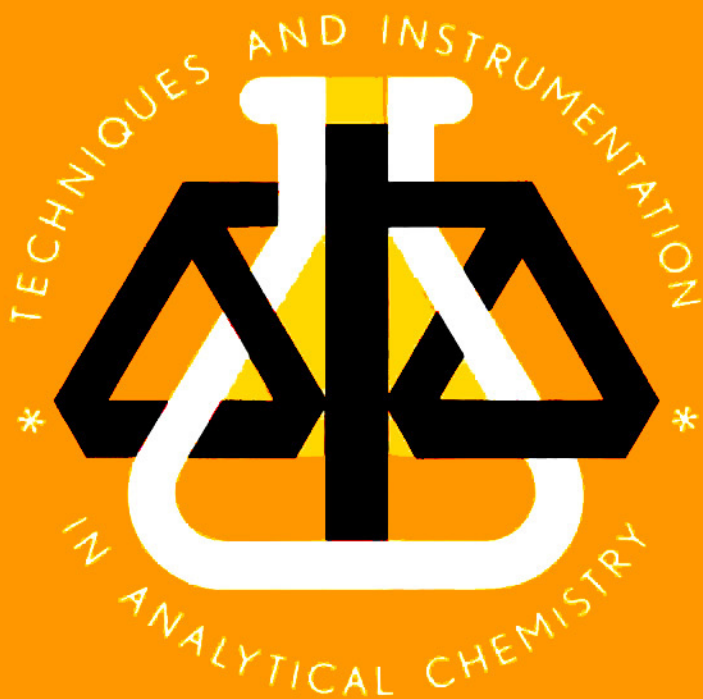


3



**PYROLYSIS MASS
SPECTROMETRY OF RECENT
AND FOSSIL BIOMATERIALS
COMPENDIUM AND ATLAS**

H.L.C. Meuzelaar, J. Haverkamp and F.D. Hileman

ELSEVIER SCIENTIFIC PUBLISHING COMPANY

TECHNIQUES AND INSTRUMENTATION IN ANALYTICAL CHEMISTRY – VOLUME 3

**PYROLYSIS MASS SPECTROMETRY OF RECENT AND
FOSSIL BIOMATERIALS**

COMPENDIUM AND ATLAS

TECHNIQUES AND INSTRUMENTATION IN ANALYTICAL CHEMISTRY

- Volume 1 Evaluation and Optimization of Laboratory Methods and Analytical Procedures. A Survey of Statistical and Mathematical Techniques**
by D.L. Massart, A. Dijkstra and L. Kaufman
- Volume 2 Handbook of Laboratory Distillation**
by E. Krell
- Volume 3 Pyrolysis Mass Spectrometry of Recent and Fossil Biomaterials. Compendium and Atlas**
by H.L.C. Meuzelaar, J. Haverkamp and F.D. Hileman

TECHNIQUES AND INSTRUMENTATION IN ANALYTICAL CHEMISTRY – VOLUME 3

PYROLYSIS MASS SPECTROMETRY OF RECENT AND FOSSIL BIOMATERIALS

COMPENDIUM AND ATLAS

Henk L.C. Meuzelaar

Biomaterials Profiling Center, University of Utah, Salt Lake City, UT, U.S.A.

Johan Haverkamp

*Department of Biomolecular Physics, F.O.M. Institute for Atomic and Molecular
Physics, Amsterdam, The Netherlands*

Fred D. Hileman

Analytical Chemistry Division, Monsanto Research Corporation, Dayton, OH, U.S.A.



ELSEVIER SCIENTIFIC PUBLISHING COMPANY
Amsterdam – Oxford – New York 1982

ELSEVIER SCIENTIFIC PUBLISHING COMPANY
Molenwerf 1
P.O. Box 211, 1000 AE Amsterdam, The Netherlands

Distributors for the United States and Canada:

ELSEVIER SCIENCE PUBLISHING COMPANY INC.
52, Vanderbilt Avenue
New York, NY 10017

ISBN 0-444-42099-1 (Vol. 3)
ISBN 0-444-41744-3 (Series)

© Elsevier Scientific Publishing Company, 1982

All rights reserved. No part of this publication may be reproduced, stored in a retrieval system or transmitted in any form or by any means, electronic, mechanical, photocopying, recording or otherwise, without the prior written permission of the publisher, Elsevier Scientific Publishing Company, 1000 AH Amsterdam, The Netherlands

Printed in The Netherlands

*Dedicated to Professor Dr. Jaap Kistemaker
in honour of his 65th birthday*



*"Is rational mass spectrometric analysis possible if molecular
size is such that thermal dissociation . . . is unavoidable?"*

Without a doubt the answer is yes."

J. Kistemaker (1954)

This Page Intentionally Left Blank

CONTENTS

Abbreviations used	IX
Preface	XI
Acknowledgements	XIII
PART I COMPENDIUM OF BASIC PRINCIPLES AND APPLICATIONS	1
Chapter 1. ORIGINS AND DEVELOPMENT OF PYROLYSIS MASS SPECTROMETRY OF BIOMATERIALS	3
1.1. The first reports	3
1.2. Direct probe Py-MS	4
1.3. Laser Py-MS	5
1.4. Filament Py-MS	6
Chapter 2. FROM FINGERPRINTING TO STRUCTURAL INVESTIGATION	9
2.1. Operational fingerprinting; a new concept	9
2.2. Complexity of the sample	9
2.3. Additivity of component spectra	10
2.4. Availability of reference spectra	10
2.5. Availability of standard reference materials	11
2.6. Knowledge of relevant pyrolysis mechanisms	13
2.7. Availability of ancillary analytical methods	13
Chapter 3. PYROLYSIS MECHANISMS IN BIOMATERIALS	15
3.1. General aspects	15
3.2. Polysaccharides	16
3.3. Nucleic acids	19
3.4. Proteins	21
3.5. Lipids	24
3.6. Miscellaneous biopolymers	25
Chapter 4. THE TECHNIQUE OF CURIE-POINT PYROLYSIS MASS SPECTROMETRY	29
4.1. Sample preparation	29
4.2. Pyrolysis	33
4.3. Pyrolysate transfer	37
4.4. Ionisation	41
4.5. Mass analysis	42
4.6. Ion detection	45
4.7. Signal recording	45
Chapter 5. REPRODUCIBILITY IN CURIE-POINT PYROLYSIS MASS SPECTROMETRY	47
5.1. Qualitative reproducibility	47
5.2. Quantitative reproducibility	49
5.3. Factors influencing long-term reproducibility	50
5.4. Prospects for inter-laboratory reproducibility	52

VIII

Chapter 6.	DATA ANALYSIS PROCEDURES	55
6.1.	Available computer programs	55
6.2.	Data pre-processing	56
6.2.1.	Pattern scaling	56
6.2.2.	Feature scaling	58
6.3.	Univariate statistical analysis	60
6.4.	Multivariate statistical analysis	62
6.5.	Visualisation techniques	66
6.6.	Computer-assisted chemical interpretation	68
6.6.1.	Subtraction techniques	68
6.6.2.	Factor analysis	69
6.7.	Computer-assisted quantitative analysis of mixtures	70
6.8.	Future developments	73
Chapter 7.	SELECTED APPLICATIONS TO BIOMATERIALS	77
7.1.	Scope of analytical pyrolysis techniques	77
7.2.	Medical applications	77
7.2.1.	Clinical microbiology	77
7.2.2.	Other clinical applications	83
7.2.3.	Quality control	85
7.3.	Biological applications	86
7.4.	Environmental applications	89
7.5.	Biogeochemical applications	92
PART II	ATLAS OF SELECTED PYROLYSIS MASS SPECTRA	99
Contents	101
1.	INTRODUCTION	105
1.1.	General remarks	105
1.2.	Sample preparation	105
1.3.	Analytical conditions	106
1.4.	Spectrum presentation format	106
1.5.	Spectrum contributions from inorganic constituents	107
1.6.	Protein spectra (group B)	109
1.7.	Nucleotide and nucleic acid spectra (group C)	110
1.8.	Lipid spectra (group D)	110
1.9.	Spectra of humic materials and geopolymers (group F)	110
1.10.	Spectra of other biochemically important compounds (group G)	111
2.	PYROLYSIS MASS SPECTRA	113
Group A.	Carbohydrates and Glycoconjugates	113
Group B.	Peptides and Proteins	151
Group C.	Nucleotides and Nucleic Acids	167
Group D.	Lipids	179
Group E.	Natural Products	195
Group F.	Humic Materials and Geopolymers	213
Group G.	Other Biochemically Important Compounds	245
Group H.	Polymers of Non-Biological Origin	259
REFERENCES	275
SUBJECT INDEX	287

Abbreviations used

amu	Atomic mass units
CI	Chemical ionisation
CID	Collision-induced dissociation
EI	Electron impact ionisation
E_{e1}	Energy of ionising electrons
FD	Field desorption
FI	Field ionisation
GC/MS	Gas chromatography in tandem with mass spectrometry
HRMS	High resolution mass spectrometry
MS	Mass spectrometry
MS/MS	Mass spectrometry in tandem with mass spectrometry
MW	Molecular weight
m/z	The mass of the ion divided by its charge (usually unity)
Py-GC	Pyrolysis-gas chromatography
Py-MS	Pyrolysis-mass spectrometry
Py-TRMS	Time-resolved pyrolysis-mass spectrometry
T_c	Curie-point temperature
T_{eq}	Equilibrium temperature
t_{Σ}	Total heating time
t_T	Temperature rise time

This Page Intentionally Left Blank

Preface

In recent years pyrolysis mass spectrometry (Py-MS) has played an increasingly important role in analytical pyrolysis, which is traditionally dominated by pyrolysis gas chromatographic methods. This tendency first became evident during the IIIrd International Symposium on Analytical Pyrolysis held in July 1976 in Amsterdam, and has continued to manifest itself during the 1978 conferences in Budapest (IVth International Symposium on Applied and Analytical Pyrolysis) and Plymouth, New Hampshire (Gordon Conference on Analytical Pyrolysis), and also at international mass spectrometry conferences and in the recently established *Journal of Analytical and Applied Pyrolysis*.

Whereas specially designed Py-MS systems using galvanically heated filament or direct probe pyrolysers have been quite successful in structural investigations and kinetic studies involving synthetic polymers and model compounds, Curie-point Py-MS systems have proved to be uniquely advantageous in applications that require maximum reproducibility in fingerprinting and also in applications that require routine analysis of hundreds or thousands of samples. This has made the Curie-point approach especially valuable for extremely complex samples, such as are encountered among materials of biological origin, ranging from biopolymers, cells, microorganisms and tissues to humic substances, sediments, peats, coals and shales.

Probably the most extensively used Py-MS system is the fully automated Curie-point Py-MS system at the F.O.M. Institute for Atomic and Molecular Physics in Amsterdam. From January 1977 to January 1980 this system produced about 18,000 pyrolysis mass spectra for over 100 different users. One visitor to this facility, Dr. F. W. McLafferty, described his impressions as follows: *"For biopolymers and other high molecular weight substances, automated pyrolysis-MS, developed by H.L.C. Meuzelaar, P. G. Kistemaker, W. Eshuis, M. A. Posthumus and A. J. H. Boerboom of the FOM Institute in Amsterdam, is now an impressive routine analytical tool running literally thousands of samples per year, such as geo- and synthetic polymers, coal, sewage, and urine without sample workup. The capability to characterise bacteria is particularly impressive and could revolutionize the classical methods which have been used by clinical laboratories since Pasteur."*

In the course of their own involvement with the Py-MS facility at the F.O.M. Institute, the authors* have sensed an increasing need for a compendium describing the

* H.L.C. Meuzelaar was founder and Director of the F.O.M. Pyrolysis Centre from 1970 to 1978; J. Haverkamp is the present Director of the F.O.M. Pyrolysis Centre; and F. Hileman was a guest scientist at the Centre in 1978.

basic principles, techniques and applications of Curie-point Py-MS aimed at past, present and future users of the method. The authors further felt that this compendium should focus on recent and fossil biomaterials rather than on synthetic compounds because of the above-mentioned unique advantages of Curie-point Py-MS for the analysis of extremely complex samples.

The need for a compendium became even more urgent with the advent of commercially available Curie-point Py-MS systems from at least two different manufacturers* in 1979. This prompted the authors to include a small Atlas of reference spectra of carefully selected biomaterials which should help new users of Curie-point Py-MS systems to "tune" their instruments to the existing systems and to evaluate unknown spectra.

A few compounds of non-biological origin, e.g. synthetic polymers, are included in the Atlas to demonstrate the applicability of the technique to these classes of compounds and to provide some relatively simple spectra for "tuning" purposes. Moreover, synthetic compounds are often encountered as constituents or contaminants in biomaterials offered for analysis.

In order to avoid confusions and disappointment it should be stressed that the Atlas part of this book will primarily assist in the qualitative interpretation of pyrolysis mass spectra. In general, the peak assignments given are tentative and have not yet been confirmed by high resolution MS or MS/MS. Although a definite level of interlaboratory reproducibility can be shown to exist between Curie-point Py-MS systems of the same basic design, as discussed in Chapter 5, the establishment of a library for quantitative comparison between spectra from different instruments, e.g. for fine differentiation between bacterial patterns, is still beyond the present state of the art.

Although many applications of this technique deal with the classification and identification of microorganisms, fungi and cells, model spectra of such materials have not been included in the Atlas as their "fingerprints" depend strongly on experimental conditions such as cultivation and preparation methods.

Finally, an important category of readers to whom this Compendium and Atlas should prove helpful are those considering the application of Py-MS techniques to their own specific problems in the analysis of biomaterials of widely different types. The authors hope that the broad range of applications and spectra presented will enable a fair assessment of the present capabilities and limitations of Curie-point Py-MS in the analysis of complex biomaterials, with regard both to known applications and to more or less closely related new applications not specifically covered in this text.

* Extranuclear Laboratories Inc., Pittsburgh, U.S.A., and V.G. Micromass Ltd., Winsford, U.K.

Acknowledgements

The authors gratefully acknowledge the gift of samples by the National Bureau of Standards (Washington, U.S.A.), Drs. E. C. Beuvery (Rijksinstituut voor de Volksgezondheid (R.I.V.), Bilthoven, The Netherlands; polysaccharide antigens), Dr. J. Borst (R.I.V., Bilthoven, The Netherlands; *Neisseria gonorrhoea* strains), Dr. H.W.B. Engel (R.I.V., Bilthoven, The Netherlands; *Mycobacterium* strains), Dr. H.M. Greven (Organon, Oss, The Netherlands; synthetic oligopeptides), Dr. K. Haider and Dr. C. Saiz-Jimenez (Forschungsanstalt für Landwirtschaft, Braunschweig, W. Germany; humic materials), Dr. S.M. Kunen (University of Utah, U.S.A.; air particulates) Dr. S. R. Larter (Union Oil Company, U.S.A.; kerogens), Dr. J. W. de Leeuw and Prof. P.A. Schenck (Technical University of Delft, The Netherlands; oil shales, coals and lignite), Dr. T. Meindersma (Academisch Ziekenhuis Dijkzigt, Rotterdam, The Netherlands; *Klebsiella* strains), Dr. J. H. Petajan (University of Utah, U.S.A.; muscle samples), Dr. G. Schutgens (Binnengasthuis, Amsterdam, The Netherlands; urine samples), Dr. G. Sposito (University of California, Riverside, U.S.A.; sludge samples) and Ir. A. L. van Wezel (R.I.V., Bilthoven, The Netherlands; poliomyelitis virus preparations).

Further, the authors are indebted for unpublished data to Dr. P. G. Kistemaker (F.O.M. Institute for Atomic and Molecular Physics, Amsterdam, The Netherlands; laser Py-MS of DNA), Dr. M. A. Posthumus (Agricultural University, Wageningen, The Netherlands; Py-MS of nucleic acids), Dr. H. -R. Schulten (University of Bonn, W. Germany; scheme of pyrolytic degradation of glycogen), and Dr. W. Windig (F.O.M. Institute; factor analysis with rotation). Finally, the authors thank Ms. A. Tom and Ms. B. Brandt (F.O.M. Institute for Atomic and Molecular Physics, Amsterdam) for preparing most of the analyses, Dr. W. Eshuis for computer analysis of the data, Dr. P. G. Kistemaker, Dr. M. A. Posthumus and Dr. J. W. de Leeuw for critical reading of the manuscript and Mrs. M. Van for typing and editing the manuscript. The research reported in this book was supported by the Foundation for Fundamental Research on Matter (F.O.M.) and the Ministry of Health and Environmental Hygiene in The Netherlands and by the United States Department of Energy.

This Page Intentionally Left Blank

PART I

COMPENDIUM OF BASIC PRINCIPLES AND APPLICATIONS

This Page Intentionally Left Blank

Chapter 1

ORIGINS AND DEVELOPMENT OF PYROLYSIS MASS SPECTROMETRY OF BIOMATERIALS

1.1. THE FIRST REPORTS

As early as 1952, Zemany (ref. 1) pioneered the application of pyrolysis mass spectrometry (Py-MS) to the characterisation of biopolymers such as albumin and pepsin. Although he employed a relatively primitive off-line filament pyrolysis technique, his results showed that characteristic and reproducible fingerprints could be obtained. After Zemany's publication, no further Py-MS studies of biomaterials appear to have been reported for more than a decade. Instead, two years later Davison, Slaney and Wragg (ref. 2) published the first account of a different analytical pyrolysis technique, namely pyrolysis gas chromatography (Py-GC), which required less expensive and complicated instrumentation than Py-MS and soon found application in the synthetic polymer field and a number of related areas. In the early 1960's, the search for extraterrestrial life - or, at least, complex organic compounds - as part of the scientific mission of planned space probes prompted the application of Py-GC to biochemical problems, e.g., studies of biopolymers and microorganisms by Wilson *et al.* (ref. 3) and Oyama (ref. 4). This, in turn, triggered an extensive series of studies by Reiner *et al.* (refs. 5 - 7), who pioneered the application of Py-GC in microbiology.

Meanwhile, Zemany's report on Py-MS seemed almost forgotten, in spite of the strong potential advantages of Py-MS over Py-GC with regard to speed of analysis, long-term reproducibility and suitability of the data for computer processing. Towards the end of the 1960's, however, scattered reports on the use of direct Py-MS for the characterisation of complex organic materials appeared in the literature. Hummel's group in Cologne started an impressive series of experiments (refs. 8, 9) using both direct probe and filament pyrolysis in combination with field ionisation and electron impact ionization mass spectrometry for structural elucidation of synthetic polymers. Also, publications dealing with biochemical applications of Py-MS appeared, revealing the existence of at least three different pyrolysis approaches namely, direct probe pyrolysis, laser pyrolysis and filament pyrolysis. This diversification reflected the existence of the same three approaches in Py-GC since direct probe pyrolysis, using a heated capillary, can be regarded as the equivalent of "oven" or "furnace" pyrolysis in Py-GC. For a detailed account of the development of pyrolysis techniques up to 1967, the reader is referred to the excellent review by Levy (ref. 10). Developments up to 1979 are described in two highly detailed and complete reviews by Irwin and Slack (ref. 11) and Irwin (ref. 12),

which should be consulted by every worker in the field of analytical pyrolysis. Since the above three pyrolysis approaches still persist in Py-MS today, the further evolution of these techniques will be discussed in the following paragraphs.

1.2. DIRECT PROBE PY-MS

The first application of this technique to biopolymers may well have been the study of DNA pyrolysed directly in the source of a high resolution magnetic sector instrument reported by Boettger and Kelly (ref. 13) in 1969. This study was primarily motivated by the search for extraterrestrial life, and was published as an extended abstract only. Among the pyrolysis products identified were intact bases. One year later, Charnock and Loo (ref. 14) independently reported an almost identical experiment. A curious aspect of this publication is that the authors completely avoided the use of the term pyrolysis - or equivalent terms - thus creating the misleading impression that the DNA sample was somehow evaporated from the direct probe rather than pyrolysed. This ambiguity has persisted in some of the later literature reports on direct probe Py-MS by other authors, reflecting a basic difficulty in accurately defining the boundaries between evaporation and pyrolysis in practical experimental conditions. As a result, the literature on direct probe mass spectrometry abounds with vaporisation experiments where the larger, less volatile molecules were inadvertently pyrolysed, and with pyrolysis experiments in which the more volatile molecules were undoubtedly evaporated intact.

After 1970, further direct probe Py-MS studies on biomaterials were reported by Wiebers *et al.* (refs. 15 - 17), Anhalt and Fenselau (ref. 18), Risby and Yergey (refs. 19, 20), Buchhorn *et al.* (ref. 21) and Lüderwald (ref. 22). The work of Wiebers *et al.* on nucleic acids appears to represent a direct continuation of Charnock and Loo's experiments. The report by Anhalt and Fenselau deals with the differentiation of microorganisms on the basis of lipid patterns in the higher mass range, illustrating the above-mentioned problems of defining the boundaries between pyrolysis and vaporisation. Risby and Yergey's studies opened a new dimension in direct probe Py-MS through the introduction of time-resolved recording of pyrolysis patterns referred to by the authors as linear programmed thermal degradation mass spectrometry (LPTDMS) and applied to the analysis of microorganisms and leukaemic white blood cells. In order to detect large evaporated or pyrolysed molecules - most probably of a lipid nature - they used chemical ionisation rather than electron impact ionisation techniques. Finally, Lüderwald and Buchhorn described the analysis of connective tissue samples for the presence of poly(ethyleneterephthalate) particles originating from prosthetic implant devices.

Characteristic features of the above described direct probe Py-MS experiments are the slow heating rates (typically less than 1°C/s), the low pyrolysis temperatures (generally below 400°C) and the relatively long residence time of the products in the pyrolysis zone. The slow heating rate technique has the advantage of allowing

pyrolysis to occur directly in the ion source, thus avoiding loss of products through adsorption on transfer lines. This enables the technique to be used with slow scanning magnetic sector instruments while still affording time-resolved registration of the pyrolysis patterns. Also, minimal specialised instrumentation is required since direct probe inlets are available with most mass spectrometers. Disadvantages of the approach are considerable contamination of the ion source (which may have an adverse influence on long-term reproducibility), excessive charring because of the slow heating rate (ref. 23) and the occurrence of secondary pyrolysis reactions because of the long residence time of the products in the pyrolysis zone.

1.3. LASER PY-MS

A second line of Py-MS studies on biomaterials which has its foundations in the late 1960's, is laser Py-MS. Here pioneering studies were reported in 1966 by Vastola and Pirone (ref. 24), who used a ruby laser in combination with a time-of-flight mass spectrometer for the analysis of coal samples. Similar experiments were published by Joy *et al.* (ref. 25) in 1968, whereas in 1970 Karn *et al.* (ref. 26) described laser Py-MS of coal using an off-line pyrolysis technique with a ruby and a CO₂ laser and analysing the pyrolysis products by high resolution mass spectrometry. Laser Py-MS creates yet another definition problem. During intense laser radiation, fragmentation of molecules may occur by direct bond scission due to electronic excitation (photolysis) rather than by relaxation of vibrational excitation resulting in heating of the whole molecule (pyrolysis or thermolysis). Some of the later Py-MS studies tried to avoid this ambiguity by using infrared lasers (mainly CO₂ lasers) at beam intensities which precluded the occurrence of multi-photon excitation. Examples of such studies include the work of Vanderborgh and Fletcher on synthetic polymers and geopolymers (ref. 27) and the studies of Kistemaker *et al.* on synthetic polymers (ref. 28) and nucleic acids (ref. 29). To confuse further the issue of process definitions in laser mass spectrometry: even when using infrared lasers, spontaneous ionisation of organic molecules occurs through ion-molecule reactions between small inorganic cations or anions and neutral organic molecules (refs. 30, 31). Apart from these intact ion-molecule complexes, often referred to as "quasi-molecular ions", fragment ions can also be found, obviously formed by thermal fragmentation either before or after the ion-molecule reaction (ref. 30).

The most recent development in laser Py-MS appears to be the laser microprobe mass analyser (LAMMA) developed by Kaufmann *et al.* (ref. 32) and further improved by Wechsung *et al.* (ref. 33). Originally developed for the analysis of intracellular electrolytes and trace metal concentrations, the LAMMA system has also produced spectra exhibiting characteristic fragment patterns of polymeric organic materials (ref. 34) and cells (refs. 35, 36) as well as the above described class of

ion-molecule complexes (ref. 37). The high spatial resolution (better than $0.5 \mu\text{m}$) allows fingerprinting of less than 10^{-12} g of sample. However, neutral fragments are not registered by the LAMMA instrument since the minute amounts of products produced per laser shot preclude the use of further ionisation procedures. Therefore, most of the detected ions are probably photolysis products and/or intact ion-molecule complexes and due caution should be exercised in referring to these spectra as "pyrolysis mass spectra".

In principle, laser Py-MS has tremendous potential because it allows rapid direct heating of the sample while heating of large reactive substrate areas is avoided. Moreover, the high spatial resolution achievable opens up a whole new dimension in the analysis of many different types of samples. Nevertheless, there are serious practical problems in controlling the amount of energy deposited per unit sample volume, in defining optimum parameters and in constructing suitable mass spectrometers for recording laser pyrolysis phenomena. These problems may take many more years before being adequately resolved.

A highly promising approach towards the simultaneous detection of ions from laser processes, without resorting to time-of-flight systems or photographic plates, is the development of electro-optical ion detectors using channel electron multiplier arrays in combination with vidicon or photodiode array readout systems (refs. 38, 39). This approach, however, is costly, technically complex and still in a relatively early stage of development.

1.4. FILAMENT PY-MS

The third line of Py-MS still actively pursued today is the filament pyrolysis approach. In 1970, Simon's group in Zurich published the results of preliminary Py-MS studies on fatty acid salts, pigment dyes and substituted benzoic acids (ref. 40) using a Curie-point pyrolyser connected to a magnetic sector mass spectrometer system through an empty capillary column and a molecular separator. Curie-point pyrolysis, as first described by Giacobbo and Simon (ref. 41), belongs to the broad group of filament pyrolysis techniques but differs from the other members of the group in that the filament is inductively heated by a high-frequency coil rather than heated by a galvanic current, and the equilibrium temperature of the filament is determined by the Curie-point of the ferromagnetic filament rather than by a servo-controlled power supply. The induction heating principle allows for batch processing of samples since the filaments are completely interchangeable, provided that the filament dimensions and the ferromagnetic alloy are kept constant. In fact, because of the low cost, Curie-point filaments are disposable. Moreover, the contactless heating principle allows for easy automation of sample exchange procedures, as demonstrated by the successful construction of fully automated Py-GC (ref. 42) and Py-MS (ref. 43) systems. Apart from these technical differences, however,

Curie-point techniques are fully comparable to other filament pyrolysis techniques employing similar heating rates and equilibrium temperatures.

In 1973, Meuzelaar and Kistemaker at the F.O.M. Institute for Atomic and Molecular Physics in Amsterdam reported the development of a Curie-point Py-MS technique for fast differentiation of bacterial strains (ref. 44). The Py-MS system differed from Simon's original system in that the pyrolysis reactor was enclosed in the vacuum system and was connected to the open electron impact ioniser of the quadrupole mass filter through a heated, gold-coated expansion chamber. A liquid nitrogen-cooled screen surrounded the expansion chamber and a signal averager allowed recording of fast repetitive mass scans.

During the next few years, the F.O.M. group reported further technical developments, such as the use of high speed ion counting (ref. 43), full automation (ref. 43) and computerised data processing techniques (ref. 45). Also, new applications to biomaterials were reported (refs. 46 - 49), including characterisation of humic materials (ref. 50) and whole soils (ref. 51), as well as geochemical applications (ref. 52) and medical applications (described in Chapter 7). The analysis of biomaterials by filament pyrolysis techniques in direct combination with mass spectrometry was also described by other groups, e.g. Schulten and Görtz (ref. 53), employing Curie-point pyrolysis in the ion source of a high-resolution field ionisation mass spectrometer for the analysis of glycogen, and by Hileman (ref. 54) using a Pyroprobe (Chemical Data Systems, Inc.) filament pyrolyser in the reagent gas inlet of a chemical ionisation mass spectrometer for the characterisation of muscle tissue samples.

Recently, the distinction between filament and oven pyrolysis techniques has become less marked through the introduction of a new Curie-point pyrolysis technique in Py-MS (refs. 55, 56). Instead of employing a ferromagnetic filament, this technique uses small, hollow ferromagnetic cylinders in which the sample is placed. The heating characteristics of these cylinders are similar to the heating profiles of the wires. The pyrolysis process differs from filament pyrolysis, however, in that the pyrolysis products experience multiple collisions with the hot cylinder wall. In this respect, the technique resembles direct probe and other oven pyrolysis techniques. It differs from the latter, however, in that the heating rates are orders of magnitude higher than in classical oven pyrolysers. Applications of this technique in Py-MS include the study of pyrolysis mechanisms in relatively volatile model compounds (refs. 55, 57 - 59), pigment dyes (refs. 55, 60) and antibiotics (ref. 61). Apart from its application to the pyrolysis of relatively volatile compounds, however, it remains to be determined whether this new approach offers any significant advantage over filament pyrolysis in the analysis of biomaterials. Because of the transient high pressures in the oven during pyrolysis secondary reactions may occur in the gas phase, e.g. formation of dibenzyl upon pyrolysis of phenylbutanoic acid (ref. 57). These reactions can be minimised by using

submicrogram amounts of sample (ref. 56). At these sample levels, however, it becomes increasingly difficult to avoid significant contributions from instrument background due to residual contaminations of oven and/or vacuum system. In our experience, the above-mentioned problems have an adverse effect on repeatability and reproducibility.

Finally, a highly specialised Py-MS technique reported by Schulten *et al.* (ref. 62) should be mentioned. In this experiment, a DNA sample was pyrolysed directly on the heated emitter of an FD source and the ions were analysed by a high resolution mass spectrometer equipped with a photoplate detector. This Py-FD/MS technique allowed the detection of unusually large pyrolysis fragments of DNA, including some intact dinucleotide ions.

Chapter 2

FROM FINGERPRINTING TO STRUCTURAL INVESTIGATION

2.1. OPERATIONAL FINGERPRINTING; A NEW CONCEPT

The classical applications of fingerprinting techniques are classification and identification of the original material, using a library of reference fingerprints. Generally in these applications, little or no chemical interpretation of the pattern is attempted or even required. Computer evaluation of pyrolysis fingerprints (pyrograms) in combination with the greatly increased speed of analysis afforded by modern Py-MS techniques has opened up important new areas of application, namely screening, quality control and process monitoring (ref. 48, 49, 63). These procedures can be regarded as "operational fingerprinting" techniques in that no library of reference spectra is required but reference samples are usually present in the batch of samples submitted for analysis. In most applications of this type, a single class of samples dominates (e.g. pure samples) and only a minor fraction of the samples belongs to one or more different classes (e.g. contaminated samples).

In our experience, operational fingerprinting automatically leads to the question: what is the biochemical nature of the observed variation or changes which make the outliers different from the central cluster. Thus, as shown in several of the above cited literature references (ref. 49, 50, 52, 53), Py-MS techniques are increasingly employed to address directly problems concerning the biochemical nature, composition and structure of the sample. The success of attempted biochemical interpretation of interesting features in pyrolysis mass spectra, whether distinguished by eye or with the aid of numerical computer techniques, depends critically on the following factors: complexity of the sample, additivity of component spectra, availability of reference spectra from standard materials, knowledge of relevant pyrolysis mechanisms and availability of ancillary analytical methods. These factors will be discussed in the following paragraphs.

2.2. COMPLEXITY OF THE SAMPLE

Obviously a multicomponent sample generally provides a spectrum more difficult to interpret than that of a sample consisting of a single, pure component. However, with multicomponent samples - even extremely complex samples such as whole cells - often only one or two components will suffice to adequately describe the analytical problem. Therefore, if suitable control samples are available, subtraction of patterns may yield a much simpler pattern, mainly representative of the component(s) of interest.

Even when comparing multiple samples, e.g., bacterial strains differing in more than one component, factor analysis techniques may be called upon to reveal relatively simple factor spectra representative of the various components involved (see Chapter 6). These techniques can only be used if the component spectra are additive which, in turn, requires that the respective pyrolysis pathways are mutually non-interfering.

2.3. ADDITIVITY OF COMPONENT SPECTRA

Only pyrolysis techniques which minimise the occurrence of bimolecular reactions and secondary reactions, e.g. recombinations between pyrolysis products, can be expected to reasonably fulfill the condition of additivity. In studies by Posthumus and Nibbering (ref. 58) the Curie-point oven pyrolysis of microgram amounts of amino acids did not cause appreciable recombination reactions. This was shown by the absence of diketopiperazine formation, a reaction that readily occurs during classical oven pyrolysis (ref. 64). In the case of 4-phenylbutanoic acid (and not for other ω -phenylalkanoic acids) a recombination reaction, i.e. the formation of dibenzyl, could be observed (ref. 57). However, this reaction could be eliminated by further reducing the amount of sample to submicrogram levels (ref. 56).

When using Curie-point filament pyrolysis, additivity of spectra is readily observed for such classes of compounds as polysaccharides (refs. 65, 66) and lignins (ref. 67) and, less well established, also for lipids and proteins (ref. 68). The additivity of "component subspectra" is an important requirement for (semi)quantitative applications of Py-MS, e.g. in monitoring ppm concentrations of the toxic, technical polymer DEAE-dextran in poliomyelitis virus vaccine preparations (ref. 63).

The admixture of inorganic salts, and also changes in pH of the sample solutions or suspensions markedly influence the pyrolysate patterns of polar organic compounds, even if no direct organic salts can be formed. This phenomenon, further discussed in Section 4.1, and in some of the Atlas spectra, should be kept in mind when evaluating spectra of complex samples for the presence of a particular organic component. Highly reactive organic groups have been found to react with inorganic components, e.g. the methyl groups of the trimethylammonium function of choline residues or ester methyl groups (see Atlas) can react with chloride ions to form methylchloride. In fact, the latter reaction is quantitative and can be used to measure the concentration of acetylcholine in brain tissue, as described by Szilagyi *et al.* (ref. 69). Similar formation of methylchloride can be observed during pyrolysis of choline-containing phospholipids (ref. 70).

2.4. AVAILABILITY OF REFERENCE SPECTRA

Until now, reference spectra have not been readily available from literature sources since the Py-MS techniques used vary too widely to allow close comparison of spectra. However, from building four Curie-point Py-MS systems over the past ten years, we know that reproducibility between instruments of the same basic

design is remarkably good. Moreover, as demonstrated in Chapter 5, even a definite degree of inter-laboratory reproducibility is readily achieved with comparable instruments. This has encouraged the F.O.M. Pyrolysis Centre to compile a collection of several hundred pyrolysis mass spectra of natural and synthetic compounds. A selection of these spectra is included in Part II of this volume. The purpose of this Atlas is primarily to enable the reader to evaluate the applicability of Curie-point Py-MS to different problems in the analysis of biomaterials, geopolymers, humic compounds and, to a limited extent, drugs and technical polymers. At the same time, this collection of Py-MS reference spectra enables scientists working with comparable Py-MS techniques to evaluate the degree of inter-laboratory reproducibility achievable by appropriate "tuning" of their instruments. However, as was pointed out in the Preface, this collection of spectra should primarily enable a qualitative comparison of pyrolysis mass spectra. The establishment of a library for quantitative comparisons between spectra from different instruments, e.g. for fine differentiation between bacterial strains, is beyond the present state of the art.

It should further be noted that extensive chemical interpretation of the various mass peaks in the Atlas spectra was not possible; only tentative assignments could be made on the basis of comparison with results of other techniques such as Py-HRMS (refs. 53, 71, 72) or Py-GC-MS (refs. 73, 74). The use of such data from the literature may give incorrect results, however, as pyrolysis and sample transfer conditions for different techniques are often very different. Therefore, tandem mass spectrometer systems for collisional induced dissociation (refs. 75 - 81) should prove invaluable for establishing the chemical identity of peaks observed in Py-MS, since this approach allows precise duplication of pyrolysis and sample transfer conditions normally used in Py-MS (see Section 2.7).

Regardless of the size of any library of pyrolysis mass spectra, the variety of biomaterials that can be investigated is so immense that often pyrolysis patterns not represented in the library will be generated. Even in these cases, a limited amount of chemical interpretation of such patterns may still be possible on the basis of insight into - or empirical knowledge of - relevant pyrolysis mechanisms (see Section 2.6.).

2.5. AVAILABILITY OF STANDARD REFERENCE MATERIALS

A difficult problem in the compilation of a reference collection of pyrolysis mass spectra of complex biomaterials is the limited availability of suitable standard materials. Although complex biomaterials can be found among the large collection of Standard Reference Materials issued by the National Bureau of Standards (ref. 82), these materials have not been thoroughly characterised and defined with respect to their organic structure and composition. Moreover, although NBS Standard Materials of biological origin are usually available as a thoroughly homogenised,

fine powder, the NBS does not guarantee (ref. 83) homogeneity of the material down to sample sizes below 100 micrograms such as are normally used in Py-MS. Of course, inhomogeneity problems may be detected by repeated Py-MS analyses and, if necessary, can be corrected by averaging the results of multiple determinations.

Table 1 lists NBS Standard Reference Materials which in the opinion of the authors may have potential value as complex biological reference samples in Py-MS, and spectra from some of which can be found in this book. Preliminary studies on four materials indicated in Table 1 failed to detect marked inhomogeneities at the 10 microgram level (ref. 84). Less sophisticated, but inexpensive and generally available reference materials for less demanding applications in Py-MS studies on biomaterials are, for instance, the polysaccharides amylose and cellulose, the proteins albumin and keratin and complex materials such as milk homogenate and soft wood powder (Douglas fir). Homogenised bovine milk is especially useful as different samples show relatively little variation in their pyrolysis mass spectra. Moreover, it is composed of a wide variety of biological compounds, needs little sample preparation (dilution with water) and produces a thin, uniform coating on the pyrolysis filament. Convenient sources of some high purity synthetic polymers are stationary phases for gas chromatography and ion exchange resins. However, considerable differences in pyrolysis patterns may be found between products from different manufacturers or even between different batches from a single commercial source.

TABLE 1

NBS Standard Reference Materials of recent and fossil biological origin. For spectra of the materials marked with * see further in this Volume.

Nr.	Material	NBS cat. nr.
1	Bovine serum albumin	SRM 926
2	α -Cellulose	SRM 1006a
3	Natural rubber	SRM 385b
4	Orchard leaves	SRM 1571
5	Tomato leaves	SRM 1573
6	Pine needles	SRM 1575
7	Spinach	SRM 1570
8	Rice flour	SRM 1568
9	*Wheat flour	SRM 1567
10	*Brewer's yeast	SRM 1569
11	Oyster tissue	SRM 1566
12	Albacore tuna	RM 50
13	Freeze-dried urine	SRM 2671
14	*Urban particulate	SRM 1648
15	*River sediment	SRM 1645
16	Estuarine sediment	SRM 1646
17	Subbituminous coal	SRM 1635
18	Bituminous coal	SRM 1632a

In conclusion, it can be stated that satisfactory standard reference materials for Py-MS analysis of complex biomaterials do not yet seem to exist. An ideal biomaterial for calibration ("tuning") of the Py-MS systems should exhibit long-term chemical stability and should preferably be completely soluble in a simple solvent with good coating characteristics. Further, it should be sensitive to changes in analytical conditions and it should provide a pyrolysate with components representative of a wide range of chemical classes and molecular sizes. An example of a potentially good standard reference material for Py-MS is lignin. Some lignins are completely soluble in methanol or ethanol (ref. 85); lignins are chemically very stable and provide a wide range of pyrolysis products. Nitrogen-containing products are usually absent, however, and lignin is not highly sensitive to changes in pyrolysis or mass spectrometry conditions. Instant milk powder might be another interesting candidate, as it also is readily soluble and contains a wide range of biological compounds, e.g. nitrogen-containing compounds and lipids. However, the chemical stability of milk powder might prove to be inadequate.

There is no doubt that the field of analytical pyrolysis would benefit greatly if NBS or other internationally recognised organisations would develop a set of carefully homogenised and stored biomaterials, 10 or 100 mg aliquots of which could be made available to the scientific community as standards for analytical pyrolysis.

2.6. KNOWLEDGE OF RELEVANT PYROLYSIS MECHANISMS

Our present knowledge of pyrolysis mechanisms in biomaterials is at best very sketchy and does not compare with the level of knowledge of and insight into fragmentation mechanisms occurring during electron impact ionisation. Although Posthumus *et al.* (refs. 57, 58) have presented strong evidence for the basic simplicity and straightforwardness of pyrolysis mechanisms in selected organic model compounds, which compare favourably with electron impact fragmentation mechanisms in these molecules, the extreme complexity of many biomaterials will undoubtedly prevent the achievement of a satisfactory degree of insight into the precise pyrolysis mechanisms involved. A more detailed overview of our present knowledge of pyrolysis mechanisms in biomaterials is presented in Chapter 3.

2.7. AVAILABILITY OF ANCILLARY ANALYTICAL METHODS

A very difficult task is the qualitative interpretation of a single significant mass peak in a pyrolysis mass spectrum. With the exception of a few peaks in the lower mass range, e.g. at m/z 34 (hydrogen sulphide) or m/z 17 (ammonia), the chemical identity of such a peak cannot be established with certainty, let alone its molecular origin. High-resolution mass spectrometry can be used to establish the elemental composition of a peak in a pyrolysis mass spectrum (refs. 53, 71), provided that the pyrolysis experiment can be repeated closely under these conditions. Photoplate registration may be the method of choice if the original spectrum was

obtained with a fast-scanning mass spectrometer. Alternatively, a few selected multiplets may be rapidly scanned by varying the electrical potentials on a high-resolution magnetic sector instrument and by recording the signals with a signal averager, as described by Freudenthal and Gramberg (ref. 86). High resolution mass spectrometry, of course, does not distinguish between isomeric structures. Application of Py-GC/MS techniques to establish the chemical identity of a Py-MS peak is severely handicapped by differences in pyrolysis conditions and transmission characteristics of the systems.

A promising approach, though requiring extremely specialised instrumentation, is the use of MS/MS for the identification of selected nominal mass peaks. Using a collisional induced dissociation (CID) technique Levsen and Schulten (ref. 75) were able to identify several molecular ions in the low-energy EI mass spectrum of a DNA pyrolysate. Another MS/MS system, especially designed for measuring very short-lasting pyrolysis processes has been described by Tuithof *et al.* (ref. 76), using simultaneous electro-optic ion detection. With this instrument, a preliminary study of a component in the pyrolysates of *Mycobacterium* cells, important for sub-species identification has been described (ref. 80). In this study it was demonstrated that isomeric molecular ions such as those of trimethylamine and propylamine show significantly different collision-induced fragment patterns.

McLafferty (ref. 77) and Todd (ref. 81) constructed a high resolution instrument consisting of two double-focussing mass spectrometers in tandem for the analysis of multicomponent mixtures. A highly interesting development for structure analysis is the tandem mass spectrometer consisting of three quadrupole assemblies recently described by Yost and Enke (ref. 87), and of a double quadrupole system, reported by Siegel (ref. 88). These developments may bring the use of MS/MS techniques within the reach of a much larger number of laboratories during the next few years since commercial versions are already available (refs. 88, 89).

Other promising approaches to a more detailed qualitative analysis of mixtures of pyrolysis products are the use of selective reagent gases in CI-MS systems or the differentiation of pyrolysis products with the same nominal mass but derived from different parent compounds by comparing time-resolved pyrolysis patterns such as those obtained by Risby and Yergey (refs. 19, 20).

Chapter 3

PYROLYSIS MECHANISMS IN BIOMATERIALS

3.1. GENERAL ASPECTS

Knowledge of vacuum pyrolysis mechanisms in biomaterials is most advanced for some classes of relatively simple compounds, such as amino acids (ref. 59). However, relatively little is known about these mechanisms for most biopolymers, with the exception of the thermal degradation of polysaccharides such as cellulose (ref. 90) or glycogen (ref. 53). Whereas some synthetic polymers such as polystyrene or polytetrafluoroethylene produce extremely simple pyrolysis mass spectra, provided that soft ionisation techniques are used (see Figure 1), the pyrolysis mass spectra of biopolymers are usually much more complex.

To some extent, this is caused by a general difference in pyrolysis mechanisms. In polystyrene and polytetrafluoroethylene the major degradation reaction is a straightforward depolymerisation by β -bond scission (initiation followed by unzipping) (ref. 9). This yields styrene (MW 104) and tetrafluoroethylene (MW 100), respectively, and thus the low voltage electron impact spectra show almost exclusively the molecular ion of the monomers and, at a much lower intensity, the molecular ions of the dimers and trimers provided that the higher mass range is scanned.

None of the more common biopolymers possesses a structure wherein each of the monomeric building blocks contributes a two-carbon segment to the polymer backbone which could lead to simple depolymerisation by β -scission. Natural rubber, a polyisoprene, is perhaps the only biopolymer to yield marked amounts of monomer under analytical pyrolysis conditions (see Section 3.5). Instead, most biopolymers decompose by a variety of mechanisms often characterised by the elimination of stable neutral molecules, such as H_2O , HCN, CH_2O , CH_3OH , H_2S , CO, CO_2 , C_2H_4 and H_2 , accompanied by the break-up of the polymer chain into larger fragments. Fortunately, these fragments often retain characteristics of the original monomeric building blocks.

It should be noted that since the initial pyrolytic reactions are heterolytic, the course of the thermal degradation and the relative yields of the various pyrolysis products can be significantly influenced by the presence of acidic or alkaline catalysts or of salts (ref. 91).

In the following paragraphs the present state of knowledge of vacuum pyrolysis mechanisms for the major groups of biopolymers will be briefly discussed.

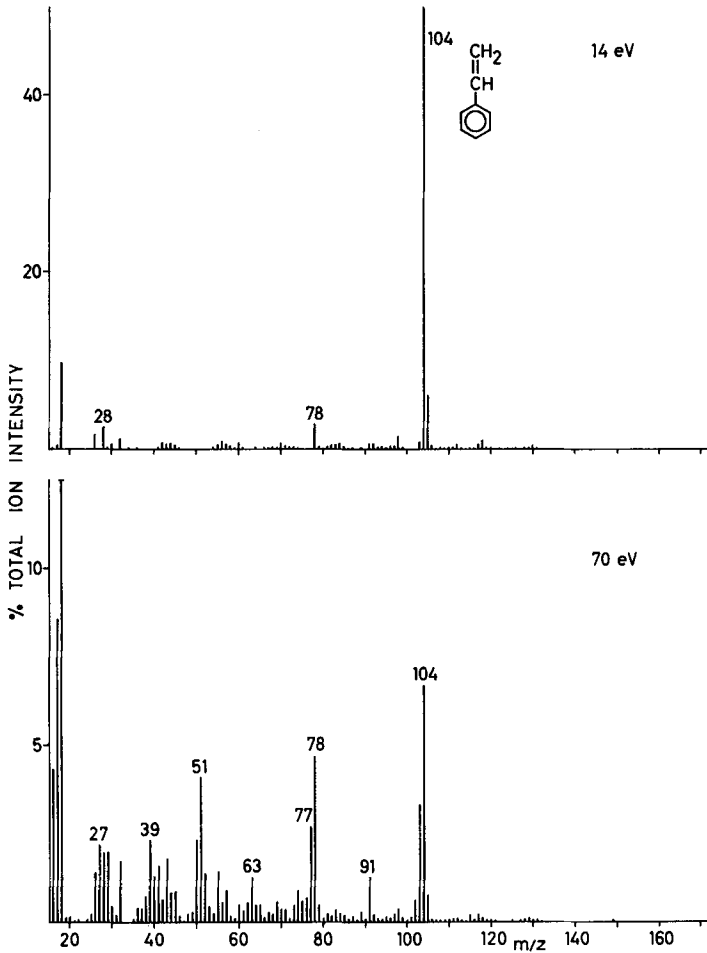


Figure 1. Pyrolysis mass spectra of polystyrene obtained at low voltage (14 eV) and normal (70 eV) EI ionisation energies. Conditions: sample 2 μg ; T_c 510°C.

3.2. POLYSACCHARIDES

The general pathways for pyrolytic degradation of polysaccharides, mainly derived by Shafizadeh *et al.* (refs. 91, 92) from model studies on cellulose [$\beta(1 \rightarrow 4)$ glucan], involve splitting of the polymer chain by three basic chemical reaction mechanisms, viz. dehydration, retroaldolisation and decarboxylation. Using these basic mechanisms, Schulten and Görtz (ref. 53) were able to explain the pyrolytic degradation of glycogen [a branched glucan with $\alpha(1 \rightarrow 4)$ and $\alpha(1 \rightarrow 6)$ linkages]. The hexose degradation pathways illustrated for glycogen in Figure 2 result in the formation of furan and pyran-type fragments and smaller acyclic aldehyde and ketone

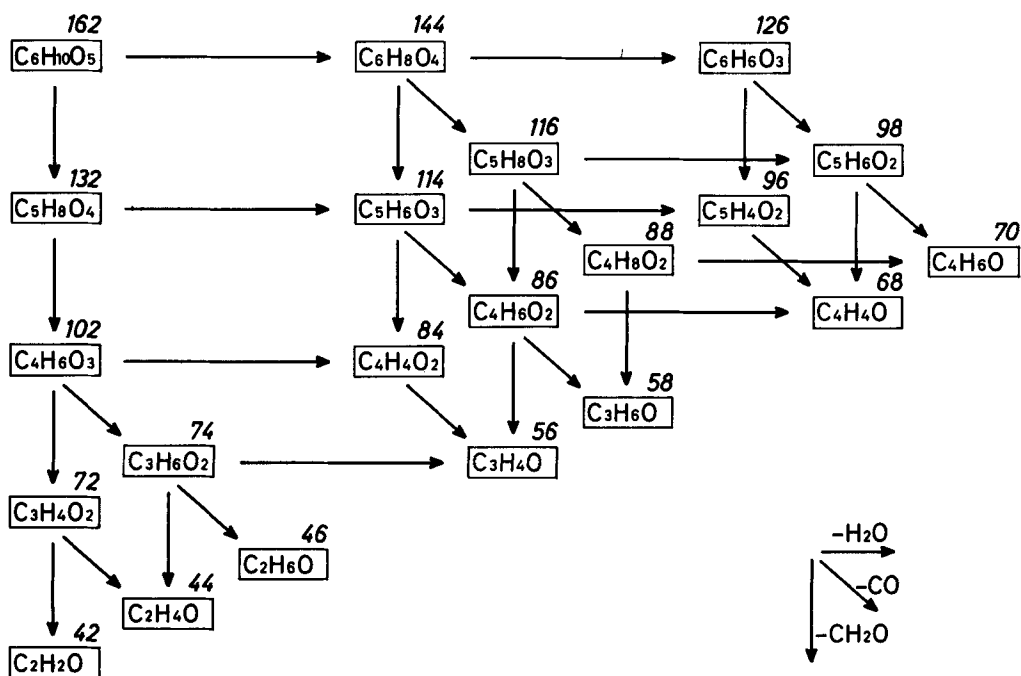


Figure 2. Some pyrolytic degradation pathways proposed for hexose polymers. This scheme is mainly based on a compilation of pyrolysis products of glycogen as observed by Schulten *et al.* (refs. 53, 94) using Curie-point pyrolysis-FI-HRMS at various pyrolysis temperatures. The m/z values are indicated in italic numerals. It should be noted that some fragments are hardly present in the Curie-point low voltage-EI spectra of hexose polymers such as those included in the Atlas. Moreover, some molecular ion peaks, regularly observed in the spectra, e.g. at m/z 32, 60, 110, 112 and 124, are not explained by this degradation scheme.

fragments. As an example, the largest commonly found cellulose fragment is levoglucosan (m/z 162), whereas a peak at m/z 126 can be attributed to hydroxymethylfurfural (ref. 90) or levoglucosenone (ref. 53) (see Atlas).

Although as yet relatively little work has been carried out to elucidate reaction pathways in non-hexosyl polysaccharides, e.g. *N*-acetylhexosaminy polymers (ref. 93), the pyrolysis mass spectral patterns shown for cellulose and its *N*-acetylglucosamine analogue chitin (Figure 3) indicate a marked degree of correspondence in basic pyrolysis fragments. As this may also hold for other types of carbohydrates, the hexose model studies should aid considerably in the qualitative interpretation of non-hexosyl polysaccharides.

Notwithstanding these apparent basic similarities in pyrolysis pathways, different types of sugar moieties, e.g. pentoses, amino sugars, *N*-acetyl aminosugars, hexuronic acids and deoxy- and anhydro sugars, often contribute characteristic fragment series

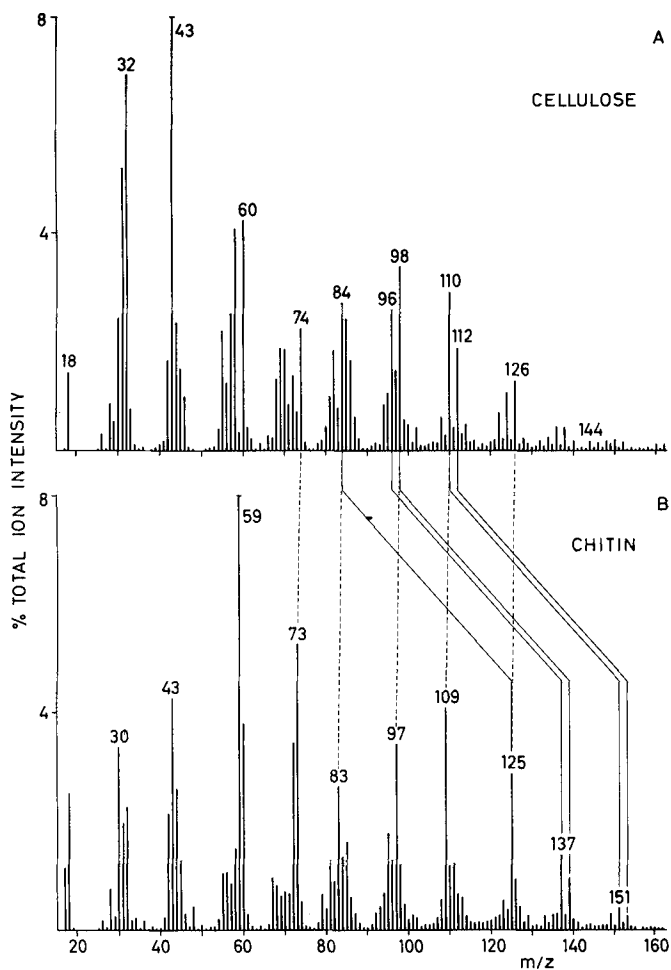


Figure 3. Pyrolysis mass spectra of cellulose (a) and chitin (b). Note the predominance of even masses in the cellulose spectrum indicating almost complete absence of fragment ions. For the chemical identity of the main ion signals see ref. 53. The characteristic ion series in the chitin spectrum appears to be shifted by 1 or 41 amu, respectively, relative to the cellulose pattern, indicating the presence of NH_2 or N-acetyl functional groups instead of an OH group in the fragments. Conditions: samples 10 μg ; T_c 510°C; E_e 14 eV (see Atlas).

to the pyrolysis mass spectrum by virtue of their different structures. For typical fragment series obtained from these carbohydrate building blocks we refer to the Atlas.

An example of the sensitivity of Py-MS for structural details was also given by Haverkamp *et al.* (ref. 49) in the analysis of N-acetyl neuraminic acid polymers (sialopolymers). This study shows that the presence of O-acetyl substituents as

well as of neutral hexosyl moieties in the native polymers is readily detected by Py-MS analysis as simple cleavage reactions give rise to acetic acid from the former and intact ring fragments such as that at m/z 126 (probably levoglucosone) from the latter. Further, differentiation of $\alpha(2 \rightarrow 8)$ and $\alpha(2 \rightarrow 9)$ linkage types between the monomeric units seems to be possible as the primary alcoholic function present in each of the monomeric moieties in the $\alpha(2 \rightarrow 8)$ chain gives rise to an increased amount of methanol as a simple pyrolytic cleavage product.

The noted scarcity of alternative analytical techniques for the rapid chemical characterisation of microgram samples of carbohydrates makes Py-MS a powerful tool, especially for the analysis of insoluble polysaccharides.

3.3. NUCLEIC ACIDS

In the field of nucleic acid analysis, pyrolysis mass spectrometry techniques have produced intriguing, sometimes paradoxical results. The work of Wiebers *et al.* (refs. 15 - 17) shows that direct probe pyrolysis produces large characteristic fragments, apparently representing intact bases or even more or less severely dehydrated nucleosides. As a result, they successfully applied this technique to the characterisation of unusual base moieties in nucleic acids. However, when applying Curie-point pyrolysis techniques to the analysis of nucleic acids, Meuzelaar *et al.* (ref. 48) obtained pyrolysis mass spectra showing only ribose and/or deoxyribose fragments (see Figure 4). Although this enabled a clear differentiation to be made between RNA and DNA samples, the complete lack of signals derived from the base moieties was both disappointing and puzzling. Later studies by Posthumus *et al.* (ref. 72) and Schulten *et al.* (ref. 62), employing high-resolution field ionisation and field desorption techniques, respectively, as well as laser Py-MS studies by Kistemaker *et al.* (ref. 29) (see Figure 5) and direct probe CID measurements by Levsen and Schulten (ref. 75) succeeded in detailing the degradation behaviour of nucleic acids.

The main mechanism taking place at temperatures as low as 180°C appears to be the expulsion of the sugar moiety with the simultaneous formation of base-phosphate condensates (ref. 72). Under standard Curie-point Py-MS conditions only the sugar moiety is detected, since the base-phosphate complex is trapped intact on the relatively cold wall of the reaction chamber. In direct probe pyrolysis, however, the base-phosphate complex is apparently further pyrolysed, yielding the base fragments. Alternatively, some of the base-phosphate complexes may conceivably reach the ion source without further wall collisions and then may fragment during electron impact ionisation, again producing ions corresponding to the base moieties. A second important reaction mechanism appears to be the formation of polyphosphates (ref. 62) with the expulsion of intact nucleosides. Again, these nucleosides can only contribute to the mass spectrum by secondary pyrolysis into more volatile fragments, or by direct diffusion into the ion source without further wall collisions.

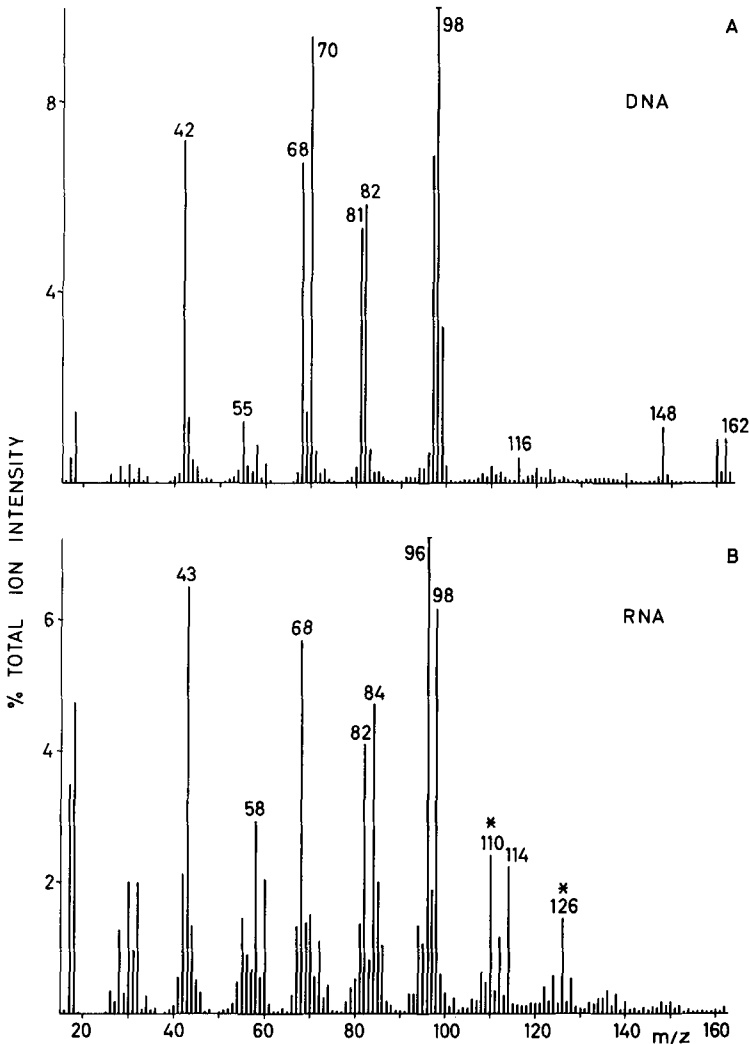


Figure 4. Pyrolysis mass spectra of DNA and RNA. Note the absence of signals from the nucleic acid bases and the dominance of water-loss fragments from the deoxyribose and ribose moieties, respectively. Peaks marked with * in the RNA spectrum denote possible contamination with hexose-type compounds. Conditions: sample 10 μg ; T_c 510°C; E_{e1} 14 eV.

A highly interesting third degradation pathway appears to be direct scission of the polymer chain into nucleotides (mono- or diphosphates) or even dinucleotides, as observed by Schulten *et al.* (ref. 62). These large phosphate-containing products cannot be expected to produce significant molecular ion signals using electron impact ionisation techniques, even if they somehow might reach the ion source.

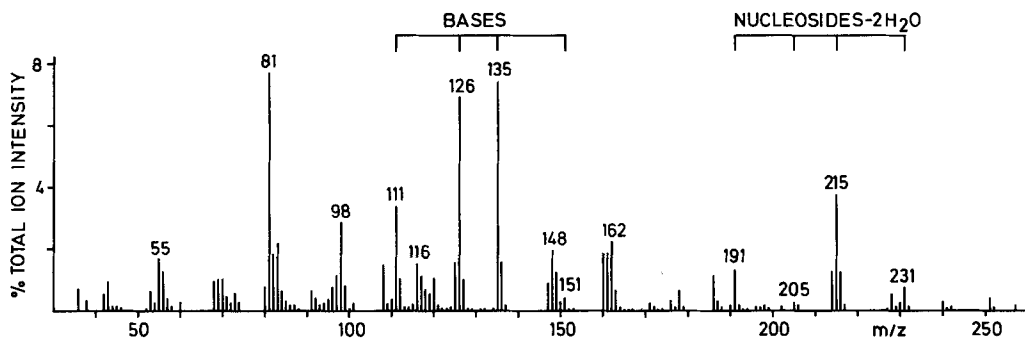


Figure 5. Laser pyrolysis mass spectrum of herring DNA showing prominent signals derived from the base and nucleoside moieties. Conditions: cw CO₂ laser, 50 W/cm², pulse time 0.1 s; E_{e1} 14 eV. For experimental set-up see reference 48.

Compared with polysaccharides, the application of Py-MS techniques to the analysis of nucleic acids is still in its infancy. However, taking into account the impressive successes obtained with the mass spectral analysis of intact nucleosides and nucleotides using some of the newer desorption techniques, significant breakthroughs in the Py-MS analysis of nucleic acids, using combinations of pyrolysis and desorption techniques, as pioneered by Schulten *et al.* (ref. 62), may well occur in the near future.

3.4. PROTEINS

As mentioned in the first paragraph of this chapter, the analysis of proteins is one of the oldest applications of Py-MS (ref. 1). Rather than break-up of the polymer backbone into large fragments characteristic of the original building blocks, the dominant mechanism appears to be the splitting off of appendages (ref. 95). As a rule, highly characteristic signals are found for the aromatic- and sulphur-containing amino acid moieties, e.g. hydrogen sulphide for cyst(e)ine and in combination with methanethiol also for methionine; pyrrole, pyrrolidine and methylpyrrole for (hydroxy)proline; phenol and cresol for tyrosine; toluene, styrene and phenylacetonitrile for phenylalanine; and indole and methylindole for tryptophan (see Figure 6). As is evident from this far from extensive list, some fragments, e.g. pyrroles and phenylacetonitrile, must involve scission of the polymer chain. In fact, some of the aliphatic amino acid moieties also produce corresponding nitriles. Nevertheless, significant nitrile formation is not observed for tyrosine or tryptophan.

There seem to be two possible explanations for the limited amount of structural information obtained thus far from the Py-MS analysis of proteins. First, proteins are composed of a greater variety of building blocks than any other class of biopolymers. This in turn provides for a great variety of pyrolysis products, many of which possess the same nominal mass. Nominal resolution mass spectra obviously

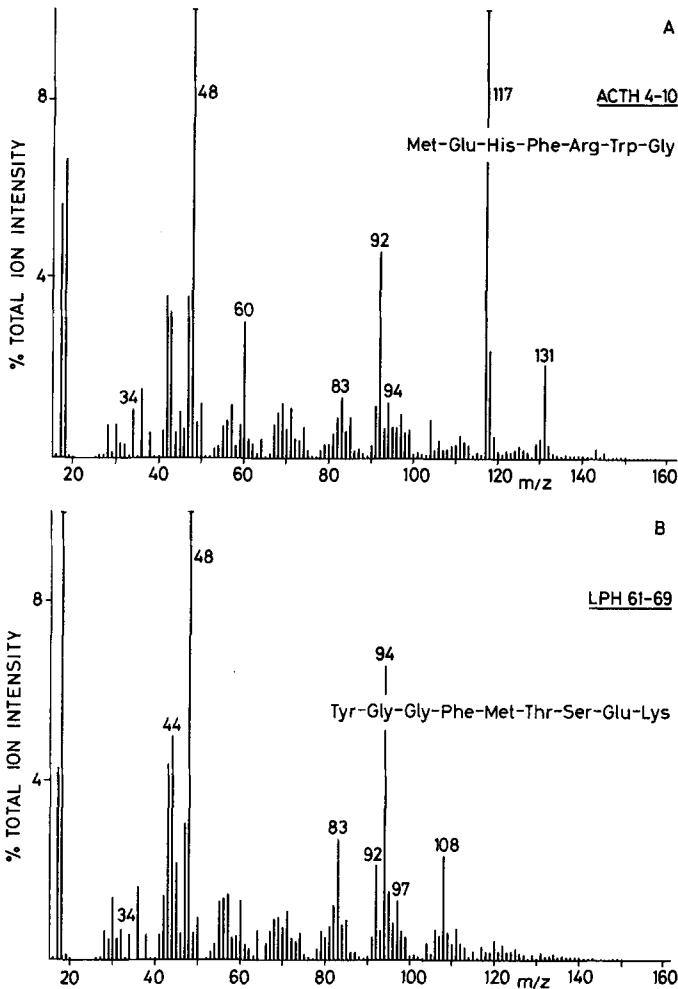


Figure 6. Curie-point pyrolysis mass spectra of synthetic oligopeptides representing sequences from adrenocorticotropin and p-lipotropin. Note characteristic ion signals of methionine (m/z 34, 48), phenylalanine (m/z 92, 104, 117), tyrosine (m/z 94, 108, 120, 122) and tryptophan (m/z 117, 131). Conditions: samples 10 μ g; T_c 510°C; E_e 14 eV.

provide very limited information on such an extremely complex pyrolysate. Secondly, there may well be a fundamental problem in the pyrolysis reaction mechanisms of proteins, namely a pronounced tendency for charring (ref. 95) involving the polymer backbone. This prevents the release of more or less complete amino acid moieties and instead results in the splitting off of appendages such as the phenol and indole fragments. As charring during pyrolysis appears to be inversely proportional to the rate of heating of the sample (ref. 23) - providing an important argument for

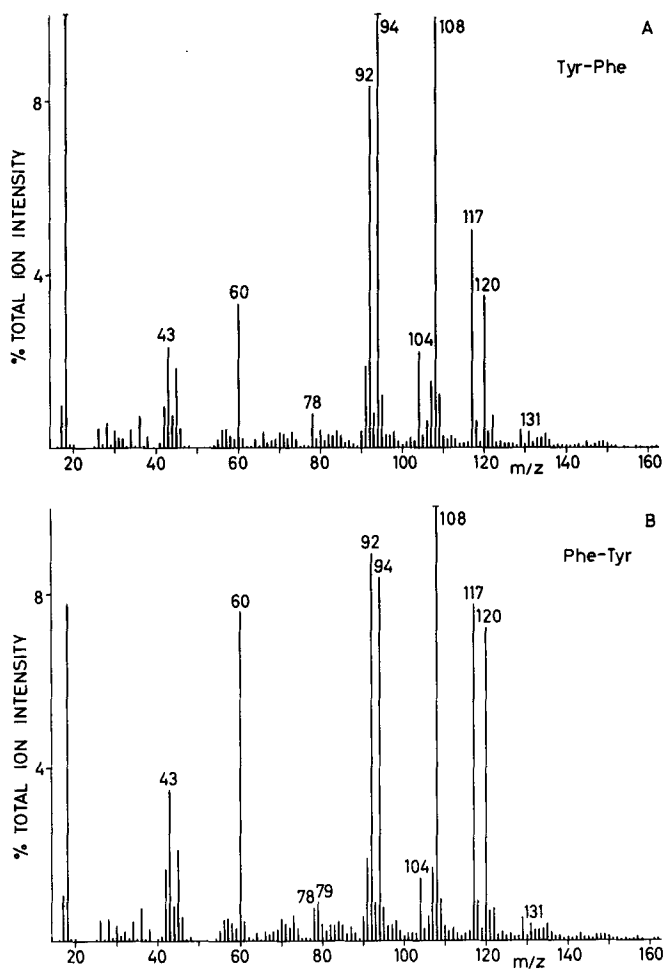


Figure 7. Curie-point pyrolysis mass spectra of two closely related dipeptides, differing only in the amino acid sequence. Note changes in relative intensities at m/z 79, 92, 94, 104, 108, 117 and 120. The difference in intensity at m/z 60 may be unrelated to structural features and probably represents acetic acid derived from the acetate counter-ion of the terminal amino group. Conditions: sample 10 μ g; T_c 510°C; E_{el} 14 eV.

preferring faster filament pyrolysis techniques over slow furnace pyrolysis techniques such as direct probe pyrolysis - fast laser pyrolysis might help to produce larger building blocks in protein pyrolysis. Preliminary experiments by Kistemaker *et al.* (ref. 29), however, failed to demonstrate these larger fragments.

In summing up the present situation, we have the distinct impression that, because of the limited success obtained and the availability of powerful alternative techniques, Py-MS techniques may not gain as much momentum in the chemical

characterisation of proteins as for some other biopolymers. However, it should be kept in mind that some important classes of proteins, such as glycoproteins, are less amenable to conventional techniques and may therefore constitute an important potential field of application. Also, Py-MS may prove to be of value in the rapid characterisation of protein preparations, when only a limited amount of chemical interpretation is desired (ref. 96). Alternatively, the sensitivity of Py-MS might perhaps allow its use in tandem with conventional protein characterisation techniques, e.g. for the analysis of electrophoretic bands or spots. Finally, Py-MS has proved to be of value in the characterisation of unusual oligopeptide structures such as those encountered in some antibiotics (ref. 61). An example of the Py-MS spectra of two closely related dipeptides is shown in Figure 7, demonstrating the sensitivity of the Curie-point Py-MS technique to minor structural details.

3.5. LIPIDS

Lipids constitute another important group of biomaterials which often have insufficient volatility to be analysed by direct chromatographic or mass spectrometric techniques. With the exception of the terpenes, which could be regarded as oligomers or polymers of isoprene, lipids usually do not possess the repeating subunits which are the hallmark of polymeric materials. Figure 8 shows the pyrolysis mass spectrum of natural rubber, a polyterpene (*cis*-1,4-polyisoprene). The dominant pyrolysis products appear to be the isoprene monomer at m/z 68 and the dimer at m/z 136. Most other prominent mass signals appear to be residual EI fragments in spite of the low electron energy conditions. The strong EI fragmentation tendency is explained by the aliphatic, branched hydrocarbon nature of the pyrolysis products. Natural rubber is perhaps one of the few biopolymers that show a more or less regular depolymerisation behaviour under pyrolysis conditions. In other biopolymers thermal degradation prevails over depolymerisation, as discussed in Section 3.1.

Curie-point Py-MS has had only limited success in the study of non-polymeric lipids because the rapid heating and short residence time of the products in the reaction zone results in the escape of intact or at most minimally fragmented lipid moieties, e.g. complete fatty acids, which are easily lost by condensation on the walls of the reaction chamber. Thus, lipid moieties tend to be strongly under-represented in the pyrolysis mass spectra of complex lipid-containing samples. By using heated reaction chamber walls and pyrolysing directly in front of the ion source, however, lipid molecules may provide intense signals, as shown by the work of Anhalt and Fenselau (ref. 18). Even then, the use of electron impact ionisation, especially at the 70 eV electron energy used by these authors, results in severe further fragmentation of the lipid products. In this respect, the use of chemical ionisation techniques for the analysis of lipid products from direct probe pyrolysis, as reported by Risby and Yergey (ref. 19, 20), may be regarded as an improvement. From the point of view of pyrolysis conditions, however, it would seem to be

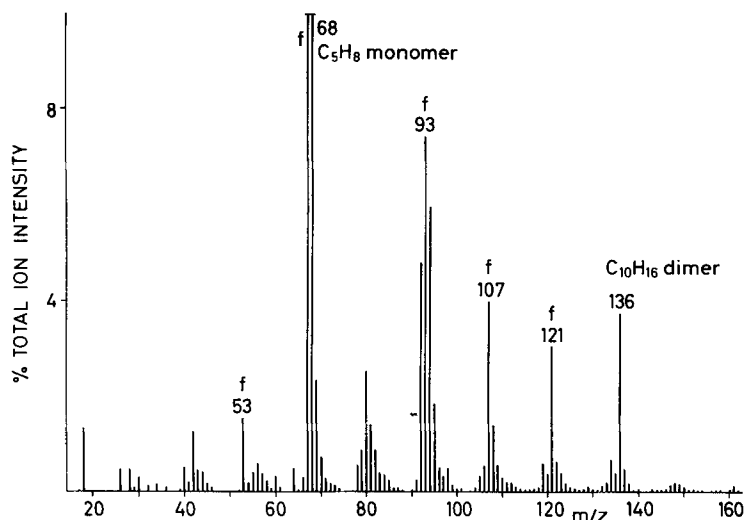


Figure 8. Curie-point pyrolysis mass spectrum of natural rubber (*cis*-1,4-polyisoprene). Note prominent ion signals at m/z 68 and 136, apparently representing the molecular ions of monomeric and dimeric units. (f) designates EI fragment ions. Conditions: sample 10 μg ; E_{e1} 14 eV (see Atlas).

preferable to use rapid filament pyrolysis rather than direct probe pyrolysis techniques, in order to avoid unnecessary secondary pyrolysis reactions resulting in the production of multiple unsaturated or even aromatic pyrolysis products.

Interesting results have also been obtained with phospholipids owing to the presence of highly characteristic moieties such as choline. Weijman (ref. 70) reported the occurrence of a characteristic ion series at m/z 59, 71 and 89, presumed to be trimethylamine, vinyl dimethylamine and *N,N*-dimethylaminoethanol, respectively (see Figure 9), in the pyrolysate of fungal phospholipids. The abovementioned identity of the m/z 59 fragment molecule in the pyrolysate of lecithin (phosphatidylcholine) was proved by Louter *et al.* (ref. 80) using Py-MS/MS. A curious phenomenon is regularly observed in the pyrolysis of phospholipid preparations, namely the methylation of chloride ions resulting in methylchloride (m/z 50, 52 in Figure 9), (see also Section 2.3.).

3.6. MISCELLANEOUS BIOPOLYMERS

An important biopolymer which lends itself extremely well to Py-MS analysis is lignin. Upon pyrolysis, whether rapid or slow, lignin degrades into its phenolic building blocks with relatively little formation of smaller pyrolysis products (see Figure 10). Depending upon the type of lignin analysed, various characteristic phenyl, methoxyphenyl (guaiacyl), and dimethoxyphenyl (syringyl) series are readily

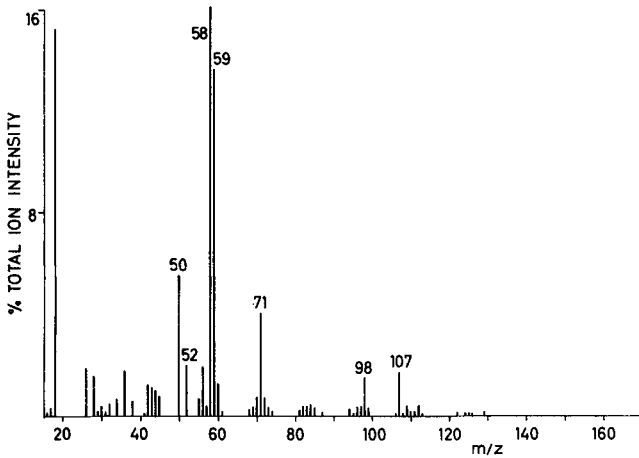


Figure 9. Pyrolysis mass spectrum of a fungal lipid fraction showing the characteristic ion series of choline-containing phospholipids namely at m/z 58 (C_3H_8N), 59 (trimethylamine), 71 (N,N -dimethylvinylamine) and 89 (N,N -dimethylaminoethanol; sometimes more pronounced, depending on the sample matrix). Note also typical methylchloride ion signals at m/z 50 and 52. The peaks at m/z 107 and 109 should probably be assigned to N,N -dimethylvinylammoniumchloride. As discussed in the text, the lipid part of the molecule is strongly under-represented in the spectrum. Conditions: sample 10 μ g; T_c 510°C; E_e 14 eV.

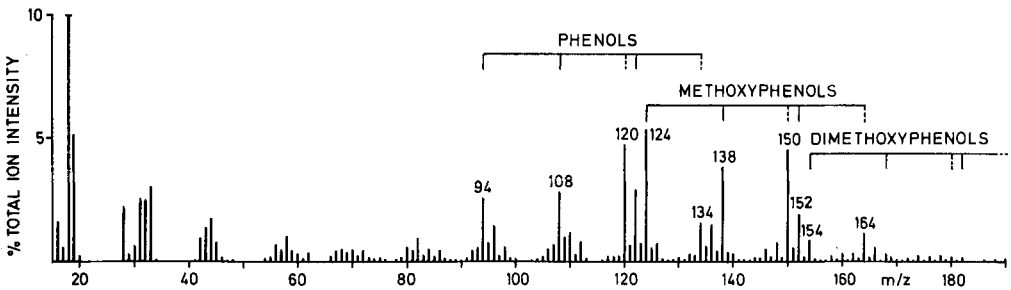


Figure 10. Pyrolysis mass spectrum of a Björkmann lignin, obtained from straw, showing the presence of all three characteristic lignin building blocks in grass lignins. Conditions: sample 10 μ g; T_c 610°C; E_e 15 eV.

distinguishable, as reported by Meuzelaar *et al.* (ref. 50). The chemical identities of the main pyrolysis products of lignin have been established by several authors, e.g. using Py-GC-MS techniques (refs. 52, 97).

Soil polymers, e.g. humic acids, as well as geopolymers, e.g. coals and kerogens although not strictly polymers in the sense of having well defined repeating subunits, are another class of macromolecular substances amenable to Py-MS analysis (ref. 52). The more random, highly complex configurations of these substances however, have so far eluded precise structural elucidation. With regard to coal structure, a recent report by the Committee of Chemical Sciences of the National Research Council, The Department of Energy, USA (ref. 98), notes that:

"It probably will not be possible in the foreseeable future actually to determine the "structure" of coal absolutely in the way we can with, say, organic compounds. Coal is heterogeneous by nature and it varies in structure no less from millimeter to millimeter in the same seam than between coals from different rank formed from different species of plant matter in swamps hundreds or thousands miles apart. The committee believes, however, that it is possible to determine in coals the key structural features that affect utility and reactivity".

As a result, understanding of pyrolysis mechanisms in these materials is highly speculative at most, and chemical interpretation of their pyrolysis-mass spectra is generally confined to the labelling of characteristic ion series as "alkenes", "benzenes", "naphthalenes", "phenols", "pyrroles", etc. (see Section 7.5). Nevertheless, this may provide useful insight into the degree of aromaticity or unsaturation, into the presence of heteroatomic compounds, e.g. sulphur compounds, and into reactivity, e.g. coal conversion behaviour (ref. 99). This information is often not available as easily from conventional techniques.

This Page Intentionally Left Blank

Chapter 4

THE TECHNIQUE OF CURIE-POINT PYROLYSIS MASS SPECTROMETRY

4.1. SAMPLE PREPARATION

In filament pyrolysis techniques, ideally the sample is coated on the filament by applying one or more drops of a solution followed by drying in air, in an inert gas or in a vacuum chamber. Although readily soluble samples may be found among both synthetic and natural polymers, more often than not the sample is insoluble in most chemically inert solvents. Generally, insoluble samples can be handled by mechanical grinding or milling to form a fine powder (with admixture of quartz sand to aid homogenisation), followed by ultrasonic suspension in a suitable solvent. Among the refractory samples which have been successfully processed in this manner are cells, tissues, whole soils, coals and shale rocks. Sampling and homogenisation of sticky or elastic materials, e.g. certain microorganisms and natural rubber, can be aided by grinding with cooling in liquid nitrogen. Some samples, e.g. bacterial colonies, sludges or urine, can be applied directly to the filament. Suitable solvents or suspending media are methanol, carbon disulphide and water. Carbon disulphide is most easily dried and produces relatively stable suspensions by virtue of its high specific density. However, it is toxic and stored samples tend to dry out rapidly. Water, although often the most natural choice for biomaterials, dries very slowly and therefore requires vacuum drying if time is an important factor. Methanol has been the preferred solvent or suspending medium in most of our recent studies.

Further important factors in sample preparation are the pH and ionic strength of the sample solution or suspension, as these factors may strongly influence the pyrolytic fragmentation of (especially polar) organic compounds. This is demonstrated in Figure 11, where pyrolysis mass spectra of polygalacturonic acid sampled from different suspension or solution media are compared. Such "matrix effects" may lead to artifacts on comparative analysis of samples by Py-MS. A suitable means of preventing such artifacts is to "standardise" solutions or suspensions throughout the series of samples to be compared by using buffered saline, e.g. aqueous PBS buffer (0.01 M phosphate, 0.145 M Cl^- , 0.17 M Na^+ ; pH 7.2). Even when disregarding any signals directly derived from residual solvent, a change of solvent, e.g. from methanol to water or carbon disulphide may appreciably influence the pyrolysis pattern (refs. 100, 101).

Careful attention should be paid to the cleanliness of the pyrolysis wire and of the glass or quartz reaction tube surrounding the filament. The use of ferromagnetic wires made of a fast rusting alloy and in particular pure iron wires ($T_c = 770^\circ\text{C}$),

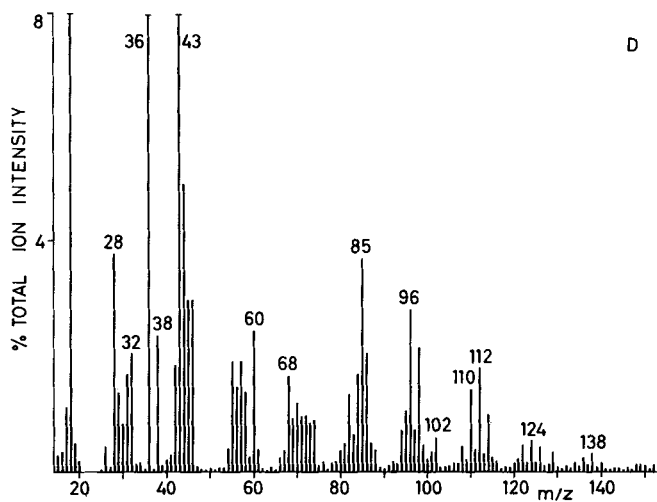
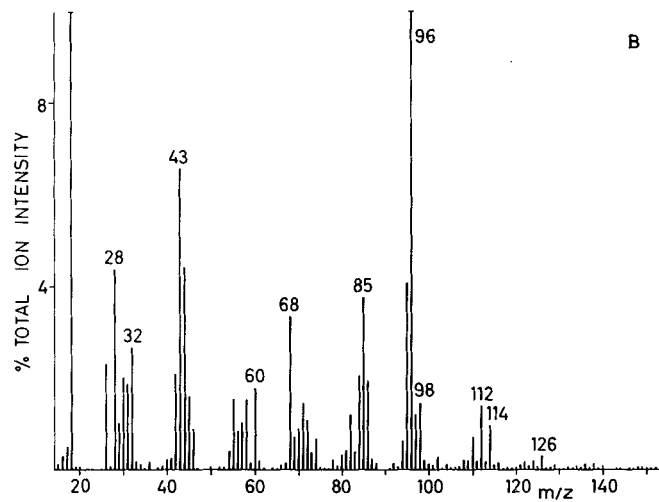
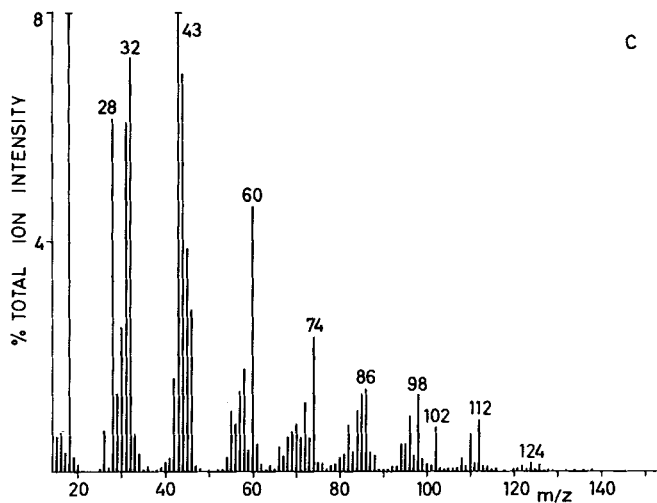
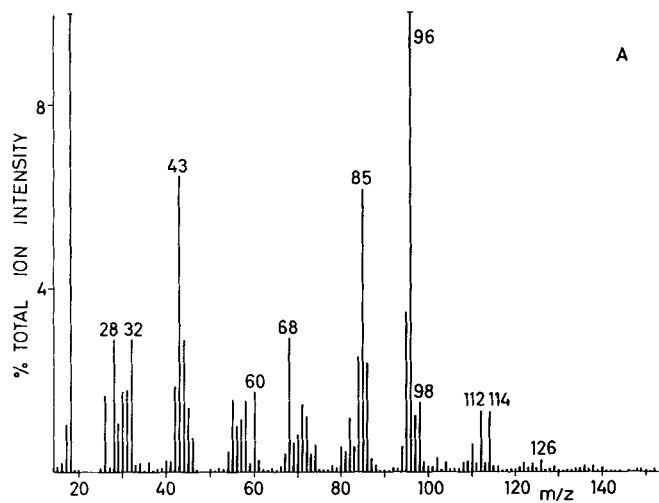


Figure 11. Pyrolysis mass spectra of polygalacturonic acid, using different sample solvents. (a) Suspension in methanol; (b) suspension/solution in water, pH 3.8; (c) solution in aqueous sodium hydroxide, pH 9.5; (d) solution in phosphate buffered saline (PBS), pH 6.5. Conditions: sample concentrations 1 mg/ml; samples 10 μ g; T_C 510°C; E_{e1} 14 eV. Note that the acidic aqueous and methanolic suspensions (a, b) give similar spectra. Use of the alkaline medium (c) results in marked intensity changes, e.g. at m/z 31, 32, 60, 68, 74, 85, 96, 102 and 114. The formation of furanoic components seems to be reduced under the influence of alkali. The neutral buffered solution gives an intermediate spectrum; the high concentration of chloride ions gives rise to the intense peaks at m/z 36 and 38 (HCl^+).

in combination with aqueous solutions or suspensions should be avoided. As Curie-point wires are very inexpensive, they may be discarded after use. Used glass or quartz reaction tubes, however, can be cleaned by boiling in acids (e.g. chromic acid), rinsing in de-ionised water and subsequent oven drying. The choice of the filament cleaning method, e.g. prolonged heating in a water-saturated hydrogen atmosphere, ultrasonic cleaning in organic solvents or pre-pyrolysing in a vacuum environment, also noticeably influences the pyrolysis pattern (refs. 100, 101). We most frequently use the reductive hydrogen cleaning technique because it removes oxide layers which may cause catalytic reactions and/or change the emissivity of the filament surface. However, it should be noted that reductive cleaning techniques can cause severe hydrogen absorption by the metal. This may influence the pyrolytic reactions, as demonstrated by Kutter *et al.* (ref. 102) using small ferromagnetic cylinders for the pyrolysis of nitro and azo compounds. Hydrogen can also be formed pyrolytically from residual solvents (methanol, water).

To apply the sample from a solution or suspension, a micropipette is used to deposit a 5-microlitre drop close to the tip of the ferromagnetic wire. Figure 12 shows a batch of 12 wires being coated while protruding from the glass reaction tubes and slowly rotating to ensure uniform distribution of the sample. If necessary, the whole assembly can be pumped off in a vacuum enclosure for fast drying. After drying, the wires are retracted to the proper position in the glass reaction tube, which also serves as a protective cover and even allows shipping of coated wires by mail (see Figure 13). An alternative coating technique may be used with slurries, sludges or pastes which are too thick for micropipetting. Such samples can be simply smeared on the wire using a platinum sample loop or by sticking the wire directly into the sample. With bacterial colonies, this technique, although providing less uniform sample coatings than the drop technique, has considerable advantages over sequential washing, freeze-drying and re-suspending procedures which may cause irreproducible changes in the chemical composition of the sample and loss of characteristic metabolites (ref. 103). Preferred amounts of sample in Curie-point Py-MS vary between 1 and 20 micrograms. Below 1 microgram, background signals may significantly contribute to the patterns. As reported by Meuzelaar (ref. 100) and Windig *et al.* (ref. 101) changing the amounts of sample from 2 to 20 micrograms causes minimal changes in the relative peak heights of the patterns of glycogen and

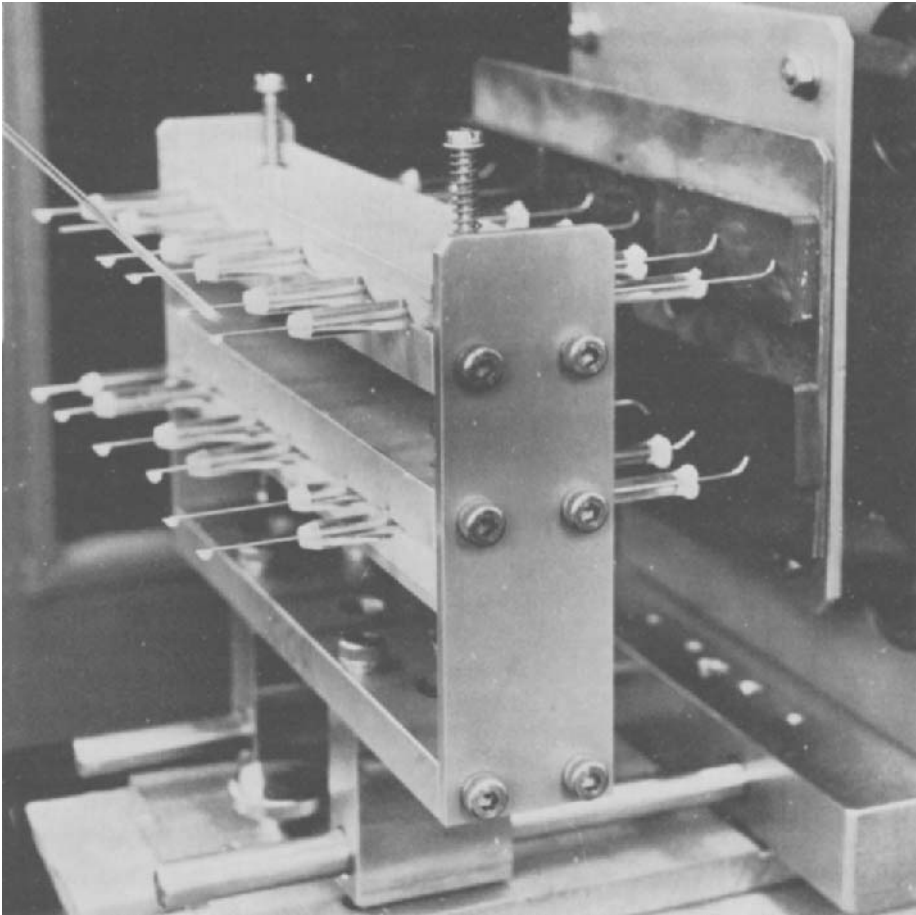


Figure 12. Apparatus for the batch coating and drying of Curie-point wires. Note that the wires are revolved by magnetic attraction to the base plate assembly (right) which makes a slow circular movement. All wires can be withdrawn simultaneously into the reaction tubes by sliding the manifold away from the base-plate.

albumin. Above 20 micrograms, however, the increase in overall peak height is no longer proportional to sample weight, indicating that parts of the material are blown off the wire before being pyrolysed. Occasionally, the use of amounts of samples up to 60 - 70 μg cannot be avoided, e.g. when pyrolysing whole soil samples containing less than 1% of organic material (ref. 51). In this case, however, sample blow-off is not as severe, as the inorganic part of the sample usually does not produce large amounts of gaseous pyrolysis products.

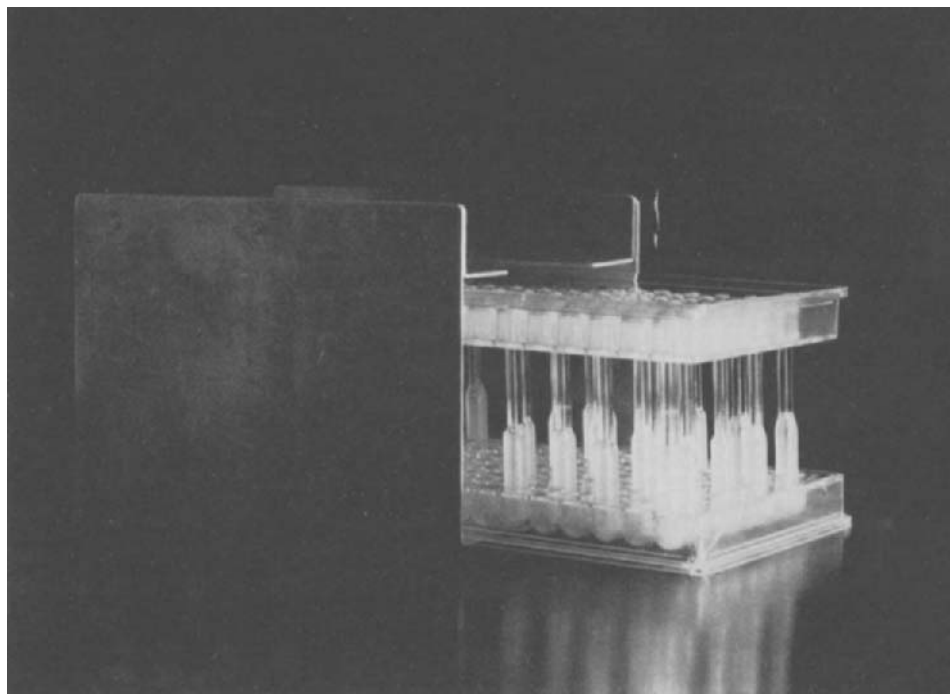


Figure 13. Coated Curie-point wires and reaction tubes in shipping container which can hold up to 96 tubes.

Typical concentrations of solutions or suspensions used for sample coating are 1 - 2 mg/ml. When applying 5 μ l drops, this amounts to 5 - 10 micrograms per drop. The normal repeatability of sample amounts applied to the filaments is approximately $\pm 10\%$ when using the drop technique and $\pm 50\%$ when using the smear technique.

4.2. PYROLYSIS

The Curie-point technique involves placing a thin ferromagnetic wire in an induction coil connected to a high frequency power supply (Figure 14). When the h.f. field is switched on, the ferromagnetic wire inductively heats to its Curie-point temperature, at which the wire loses its ferromagnetism and becomes paramagnetic. This causes a drastic loss in energy absorption from the h.f. field in the coil. Provided that the wire dimensions and h.f. field parameters are properly matched, the equilibrium temperature (T_{eq}) of the wire stabilizes close to the Curie-point temperature, at a point where the residual energy absorption by Eddy currents ("skin

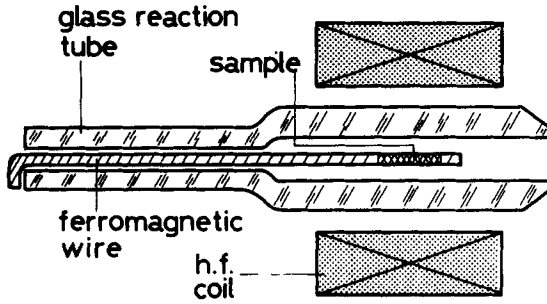


Figure 14. Schematic diagram of the Curie-point wire/reaction tube assembly located within the high frequency coil.

effect") is balanced by the loss of heat through radiation and conduction (ref. 104). Temperature/time profiles for wires of different ferromagnetic materials, when using a Fischer Labortechnik 1.5 kW, 1.1 MHz h.f. power supply, are shown in Figure 15. Intermediate curves can be obtained by using various alloys of these ferromagnetic materials. At 600°C, typical degradation reactions in polymers are completed in less than milliseconds (ref. 105). Therefore, even with temperature-rise times (t_T) in the millisecond range, pyrolysis will be complete at temperatures well below 600°C. As a consequence, it is not surprising that changing T_{eq} from 510 to 610°C does not drastically influence the pyrolysis patterns of biopolymers such as glycogen and albumin (refs. 100, 101). For the same reason, changing the total heating time (t_{Σ}) from 0.3 to 1.2 s also does not cause appreciable changes in these patterns (refs. 100, 101). However, a very low T_{eq} , e.g. below 400°C, may cause drastic changes in pyrolysis patterns. This is explained by the fact that at these

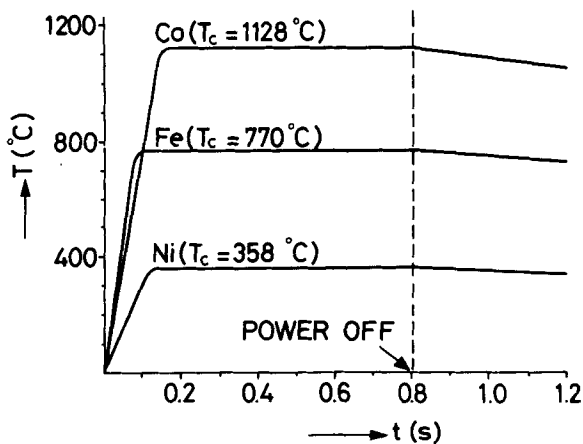


Figure 15. Temperature/time profiles and Curie-point temperatures for pure Ni, Fe, and Co wires (diameter 0.5 mm) when using a 1.5 kW, 1.1 Mhz h.f. power supply.

temperatures the half-life of a degradation reaction may become long compared with the temperature-rise time. In this situation, pyrolysis may be incomplete when T_{eq} is reached and thus changing t_{Σ} strongly influences the pyrolysis pattern. On the other hand, a high T_{eq} , e.g. above 700 or 800°C, may also cause changes in the pyrolysis patterns owing to the strong radiant heating of the reaction tube, and may lead to either evaporation or secondary pyrolysis of compounds condensed on the walls of the tube during the initial pyrolysis stages of the sample.

It should be noted that varying T_{eq} may be used to enhance or reduce the relative contribution of a particular component or moiety in the pyrolysis mass spectrum of a complex mixture or conjugate. For instance, because of the relative thermolability of carbohydrates in comparison with proteins, carbohydrate signals may be specifically enhanced in spectra of carbohydrate-protein mixtures or glycoproteins by selecting lower pyrolysis temperatures. This is shown in Figure 16 for an oligosaccharide-oligopeptide mixture. In the 358°C spectrum (a) the peptide contributes a characteristic series of fragments at m/z 48 (CH_3SH , from the Met-residues), 56 (C_4H_8 isomers, and acrolein), 94 (phenol, from Tyr), 108 (cresol, from Tyr) and 117 (indole, from Trp), whereas contributions of the Phe-residue (m/z 92, toluene, and 104, styrene) are relatively low. Most of the fragment peaks in the spectrum originate from the carbohydrate constituent. In the 610°C spectrum (b) the peptide sub-pattern (arrows) is much more pronounced with respect to the carbohydrate sub-pattern. Moreover, additional information about the peptide constituent is obtained by the increase in relative intensities at m/z 34 (H_2S , an additional fragment from the Met residues), 92, 104, 120 (hydroxystyrene, additional fragment from Tyr) and 131 (methylindole, from Trp). The relative intensities of high mass range carbohydrate fragments (m/z 112, 114, 124, 126, 144) have decreased.

The t_T is determined by the diameter of the wire, the composition of the alloy, the strength of the high frequency field and the field frequency (ref. 104). Since under practical Py-MS conditions pyrolysis takes place before the wire reaches T_{eq} , the heating rate is generally thought to have a critical influence on the pyrolysis patterns (ref. 105). Unexpectedly, however, varying the heating rate by a factor of 10 (changing t_T of a 510°C wire from 0.1s to 1.0s) does not appreciably change the Py-MS patterns of glycogen and albumin (refs. 100, 101). Therefore, the emphasis placed on accurate reproduction of the temperature/time profile in the pyrolysis gas chromatography literature (e.g. refs. 10, 11, 106, 107) does not seem to be as stringent under vacuum pyrolysis conditions, provided that T_{eq} is neither too low nor too high. Other factors, such as the choice of the filament cleaning technique and of the solvent, and factors that govern transfer of the pyrolysate to the ion source or influence ionisation conditions, appear to determine the reproducibility of Py-MS more strongly than the temperature/time profile, especially with respect to long-term reproducibility (refs. 100, 101).

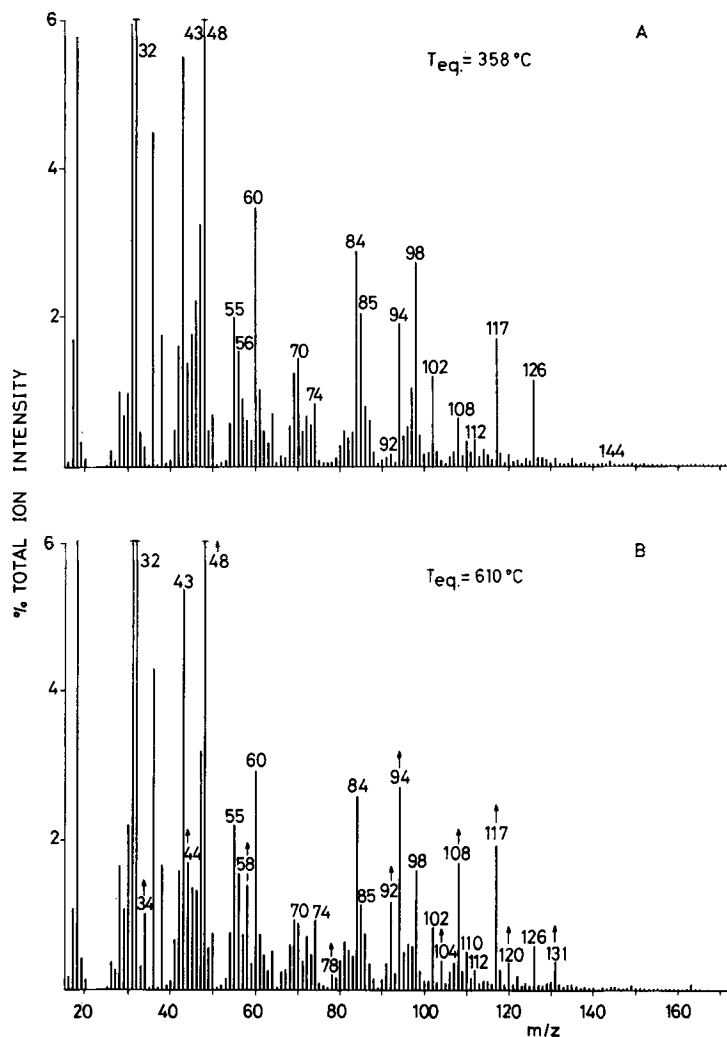


Figure 16. Pyrolysis mass spectra of an oligosaccharide-oligopeptide mixture (maltopentaose and Phe-Asp-Met-Trp-Gly-Met-Tyr, 1:1 w/w ratio) showing the differences in fragmentation behaviour of both molecular components when different equilibrium temperatures are used.

In contrast to the relatively mild influence of changes in temperature profile, substitution of a ferromagnetic tube ("oven" pyrolysis) for the ferromagnetic wire produces pronounced changes in the pyrolysis mass spectra of most compounds as shown in Figure 17. As can be seen, oven pyrolysis of carbohydrate and proteinaceous materials produces a range of products due to secondary pyrolysis reactions, e.g. unsaturated and aromatic hydrocarbons. Moreover, spectra of chemically related materials produced by oven pyrolysis tend to show fewer characteristic differences

than the corresponding filament spectra, whereas for obtaining reproducible oven-spectra smaller tolerances in pyrolysis and sample conditions exist. In conclusion, the use of ferromagnetic tubes is recommended only for relatively volatile samples which cannot be pyrolysed effectively by the filament technique, or in special cases where more rigorous thermal degradation is desired.

4.3. PYROLYSATE TRANSFER

In the previous steps, sample preparation and sample pyrolysis, the original sample was transformed into a multicomponent mixture of pyrolysis products (the pyrolysate). Reproducible mass spectrometric analysis of this multicomponent mixture requires careful control of several factors, including the transfer conditions between the pyrolysis zone and the ion source, the ionisation conditions and the subsequent mass analysis and ion detection conditions.

Ideal pyrolysate transfer conditions should allow the pyrolysis products to reach the ionisation zone without any loss, degradation or recombination of products during transfer; in practice these conditions are almost never fulfilled. First, some pyrolysis products tend to remain on the filament in the form of nonvolatile chars and thus are completely inaccessible to further analysis. Presently available evidence indicates that the amount of char formed is inversely proportional to the heating rate (ref. 23) and thus can be minimised by avoiding excessively slow heating rates. Some products volatile enough to escape from the pyrolysis zone may be difficult to transfer to the ionisation zone. These products may have a tendency to condense on the walls of the reaction chamber and/or subsequent transfer lines. Heating these walls to a high enough temperature to avoid condensation may result in further thermal degradation of the products. Obviously, the ideal solution would be to achieve a wall-less transfer of pyrolysis products, that is, by pyrolysing directly in front of the ion source, or by analysing only those molecules which reach the ionisation region without previous wall collisions. However, in practice it is difficult to avoid strong contamination of the ion source under these conditions. If the beam of pyrolysis products is sufficiently collimated to avoid wall contact in the ion source, then contamination may be minimised but the signal intensity will be strongly reduced. Therefore, the glass reaction tube shown in Figure 14 serves two purposes, namely to trap the relatively involatile pyrolysis products which might contaminate the ion source and to obtain maximum signal intensity by producing a forward oriented beam of volatile pyrolysis products which may directly enter the expansion chamber or the ion source.

The expansion chamber shown in Figure 18 serves to broaden the pressure/time profile in the ion source, in order to enable a sufficient number of mass scans to be made to obtain a representative averaged mass spectrum of the pyrolysate. The expansion chamber should have chemically inert walls, e.g. quartz or gold-coated, in order to avoid degradation of pyrolysis products. Moreover, these walls should be

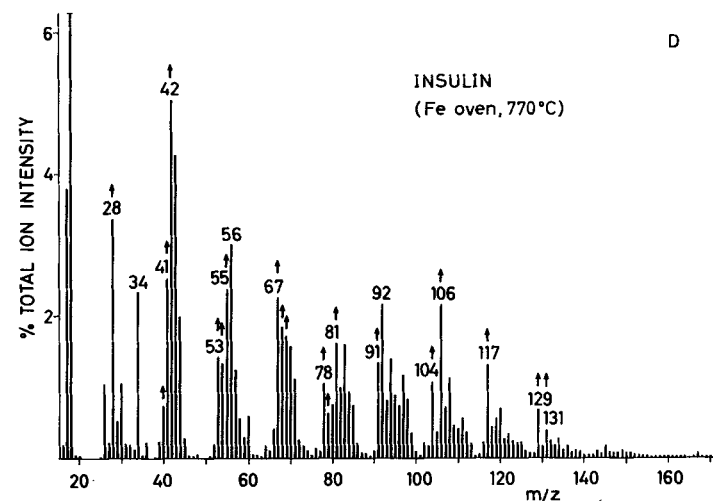
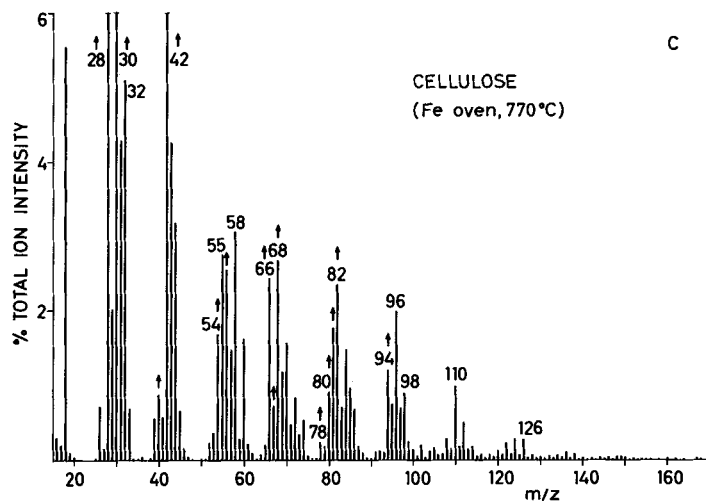
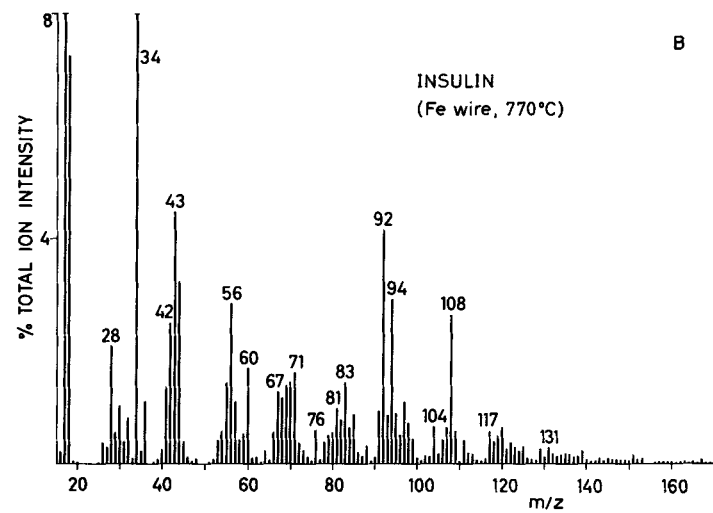
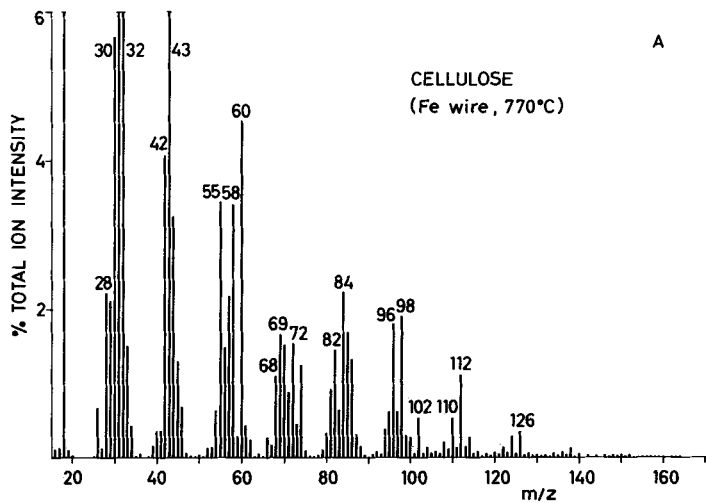
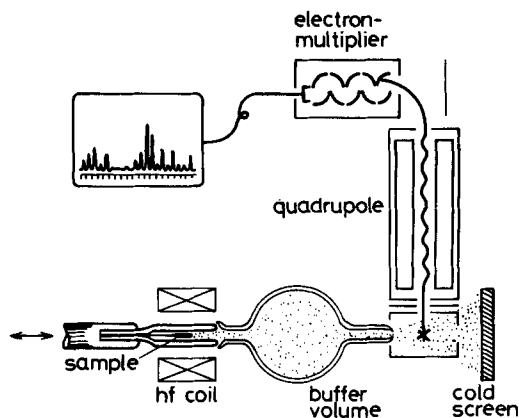


Figure 17. Comparison of pyrolysis mass spectra of biopolymers obtained by the filament technique (Fe wire, T_C 770°C; spectra a, b) and the oven technique (Fe tube, T_C 770°C; spectra c, d). The oven spectra are corrected for background, in the filament spectra background contributions are negligible. Note the considerable increase in relative peak intensities in the oven spectra (arrows) when compared to the corresponding filament spectra.



CURIE-POINT PYROLYSIS MS SYSTEM

Figure 18. Schematic diagram of a Curie-point Py-MS system. Typical operating conditions: buffer volume (expansion chamber) temperature 150-175°C; E_{e1} 13-15 eV; ion energy 5-10 eV; mass range m/z 15 to between m/z 130 and m/z 200; scanning speed 8-10 spectra/s; total scanning time 15-30 s.

heated to a temperature high enough to prevent condensation of pyrolysis products from leaving the reaction tube, yet low enough to avoid secondary pyrolysis reactions. A good compromise temperature range appears to be 150-200°C. The temperature should be kept fairly constant in order to avoid variations in ionisation fragmentation patterns due to different initial temperatures of the molecules entering the ionisation region (ref. 101, 108, 109). In the configuration shown in Figure 18, the walls of the reaction tube are heated by radiation from the pyrolysis filament only and are the coldest location in the transfer line. As a consequence, most pyrolysis products with low volatility and also large evaporated compounds, e.g. lipids, will condense on the wall of the reaction tube directly around the pyrolysis zone. Although the loss of such substances leads to a loss of valuable information, the advantage of this situation is that contamination of expansion chamber and ion source is minimal. In fact, a system such as that shown in Figure 18 can be used for over 1 year, analysing more than 1,000 samples, without cleaning the ion source (ref. 100, 101).

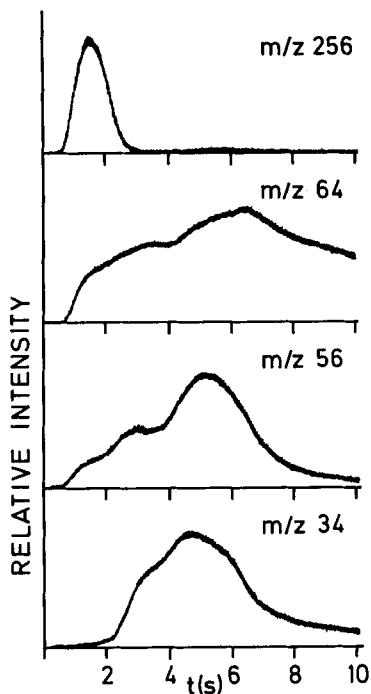


Figure 19. Selected ion profiles from time-resolved Py-MS analysis of an oil-shale kerogen sample. The profiles were obtained by removing the modular expansion chamber, prolonging t_T to approximately 6 s. The profiles at m/z 56, believed to represent mainly C₄-alkenes, shows at least four overlapping kinetic events. The ion profiles at m/z 34 (H_2S^{+}) and m/z 64 (SO_2^{+} and/or S_2^{+}) are even more complex. Especially the m/z 64 profile shows many overlapping events, the first of which appears to represent early distillation of elemental sulphur from the sample, thus producing an S_8^{+} molecular ion signal at m/z 256 as well as a suite of fragment ions, among which the S_2^{+} ion contributes to the ion profile at m/z 64. Conditions: Sample 10 μ g (from methanol suspension); T_C 610°C; t_T 6 s (estimated); t_S 10 s; E_{e1} 20 eV.

A newly designed version of the Py-MS inlet system (ref. 110) incorporates a modular design which allows easy removal of the expansion chamber, thus positioning the reaction tube directly in front of the ion source. In addition, the reaction tube is designed in such a way that the walls around the pyrolysis zone may be pre-heated to several hundred degrees without heating the sample, which is temporarily kept in a cool portion of the reaction tube. The potentially stronger contamination of the ion source can be controlled by operating the ion source at a slightly higher temperature than the reaction tube, e.g. at 200 and 175°C, respectively. The pressure/time profile of pyrolysis products entering the ion source can be broadened sufficiently by slowing the heating rate of the wire to 100°C/s. As demonstrated in Figure 19 this allows for efficient scanning of the pressure/time profile by the

quadrupole, but is still orders of magnitude faster than the heating rates of direct probe systems, thus minimizing excessive char formation. In principle, this configuration combines the advantages of Curie-point pyrolysis (batch processing, easy automation) and fast filament heating (minimal char formation, minimal secondary reactions) with those of direct probe techniques (minimal loss of low-volatility pyrolysis products, possibility of obtaining time-resolved pyrolysis profiles).

4.4. IONISATION

In selecting the ionisation technique, two criteria are considered essential. First, minimal ionisation fragmentation of pyrolysis products should occur with principally molecular ions being formed. Secondly, the ionisation process must be stable enough to provide a high degree of long-term reproducibility. While no ionisation technique is ideal in both respects, the advantages and disadvantages of the three major "soft" ionisation techniques, i.e. low voltage EI, CI and FI, will be briefly discussed.

Low voltage EI has been the principal technique used throughout the Curie-point Py-MS studies reported so far. Trial studies using compounds typical of pyrolysates indicate that electron energies between 13 and 15 eV appear to be a good compromise between minimum yield of fragment ions and maximum yield of molecular ions (ref. 46). Once the electron energy has been chosen, every effort should be made to keep this energy constant to within 0.1 eV. In reproducibility studies, a variation in electron energy from 13.9 to 14.1 eV resulted in a 3.4% and 4.0% mean relative deviation in the intensities of the 40 most intense peaks in the spectra of albumin and glycogen, respectively (refs. 100, 101). In spite of this sensitivity to minor changes in operating conditions, low voltage EI has the unique advantage of being able to ionise molecular beams efficiently. This allows for a very open design of the ion source and minimises memory effects. In contrast, both CI and FI involve considerable interaction of pyrolysis products with surfaces during the ionization procedure (FI only for polar products). Finally, low voltage EI is readily obtainable on most mass spectrometers whereas the CI and FI techniques may require elaborate equipment modification.

The CI technique is extremely efficient in generating (quasi-)molecular ions thereby allowing the detection of these ions even when the sample is present in very low concentrations (ref. 111). An additional feature of CI is the degree of selectivity as to which particular chemical moiety can be ionised, depending on the selection of the reagent ion (ref. 112). As an example of how this could be used in Py-MS studies, one might conceivably enhance the contribution of nitrogen-containing pyrolysis products, e.g. derived from proteins in the sample, by using a reagent ion with a high proton affinity, such as $C_4H_5^+$. However, several inherent features of CI ion source design potentially limit its usefulness in Py-MS studies. First, the

prolonged residence time in the tight ion source may cause drastic changes in the chemical composition of the pyrolysate. Secondly, unless the sample is pyrolysed slowly and the products are diluted with reagent gas, pyrolysis compounds formed in high concentrations (e.g. H_2O , NH_3) could modify the ionisation process by substituting for the original reagent gas (ref. 54). Thus the ionisation process may then be determined by sample-dependent factors. Although CI studies of multicomponent hydrocarbon mixtures have been reported (ref. 113), so far no long-term reproducibility studies on multicomponent mixtures containing highly polar compounds appear to have been carried out. Until such data become available the value of CI in quantitative Py-MS studies ("fingerprinting") cannot be established with certainty. As discussed on page 14, however, CI is potentially a very valuable ancillary technique for qualitative studies of the pyrolysate, using selective reagent gases.

In FI the ionisation process is dependent to some extent on the condition of the emitter surface, especially with polar compounds. This is shown by the frequent occurrence of protonated molecular ions, indicating the role of surface ionisation processes in FI of these compounds (ref. 114). Changes in the condition of the emitter surface may thus change the character and distribution of the ions produced from multicomponent mixtures containing relatively polar compounds. This problem does not exist with mixtures of apolar substances. In fact, FI has been shown to be superior to low voltage EI in the quantitative analysis of hydrocarbon mixtures (ref. 115). Except for some selected geopolymers and synthetic polymers, however, most complex organic materials will yield pyrolysates containing varying amounts of polar components. Therefore, FI is unlikely to become a routine ionisation technique in fingerprinting of biomaterials by Py-MS. However, FI can be a very valuable tool for determining the elemental composition of intact molecular ions in pyrolysates especially in combination with high-resolution mass spectrometry (refs. 53, 71, 116).

Although low-voltage EI may have the drawbacks of residual fragmentation and poor sensitivity in comparison with CI or FI, the inherent advantages of simplicity and ability to operate in a beam mode, thus reducing contamination, have made it the method of choice in most Curie-point Py-MS studies reported so far. Further, it is worth mentioning that the problem of residual fragmentation during low voltage EI is to some extent compensated for by the fact that pyrolysis products represent an unusual collection of relatively stable compounds which often produce stable molecular ions during low-voltage EI (ref. 100). Among the more common biomaterials, lipids are the only class of compounds which consistently produce low voltage EI Py-MS patterns strongly dominated by fragment ions.

4.5. MASS ANALYSIS

The choice of the mass spectrometer in Py-MS is dictated by the pyrolysis conditions, the analysis speed required, the mass range and resolution desired, the

preferred ionisation mode, the cost of the instrument and the need for computerisation. Fast heating rates generally demand either instruments with simultaneous ion detection capability, i.e. incorporating photoplate or channelplate detectors, or fast scanning instruments such as quadrupoles, time-of-flight spectrometers or voltage-scanned magnetic sector instruments. However, the requirements of high analysis speed and sample throughput may rule out the use of photoplate systems. Also, cost factors may weigh against the use of photoplate instruments. Mass range may become a problem with time-of-flight instruments, especially if coupled with the requirement of unit resolution at higher mass ranges. If ionisation techniques other than EI are required, e.g. FI or CI, only magnetic sector instruments and quadrupoles come into consideration. Finally, ease of computerisation provides a strong argument in favour of quadrupoles.

Most of the Curie-point Py-MS work reported has been performed with quadrupole instruments. The only real disadvantages of quadrupoles for Py-MS studies are the limited ion transmission at higher mass ranges and the inability to perform high resolution studies. If further major breakthroughs were to be made in the development of Fourier transform ion cyclotron resonance mass spectrometry for routine analytical applications (ref. 117), this technique might well become the preferred approach for Py-MS studies. Alternatively, the recent introduction of commercial magnetic sector instruments featuring fast voltage scanning over several mass decades (ref. 118) might also become an attractive alternative to quadrupole systems, especially if high-resolution versions of these magnetic sector instruments could be developed.

When using quadrupoles in a Curie-point Py-MS configuration, as shown in Figure 18, typical operating conditions are: electron energy 14 eV (open cross-beam ioniser), ion energy 5-10 eV, mass range m/z 16 (lowest organic molecular ion is CH_4) to m/z 200, scanning speed 8-10 spectra/s and total scanning time 10-30 s. Whereas the expansion chamber is heated to 150-200°C, the ion source is not specially heated and the mass spectrometer housing is usually at room temperature. The liquid nitrogen-cooled shroud around the ion source acts as a very efficient pump for organic molecules, which traps most pyrolysis products escaping ionisation. This prevents them from re-entering the ion source after multiple collisions with the poorly defined surfaces of the vacuum envelope or quadrupole head. Apart from being a very efficient pump, the liquid nitrogen-cooled screen is also a pump with a highly constant performance, mainly defined by elementary parameters such as temperature and surface area. The constant pumping characteristics of the cold screen are an important factor in the achievement of long-term reproducibility in the analysis of multicomponent samples. The other solution to this problem, diffusion-limited pumping (ref. 119), does not achieve the same pumping efficiency as the cold screen by far. To prevent the accumulation of excessive amounts of trapped products, the screen is not permanently cooled but is allowed to heat up to room temperature at the end of each day. The molecules released during the heating up period are then pumped off by the main vacuum pump of

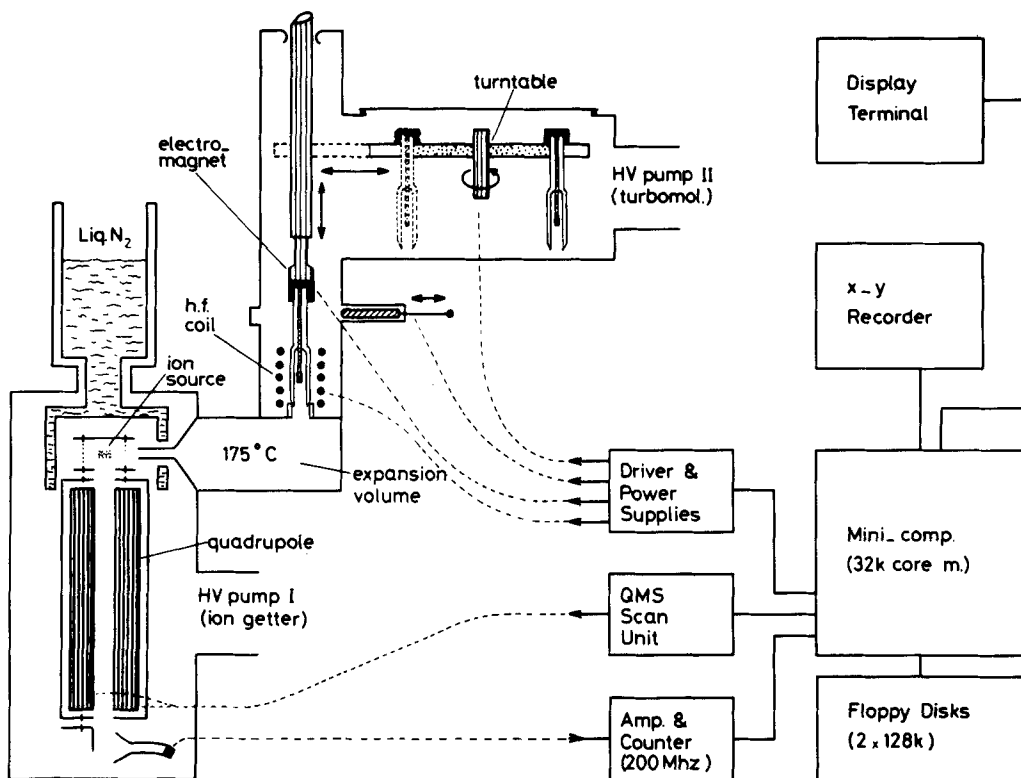


Figure 20. Schematic diagram of an automated Curie-point Py-MS system. For a detailed description, see reference 43. Note the 36-position turntable; the liquid nitrogen-cooled screen completely surrounding the ion source and the high-speed ion counting channel. Typical time needed to analyse one batch of 36 samples is 1 hour.

the system, which may either be a diffusion pump or a turbomolecular pump. Finally, the cold screen, by virtue of its high pumping speed (approximately 10 l/s.cm^2) provides for extremely low organic background signals and fast recovery of the system after each analysis.

Figure 20 shows a completely automated Curie-point Py-MS system. This automated system was built at the F.O.M. Institute for Atomic and Molecular Physics in Amsterdam (ref. 43) and has been in operation since 1976. Manual versions based on the principles shown in Figure 18 or following a somewhat different approach are commercially available (ref. 120). Removal of the expansion chamber and pre-heating of the reaction tube walls requires mass ranges up to m/z 800 or higher if full use is to be made of the information available from large evaporated or pyrolysed molecular species, e.g. lipids. The increased scanning time per spectrum caused by this large mass range has to be compensated for by slower heating rates of the sample or longer residence times of the pyrolysate in the expansion chamber, if used.

4.6. ION DETECTION

In principle, ion counting has considerable advantages over analogue ion current monitoring. The large bandwidth of pulse amplifiers used in ion counting systems allows the recording of extremely small signals at maximum scanning speed of the quadrupole mass spectrometer. Current amplifiers, in contrast, have lower bandwidths at high amplifications, thus limiting the scanning speed or spoiling peak resolution. Moreover, the use of pulse amplifiers greatly facilitates the automation of Py-MS systems since samples producing unexpectedly small or large signals do not require a change in amplification setting by the operator. Further advantages of pulse counting systems are the direct insight into the signal sampling statistics for each peak, the lack of immediate signal reduction with decreases in multiplier gain (provided that the gain remains above a certain minimum level), and the absence of signal fluctuations caused by mechanical vibrations in multi-stage dynode multipliers (e.g. caused by mechanical pumps). A serious disadvantage of ion counting, however, is the limited counting rate of commercially available systems. Typical maximum counting rates are of the order of 10^6 ions/s. Assuming a scan rate of 10^3 amu/s, the maximum number of ions accurately counted for any given mass will be less than 10^3 /s. In the Py-MS configurations shown in Figures 18 and 20, the pressure rise in the ion source after each pyrolysis lasts for about 5-10 s. Thus the total maximum number of ions measured per peak is well below $5 \cdot 10^3$. Since at least 10^2 ions are required for a reasonably well defined (10% level) peak amplitude measurement, the useful dynamic range (ratio between smallest and largest accurately measured peak in a spectrum) is less than 50:1.

For this reason, Meuzelaar *et al.* used a specially built high-speed ion counting system, capable of counting up to $2 \cdot 10^7$ ions/s (ref. 43), thus obtaining a 20-fold improvement in the useful dynamic range. Construction of the high-speed ion counting system required special precautions to be taken against interference from outside noise signals, e.g. triaxial feedthrough and cable connections from multiplier to amplifier. The multiplier used was a Bendix 4700 channeltron multiplier. When using amounts of sample below 20 μ g and ionizing at 14 eV, only a relatively small number of mass signals encountered in biomaterials exceeded the maximum count rate in this system.

4.7. SIGNAL RECORDING

Recording of pyrolysis mass spectra obtained by quadrupole instruments can be done either by a signal averager or by computer. Signal averagers are often suitable for interfacing with quadrupole mass spectrometers (ref. 44). Most signal averagers will supply a voltage ramp output which can be used to direct the mass scan of the quadrupole. Alternatively, the quadrupole may use its internal scan and the signal averager may follow the quadrupole scan in a trigger mode. Some signal averagers are even equipped with pulse count inputs allowing direct recording of signals

generated by ion counting equipment. However, as with commercially available ion-counting equipment, the maximum count rate of pulse inputs on signal averagers generally does not exceed $2 - 3 \cdot 10^6$ pulses/s. The advantages of spectrum recording by signal averagers are simplicity of operation, ease of data inspection and high scan speed. Disadvantages, in comparison with signal recording by computer, are limited memory size, unsuitability for further data processing and inability to perform more complex scanning routines, e.g. jumping to selected peaks. The limited memory size will generally preclude the recording of time-resolved pyrolysis patterns. To allow further data processing, on- or off-line transfer of spectral data to a suitable computer system will be necessary.

Various computerized quadrupole systems are now commercially available. However, when selecting a computerized system for Py-MS applications, attention has to be paid to some special requirements not fulfilled by every system. In fact, none of the presently available mass spectrometer/computer systems is ideally suited for Py-MS applications. First, the computer should be readily programmable to perform signal averaging tasks for the purpose of obtaining a single integrated mass spectrum, especially if the available memory size does not permit sequential storage of all spectra for later summation. Secondly, if time-resolved pyrolysis patterns are to be recorded, the memory size of the computer should be large enough to accommodate sequentially recorded spectra or, alternatively, fast dumping of recorded spectra to disk should be possible during the measurements. Thirdly, the computer/mass spectrometer interface should be capable of handling ion counting signals instead of analogue signals. At present, this capability is available on one of the commercial Py-MS systems (ref. 120a) but only for count rates up to $2 \cdot 10^6$ ions/second. Finally, the computer system should be evaluated with regard to its capability for numerical evaluation of the pyrolysis mass spectra. None of the commercially available mass spectrometer/computer systems provides software packages for multivariate statistical analysis such as described in Chapter 6. Therefore, the user either has to develop his own software by translating available software packages from larger computer systems, or may simply want to make an on- or off-line connection to a large system. A minimum "minicomputer" configuration suitable for developing multivariate statistical analysis programs will probably have at least 64K core memory, a floating point processor, two disks (or one disk and one magnetic tape), a printer and a graphic display terminal with hard copy unit or X/Y plotter.

Chapter 5

REPRODUCIBILITY IN CURIE-POINT PYROLYSIS MASS SPECTROMETRY

5.1. QUALITATIVE REPRODUCIBILITY

A high degree of qualitative reproducibility, that is the continuous presence of the same features in analysis patterns obtained from the same sample, is a prime requirement for any fingerprinting technique (ref. 107). In our experience, Curie-point Py-MS techniques show excellent qualitative reproducibility for all kinds of complex biomaterials analysed so far. Similar conclusions were drawn by Hickman and Jane from a comparative study of three different Py-MS techniques in the analysis of various polymeric materials (ref. 121). Considering the large number of different, possibly even competing, pyrolysis reactions that occur in highly complex biomaterials, the stability of the pyrolysis patterns of such materials, as also observed in Py-GC (ref. 122), is an intriguing phenomenon. In fact, many deliberate changes in pyrolysis conditions, e.g. a 15-fold increase (from 0.1 -1.5 s) in t_T (refs. 100, 101), fail to change the qualitative composition of the pyrolysate, provided that the occurrence of secondary reactions is minimized and T_{eq} is high enough to ensure complete pyrolysis within t_T . Marked qualitative changes in pyrograms, e.g. due to formation of recombination products, may occur, however, when samples become excessively large, or when pyrolysis is carried out inside a capillary tube rather than on the surface of a filament. Drastic changes in pyrograms can also be expected to occur if the selected T_{eq} is so low that the half-lives of degradation reactions become longer than t_T , allowing isothermal pyrolysis processes to take place at, or close to, T_{eq} of the filament. Windig *et al.* (ref. 109), who applied factor analysis (see Section 6.6.2) to the qualitative evaluation of the influence of changes in a number of pyrolytic and mass spectrometric conditions, demonstrated that an increase in T_{eq} (358 - 770°C) for polysaccharide materials results in a stronger degradation of the compounds to small, less characteristic fragment molecules, whereas the effect for a typical protein is completely different, viz. the formation of more strongly dehydrogenated pyrolysis products. Since qualitative changes in the pyrolysates are brought about only by such gross, deliberate changes in pyrolysis conditions, such changes hardly ever pose a significant problem under controlled analytical conditions.

A problem with regard to qualitative reproducibility may be encountered when a high instrument background is present due to insufficient trapping efficiency of the liquid nitrogen-cooled screen or unusually heavy contamination of the expansion

chamber or ion source. However, Curie-point Py-MS systems such as that shown in Figure 20 are specifically designed to eliminate such problems as rigorously as possible. Naturally, even a low instrumental background may strongly influence the pyrolysis patterns if the amount of sample pyrolysed is too low to provide an adequate signal-to-background ratio. For the type of instrument shown in Figures 18 and 20, the minimum sample size for obtaining satisfactory signal-to-background ratios is approximately 1 microgram for substances yielding complex pyrolysates, e.g. biopolymers (see Figure 21), as compared with 10 ng or less for compounds which yield a single dominant component, e.g. polystyrene (see Figure 1). Some types of sample tend to give low signal yields, especially samples containing relatively large amounts of inorganic constituents, e.g. whole soil samples, compounds forming large

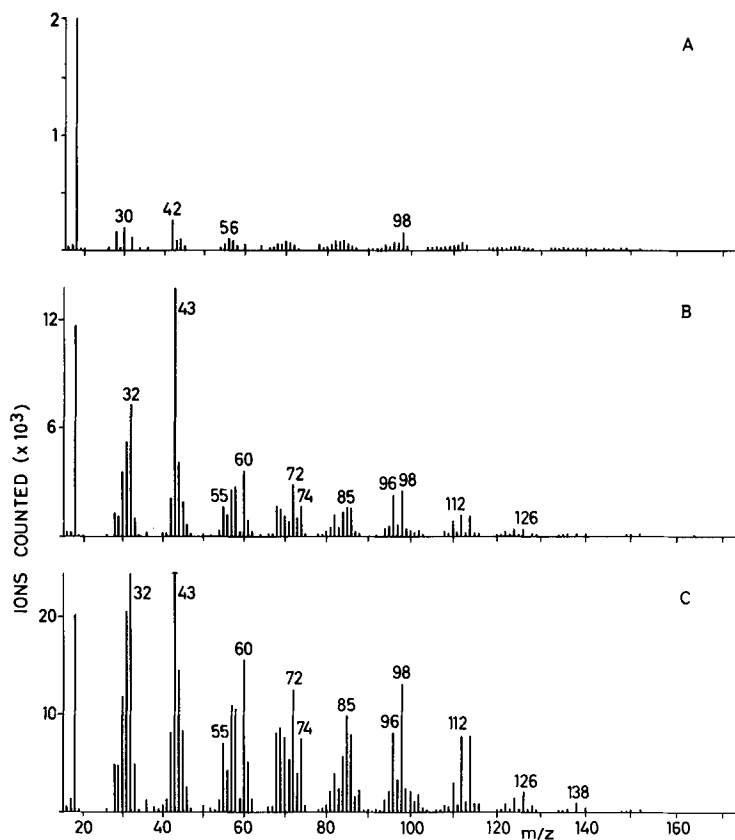


Figure 21. Pyrolysis mass spectra of (a) background produced by heating a clean wire (b) and (c) 1 and 5 μg , respectively, of a galacto-gluco-glucurono-araban. Note that the spectrum of the 1 μg sample still shows an overall signal-to-background ratio of better than 10:1. Further note that the intensity of the 5 μg spectrum is only about 4 times that of the 1 μg spectrum, indicating possible inaccuracy of actual sample size.

amounts of char, e.g. condensed polynuclear structures such as are found in high rank coals, or compounds evaporating intact and condensing on the relatively cold reaction tube wall, such as cholesterol and other relatively volatile compounds. With such samples, low signal-to-background ratios may be obtained in spite of a seemingly adequate sample size.

5.2. QUANTITATIVE REPRODUCIBILITY

Most pyrolysis mass spectrometry applications also require a definite degree of quantitative reproducibility, that is the continuous presence of features with similar relative intensities in analysis patterns obtained from the same sample. Obviously, short-term quantitative reproducibility, better termed "repeatability", is much more readily achieved than long-term quantitative reproducibility. Typical figures for short-term (less than 1 day) and long-term (more than 1 month) reproducibility as determined in Curie-point Py-MS studies on selected biopolymers (ref. 100) are in the 1-3% and 8-11% ranges (average difference observed in the relative intensities of the 40 most intense peaks), respectively. Figure 22 shows the level of long-term reproducibility observed for glycogen. The above-mentioned levels of quantitative reproducibility can be achieved only after some basic considerations regarding ion signal statistics and dynamic range of the amplifier are carefully observed. For example, an average reproducibility level of $\pm 5\%$ cannot be obtained if the average peak signal in the mass spectra is produced by less than 400 ions (for 400 detected ions the uncertainty in the signal magnitude measured is roughly $\pm 400^{1/2} = \pm 20$, or $\pm 5\%$). On the other hand, if the signals become too large, both pulse and analogue amplifiers may suffer signal loss, leading to a non-linear response. This may adversely affect the quantitative reproducibility, especially if the sample sizes vary considerably between duplicate analyses. For a more comprehensive discussion of dynamic range problems in pulse amplifiers, the reader is referred to Section 4.6.

In view of the inherent variability of many samples of biological origin, a 5 - 10% level of instrument irreproducibility is satisfactory for most Py-MS applications. Further, some applications do not require a high degree of long-term reproducibility since reference samples are co-analysed with the unknown samples, as discussed in Section 2.1 ("operational fingerprinting"). Typical examples of operational fingerprinting, where the need for library spectra is obviated, are provided by studies on the subspecies identification of mycobacteria reported by Wieten *et al.* (refs. 123 - 125), as well as by the analyses of tissue and body fluid samples described in Chapters 6 and 7, respectively. However, even if not required in some applications, a high level of long-term quantitative reproducibility is an indispensable ingredient for achieving any degree of inter-laboratory reproducibility.

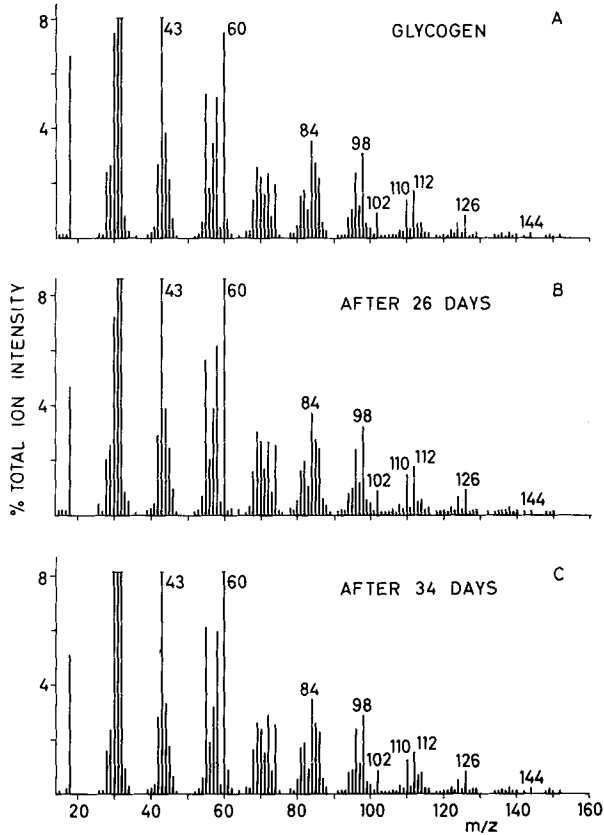


Figure 22. Long-term reproducibility of glycogen pyrolysis mass spectra. Conditions: sample 5 μg ; T_C 610°C; t_T 0.1 s; t_S 0.9 s; inlet temperature 150°C; E_{e1} 14 eV. (a) Glycogen, suspended in methanol; (b) the same suspension, analysed after 26 days of storage at -20°C; (c) fresh suspension of glycogen prepared from the same batch, analysed 34 days after the analysis of (a).

5.3. FACTORS INFLUENCING LONG-TERM REPRODUCIBILITY

Factors influencing long-term reproducibility in Curie-point Py-MS have been studied in detail by Meuzelaar (ref. 100) and Windig *et al.* (ref. 101). Table 2 lists possible factors influencing various steps of the analytical procedure in Py-MS. A detailed examination of factors involved in sample preparation and pyrolysis steps showed that some deliberate changes in experimental conditions caused changes in average peak height (40 most intense peaks) of over 20%, as listed in Table 3. In practice, however, the experimental parameters involved are controlled much more closely. Therefore, the estimated combined contribution of these factors to long-term variations observed in the spectra is less than 3 - 4%. This leads to the conclusion that the major causes of imperfect long-term reproducibility must be sought in factors influencing sample transfer and/or mass spectrometric analysis rather than in factors influencing sample preparation and pyrolysis.

TABLE 2

Factors possibly influencing long-term reproducibility

Sample Preparation	Filament Heating	Product Transfer	Mass Analysis
cleaning of sample carrier	temperature rise time	inlet temperature	ionisation
solvent/suspending liquid	equilibrium temperature	residence time	extraction
sample size	total heating time	surface activity	transmission

TABLE 3

Influence of sample preparation and pyrolysis parameters on pyrogram variability of bovine serum albumin and glycogen

Parameter Varied	Average difference in 40 most intense peaks (%)	
	Albumin	Glycogen
a. Wire cleaning method (3 techniques)*	6.0 - 17.4	14.8 - 22.7
b. Suspending liquid (H ₂ O, MeOH, CS ₂)	7.7 - 15.4	12.0 - 22.9
c. Sample size (5, 10, 20 µg)	5.7 - 8.6	5.2 - 12.8
d. Temperature rise time (0.1, 0.5, 1.0 s)	7.1 - 9.1	5.2 - 10.3
e. Equilibrium temperature (510, 610°C)	12.0	14.9
f. Total heating time (0.3, 0.6, 1.2 s)	3.2 - 4.5	3.2 - 6.5
Estimated contribution of a - f to long-term variability	2 - 3	2 - 4
Actual short-term variability (< 1 day)	0.9 - 2.4	1.0 - 2.9
Actual long-term variability (34 days)	9.9 - 11.0	8.3 - 9.7

* Cleaning techniques used: inductive heating, solvent cleaning, and heating in a reducing Bunsen burner flame (refs. 100, 101).

Electron energy in particular proved to be a highly critical parameter. Changing the electron energy settings from 14.0 to 14.1 eV caused more than a 10% difference in average relative peak intensities. Since actual electron impact energies are not readily defined to within a few tenths of an electron volt and changes of that magnitude might easily be caused by contamination of the ion source or by electronic instabilities during pyrolysis, fluctuation in electron energy may be a major factor limiting long-term reproducibility. Other possible troublesome factors are adsorption phenomena on the walls of reaction tube and expansion chamber, as well as changes in ion energies and mass resolution by contamination of ion source and quadrupole rods. Controlled heating of the ion source could reduce these problems. In view of all these possible or actual sources of variation, the degree of inter-laboratory reproducibility achieved with instruments showing considerable differences in ion-source and quadrupole design is remarkable, as will be discussed in the following paragraphs.

5.4. PROSPECTS FOR INTER-LABORATORY REPRODUCIBILITY

As yet, no systematic study has been undertaken to determine the level of inter-laboratory reproducibility obtainable with Curie-point Py-MS. Preliminary data, however, suggest that the prospects for inter-laboratory reproducibility between instruments of the same basic design as shown in Figure 18 are promising. Figures 23 and 24 show spectra of Douglas fir wood and urban particulate (NBS, SRM 1648), respectively, obtained on different Py-MS instruments in two different laboratories. In spite of a similar basic design, the two instruments, a fully automated system built at the F.O.M. Institute for Atomic and Molecular Physics in Amsterdam (see Figure 20) around a Riber QM17 mass filter, and a Py-MS system at the Biomaterials Profiling Center, University of Utah, Salt Lake City, built by Extranuclear Labs. Inc. (Pittsburgh) around a Spectrel 275 quadrupole mass filter, were significantly different with regard to the dimensions of the expansion chamber, ion source and mass filter. Also there were notable differences in the operating conditions of the pyrolyser, ion source and quadrupole mass filter. Moreover, the Douglas fir samples were obtained from different batches. Hence, in many ways the spectra in Figures 23 and 24 present "worst case" examples of inter-instrumental and inter-laboratory reproducibility and the presence of some obvious differences in these spectra is therefore not surprising. Careful examination, however, reveals the most severe differences to be attributable to different ion transmission efficiencies in the low and high mass ranges of the spectra. Note especially the high transmissivity in the high mass range shown by the Extranuclear Labs. system, which employs a quadrupole rod system of larger dimensions than the F.O.M. system.

It should be pointed out that optimal correspondence between spectra obtained on different quadrupole systems can be achieved only by trial and error, since instrument settings such as "electron energy" and "ion energy" provide only a rough

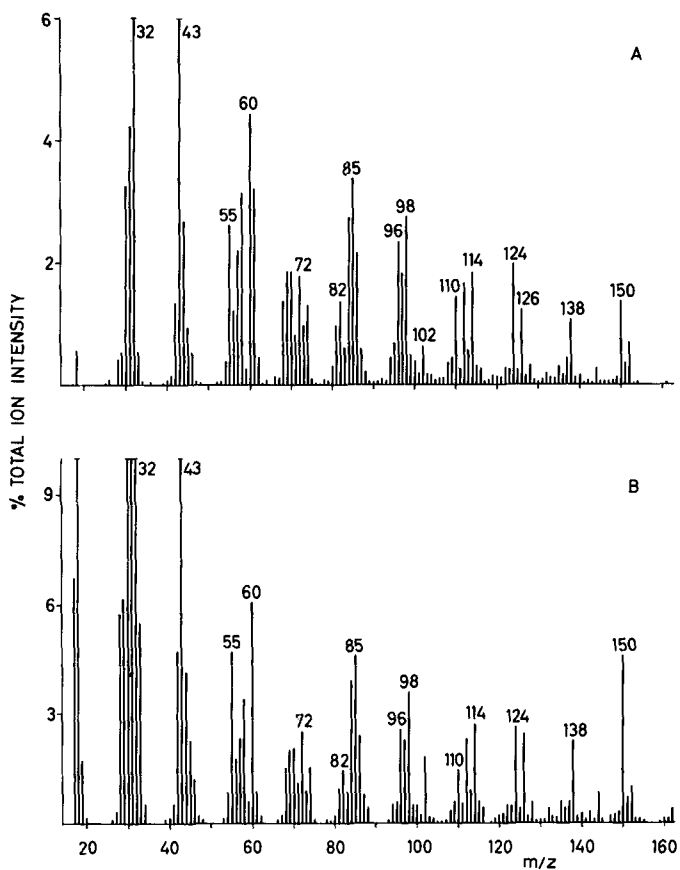


Figure 23. Comparison of pyrolysis mass spectra of Douglas fir wood obtained on different instruments: (a) Automated Py-MS apparatus; F.O.M. Institute, Amsterdam; (b) Extranuclear Labs. Py-MS instrument, Biomaterials Profiling Center, University of Utah. Difference in peak intensities in the low mass range of the spectra probably represent residual solvents (water, methanol) and/or different ion transmissivities of the quadrupole filters. Conditions: sample 10 μ g; T_C 510°C; E_{e1} (a) 14 eV and (b) 11 eV.

indication of the actual electron and ion energies involved. The spectra in Figures 23 and 24 were obtained with minimal effort to obtain optimum correspondence between the systems and thus do not represent the ultimate degree of inter-laboratory reproducibility obtainable.

Since differences in relative ion transmission are a widely recognized problem in quadrupole instruments, magnetic instruments would appear to offer considerable advantages with regard to inter-laboratory reproducibility in Py-MS. Inherent disadvantages, however, such as slower scanning rates, lower sensitivity in low and medium mass ranges and higher vulnerability to ion source contamination problems,

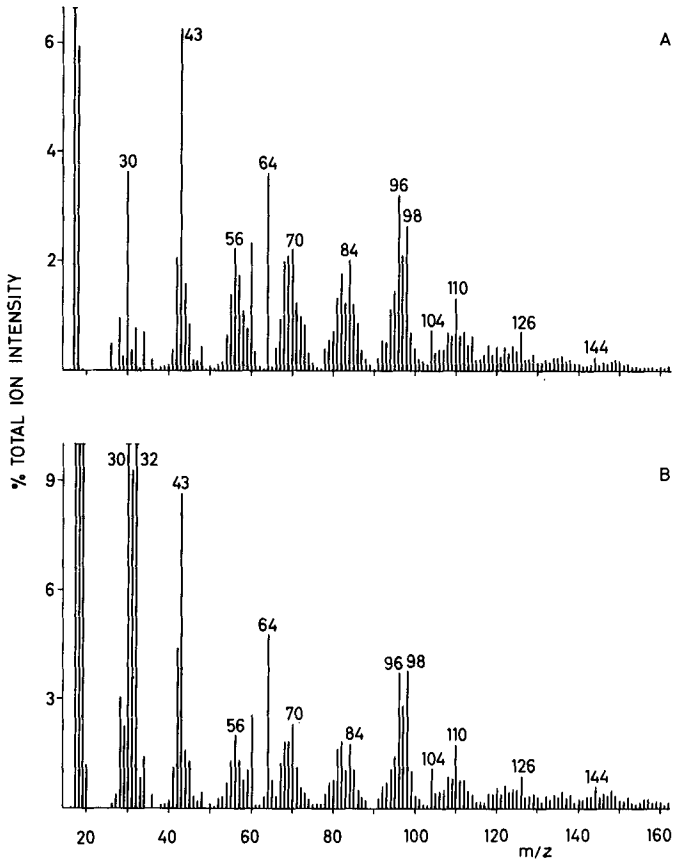


Figure 24. Comparison of pyrolysis mass spectra of urban particulate (NBS, SRM 1648) obtained on different instrument. (a) Automated Py-MS apparatus, F.O.M. Institute, Amsterdam; (b) Extranuclear Labs, Py-MS instrument, Biomaterials Profiling Center, University of Utah. For differences in the low mass range, see Figure 23. Conditions: sample 10 μg ; T_c 510°C; E_e] (a) 14 eV and (b) 11 eV.

have so far prevented the development of Curie-point Py-MS systems based on magnetic instruments for routine analytical applications. Fortunately, modern computer techniques allow some degree of compensation for transmissivity differences between quadrupoles. A simple way of correcting for transmissivity differences is to divide the spectra into sections of 14 mass units and to make comparisons between peak intensities within these sections only. Since such correction methods are far from perfect, however, the level of inter-laboratory reproducibility achievable should not be expected to allow direct comparison of minute quantitative differences in fingerprints within the foreseeable future. Rather, the degree of inter-laboratory reproducibility obtainable should enable research workers to exchange data regarding the presence and interpretation of characteristic signals in different types of materials being analysed.

Chapter 6

DATA ANALYSIS PROCEDURES

6.1. AVAILABLE COMPUTER PROGRAMS

Evaluation of pyrolysis mass spectra may either be purely quantitative, using the spectra as fingerprints only, or may involve some degree of qualitative interpretation as to the biochemical nature, composition or structure of the sample. Although in selected cases direct visual evaluation of qualitative aspects by an experienced operator is possible, computer-assisted evaluation techniques have not only greatly refined quantitative comparisons between the spectra but are also becoming indispensable tools for qualitative interpretation, as shown by Burgard *et al.* (refs. 126, 127) in the interpretation of direct probe Py-MS spectra from nucleic acids.

Computer-assisted techniques used for the evaluation of pyrolysis mass spectra include data pre-processing techniques, univariate statistical analysis techniques, multivariate statistical analysis techniques, feature selection and data reduction techniques, and display techniques. Most of these procedures are included in the special Py-MS software package developed by Eshuis *et al.* (ref. 45) at the F.O.M. Institute for Atomic and Molecular Physics, Amsterdam, and are available to interested scientists. Principal component, discriminant and factor analysis procedures are available in the widely used Statistical Package for the Social Sciences (SPSS) (ref. 128) and in the BMDP package (ref. 129). Other useful, widely available multivariate statistical analysis programs are the ARTHUR program package developed by Kowalski (ref. 130) and the CLUSTAN package (ref. 131). The latter programs are specifically oriented towards the cluster analysis approach in classification problems.

A full discussion of computer analysis techniques suitable for pyrolysis mass spectra is beyond the scope of this Chapter. Therefore, we shall discuss only the most essential data processing steps when applying the F.O.M program package to a selected medical problem, namely the comparative analysis of muscle biopsy samples from patients with Duchenne muscular dystrophy (DMD) as well as from non-dystrophic controls. Table 4 shows the clinical data for biopsied muscle tissue samples from three DMD patients and three non-dystrophic controls. It should be pointed out that DMD is an inherited, relentlessly progressive disease. DMD, which only manifests itself clinically in boys, is usually diagnosed at the age of four or five and leads to terminal illness at the age of thirteen or fourteen. Therefore increased involvement was noted for the 5, 7 and 8 year old boys (patients D, E and F). Preparation

TABLE 4

Clinical data for the muscle biopsy samples from dystrophic patients and controls

Patient	Age	Sex	Diagnosis	Muscle Type
A	26	M	control	biceps
B	2	M	control	abdominis
C	36	F	control	vastus (med.)
D	5	M	dystrophic	gastroc (med.)
E	7	M	dystrophic	biceps
F	8	M	dystrophic	biceps

of the muscle tissue samples for Py-MS analysis subsequently involved freeze-drying, grinding to a fine powder and suspending in methanol.

6.2. DATA PRE-PROCESSING

Each of the six muscle tissue samples was analysed in quadruplicate, thus generating 24 spectra in total. Representative spectra obtained by pyrolysing 10 μg of muscle tissue on filaments with a Curie-point temperature of 610°C and using electron impact ionisation at 14 eV electron energy are shown in Figure 25 for control C and patient F.

Visual examination of the spectra shows obvious similarities (note the characteristic ion cluster at m/z 91 to m/z 100) and differences (compare m/z 67) between the two spectra. The first question to be addressed is whether these differences are characteristic of the samples or due to variations introduced by the analytical procedure. Assuming that these differences indeed prove to be characteristic of the samples, the next question then becomes whether these differences in composition are correlated with the involvement in the disease or are due to intra- and inter-individual variations in the samples. Before such questions can be addressed by making numerical comparisons between the spectra, all ion intensity measurements have to be properly scaled. Two types of scaling operations are normally performed, namely pattern (= spectrum) scaling, more often referred to as "normalisation", and feature (= mass peak) scaling. Both types of scaling will be discussed in some detail since previous texts have paid little attention to these procedures, which are highly crucial to the outcome of the numerical evaluation procedure.

6.2.1. Pattern scaling

Pattern scaling (normalisation) is performed to compensate for variations in the overall ion intensity caused by phenomena not relevant to the analytical problem, such as differences in sample size or changes in instrument sensitivity. The most direct, often satisfactory way to normalise mass spectra for numerical purposes is to express peak heights as percentage total ion intensity. This procedure works

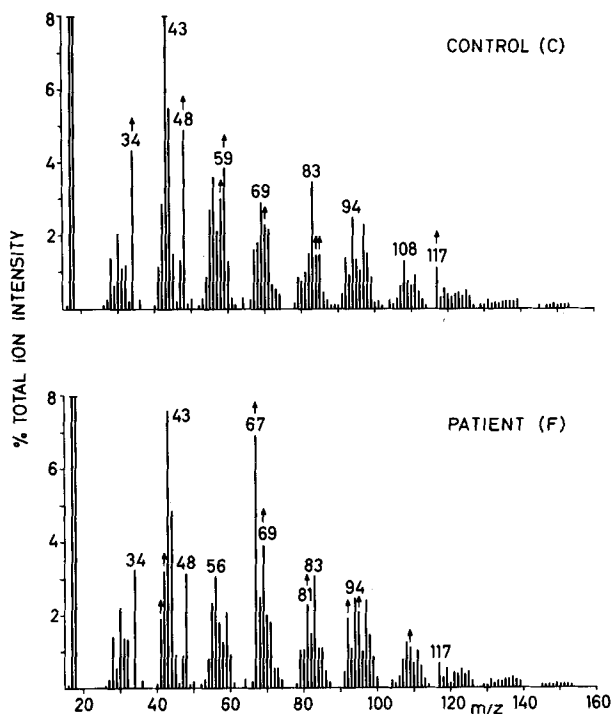


Figure 25. Pyrolysis mass spectra of muscle tissue from a control subject (C) and a dystrophic patient (F). For clinical data see Table 4. Conditions: sample 10 μg ; T_c 610°C; E_e 14 eV. Arrows indicate increased intensities as compared to the other spectrum.

better as the number of peaks increases and as the variation in individual peak heights decreases. The main problem in using this procedure is the occurrence of very large peaks, especially when these peaks exhibit a high degree of intra- and/or inter-sample deviation. If such a peak happens to be unusually high in a given spectrum, then all other peaks will be given low relative intensity values, which may considerably confuse further quantitative and qualitative comparisons between the spectra. A simple solution to this problem is to exempt all peaks larger than a certain percentage of total signal intensity, in one or more of the spectra compared, from the normalisation procedure. Once the remaining peaks have been normalised to 100% of the residual total ion intensity, the initially omitted peaks can be scaled accordingly, thus bringing the sum of the relative ion intensities to a value greater than 100%. The obvious shortcoming of this procedure is, however, that elimination of the largest peaks is at best a very rough way of eliminating potential sources of strong variation. Some large peaks may be very stable and contribute little to intra-sample (inner) or inter-sample (outer) deviation, whereas a relatively small peak may be responsible for most of the total (pooled) deviation in the system. An

alternative procedure would therefore be to exempt all peaks exhibiting more than a certain amount of inner and/or outer deviation, depending on the analytical problem. However, this requires a knowledge of these deviations, which can be calculated accurately only after adequate normalisation. Therefore, this approach requires iterative calculation of normalisation coefficients and variances while removing peaks with high deviation values until no more peaks can be found with deviation values above a certain level. Apart from being demanding on computer time, this iterative procedure needs to be used judiciously when high levels of inner or outer deviation exist in the data, otherwise all but a few small peaks might be removed, and the normalisation might be based on poor signal statistics.

For the muscle biopsy data a compromise solution was adopted. Preliminary pattern scaling was performed on the basis of percentage ion intensity using all peaks. Subsequently, inner and outer deviation values were calculated for all peaks. Those peaks showing more than 5% relative ion intensity and/or an inner or outer deviation larger than 1% of total deviation were removed from the second and final pattern scaling operation. This resulted in the temporary removal of m/z 17, 34, 43, and 67.

It should be noted that the choice of the normalisation procedure and of most of the following numerical procedures depends largely on the operator's analytical philosophy. If, for example, the pyrolysis mass spectra of polystyrene and polytetrafluoroethylene, which show peaks only at m/z 104 and 100, respectively, (see Figure 1) are to be compared numerically, then the iterative normalisation procedure will fail completely as both peaks are removed and no group of stable peaks common to both spectra is left to provide an internal reference for pattern scaling. Even if this problem is ignored by using sample weight or total ion current as a normalisation reference, further problems may be encountered when actually comparing the spectra numerically, depending on the type of similarity coefficient used. In general it can be stated that the more similar the spectra are that are being compared, the more straightforward a numerical comparison is likely to be. The more dissimilar the spectra, the greater is the difficulty in deciding which numerical procedures to use.

6.2.2. Feature scaling

Feature scaling, i.e. scaling the relative intensity values of different mass peaks, is performed to compensate for differences in relative peak intensities caused by phenomena not relevant to the analytical problem. For example, when trying to differentiate muscle biopsy samples by comparing pyrolysis mass spectra, the largest peaks do not necessarily contain the most information relevant to the problem. However, if no feature scaling is performed these large peak values will dominate the numerical comparison between spectra, with most types of algorithms.

Because it is preferable to base a classification or differentiation of muscle biopsy samples on the most reliable and characteristic features rather than on the largest, some form of feature scaling is indicated. Since multiple analyses of each sample are made, intra-sample standard deviations for each peak can be calculated and peak intensities expressed in units of standard deviation. The more duplicate analyses are available the more effectively this procedure removes intra-sample "noise" due to instrumental sources. If multiple samples had been available from each individual, "noise" from intra-individual variations in the composition of the sample could have been eliminated in the same way. An example of this scaling for the DMD data is given in Table 5 in which column (a) gives the total ion intensity for various peaks and column (b) the intra-sample deviation. Division of (a) by (b) gives the peak intensities in terms of standard deviation units. While this very common procedure brings out the most reliable features, these features are not necessarily the most characteristic features for obtaining a clear differentiation between the samples.

TABLE 5

Ion intensity parameters for the 15 masses with greatest characteristicity values in the analysis of muscle samples

Mass	(a) % Total Ion Intensity	(b) Intra-sample Deviation	(c) Inter-sample Deviation	(a)/(b) Reproducibility Value	(c)/(b) "Characteristicity" Value
67	3.45	0.19	4.39	18.16	23.60
81	1.61	0.06	0.77	26.83	13.24
32	1.40	0.09	1.09	15.56	11.50
101	0.09	0.01	0.08	9.00	10.15
31	1.33	0.08	0.75	16.63	9.53
41	1.42	0.06	0.54	23.67	8.78
40	0.11	0.01	0.05	11.00	8.56
84	1.41	0.05	0.40	28.20	8.30
68	2.03	0.07	0.57	29.00	8.24
80	0.83	0.03	0.25	27.67	7.97
48	4.34	0.19	1.44	22.84	7.54
102	0.08	0.01	0.05	8.00	6.14
74	0.37	0.02	0.13	18.50	5.71
42	3.00	0.07	0.40	42.86	5.63
34	4.07	0.14	0.73	29.07	5.29

To solve this problem, Eshuis *et al.* (ref. 45) suggested the use of a feature scaling factor based on the ratio between outer and mean inner deviation, in order to bring out those features which are both highly different between different classes of patterns (high outer deviation) and highly stable within each given class (low mean inner deviation). This "characteristicity" factor is closely related to the well known Fisher ratio. Eshuis *et al.* have shown that the use of this factor

dramatically improves the separation of two classes of *Listeria* without making previous assumptions about the existence of these two classes (ref. 45). If used in this manner, the feature scaling acts as a contrast-enhancing procedure not entirely dissimilar to the computer procedures used for contrast enhancement in digital image processing operations.

A distinct disadvantage of feature scaling techniques incorporating outer deviation values in the scaling factor, however, is the strong dependence of this factor on the particular set of samples used. Addition of a different sample to the set may appreciably change the scaling factors, sometimes making direct comparison between results obtained with different sets of samples difficult, if not impossible. This problem does not necessarily exist when mean inner deviation is used in the scaling factors only, since the sources of biological and instrumental "noise" variations may often be assumed to be similar for different sets of samples. In fact, this condition is almost a prerequisite for further statistical processing of combined data from different sets of samples. Referring again to Table 5, the column labelled "characteristicity" value lists the ratio of the outer to inner sample deviations for the fifteen masses with the largest "characteristicity" values.

6.3. UNIVARIATE STATISTICAL ANALYSIS

Feature scaling factors are primarily calculated for subsequent multivariate statistical analysis of the data. However, these factors also provide a primitive, but often effective, means of data reduction and/or feature selection. Data reduction for further numerical analysis procedures may be achieved by only considering the n mass peaks with the highest "characteristicity" values or highest reproducibility values, where n may have any value from unity to the total number of mass peaks measured. Feature selection on the basis of scaling factors can be helpful in selecting features to be displayed as one-, two- or three-dimensional plots. Alternatively, selected features may be used for further univariate statistical analysis, e.g. T-tests for the significance of observed trends in the intensity distributions.

As an example of two-dimensional feature plots, Figure 26 shows the scatter plot of the intensity distributions of the two masses with highest "characteristicity" values, namely m/z 67 and 81, respectively, for the DMD data. These masses both show a progressive increase in intensity with progressive involvement of the disease. In fact, T-test values show a significant separation between patient and control samples in spite of the small number of samples involved. At the same time, however, this two-dimensional plot shows the basic shortcoming of univariate statistical analysis techniques in that the strong correlation between the two mass signals is completely ignored. The existence of this correlation is confirmed by the high value of the calculated correlation coefficient. In contrast, the scatter plot of m/z 32 versus m/z 101 shown in Figure 27 reveals no strong correlation either with the degree of involvement in the disease or between both masses. The intensity distribution of

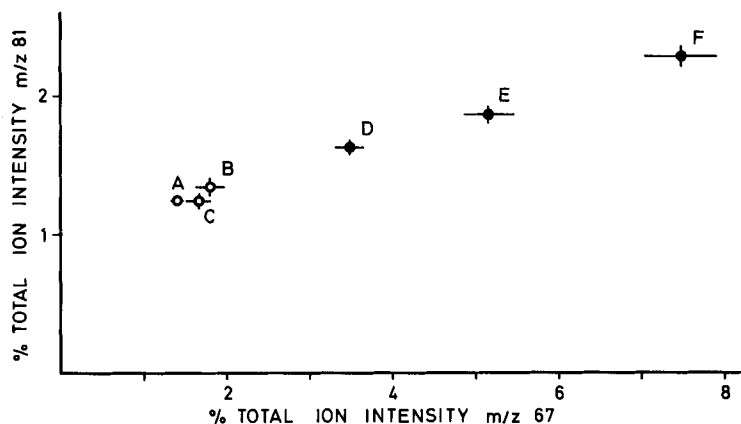


Figure 26. Scatter plot of the ion intensities at m/z 67 versus m/z 81 for muscle biopsy samples (Table 4), showing a strong increase in the dystrophic muscle (D,E,F) and a high degree of correlation (correlation coefficient 0.91) between m/z 67 and 81. T-tests for probability of chance occurrence of separation between normals and dystrophic case F yield p values less than 0.01 for both m/z 67 and m/z 81.

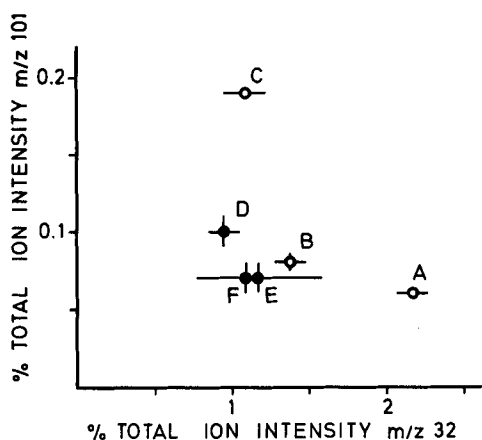


Figure 27. Scatter plot of the ion intensities at m/z 32 versus m/z 101, showing absence of correlation with the disease as well as between both ion intensity distributions. Note high value for sample C (female control) at m/z 101.

m/z 32 appears to be dominated by strong individual differences between all three controls (compare this finding with the pronounced differences in clinical data for these samples in Table 4), whereas m/z 101 shows an exceptionally high value for the only female sample (control C). Additional analyses of different samples will be required in order to confirm the significance of these observations.

Similar two-dimensional plots could be constructed, of course, for many other combinations of masses with high "characteristicity" values. However, a far more comprehensive approach is to use multivariate statistical analysis techniques which enable a comparison of intensity distributions of a much larger collection of masses to be made simultaneously. Also, this approach avoids the danger of misjudging the significance of seemingly non-random distributions when examining isolated features for an expected differentiation in intensity distributions. Obviously, a significance level of 1% ($p \leq 0.01$) does not prove differentiation if only observed a few times among a hundred or so different features inspected.

6.4. MULTIVARIATE STATISTICAL ANALYSIS

Instead of considering the intensity distribution at each individual mass value separately, as is the case in univariate statistical analysis, multivariate statistical analysis techniques allow consideration of n mass distributions in n -dimensional space simultaneously. Whereas it is relatively easy to visualize two- or even three-dimensional scatter plots obtained by plotting the intensity distributions at two or three mass values simultaneously, direct visualisation of distributions in higher dimensional space is, of course, impossible. However, as long as the higher dimensional space is metric, calculation of distances between points obeys the same metric laws as calculation of distances in two- or three-dimensional space. Therefore, consider the situation shown in Figure 28, where each of the two points represents the result of a measurement involving the same three parameters, x , y , and z . In terms of Py-MS data, this would correspond to two mass spectra containing masses x , y , and z with the ion intensities for those particular masses plotted along the corresponding axes. Since the values found for each of these parameters are different in the two measurements, the points occupy different positions in three-dimensional space. Obviously, the more different the values measured, the farther apart are the points, and *vice versa*. Thus, the distance between the points is a numerical expression of the degree of similarity between the multiparameter measurements.

The most direct way of measuring the distance between the points is to calculate the distance along a straight line through both points, the so-called Euclidean distance. A seemingly more complicated way of measuring the distance is to sum the distance when taking the shortest route from one point to another only following lines parallel to one of the three axes, the so-called city block distance (see Figure 28). The attractive property of this distance measurement is that it involves only simple additions and subtractions. Frequently, quadratic and other non-linear functions (e.g. correlation coefficients, standard deviations, chi squared coefficients or generalized Mahalanobis distances) are used to derive distance values (ref. 132). All of these functions are generally referred to as "similarity coefficients".

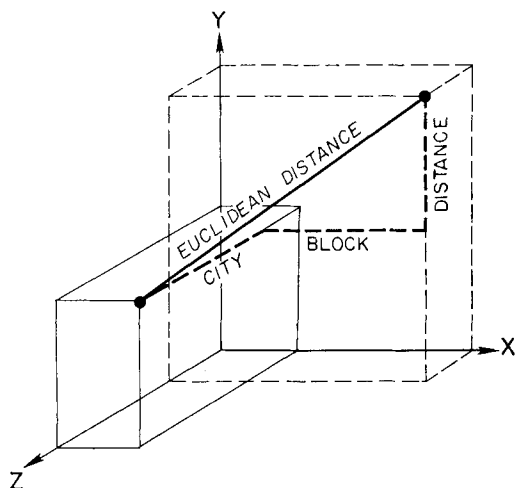


Figure 28. Three-dimensional representation of two hypothetical mass spectral patterns with features X, Y and Z, showing Euclidean distance and city block distance.

All metric similarity coefficients in two- or three-dimensional space can be visualised provided that suitable linear or non-linear axes are chosen. For a mathematical description of the various similarity coefficients used in multivariate statistical analysis, the reader is referred to specialised textbooks (refs. 132, 133) or to the SPSS User Manual (ref. 128).

In our experience, the modified Euclidean distance algorithm described by Eshuis *et al.* (ref. 45) and the closely related chi squared algorithm provide the most satisfactory results for pyrolysis mass spectra, provided that the proper feature scaling techniques are used first. Again referring to the DMD data, Table 6 shows the distance matrix obtained for the Py-MS spectra when using the 40 mass peaks with highest "characteristicity" values and employing the chi squared formula. The diagonal of the matrix shows distance values between duplicate spectra of the same sample. Examination of these values allows the detection of badly reproducing spectra, which subsequently may be deleted and the matrix re-calculated. If there are no more obvious outliers among the duplicate spectra, the matrix can be substantially reduced by listing only the distance values between the average spectrum of each sample, as illustrated in Table 7. A close scrutiny of the values in Table 7 enables a crude mental picture to be formed of the relative positions of the average spectra in multi-dimensional space. Obviously, the spectra of the non-dystrophic controls form a small cluster with the spectra of the dystrophic patients moving progressively away from this cluster with increasing age of the patient. To form such mental pictures becomes increasingly difficult, if not impossible, with

TABLE 6

Distance matrix showing chi squared coefficient values for pyrolysis mass spectra of muscle biopsy samples from three dystrophic patients (D, E, F) and three controls (A, B, C).

A1	-																							
A2	1.1	-																						
A3	1.1	.8	-																					
A4	1.1	.8	.8	-																				
B1	2.9	2.3	2.6	2.6	-																			
B2	3.5	2.8	3.0	2.8	1.8	-																		
B3	3.1	2.4	2.6	2.6	1.0	1.4	-																	
C1	5.6	5.0	5.2	5.3	3.9	4.0	3.8	-																
C2	5.2	4.7	4.9	5.1	3.7	4.2	3.7	1.4	-															
C3	5.6	4.9	5.2	5.3	3.8	3.9	3.6	1.0	1.3	-														
D1	6.6	6.1	6.3	6.3	4.7	4.5	4.5	4.4	4.6	3.9	-													
D2	6.6	6.0	6.2	6.2	4.8	4.2	4.4	4.7	5.0	4.2	1.3	-												
D3	7.3	6.6	6.8	6.8	5.3	4.7	4.9	5.2	5.5	4.7	1.8	1.2	-											
D4	7.2	6.6	6.8	6.8	5.3	4.7	4.9	5.0	5.4	4.6	1.6	1.2	.7	-										
E1	9.5	9.1	9.1	9.1	8.1	7.3	7.7	8.4	8.7	8.0	4.7	4.3	4.1	4.2	-									
E2	10.2	9.8	9.8	9.9	8.8	8.1	8.5	9.2	9.4	8.8	5.4	5.0	4.8	4.8	1.1	-								
E3	8.6	8.2	8.3	8.3	7.2	6.6	6.9	7.6	7.8	7.2	3.9	3.6	3.4	3.4	1.4	2.0	-							
E4	8.7	8.3	8.4	8.4	7.3	6.7	7.0	7.8	8.0	7.4	4.0	3.7	3.4	3.5	1.4	1.9	.8	-						
F1	14.5	14.1	14.1	14.1	13.2	12.4	12.9	13.4	13.7	13.1	9.7	9.4	9.0	9.1	5.4	4.6	6.2	6.1	-					
F2	13.1	12.7	12.7	12.7	11.8	11.1	11.4	12.0	12.2	11.6	8.2	7.9	7.5	7.6	4.0	3.3	4.7	4.6	2.0	-				
F3	13.6	13.3	13.3	13.4	12.4	11.7	12.0	12.5	12.7	12.1	8.8	8.6	8.2	8.3	4.6	3.9	5.3	5.2	1.8	1.5	-			
	A1	A2	A3	A4	B1	B2	B3	C1	C2	C3	D1	D2	D3	D4	E1	E2	E3	E4	F1	F2	F3			

TABLE 7

Reduced distance matrix showing the average distance values for each set of analyses given in Table 6 for controls (A,B,C) and patients (D,E,F).

A	1.0					
B	2.8	1.4				
C	5.2	3.8	1.2			
D	6.6	4.7	4.8	1.3		
E	9.0	7.5	8.2	4.2	1.4	
F	13.5	12.1	12.6	8.5	4.8	1.8
	A	B	C	D	E	F

larger matrices and more complex relationships. In order to obtain an accurate impression in these cases, special techniques have to be used to extract the most significant information from the distance matrix and to display this selected information in an easily visualised form. The loss of information incurred can be minimized by using a number of complementing visualisation techniques rather than a single technique. Visualisation techniques often used are: nearest neighbour tables, dendrograms, re-ordered matrices and non-linear maps (see Figure 29). Of these we most often use the non-linear maps and nearest neighbour tables, and occasionally the re-ordered matrices.

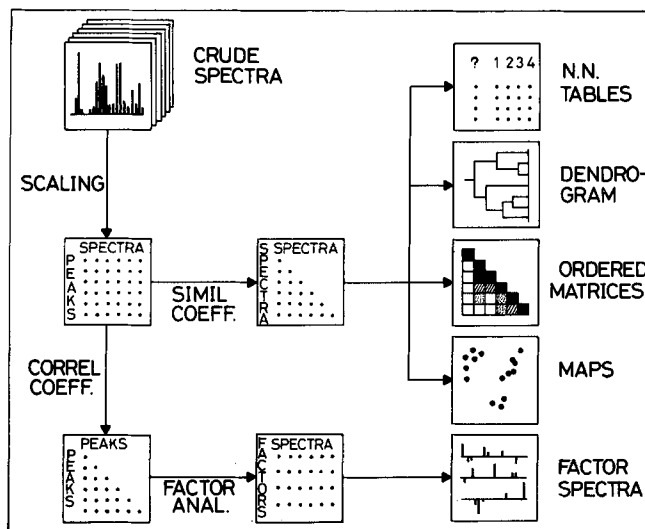


Figure 29. Schematic overview of relationships between multivariate statistical analysis procedures applicable to pyrolysis mass spectra.

6.5. VISUALISATION TECHNIQUES

Nearest neighbour tables are simple lists of the K nearest neighbours of each sample in multi-dimensional space. Table 8 shows such a list for the DMD data. Inspection of this table demonstrates that each sample recognizes other similar samples. Controls always find other controls as first neighbours and the dystrophic samples always find other dystrophic samples.

TABLE 8

Nearest neighbour table, derived from distance matrix in Table 7, for control (A,B,C) and Duchenne muscular dystrophy (D,E,F) muscle biopsy samples

Sample	Nearest Neighbour		
	1st	2nd	3rd
A	B	C	D
B	A	C	D
C	B	D	A
D	E	B	C
E	D	F	B
F	E	D	B

An ordered matrix is a direct form of representation of the distance matrix in which various colours or degrees of shading are used to represent different distance ranges. The samples in the matrix are arranged in such a way as to put nearest neighbours as close together as possible. Figure 30 gives an example of a simple ordered matrix for the DMD data. An excellent way to arrive at the best possible sequence of neighbours for the ordered matrix is to use Kruskal's multidimensional scaling technique (ref. 134), which is strongly based on neighbourhood criteria, to scale the n-dimensional distance matrix to a one-dimensional sequence.

Non-linear mapping techniques have been used extensively in this work and are sufficiently complex to be considered as multivariate statistical analysis procedures in their own right. In fact, the non-linear mapping technique most often used by us, which is based on Kruskal's multidimensional scaling method (ref. 134), has sometimes been compared with principal component factor analysis techniques (ref. 132) because of its remarkable ability to display the most prominent numerical trends in the data. The concept of non-linear mapping is complicated and therefore often a source of confusion. For instance, a Kruskal-type two-dimensional non-linear map (three-dimensional versions also exist) is not a projection of multidimensional space on to two-dimensional space, but the result of an iterative computer procedure (ref. 45) aimed at minimizing the "stress", an empirical goodness-of-fit value (ref. 135) which compares the configuration in two-dimensional space with the original configuration in multidimensional space. Low stress values (e.g. <5%) are obtained if the nearest neighbour sequence for each point in the non-linear map is nearly identical with the

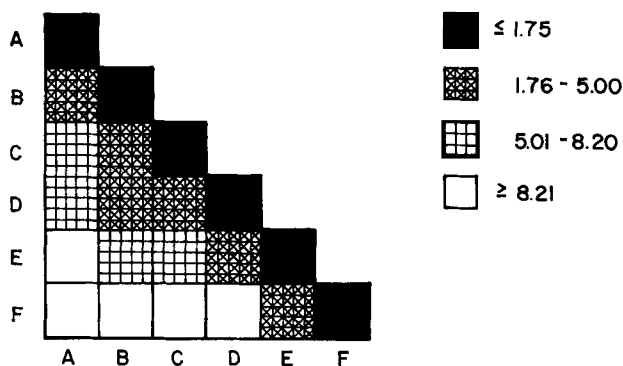


Figure 30. Ordered distance matrix derived from the distance averaged distance matrix shown in Table 7.

nearest neighbour sequence for the corresponding point in multidimensional space. Whereas "relative neighbourhood" is thus preserved as far as possible, relative distance between points is often sacrificed.

The non-linear map of the distance matrix in Table 6 is shown in Figure 31. This map conforms closely to the mental picture formed from the distance matrix, as also evidenced by the very low stress value of 0.8%. In particular, the non-linear map appears to be a synthesis of the relationships shown in the scatter plots of Figures 26 and 27.

The loss of accurate distance information limits the usefulness of the non-linear map for quantitative decisions. However, non-linear maps are powerful tools for visualising differentiation tendencies in the data. Especially when the samples form clusters of complex shape, as often occurs with biological samples, non-linear maps may be the only possible way of obtaining insight into the relationship between

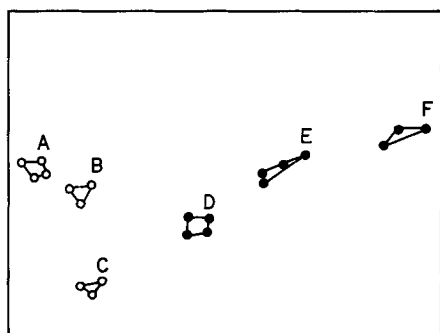


Figure 31. Non-linear map (stress 0.8%) derived from the distance matrix in Table 6, showing the approximate relationships between the muscle biopsy spectra of dystrophic patients (D, E, F) and controls (A, B, C) in 40-dimensional space (see text).

the samples. Furthermore, non-linear mapping can provide a unique insight into the influence of varying the analytical conditions, e.g. pyrolysis temperatures, on the degree of differentiation achieved. Finally, it should be noted that Kruskal's mapping technique does not require any assumptions about the statistical distribution of the data. This allows mapping of small data sets with insufficient data for a reliable principal component, factor analysis or discriminant analysis approach.

6.6. COMPUTER-ASSISTED CHEMICAL INTERPRETATION

6.6.1. Subtraction techniques

In its simplest form the question regarding the biochemical nature of an observed difference between two classes of pyrolysis mass spectra can be answered by subtraction. Calculation of average spectra for each class may improve the reliability of the procedure. Figure 32 shows the results of subtracting the average spectra of the non-dystrophic muscle biopsy samples from the dystrophic samples. The positive component of the difference spectrum shows a prominent ion series at m/z 67, 81, 95 and 109, indicating the presence of pyrroles. In biomaterials, marked pyrrole series are often derived from porphyrins (ref. 136) or from proline-containing compounds (ref. 137). The latter possibility immediately suggests the presence of relatively large amounts of collagen, a protein unusually rich in proline (12%) and

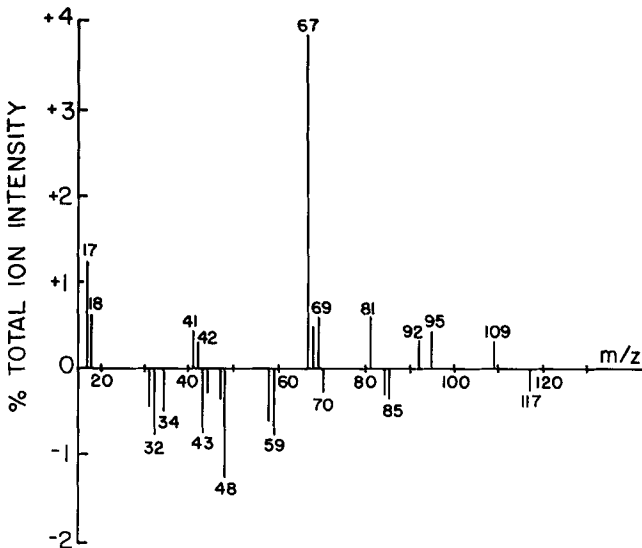


Figure 32. Difference spectrum obtained by subtracting the average pyrolysis mass spectrum of normal muscle samples from the average spectrum of dystrophic muscle samples.

hydroxyproline (9%) (see Atlas). Indeed, the relative contribution of collagen, an important constituent of connective tissue, strongly increases with progressive wasting of the muscle tissues in DMD.

The negative part of the difference spectrum appears to contain different components. The typical protein-derived peaks at m/z 34 (H_2S), 48 (CH_3SH) and 117 (probably indole) seem to point to a relative decrease in a protein component rich in cyst(e)-ine, methionine and tryptophan. Although it is tempting to associate this with the strong relative decrease in muscle proteins, e.g. myoglobin, in DMD, the situation is far less clear than with collagen. Also, it should be kept in mind that the presence of an abnormal positive component tends to lead to relatively low signals for all normal components present in spite of the elimination of m/z 67 during the normalisation procedure. Indeed the negative part of the difference spectrum shows a rough resemblance to the spectrum of normal muscle tissue in Figure 25. Finally, the presence of a typical series of carbohydrate peaks at m/z 31, 32, 43, 70, 84, and 85 merits attention. When examining the intensity distributions of these peaks, a marked degree of inter-individual variation is noted, especially among controls. The DMD cases show relatively low intensities, as evidenced by the appearance of these masses in the negative part of the difference spectrum. This tendency is shown in the intensity distribution of m/z 32 in Figure 27. The strong inter-individual variation points to a carbohydrate component present in varying concentrations. Thus, it is tempting to identify this component as muscle glycogen, the concentration of which will be strongly dependent on the physiological status of the muscle prior to the biopsy. Of course, many more samples would have to be analysed before such conclusions could be confirmed. Therefore, these data are given primarily as an example of how to attempt a limited degree of chemical interpretation with complex samples. Such a limited degree of interpretation can be extremely helpful in pointing the way to more specialised biochemical studies. Also, once the identity of a given pattern has been firmly established, e.g. the supposed collagen pattern, then the pyrolysis mass spectrum may provide a unique way of obtaining a quantitative estimate of the amount of the component present in further samples.

Apart from performing simply subtractions, computer techniques can be used for more sophisticated support of attempted chemical interpretation. For instance, if doubts exist as to the significance of features discovered in difference spectra, the computer may be used to calculate all the variances involved in order to arrive at an estimate of statistical significance of the features shown.

6.6.2. Factor analysis

A different approach is necessary when more than two classes of samples are compared and the differences between these classes are caused by multiple components. Using factor analysis techniques, the contribution of each of the different components

(factors) to each of the different sample classes can be determined (ref. 126, 127), provided the number of different spectra available is several times larger than the number of components involved. In many ways, this requirement is similar to the requirement for solving equations with multiple unknowns, namely that the number of different equations available should be equal to or greater than the number of unknowns. Apart from determining the contribution of each factor to each class of spectra, factor analysis procedures also allow the determination of the contribution of each mass peak to each factor. The resulting factor spectra can be regarded as characteristic of the corresponding components. If sufficiently large numbers of observations are available, the number of factors involved is fairly low (e.g. <10), and the components do not mutually interfere in the analytical procedure, the factor spectra should show a close resemblance to the spectra of the individual compounds. Thus far, experience with factor analysis in pyrolysis mass spectrometry is limited. Figure 33 shows the factor spectrum calculated for the main factor derived from the series of pyrolysis mass spectra of DMD muscle samples described in the earlier sections of this Chapter. The factor analysis program used was part of the SPSS package (ref. 128). Windig *et al.* (ref. 101) used factor analysis techniques for qualitative comparison of pyrolysis mass spectra of standard biopolymers on changing the pyrolysis parameters (see Section 5.3). Van Graas *et al.* (ref. 73) demonstrated that from the pyrolysis mass spectra of coals of different coalification stages a factor can be calculated which is strongly correlated with the rank of the coal.

6.7. COMPUTER ASSISTED QUANTITATIVE ANALYSIS OF MIXTURES

In case a factor describes one chemical component in a complex mixture, the factor score can be used as a quantitative measure of the compound. This is demonstrated in the application of Py-MS to the detection of ppm levels of impurities of the toxic, technical polymer diethylaminoethyl(DEAE)-dextran in batches of poliomyelitis virus vaccine as shown in Figure 34. By introducing standard virus preparations, spiked with 20, 40, or 80 ppm of DEAE-dextran in the sample series, the first factor described this polymer. Concentrations in the samples to be checked can be determined down to 20 ppm (ref. 63).

In the pyrolysis mass spectra of complex mixtures, factor spectra often represent correlated changes of a number of chemical components. Generally, this is due to mathematical reasons, e.g. the normalisation of the spectra, and the non-orthogonality of factors. In such cases, specialised factor analysis techniques such as vector rotation and renormalisation (refs. 138, 139, 140) allow the examination of mass spectra from mixtures for the presence of specific components. Other methods suitable for this purpose are target transformation factor analysis as described by Malinowski and McCue (ref. 141) and the probability-based reversed matching method

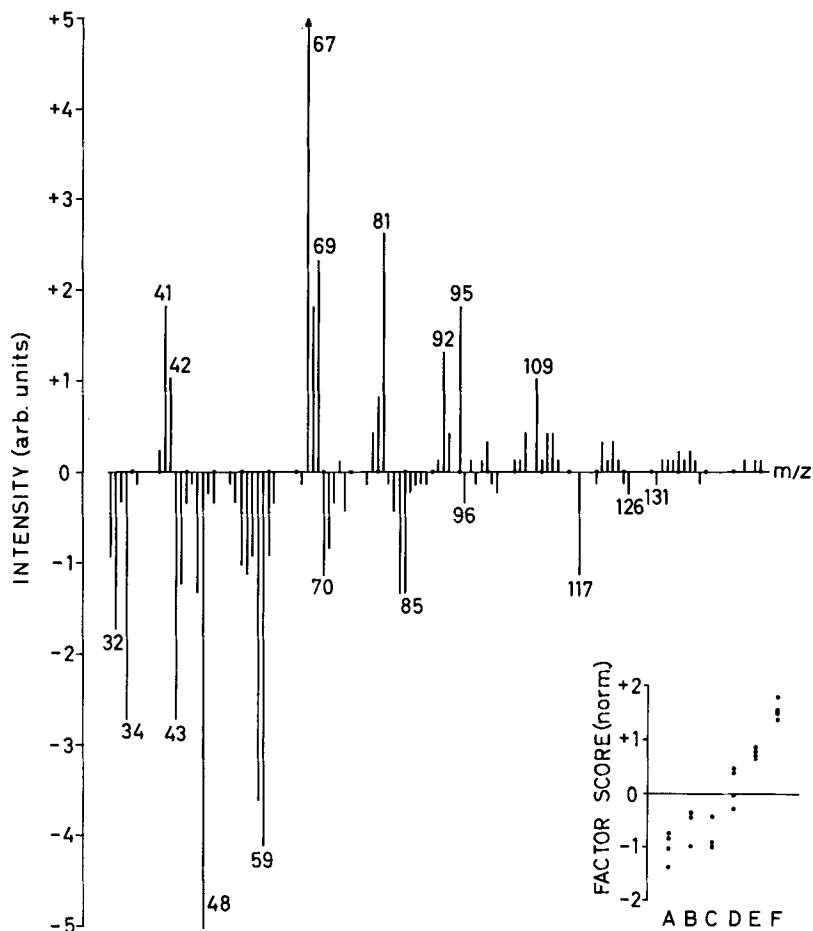


Figure 33. Factor spectrum of the first factor derived from the pyrolysis mass spectra of the set of DMD and normal tissue samples mentioned in Table 4. This main factor accounts for 59% of the total variance present in the data set. The intensities in this factor spectrum represent $\alpha_i \cdot \sigma_i$ -values (α_i = loading of the mass intensity i to the factor; σ_i = SD of the mass intensity i), so that the spectrum shows that part of the measured variation (σ_i) on each of the mass peaks, which is described by the factor (ref. 101). Because the loadings α_i can be either positive or negative (due to normalisation of the spectra to total intensity), the factor spectrum exhibits positive and negative series of intensities; both of these can be interpreted individually. The close resemblance of the positive and negative parts of this factor spectrum to the difference spectrum (Figure 32) should be noted. In the negative part of the factor spectrum three subsets of fragment peaks can be recognized more clearly than in the difference spectrum, viz. the protein series of peaks at m/z 34, 48, 117 and 131, the carbohydrate series at m/z 31, 32, 43, 60, 70, 72, 84, 85, 96 and 126, and the series at m/z 58, 59, 71 and 89, indicative of choline residues from phospholipids (see Figure 9). By factor rotation methods (see Section 6.7) these subsets of peaks could be optimized separately and thus have to represent different chemical components within the tissue materials. The factor scores of this first factor are given in the insert and represent the intensities (standardised values) at which this factor contributes to the average spectrum of each of the samples.

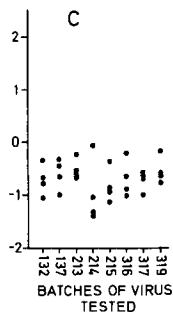
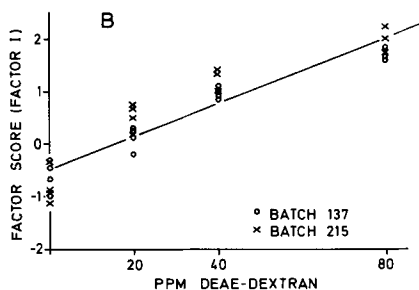
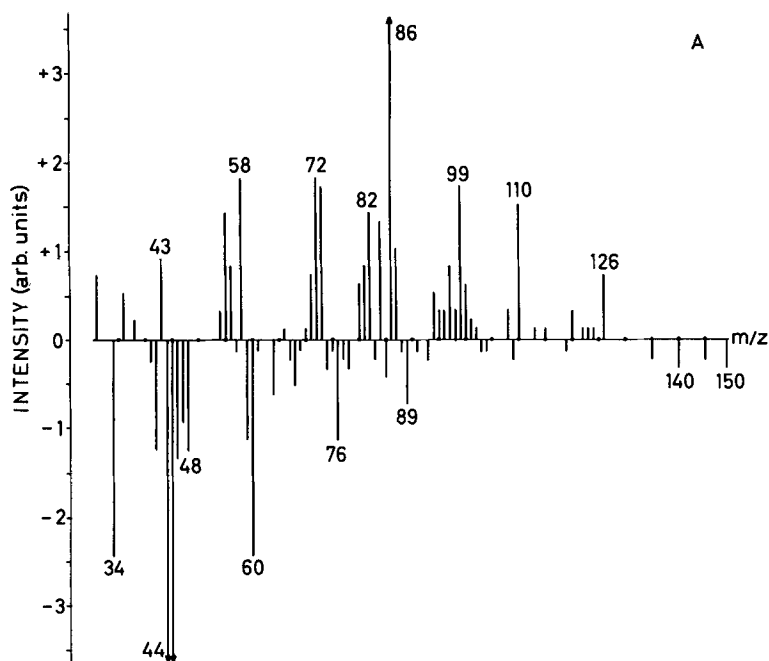


Figure 34. Factor spectrum of the main factor, derived from a series of pyrolysis mass spectra of poliomyelitis-virus concentrates, obtained by purification on DEAE-Sephadex columns. The positive part of the spectrum (a) represents the DEAE-dextran pattern (compare with Atlas); the negative part reflects mainly pyrolysis fragments of the virus material (note the sulphur-containing fragments at m/z 34, H_2S^+ ; 48, CH_3SH^+ ; 64, SO_2^+ ; 76, CS_2^+). The calculation was based on a series of eight virus batches together with some standard samples prepared from two of the batches by addition of DEAE-dextran at concentrations of 20, 40, and 80 ppm, respectively. Semi-quantitative results are given in Figure (b). A linear relationship appears to exist between the polymer concentration and the factor score of the main factor (quadruplicate determinations are given). All tested virus batches (designated by numbers 132, 137, ..., 319; Figure (c)) have DEAE-dextran concentrations not exceeding the detection limit (20 ppm).

developed by McLafferty *et al.* (ref. 142). So far, the use of these latter techniques has not been reported in Py-MS.

With respect to the factor rotation methods it should be noted that owing to the complex character of pyrolysis mass spectra mathematical criteria usually cannot be found. Therefore, rotation techniques such as Varimax (ref. 138) and the method of Knorr and Futrell (139) may not perform satisfactorily. Moreover, target transformation and matching techniques (which use library criteria) are less well suited for the analysis of complex pyrolysis mass spectra, as the component sub-patterns can be influenced by the total sample matrix (see Section 4.1). For these reasons, Windig *et al.* (ref. 140) adapted the "graphical rotation" method (ref. 143), an empirical factor rotation technique, for interpreting pyrolysis mass spectra. The example in Figure 35 represents the analysis of a small set of pyrolysis mass spectra of yeast species in order to obtain a more quantitative description of the main groups of biochemical components in these microorganisms. The spectra of such yeasts (Figure 35a) are mainly composed of series of fragment peaks indicative of neutral hexose and pentose-type carbohydrates, N-acetylamino sugars and proteins, which are building blocks present in many different homo- and hetero-biopolymers of the microorganisms. The first, unrotated factor calculated is given in Figure 35b and the positive part describes the differences in the overall protein sub-patterns very well. The negative part of this factor represents a mixed pattern of fragment peaks attributable to a number of other component groups. On rotation in the plane through the two factor axes this pattern changes, until at 60° a set of peaks is observed (Figure 35c) which optimally represents a fragment pattern of pentose-type carbohydrates (compare with Atlas). At the same rotation angle the positive part of factor 2 (Figure 35d) optimally represents the highly correlated (not separable) hexose and N-acetylhexosamine sub-patterns (see Atlas), whereas the negative part of this second factor (not shown) now represents the protein pattern of the first, unrotated factor. The factor scores of these optimized "component factors" can be used as a semi-quantitative measure of the chemical components as shown in Figure 35e.

6.8. FUTURE DEVELOPMENTS

A schematic overview of the entire set of data analysis procedures discussed in the previous sections is shown in Figure 29. With the exception of factor analysis procedures which can be found in the SPSS, ARTHUR and BMDP packages, and dendrogram procedures, which are present in the CLUSTAN programs, all procedures shown in Figure 29 are available in the F.O.II. package. A challenging development for the coming years will be to combine the most attractive features of these programs in a single package, suitable for operator-interactive processing of pyrolysis mass spectra on mini-computer systems.

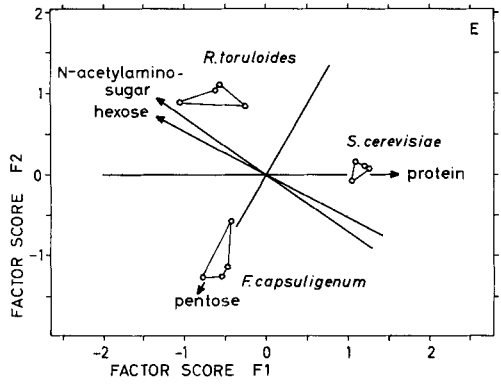
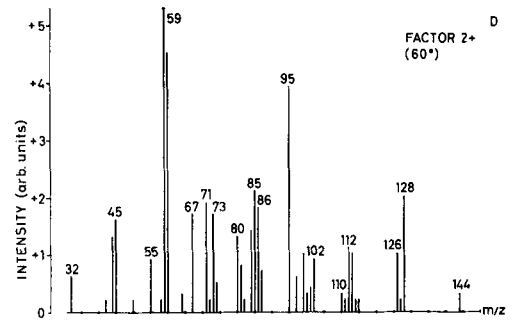
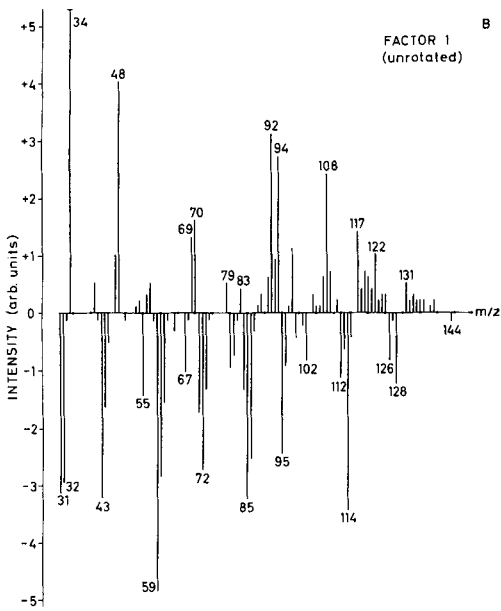
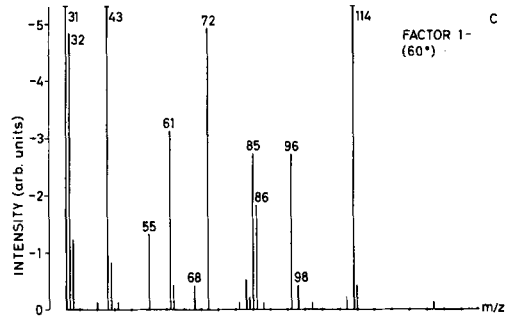
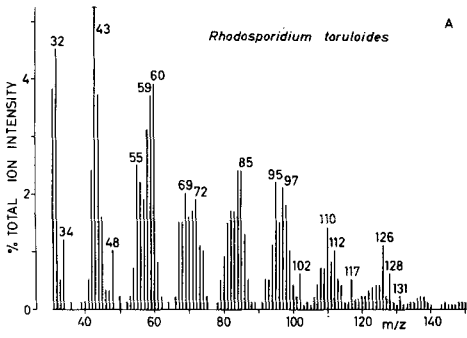


Figure 35. Pyrolysis mass spectrum of the yeast *Rhodospiridium toruloides* together with some factor spectra obtained on comparison with spectra of the other yeast species *Saccharomyces cerevisiae* and *Filobasidium capsuligenum*. The complex yeast spectra (e.g. Figure (a)) contain various sub-sets of fragment peaks attributable to main groups of biochemical components, *viz.* proteins (marker peaks at m/z 34, 48, 69, 83, 92, 94, 108, 117, 131), hexoses (m/z 55, 58, 68; 72, 74, 82, 84, 85, 96, 98, 102, 110, 112, 126, 144), pentoses (m/z 55, 58, 60, 68, 70, 72, 82, 84, 85, 86, 96, 98, 114) and N-acetylamino sugars (m/z 59, 73, 83, 97, 109, 123, 125, 137). Figure (b) shows the first factor (unrotated); the positive part represents a protein sub-pattern and the negative part a mixed pattern of mainly carbohydrate fragment peaks. Figure (c) shows the negative part of the first factor after rotation of the feature space over 60° , and represents a pentose sub-pattern. Figure (d) shows the positive part of the second factor in the 60° rotation configuration and represents the strongly correlated hexose and N-acetylhexosamine sub-patterns which cannot be further separated. The plot of the unrotated factor scores for factors 1 and 2 is given in Figure (e). The inproduct of a spectrum and a "component factor" gives the rotated factor scores; *F. capsuligenum* is relatively rich in pentose components, *S. cerevisiae* in protein and *R. toruloides* in hexoses and N-acetylaminosugars. It should be noted that this type of plot in general gives a better impression of dissimilarities between spectra in terms of chemical components than do non-linear maps such as that presented in Figure 31.

The applicability of several other important multivariate analysis techniques in Py-MS, e.g. principal component analysis or discriminant analysis, remains to be further demonstrated. Principal component analysis (ref. 132) is basically a data reduction technique. However, as a data reduction technique it has some serious disadvantages for Py-MS applications. First, the transformation from feature space to principal component space (Karhunen-Loeve transformation) is a full multivariate procedure requiring considerable computer time. Thus, in most applications, little or no gain in time or efficiency can be expected by reducing the data in this way. Secondly, the familiar m/z values are replaced by principal component values which do not necessarily have any chemical meaning. In factor analysis, an attempt is made to obtain factors which correspond directly to components of the sample and special adaptations [Varimax rotation (ref. 138)] exist to accommodate situations where the components in the sample are not mutually independent, as will be the rule rather than the exception in complex organic samples. Principal components, however, are mutually independent [orthogonality principle (ref. 132)].

Perhaps the most useful application of principal component analysis in Py-MS is to arrive at an estimate of the intrinsic ("true") dimensionality of the data set or, in chemical terms, the number of chemical components which vary between the samples of the set (ref. 144). Knowledge of this intrinsic dimensionality, which may be much lower than the number of mass peaks per spectrum, is important for assessing the suitability of the data set for supervised learning procedures, such as the LLM (linear learning machine) approach. When using discriminant analysis techniques, such as LLM, a reliable differentiation between two or more classes of spectra can be obtained only if the number of spectra per class is at least three times the intrinsic dimensionality of the data set (ref. 145). For instance, when trying to

establish a reliable discriminant function for two or more classes of pyrograms reflecting differences in twenty chemical components, then the training set of pyrograms of known class should consist of at least sixty pyrograms for each of the classes considered. If this condition is not fulfilled, the discriminant function calculated will show poor classification performance. This requirement strongly limits the application of LLM and other discriminant analysis techniques to the classification of pyrolysis mass spectra of complex biomaterials. As discussed in Section 6.5, non-supervised techniques such as Kruskal's non-linear mapping method can be extremely useful in visualising differentiation tendencies in relatively small data sets which do not satisfy the basic requirements for discriminant techniques. A different, highly promising approach to the analysis of relatively small data sets has been developed by Wold and Sjöström (ref. 146). This approach, the so-called SIMCA technique, was recently applied to Py-GC data (ref. 147) but has not yet been tested with Curie-point Py-MS data. The SIMCA program can be obtained from Infometrix (ref. 130).

Chapter 7

SELECTED APPLICATIONS TO BIOMATERIALS

7.1. SCOPE OF ANALYTICAL PYROLYSIS TECHNIQUES

Table 9 lists the current applications of analytical pyrolysis techniques. Although far from complete, this list makes it clear that analytical pyrolysis techniques are used in all scientific and technological fields dealing with complex organic materials. In the context of this book, only applications to the analysis of biomaterials in the broadest sense will be discussed. This leaves out the analysis of synthetic polymers which is of vital importance to such diverse fields as polymer science (ref. 8), forensic science (ref. 148) and the technology of plastics, fibres and coatings (ref. 149). Some excellent reviews dealing with applications of analytical pyrolysis techniques in biomedicine (refs. 11, 12) and more specifically in the identification of microorganisms (ref. 150) have recently been published. The following discussion of selected applications to biomaterials has been divided into four sections: medical, biological, environmental and biogeochemical.

TABLE 9

Current applications of analytical pyrolysis techniques

Biological & Medical	Geochemical & Environmental	Industrial & Forensic
- biopolymers - microorganisms - cells & tissues - body fluids - biochemical fractions	- geopolymers - sediments - humic matter - sludges & water - air particulates	- plastics and fibres - coatings - natural products - vaccines & drugs - foods & beverages

7.2. MEDICAL APPLICATIONS

7.2.1. Clinical microbiology

Classification and identification of bacteria is one of the best known "classical fingerprinting" applications of analytical pyrolysis techniques (see Chapter 2). As explained in Chapter 1, this interest in fingerprinting of microorganisms originated in the search for extraterrestrial life in the early 1960's. Since then, Py-MS fingerprinting has been applied to various microorganisms, as listed in Table 10.

TABLE 10

Microbiological applications of pyrolysis mass spectrometry

Purpose	Problem	Microorganism	References
Classification	intra-species heterogeneity	<i>Mycobacterium</i>	Wieten <i>et al.</i> (123-125)
		<i>Bacillus</i>	Meuzelaar <i>et al.</i> (43,151)
		<i>Listeria</i>	Böhm and Meuzelaar (152)
		<i>Neisseria gonorrhoea</i>	Risby and Yergey (19)
		<i>Pseudomonas</i>	Eshuis <i>et al.</i> (45), Meuzelaar <i>et al.</i> (43)
		<i>Escherichia coli</i>	Borst <i>et al.</i> (153)
		<i>Anthrobacter</i>	Risby and Yergey (19)
		<i>Staphylococcus</i>	Risby and Yergey (19)
		<i>Proteus</i>	Anhalt and Fenselau (18)
		<i>Streptococcus</i>	Kistemaker <i>et al.</i> (66), Meuzelaar <i>et al.</i> (48)
epidemiology (hospital infections)		<i>Klebsiella</i>	Haverkamp <i>et al.</i> (154)
Identification	pathogenicity	<i>Escherichia coli</i>	Haverkamp <i>et al.</i> (65)
		<i>Mycobacterium</i>	Wieten <i>et al.</i> (123-125)
	cariogenicity	<i>Streptococcus</i>	Kistemaker <i>et al.</i> (66), Meuzelaar <i>et al.</i> (48)

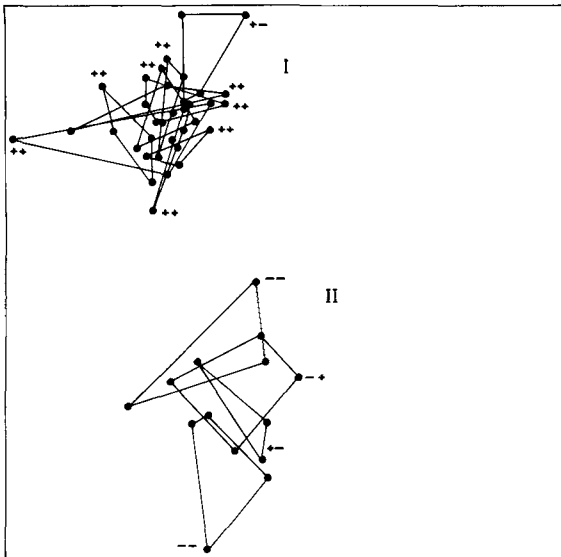


Figure 36. Non-linear map (stress 12.2%) of the pyrolysis mass spectra of 13 *Neisseria gonorrhoea* strains, showing the presence of two distinct pyrotypes. Note correlation between pyrotype II and the presence of delayed glucose utilization (- sign). Glucose utilization tests were repeated in different laboratories (see double signs).

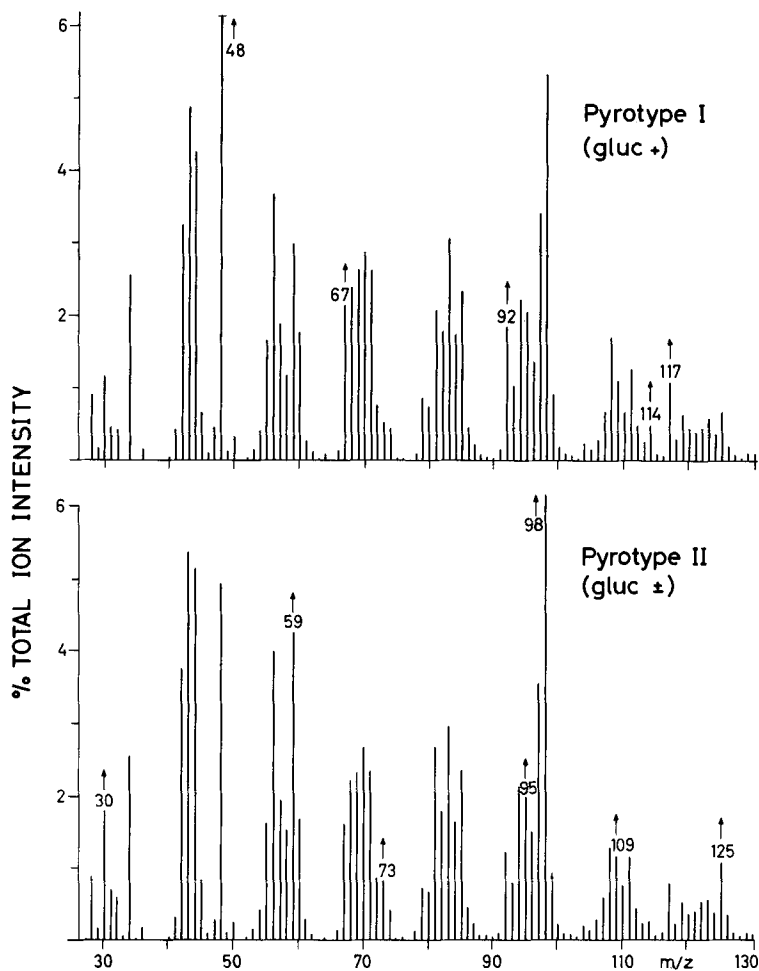


Figure 37. Examples of pyrolysis mass spectra of two different pyrotypes of *Neisseria gonorrhoea*. Arrows indicate significantly higher peak intensities. Conditions: sample 20 μ g; T_C 510°C; E_{el} 14 eV.

Figure 36 gives an example of fingerprinting results obtained by Curie-point Py-MS. Analysis of *N. gonorrhoea* strains, harvested directly from chocolate agar culture plates, showed the presence of two hitherto unknown pyrotypes. Careful study of the conventional biochemical typing results revealed a possible correlation of the two pyrotypes with the rate of glucose metabolism; pyrotype II appeared to correlate with delayed metabolic conversion of glucose. Inspection of the spectra of both pyrotypes (Figure 37) shows a complex difference, with peak intensities at m/z 48, 67, 92, 114 and 117 being higher in type I and peak intensities at m/z 30, 59, 73, 95, 98, 109 and 125 being higher in type II. Tentative biochemical interpretation

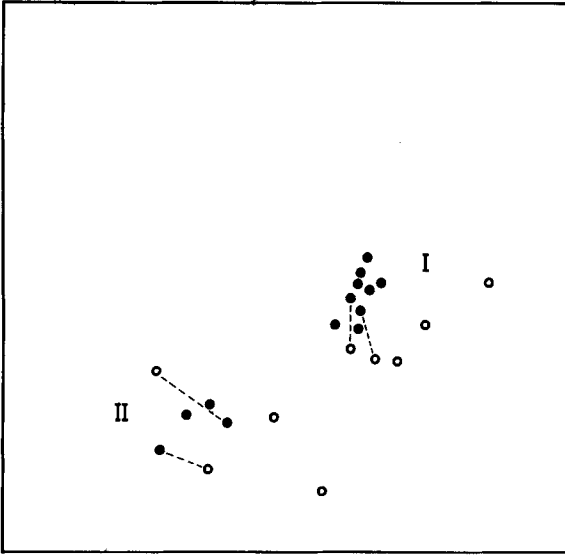


Figure 38. Non-linear map (stress 12.7%) of two sets of pyrolysis mass spectra of *Neisseria gonorrhoea* strains. One set of spectra (●) corresponds to the set shown in Figure 36 (only centroids of the replicate analyses shown here). The second set (○) was analysed 3 months later and four of these strains were identical with strains of the first set (see broken lines). Note that both pyrotypes are still clearly distinguishable after 3 months, in spite of the obvious drift in the patterns caused by changes in instrumental and/or biological conditions.

points to an increase in some N-acetylamino sugar component in type II, accompanied by a decrease in a protein component rich in methionine (m/z 48), proline (m/z 67), phenylalanine (m/z 92) and tryptophan (m/z 117). Although later analyses showed the extent of the difference to be variable, the same two pyrotypes were clearly distinguishable three months later (see Figure 38). The reproducibility of the spectra was good enough to enable the older spectra to be used as reference patterns for identifying the new spectra, even though the latter included several strains not analysed before.

Probably the most detailed studies on fingerprinting bacteria by Py-MS are those carried out by Wieten *et al.* on mycobacteria (ref. 123 - 125). The main aim of this work is the identification of clinical *Mycobacterium* strains as belonging to either *M. tuberculosis*, *M. bovis* or *M. bovis BCG*, or to other mycobacteria. The three mentioned species, together referred to as the Tuberculosis complex, are most important to man; *M. tuberculosis* and *M. bovis* are pathogenic, whereas *M. bovis BCG* is used for vaccination purposes and may also cause disease. Special computerized data processing procedures for matching unknown strains with reference strains of the Tuberculosis complex were developed so as to confirm the existing microbiological

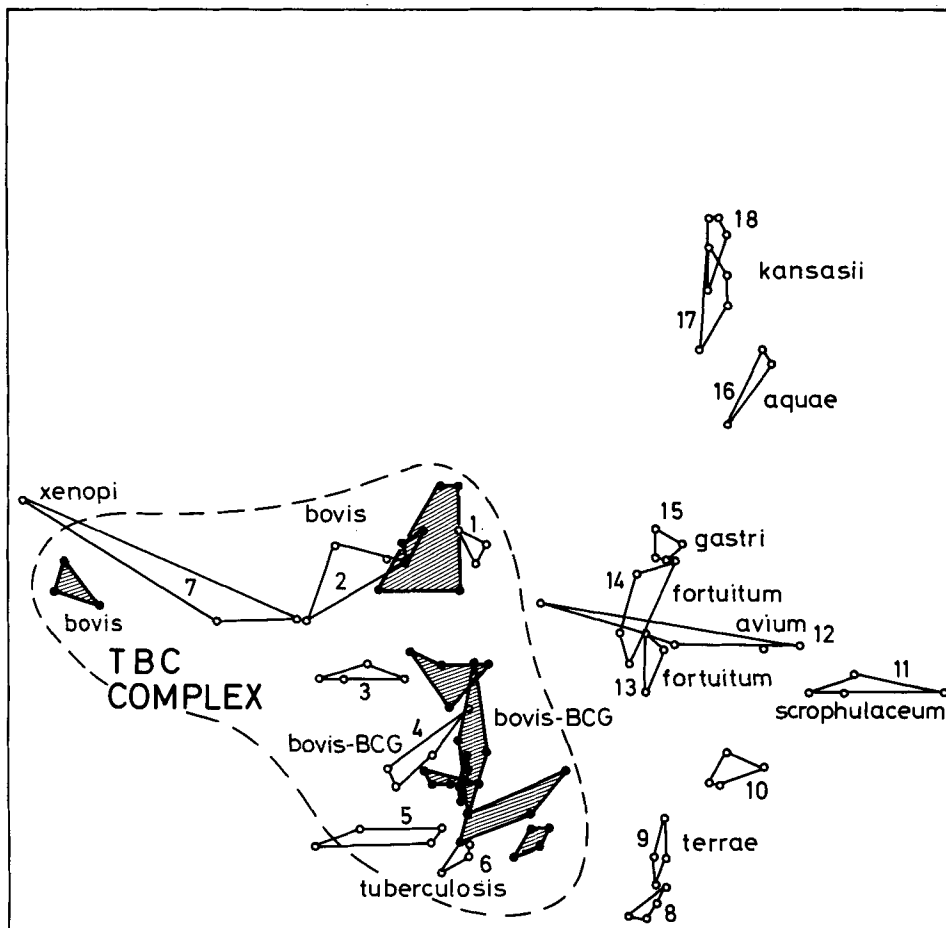


Figure 39. Non-linear map (stress 13.8%) of 18 clinical isolates of *Mycobacterium* strains and 9 reference strains of the Tuberculosis complex (shaded), calculated on the basis of the key masses m/z 31, 50, 58, 59, 71, 86, and 98. Identification of the clinical isolates as whether or not belonging to the Tuberculosis complex was made on the basis of their distance (see Section 6.4) with respect to the reference strains. In this series, strains 1-6 belong to the Tuberculosis complex, whereas strains 8-18 were identified as other, non-pathogenic mycobacteria. Strain 7, microbiologically typed as a non-Tuberculosis complex strain (*M. xenopi*), was misidentified as belonging to the Tuberculosis complex by Py-MS, using this key mass identification procedure. Note the clustering of the two strains 17 and 18, bacteriologically typed as *M. kansasii*, and also the relative closeness of strains 13 and 14 (*M. fortuitum*) and of strains 8 and 9 (*M. terrae*).

classification scheme. Identification of Tuberculosis complex strains can be made on the basis of the relative peak intensities of just seven "key masses" in the pyrolysis mass spectra (see Figure 39; ref. 124). Py-MS fingerprinting has also been used

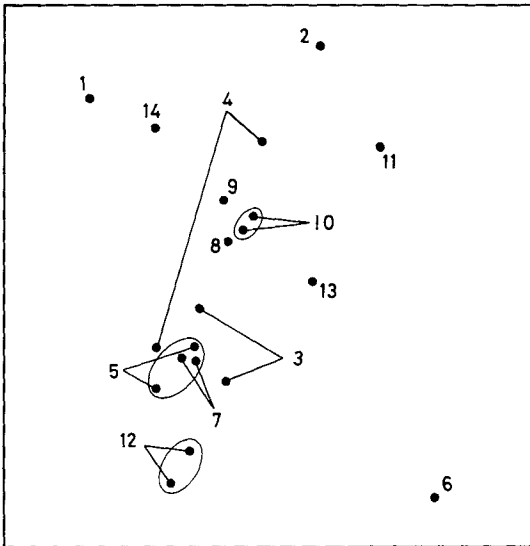


Figure 40. Non-linear map of the pyrolysis mass spectra (only centroids shown) of 20 *Klebsiella* isolates from 13 different patients (arabic numerals) in the same hospital. Encircled spectra cannot be differentiated in the distance matrix (not shown). Note that only the isolates from patients 5 and 7 are possibly identical. However, these isolates could be differentiated by conventional biotyping. Thus, no cross-infection was found to exist between patients.

for taxonomic problems within the genus *Mycobacterium* for differentiation of *M. kansasii* and *M. gastri* (ref. 125).

Apart from the above applications of fingerprinting for classification and identification, Curie-point Py-MS techniques can also be used for epidemiological purposes in microbiology, as shown in Figures 40 and 41. *Klebsiella* infections present a difficult problem in hospital epidemiology because conventional biochemical typing techniques often do not distinguish adequately between different *Klebsiella* strains and serological techniques are hampered by limited availability of reliable sera (ref. 155). The other major source of hospital infections, namely *Staphylococcus*, has so far eluded reliable classification by biochemical and serological (ref. 156) techniques, and so differentiation of *Staphylococcus* strains relies almost entirely on phage typing. However, about 10-15% of all *Staphylococcus* strains isolated in hospitals do not respond to any of the more generally available phages. In these cases, promising results have been obtained with subtyping of "phage-negative" *Staphylococcus* strains by Curie-point Py-MS (ref. 157).

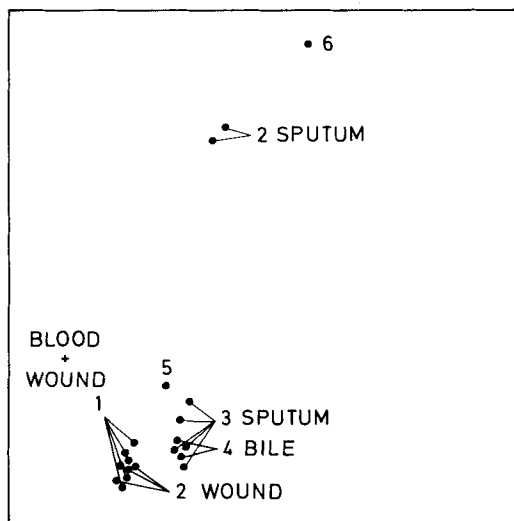


Figure 41. Non-linear map of the pyrolysis mass spectra (only centroids shown) of 20 different *Klebsiella* isolates from six patients (arabic numerals) in the same hospital. Previous analysis by conventional biotyping failed to differentiate these strains and thus the presence of a "hospital epidemic" involving six patients was concluded. Py-MS analysis, however, indicated possible cross-infections between patients 1 and 2, as well as between patients 3 and 4, only. Re-examination of the isolates of patients 5 and 6 by biotyping, showed the presence of typing errors in the first run. The isolate from patient 5 proved to be a slightly different biotype whereas the isolate from patient 6 was an altogether different species (*Enterobacter*).

7.2.2. Other clinical applications

Fast biological profiling of single drops of urine without complex sample preparation, as shown in Figure 42, is one of the newest and most promising applications of Py-MS in medicine (refs. 158, 159). Even if this approach may not be expected to detect all abnormalities detectable by a combination of other, more specific methods, such as GC or GC-MS analysis of urine extracts (refs. 160, 161), the speed and simplicity of the Py-MS technique in combination with the ease of statistical evaluation may bring biochemical profiling of urine samples as a general screening technique closer to its practical realization. A similar approach has given promising results with other body fluids such as bile (refs. 158, 159) and synovial fluids (ref. 162). Experiments with serum and spinal fluid samples also seem possible and preliminary investigations in these areas are in progress. Py-GC/MS studies (electrically heated filament) of untreated urine samples for detecting metabolic abnormalities have recently been reported by Roy (ref. 163).

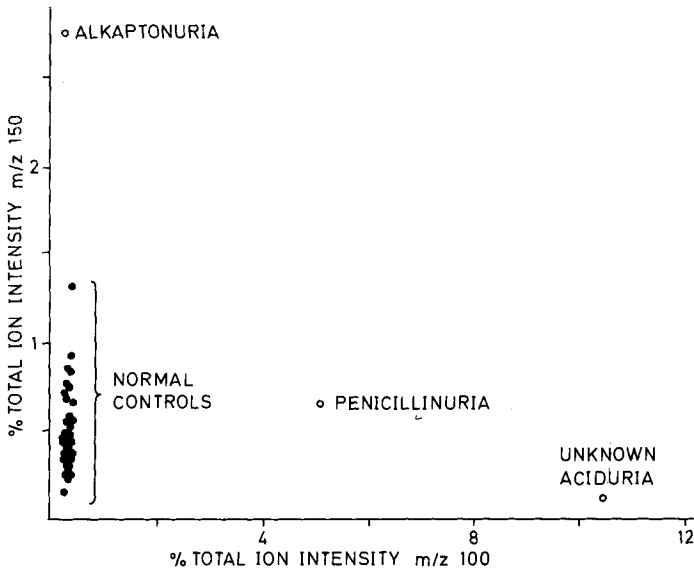


Figure 42. Scatter plot of the ion intensities at m/z 100 *versus* m/z 150 for the analysis of single drops of unprepared urine from 39 normal controls (●) and three patients (○). In the alkaptonuria case m/z 150 corresponds to the molecular ion of the (M-H₂O) pyrolysis fragment of homogentisic acid (MW 168). Similarly, in the case of the unknown aciduria m/z 100 later proved to correspond to the molecular ion of the (M-H₂O-CO₂) pyrolysis fragment of hydroxymethylglutaric acid (MW 162). The m/z 100 ion in the urine of the patient on penicillin medication is a characteristic penicillin fragment (together with other ions, e.g. at m/z 115) of unknown structure. The normal controls were not on special diets.

As shown already in the microbiological applications, Py-MS techniques are useful for the differentiation and identification of cells. In fact, some preliminary applications of differentiation of diseased *versus* normal cells, viz. fibroblasts from patients with inborn errors of metabolism (ref. 159) or leukaemic white blood cells (refs. 110, 158, 164), have been described. Despite promising results, it should be realized that the analysis of highly complex mammalian cells poses almost insurmountable problems with regard to the selection of representative samples owing to the high level of inter- and intra-individual variability encountered. These problems are even more pronounced when applying Py-MS techniques to whole tissues, e.g. the differentiation of diseased muscle tissue such as discussed in Chapter 6. However, by selecting carefully defined tissue samples the problems of inter- and intra-individual variability can be brought back to manageable proportions, as was demonstrated by Van Haard *et al.* in the analysis of cataractous eye-lens nucleus tissues (ref. 96). A model system using frog embryo cell clones was recently

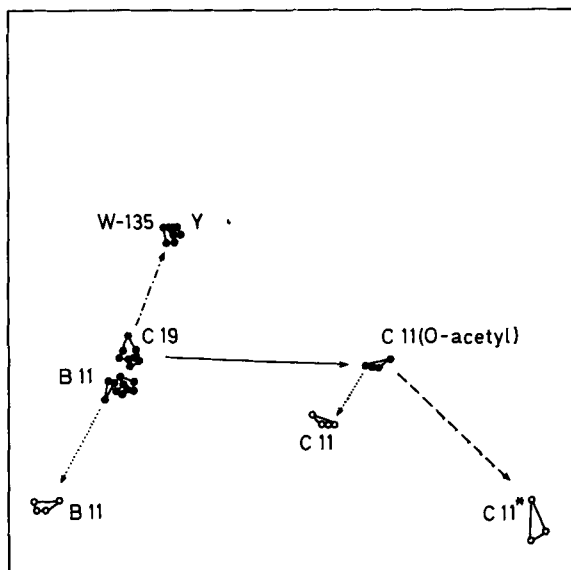


Figure 43. Non-linear map of pyrolysis mass spectra of 8 purified (●) and 3 incompletely purified (○) capsular polysaccharides of *Neisseria meningitidis* groups B, C, W-135 and Y. Groups B and C polysaccharides consist of linear chains of N-acetylneuraminic acid (sialic acid) with α (2→8) and α (2→9) glycosidic linkages, respectively. The W-135 and Y polysaccharides are composed of hexosyl-N-acetylneuraminic acid repeating units. The partially purified preparations B 11 and C 11 contain protein; the preparation C 11* contains in addition lipopolysaccharide contaminants. Note how the presence of all these differences in structure and composition results in characteristic shifts in the map: --- shift due to the presence of hexose residues; — shift due to O-acetyl substitution; ··· shift due to protein contaminants; --- shift due to lipopolysaccharide contaminants.

described as a means of evaluating the full potential of Py-MS for detecting minute biochemical differences in highly defined cell and tissue samples (ref. 165).

In spite of the above severe limitations of Py-MS applications to practical clinical samples, the technique may eventually find applications in selected clinical problems, e.g. involving early detection and diagnosis, monitoring the course and extent of a disease or evaluating the effect of therapeutic measures. As noted by Laitinen (ref. 166): "The possibilities for diagnostic use appear sufficiently promising to justify a research effort of considerable magnitude".

7.2.3. Quality control

A similar "operational fingerprinting" approach to that used in microbiology has potential application in other medical areas, as demonstrated in Figures 42 and 43. Py-MS analysis of biochemical preparations such as bacterial antigens or virus preparations to be used in vaccines (see also Section 6.7) allows rapid testing of

the overall biochemical composition of the sample (ref. 49, 63). Although this approach may not obviate the need for more specific tests, e.g. tests directly relating to the biological activity of the sample, it should provide manufacturers of complex biochemical preparations such as vaccines, drugs, beverages or foods with a unique tool for detecting the presence of unexpected contaminants or chemically altered components incurred during the manufacturing process.

7.3. BIOLOGICAL APPLICATIONS

Biological applications encompass a potentially broad area ranging from the analysis of biopolymers and lower unicellular or multicellular organisms, to plant and animal tissues or even whole ecological systems. Most of this vast area still remains unexplored by pyrolytic techniques. The analysis of biopolymer preparations (refs. 46 - 48) and the differentiation of yeasts and fungi (refs. 70, 167 - 169) represent areas where Py-MS techniques have made some progress. Classification of fungi presents challenging problems in view of the inaccessibility of some types of fungi to conventional morphological classification techniques. Examples are the differentiation of *Endogonaceae* species reported by Weijman and Meuzelaar (ref. 170) using Curie-point Py-MS, and the characterization of rust spores, including the economically highly important coffee rust *Hemileia vastatrix* by Meuzelaar (ref. 171). A Curie-point Py-MS spectrum of *Hemileia vastatrix* is shown in Figure 44. Analysis of this spectrum reveals the presence of considerable amounts of N-acetylamino sugar fragments, probably originating mainly from chitin (see Atlas) localised in the spores, which could point the way to new approaches towards coffee rust control. As already mentioned in Section 6.7, factor analysis techniques have been used for the comparative analysis of pyrolysis mass spectra of yeasts and provide a powerful method for chemotaxonomic studies of yeast species.

Boon *et al.* (ref. 172) studied the variations in the cell wall composition of *Bacillus subtilis* resulting from differences in the composition of the culturing medium. The microorganism synthesises the acidic polysaccharide teichoic acid when grown in a phosphate-rich environment, whereas under phosphate limiting conditions mainly the phosphorus-free polysaccharide teichuronic acid is produced. These differences in cell wall compositions become directly clear on Py-MS analysis of the complete cells or of the isolated cell walls. Py-MS is also a valid tool for studying the biodegradation of organic matter in sediments, as was demonstrated in a study of sediment digestion by the lugworm *Arenicola marina* in a benthic marine ecosystem (ref. 173).

An intriguing application of pyrolysis techniques in the detection of plant diseases was reported by Myers and Watson in 1969 (ref. 174) and more recently by Marais and Kotzé (ref. 175). Using Py-GC techniques, these authors detected characteristic changes in the pyrolysis patterns of whole plant tissues diagnostic of a

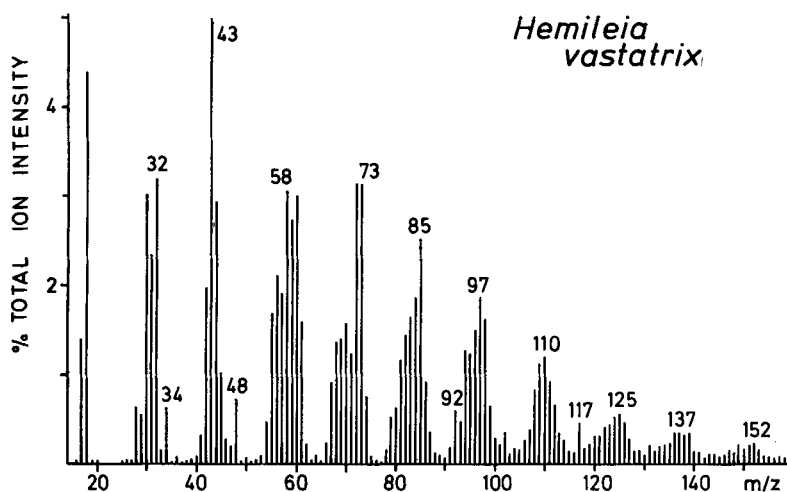


Figure 44. Pyrolysis mass spectrum of *Hemileia vastatrix* (coffee rust). Conditions: sample 5 μ g; T_c 510°C; E_{e1} 14 eV.

given type of infection. Recent studies of virus-infected leaf tissues by Py-MS confirmed the existence of characteristic changes in the pyrolysis profiles in some cases where the morphological lesions were indistinguishable and the infection could be firmly diagnosed only by lengthy virus culturing techniques (ref. 176).

An important class of problems in agricultural science which can be addressed by Py-MS techniques is the elucidation of the composition and structure of soil humic compounds such as humic acids and fulvic acids, and the relationship with soil fertility and plant development. Analytical pyrolysis studies of these compounds were first reported by Nagar (ref. 177) using Py-GC. Later studies by other authors included Py-GC (ref. 178), Py-GC-MS (refs. 180 - 182) and direct Py-MS (refs. 179, 183 - 186). Halma *et al.* (ref. 51) and Bracewell *et al.* (ref. 183) showed the possibility of characterising the organic material in soil by directly pyrolysing whole soil samples, obviating the lengthy and ill-defined extraction and fractionation steps for isolating humic substances. Progression of the stage of humification can readily be detected, as the pyrolysis mass spectrum shows the gradual loss of methoxyphenols (lignin), the loss of some polysaccharide products, and increase of aromatic components and alkyl-pyrroles (ref. 186). Py-MS investigations of seasonal changes in fulvic acid patterns from lake water were carried out by De Haan *et al.* (ref. 187). As examples of pyrolysis mass spectra of these types of complex organic materials, some typical spectra of soil and soil fractions are given in Figure 45.

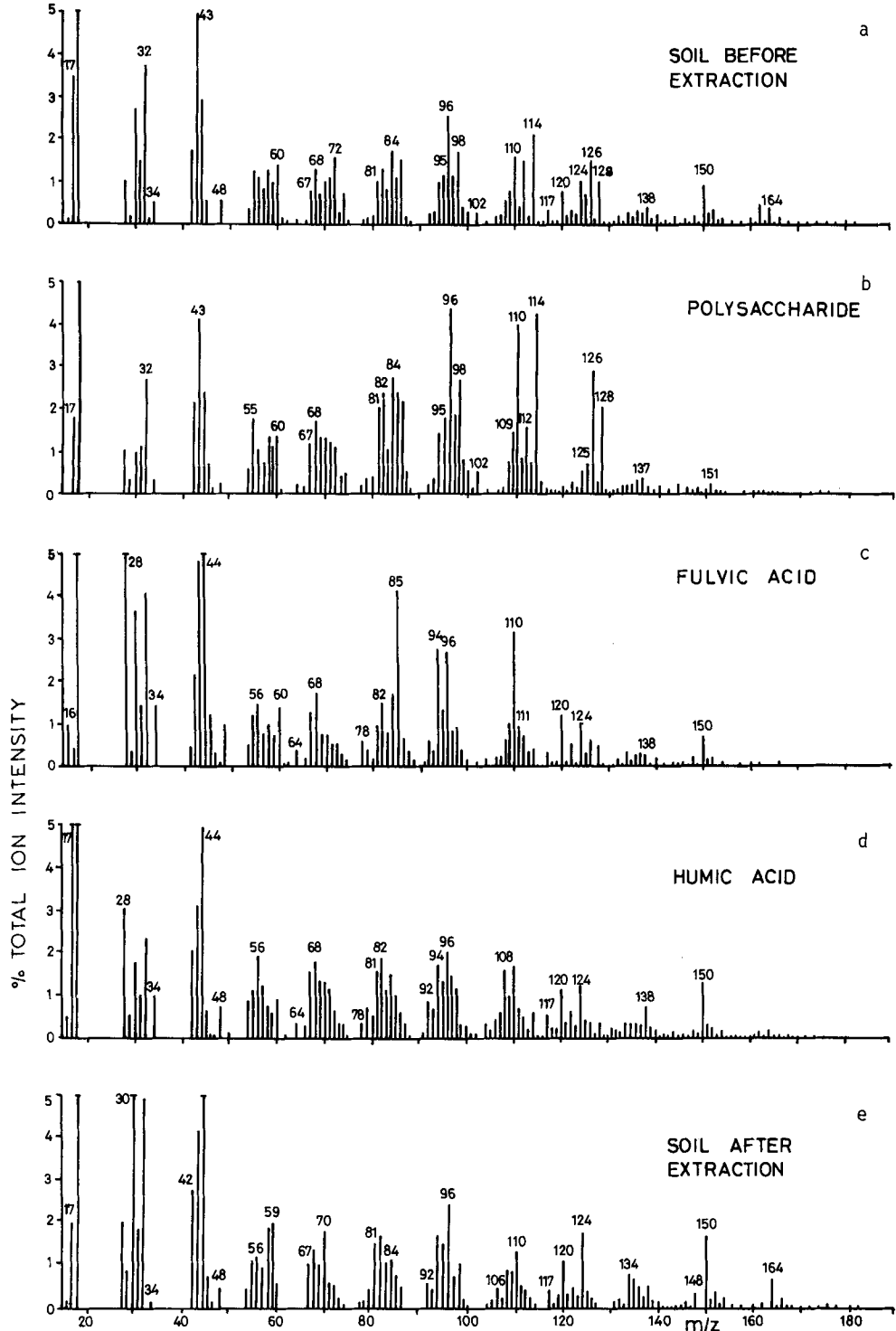


Figure 45. Pyrolysis mass spectra of whole soil, soil humic fractions and extracted soil from the A1 horizon of a brown soil on granite (Typic Xerochrept) as described by Saiz-Jimenez *et al.* (refs. 185, 188). Note the dominance of carbohydrate-type signals in the unextracted soil sample (a). Most of these carbohydrates are removed in the first water-extraction step and form the highly complex polysaccharide fraction (b) which exhibits typical hexose (m/z 102, 126), pentose (m/z 114), deoxyhexose (m/z 128) and hexosamine (m/z 125, 137, 151) signals. The fulvic acid pattern (c) appears to consist of a mixture of furan-type fragments (e.g. m/z 68, 82, 96, 110) and aromatic fragments (e.g. m/z 78, 94, 120, 124, 138, 150), several of which are lignin-derived molecular units. Compared with that of fulvic acid, the humic acid pattern (d) shows even more prominent aromatic signals, in addition to pyrrole (m/z 67, 81, 95) and indole (m/z 117, 131) series. The pattern of extracted soil (e) shows a high degree of similarity to the humic acid pattern indicating the presence of unextractable humic acid-like materials, known as humins. Also note that characteristic lignin-type fragments at m/z 124, 150 and 164 are abundant in extracted soil. Throughout all spectra, sulphur-containing ion signals are more or less apparent at m/z 34 (H_2S), 48 (CH_3SH) and 64 (SO_2), although these appear to be equally pronounced in the fulvic and humic acid fractions.

7.4. ENVIRONMENTAL APPLICATIONS

Environmental samples studied by pyrolytic techniques encompass soil, water, and air. Although primarily studied for their possible role in soil fertility and stability, as discussed in the previous section, it is now recognised that humic substances play an important role in environmental problems because of their capacity for binding large amounts of organic and inorganic substances such as pesticide residues and heavy metals, which constitute potential environmental threats (ref. 189). A Curie-point Py-MS study of the organic fraction of river sludge samples from the Rhine delta, containing relatively high heavy metal concentrations, was recently reported by Van de Meent *et al.* (ref. 190). Although heavy metals appear to be effectively trapped by the strong chelating action of fulvic acids and other organic fractions, drastic changes in sediment pH or other physicochemical parameters might possibly lead to a sudden release of these metals into the environment. As a consequence, further studies of the organic structure and chelating properties of soil humic compounds in marine and terrestrial environments are strongly indicated.

An artificial "soil" unusually rich in organic compounds, but probably influenced by the same microflora as active in natural soils, is sewage sludge. Figure 46 shows spectra of aerobic and anaerobic sewage sludge. The pattern of the aerobically degraded sludge shows dominant protein patterns presumably derived from the bacterial cell mass composing most of the organic material. Other noteworthy features are the large nitric oxide peak at m/z 30, derived from pyrolytic degradation of nitrates, and the series of phenolic peaks in the higher mass range, typical of lignin thus showing the unusual resistance of this plant polymer against microbial degradation. As shown by De Leeuw (ref. 191), the lignin contribution in sewage sludge is mainly derived from toilet paper. The anaerobic (fermented) sludge spectrum is dominated by series of polysaccharide peaks, either signifying a basic difference in the composition of anaerobic microorganisms or showing the presence of incompletely degraded

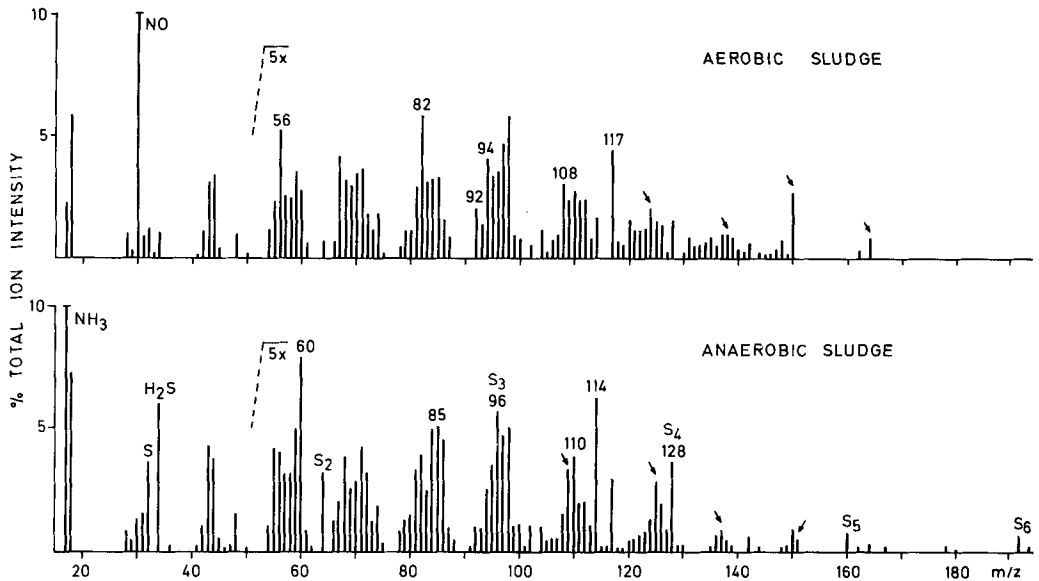


Figure 46. Pyrolysis mass spectra of sludge samples from an aerobic (Pasveer ditch) and an anaerobic (fermentative) sewage treatment plant. The arrows in the upper spectrum point to a typical lignin series at m/z 124, 138, 150 and 164. The arrows in the lower spectrum reveal an ion series (m/z 109, 125, 137 and 151) characteristic of N-acetylamino sugars. For further biochemical interpretation, see text. Conditions: samples 20 μg ; T_c 610°C; E_e 15 eV.

carbohydrate input materials. The anaerobic nature of the sludge is demonstrated well by the strong NH_3 peak at m/z 17 and the H_2S and S_2 peaks at m/z 34 and 64, respectively. A remarkable feature is the presence of S_5^+ and S_6^+ ions at m/z 160 and 192, respectively. Separate experiments showed these signals to be derived from electron impact ionization of S_8 , formed by direct evaporation of elemental sulphur, present in the sample. The molecular ion peak (at m/z 256) is outside the mass range of this spectrum. At the higher end of the mass scale a typical N-acetylamino sugar series is found (at m/z 109, 125, 137, 151), possibly derived from the muramic acid moieties of bacterial cell walls. The ability of Py-MS techniques to characterise sludges is potentially valuable in the process control of sludge treatment procedures as well as in judging the suitability of sewage and other sludges for recycling as cattle food, soil fertilizer or building material.

The possibility of characterising water samples by Py-MS is illustrated in Figure 47, showing spectra obtained from single drops of water taken from the inlet and outlet systems of anaerobic and aerobic sewage treatment plants. The lower mass range of the spectra shows the obvious decrease in organic signals after treatment in both cases. However, whereas the aerobically treated water is extremely rich in

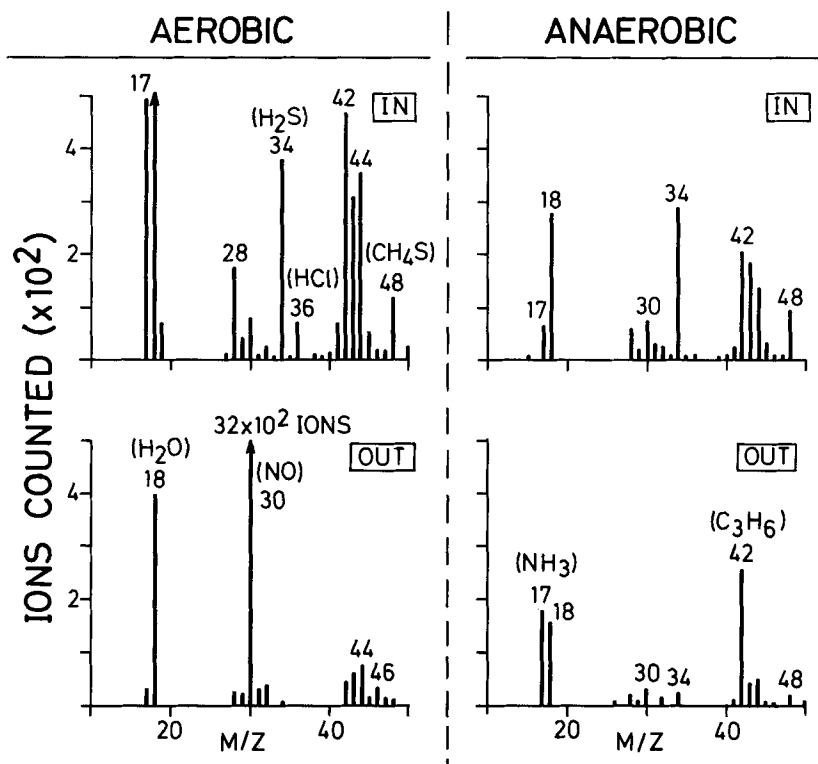


Figure 47. Pyrolysis mass spectra of single drops of unprepared water samples from the inlet and outlet process streams of aerobic and anaerobic sewage treatment plants. Conditions: samples 5 μ l; T_c 610°C; E_{e1} 15 eV.

nitrates as evidenced by the high peak at m/z 30, the spectrum of the anaerobically treated sample shows a strong NH_3^+ peak and an aliphatic signal at m/z 42. Obviously, the information obtainable from the water samples may be used to complement the results of the sludge analyses. Moreover, the water profiles might be used directly to judge the efficiency of the treatment procedure as well as the suitability of the treated water for different types of use. Other potential applications of profiling the organic (as well as some of the inorganic) compounds in water samples are the analysis of samples from streams and ponds for the presence of lignin sulphonates and other non-volatile organic pollutants.

The application of Curie-point Py-MS to the characterisation of organic pollutants in air, by analysing trapped air particulates, has been reported by Voorhees *et al.* (ref. 192). Samples were collected on quartz filters and the exposed portions of these filters ground and suspended in methanol. An aliquot of this suspension was applied to the Curie-point wire for analysis. Particulates from several well characterised sources were collected and analysed, as shown in Figure 48. Particulates of unknown origin might be identified by comparing their Py-MS patterns with those of

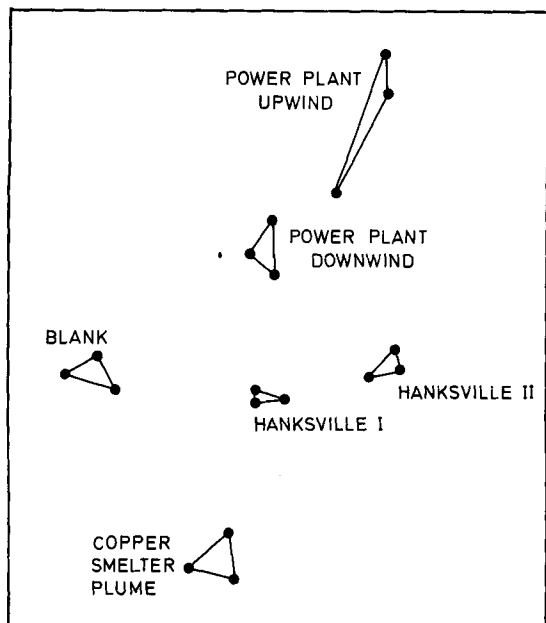


Figure 48. Non-linear map (stress 4.2%) of the pyrolysis mass spectra of air particulates collected at various discrete sources ("Power plant" is a coal-fired power plant; "Hanksville I" is a desert sample; "Hanksville II" is a sample taken two days later at the same location; "Blank" is a sample of clean, unused quartz filter).

reference particulates. In principle, this technique might also be extended to the characterisation of organic particulates generated in fires, e.g. for the purpose of assessing the chemical nature of substances inhaled by firefighters.

7.5. BIOGEOCHEMICAL APPLICATIONS

Figure 49 shows the pyrolysis mass spectra of two different types of peat. Whereas the Sphagnum peat exhibits an almost strictly polysaccharide pattern, the bog peat spectrum exhibits additional strong phenolic ion series typical of lignins (see lignin spectrum in Figure 10). This agrees with the absence of true lignins in Sphagnum moss. The only lignin-like constituent of Sphagnum moss - sphagnol (ref. 85) - probably gives rise to the non-methoxylated phenolic series at m/z 94, 108, 120 and 134. Also note the absence of pyrolytic methane formation from methoxyl groups in Sphagnum peat. Bog peat, however, is composed to a large extent of wool grass and other higher plant residues (ref. 184). Therefore it contains grass lignins characterised by the presence of methoxylated phenolic series derived from guaiacylic (m/z 124, 138, 150 and 164), and syringylic (weak signals at m/z 154, 168, and 180) building blocks in addition to the non-methoxylated series found in sphagnol (ref. 97).

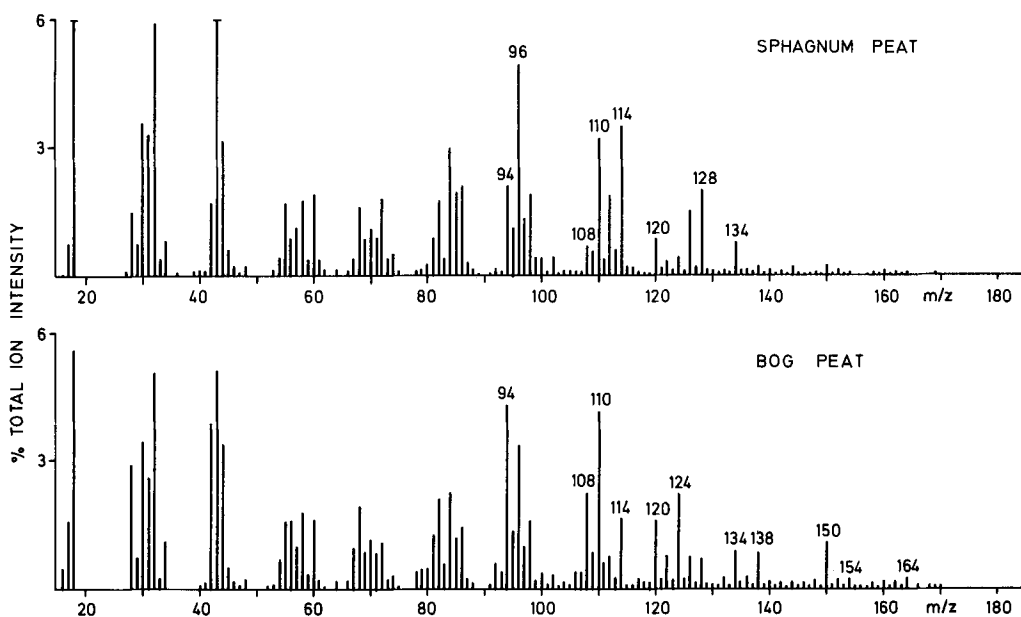


Figure 49. Pyrolysis mass spectra of peat samples, showing predominant polysaccharide patterns plus typical phenolic series derived from sphagnol (m/z 94, 108, 120, and 134; upper trace) and grass lignins (m/z 124, 138, 150, 154, and 164; lower trace). Conditions: samples 25 μg ; T_c 510°C; E_e 15 eV.

Lignin-derived signals can even be found in much older geochemical formations, such as brown coals or oil shales. In this context, it is interesting to note that lignin-type fragment series have been observed in the pyrolysates of fossil wood, petrified under various conditions, e.g. the silicified wood of the Petrified Forest National Park in Arizona (ref. 193). The German brown coal sample shown in Figure 50 (b) exhibits a strong dominance of phenolic signals which closely resemble the spectrum of recent lignins (see Figure 10). Since this brown coal, a Herzogenrath lignite of Miocene age, is mainly composed of redwood residues, the lignin originally must have been accompanied by large amounts of cellulose and hemicelluloses (see Figure 50 (a)). Apparently, the latter have disappeared selectively, leaving only the lignin-like materials. When coalification progresses further these lignin-like materials rapidly lose their methoxyl groups by demethylation, resulting in the formation of dihydroxybenzene moieties. A prominent dihydroxybenzene peak at m/z 110 is already visible in the lignite spectrum in Figure 50 (a) and is still a dominant feature in the subbituminous coal spectrum in Figure 51 (a). However, as shown in Figure 51 the dihydroxybenzene series strongly decreases with increasing degree of coalification ("rank"), followed by the phenols and sulphur-containing ion signals.

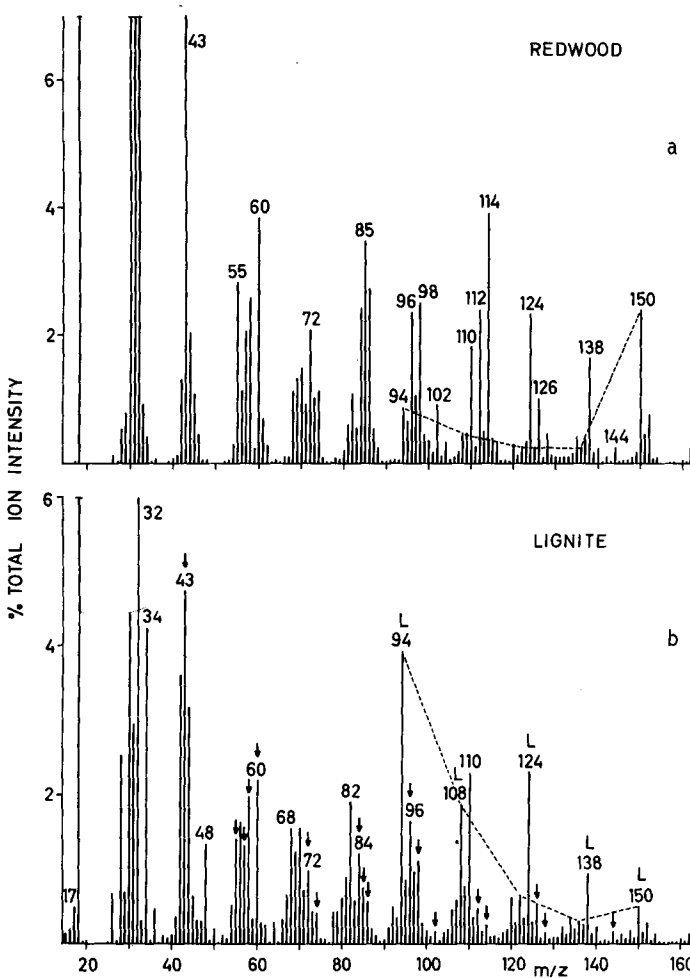


Figure 50. Pyrolysis mass spectra of (a) a recent redwood and (b) a brown coal (Herzogenrath lignite). Note the obvious decrease of the cellulose and hemicellulose fragment series (m/z 43, 55, 57, 58, 60, 72, 74, 84, 85, 86, 96, 98, 102, 112, 114, 126, 128, 144) in the lignite spectrum with respect to the recent redwood (indicated by arrows). Conditions: samples 10 μg ; T_c 510°C; E_{e1} 14 eV.

The relative intensity of hydrocarbon series, e.g., alkenes, naphthalenes and benzenes, increases with rank. That the differences between the spectra in Figure 51 are indeed mainly due to rank was established by Meuzelaar *et al.* (ref. 194) in a study of over 100 coals from the Rocky Mountain Province. However, this study also showed that the influence of differences in depositional environment on the pyrolysis patterns is often difficult to distinguish from the influence of differences in rank. The effects of depositional environment and degree of coalification on conventional

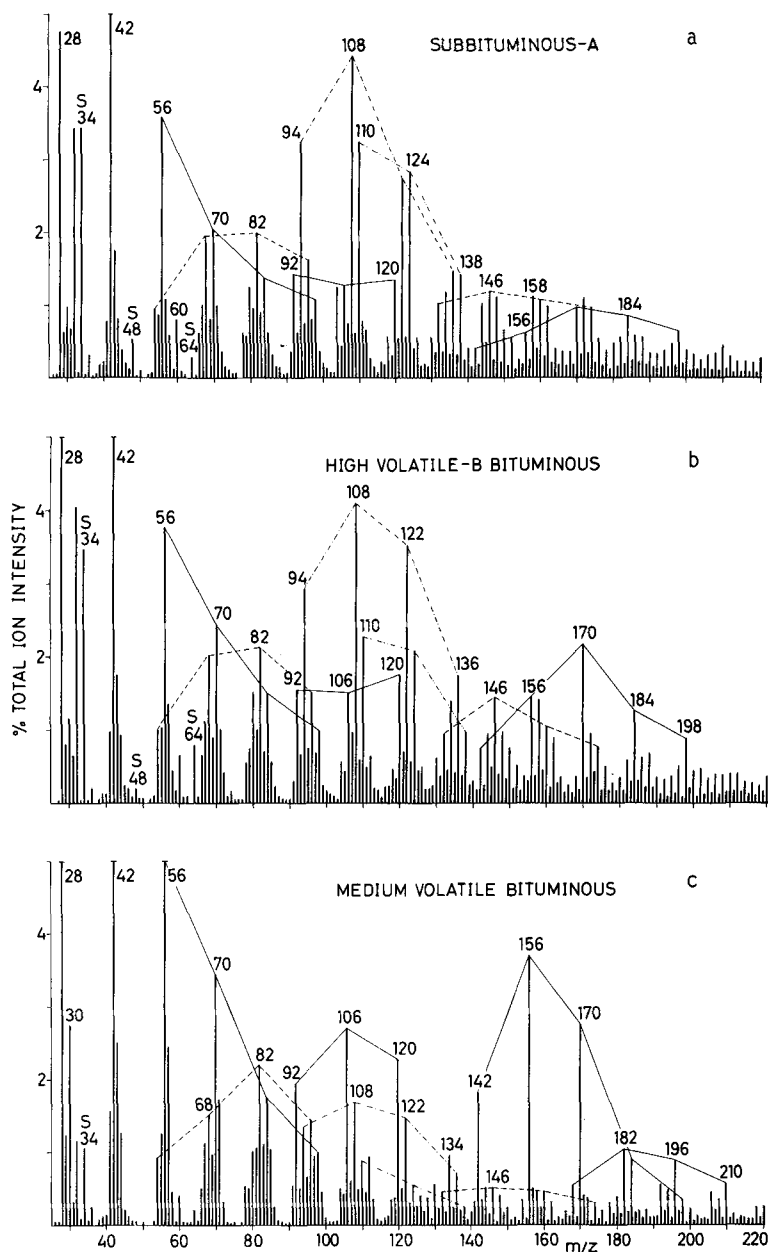


Figure 51. Pyrolysis mass spectra of three coal samples of different rank from the Uintah Region in the Rocky Mountain Coal Province (USA). Note the rapid decrease in dihydroxybenzenes (m/z 110, 124, 138) followed by phenols (m/z 94, 108, 122, 136) and sulphur-containing ions (m/z 34, 48, 64) as opposed to the strong increase in naphthalenes (m/z 142, 156, 170, 184, 198), benzenes (m/z 92, 106, 120, 134) and alkenes (m/z 56, 70, 84). Each spectrum was obtained by averaging quadruplicate analyses. Conditions: samples 50 μ g; T_c 610°C; E_e 15 eV.

coal parameters, e.g. elemental composition, moisture content, calorific value, etc., have been authoritatively described by Teichmüller and Teichmüller (ref. 195).

No spectra of coals of higher rank than medium volatile bituminous are shown here because the highly condensed aromatic nature of such coals results in abundant char formation accompanied by very low yields of detectable pyrolysis products (see also Chapter 5.1). However, it should be pointed out that the rank of a coal is to a large extent independent of its age. Some low rank, e.g. high volatile bituminous, coals were deposited during the Carboniferous Period whereas the medium volatile bituminous coal shown in Figure 51 (c) is only of Cretaceous age but was coalified more rapidly because of locally high geothermal gradients.

Van Graas *et al.* (refs. 73, 196) analysed series of coal samples by Py-MS and Py-GC/MS. They demonstrated that the spectra can be explained in terms of the maceral ("coal mineral") composition of the samples. The pyrolysis mass spectra of macerals included in the Atlas part of this volume show the marked differences between these materials. Factor analysis (see Section 6.6.2) of the pyrolysis mass spectra of a series of diagenetically different humic coals (same input materials) revealed that the main factor calculated represented a series of alkyl-substituted phenols, indanes, indenes and benzofurans. Although this set of aromatic fragments cannot simply be ascribed to one particular macromolecular component of the coals, the score of this factor is strongly correlated with the coal rank, i.e. the degree of coalification (ref. 73). Also other chemical features of coal, e.g. the degree of aromaticity or unsaturation, and the presence of sulphur- or oxygen-containing moieties - important factors in industrial coal processing - can be monitored by Py-MS (ref. 98). Altogether, Py-MS appears to be rapidly evolving into an important tool for coal characterisation.

Applications of Py-MS to the characterisation and structural analysis of oil shales and their kerogens have been reported by Maters *et al.* (ref. 52) and Wojcik *et al.* (ref. 197) employing the Curie-point and other pyrolysis methods. Different approaches, based on Py-GC/MS and selected ion monitoring have been reported by Solli *et al.* (refs. 198 - 199), Larter *et al.* (ref. 200) and Van de Meent *et al.* (ref. 201). Figure 52 shows the pyrolysis mass spectra of kerogens from three different oil shales, namely Green River shale, Tasmanite and Messel shale. In spite of considerable age difference, the Tasmanite kerogen (250 million years) closely resembles the Green River shale kerogen (50 million years). Whereas Tasmanite and (probably) Green River shale are primarily of algal origin (ref. 52), Messel shale was deposited 50 million years ago in a lacustrine environment and contains considerable amounts of plant residues (ref. 52). The spectrum of Messel shale differs from the other two shales in that it shows the presence of phenolic series typical of lignin, e.g., at m/z 124, 138, 150 and 164. The presence of such methoxylated phenols was confirmed by Maters *et al.* (ref. 52) using Py-GC/MS techniques. A more detailed inspection of the pyrolysis mass spectra of Tasmanite and Green River shale kerogen shows the

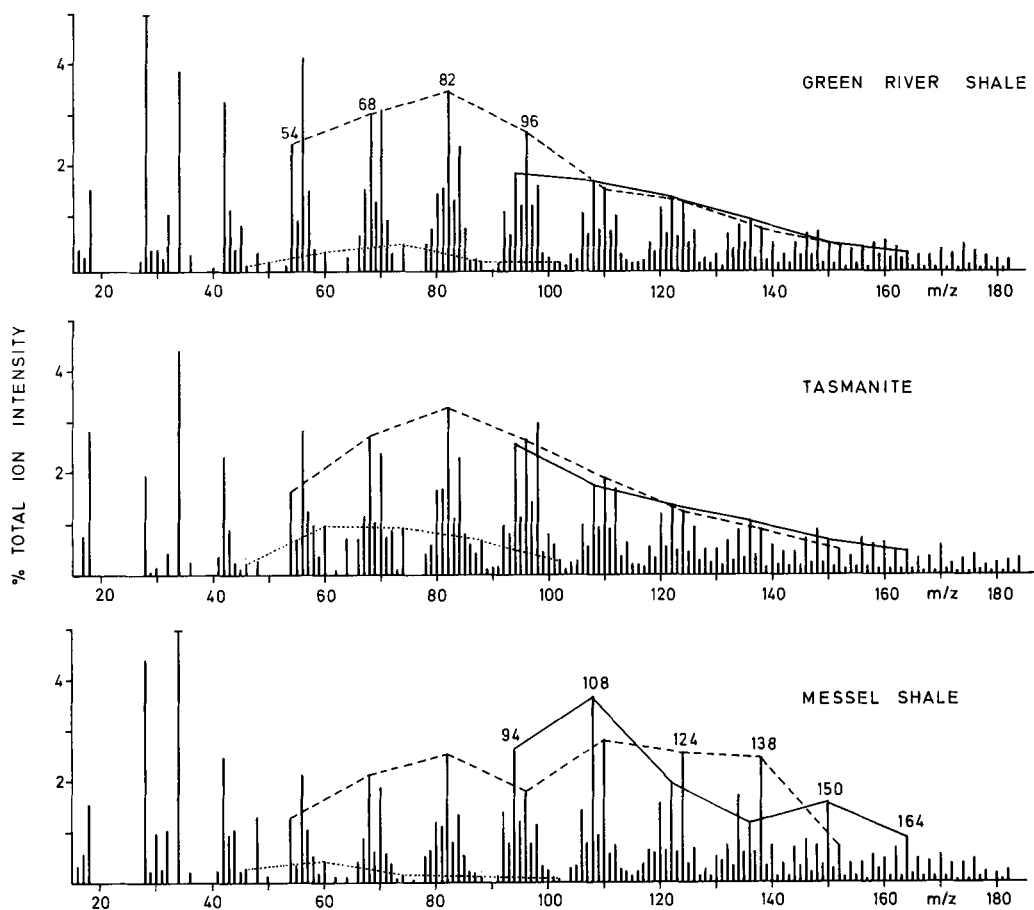


Figure 52. Pyrolysis mass spectra of kerogens from three different oil shales. Note the strong similarity between patterns of Tasmanite (algal) kerogen and of Green River shale kerogen. Further note typical "lignin" series (m/z 94, 108, 124, 138, 150 and 164) in Messel kerogen. Conditions: samples 20 μg ; T_c 610°C; E_e 15 eV.

pyrolysates to be mainly composed of aliphatic hydrocarbons exhibiting varying degrees of unsaturation. Apart from small ammonia peaks (m/z 17), no strong nitrogen-containing ion series appear to be present. Marked sulphur-containing ions at m/z 34 (H_2S), 48 (CH_3SH) and 64 (SO_2 and/or S_2) point to the marine origin of the samples. All of these conclusions, which can be reached by direct inspection of the pyrolysis mass spectrum, confirm the currently held views about the chemical structure of algal kerogens (ref. 202). Moreover, Py-MS can sometimes be applied directly to the whole shale samples without the need for elaborate preparation of kerogens, since spectra obtained from the whole shales may closely match the kerogen spectra (ref. 52).

Whereas the above discussed results show the potential importance of Py-MS techniques for the characterisation of geopolymers of interest, Py-MS techniques have also been applied to more fundamental problems in biogeochemistry. Van der Meide *et al.* (ref. 203) have reported the use of Curie-point Py-MS for structural studies on organic fractions from fossil Nautilus shells. It would also be interesting to compare fingerprints of well-defined plant remains preserved in coal seams. In spite of the extensive chemical transformation, characteristic differences might still be found. Such differences could be of potential use in palaeotaxonomy. In this context, the Py-MS (and Py-GC/MS) studies of Schenck *et al.* on differentiation between pollen and spores of different origins (ref. 74) as well as between defined entities within the kerogen matrix should be mentioned.

PART II

ATLAS OF SELECTED PYROLYSIS MASS SPECTRA

This Page Intentionally Left Blank

PART II ATLAS OF SELECTED PYROLYSIS MASS SPECTRA

CONTENTS	101
1. INTRODUCTION	105
1.1. General remarks	105
1.2. Sample preparation	105
1.3. Analytical conditions	106
1.4. Spectrum presentation format	106
1.5. Spectrum contributions from inorganic constituents	107
1.6. Protein spectra (group B)	109
1.7. Nucleotide and nucleic acid spectra (group C)	110
1.8. Lipid spectra (group D)	110
1.9. Spectra of humic materials and geopolymers (group F)	110
1.10. Spectra of other biochemically important compounds (group G)	111
2. PYROLYSIS MASS SPECTRA	113
GROUP A. CARBOHYDRATES AND GLYCOCONJUGATES	113
A.1 CELLULOSE	115
A.1a CELLULOSE	116
A.2 AMYLOSE	117
A.3 NIGERAN	118
A.4 GLYCOGEN	119
A.5 CARRAGHEENAN	120
A.6 AGAROSE	121
A.7 INULIN	122
A.8 POLYGALACTURONIC ACID	123
A.9 ALGINIC ACID	124
A.10 FUCOIDAN	125
A.11 ARABINAN	126
A.12 CHITOSAN	127
A.12a CHITOSAN	128
A.13 CHITIN	129
A.13a CHITIN	130
A.14 CAPSULAR POLYSACCHARIDE <i>N. meningitidis</i> group X	131
A.15 CAPSULAR POLYSACCHARIDE <i>N. meningitidis</i> group A	132
A.16 HYALURONIC ACID	133
A.17 CHONDROITIN SULPHATE C	134
A.17a CHONDROITIN SULPHATE C	135
A.18 CHONDROITIN SULPHATE A	136
A.18a CHONDROITIN SULPHATE A	137
A.19 TEICHURONIC ACID	138
A.19a TEICHURONIC ACID	139
A.20 CAPSULAR POLYSACCHARIDE <i>N. meningitidis</i> group 29E	140
A.20a CAPSULAR POLYSACCHARIDE <i>N. meningitidis</i> group 29E	141
A.21 2-KETO-3-DEOXYOCTONATE (KDO)	142
A.22 TEICHOIC ACID <i>B. subtilis</i>	143
A.23 CAPSULAR POLYSACCHARIDE <i>N. meningitidis</i> group B	144

A.24	CAPSULAR POLYSACCHARIDE <i>H. influenzae</i> type B	145
A.25	PEPTIDOGLYCAN <i>B. subtilis</i>	146
A.25a	PEPTIDOGLYCAN <i>B. subtilis</i>	147
A.26	TETRAHEXOSYLCERAMIDE	148
A.27	GANGLIOSIDE GT1b	149
GROUP B.	PEPTIDES AND PROTEINS	151
B.1	ADRENOCORTICOTROPIC HORMONE fragment ACTH 1-24	153
B.2	ADRENOCORTICOTROPIC HORMONE fragment ACTH 1-10	154
B.3	ADRENOCORTICOTROPIC HORMONE fragment ACTH 11-24	155
B.4	INSULIN	156
B.4a	INSULIN	157
B.5	RIBONUCLEASE-A	158
B.6	DEOXYRIBONUCLEASE I	159
B.7	LYSOZYME	160
B.8	HEMOGLOBIN	161
B.9	CYTOCHROME C	162
B.10	MYOGLOBIN	163
B.11	KERATIN	164
B.12	COLLAGEN	165
B.13	CERULOPLASMIN	166
GROUP C.	NUCLEOTIDES AND NUCLEIC ACIDS	167
C.1	RIBONUCLEIC ACID (RNA)	169
C.2	DEOXYRIBONUCLEIC ACID (DNA)	170
C.3	ADENOSINE-5'-PHOSPHATE (5'-AMP)	171
C.4	ADENOSINE-5'-PHOSPHATE (5'-AMP)	172
C.5	ADENOSINE-3'-PHOSPHATE (3'-AMP)	173
C.6	ADENOSINE-3',5'-PHOSPHATE (cyclic AMP)	174
C.7	THYMIDINE-5'-PHOSPHATE (5'-TMP)	175
C.8	NICOTINAMIDE ADENINE DINUCLEOTIDE PHOSPHATE (NADPH)	176
C.9	NICOTINAMIDE ADENINE DINUCLEOTIDE (NADH)	177
GROUP D.	LIPIDS	179
D.1	SODIUM LAURYL SULPHATE	181
D.2	LINOLIC ACID	182
D.3	α -LINOLEIC ACID METHYL ESTER	183
D.4	γ -LINOLEIC ACID METHYL ESTER	184
D.5	OCTADECADIENOIC ACID	185
D.6	TRICAPRYLIN	186
D.7	TRILAURIN	187
D.8	TRIPALMITIN	188
D.9	CHOLESTEROL	189
D.10	STIGMASTEROL	190
D.11	ERGOSTEROL	191
D.12	L- α -LECITHIN	192
D.12a	L- α -LECITHIN	193
GROUP E.	NATURAL PRODUCTS	195
E.1	COTTON	197
E.2	FLAX	198
E.3	BURLAP	199
E.4	SILK	200
E.5	SHEEP WOOL	201
E.6	CAMEL HAIR	202
E.7	NATURAL RUBBER	203

E.8	TANNIN	204
E.9	WHEAT STRAW LIGNIN	205
E.10	WHEAT STRAW LIGNIN	206
E.11	DOUGLAS FIR WOOD	207
E.12	CORK	208
E.13	POLLEN	209
E.14	BREWER'S YEAST	210
E.15	WHEAT FLOUR	211
E.16	SPHAGNUM MOSS	212
GROUP F.	HUMIC MATERIALS AND GEOPOLYMERS	213
F.1	GRANITE BROWN SOIL	215
F.2	RIVER CLAY	216
F.3	RIVER SEDIMENT	217
F.4	SOIL POLYSACCHARIDE	218
F.5	FULVIC ACID	219
F.6	HUMIC ACID	220
F.7	HUMIC ACID	221
F.8	COORONGITE	222
F.9	TORBANITE	223
F.10	TORBANITE	224
F.11	GREEN RIVER SHALE	225
F.12	MESSEL SHALE	226
F.13	GILSONITE	227
F.14	BOG PEAT	228
F.15	SPHAGNUM PEAT	229
F.16	LIGNITE	230
F.17	HIGH VOLATILE C BITUMINOUS COAL	231
F.18	HIGH VOLATILE C BITUMINOUS COAL	232
F.19	HIGH VOLATILE B BITUMINOUS COAL	233
F.20	HIGH VOLATILE A BITUMINOUS COAL	234
F.21	MEDIUM VOLATILE BITUMINOUS COAL	235
F.22	BOGHEAD COAL	236
F.23	BOGHEAD COAL	237
F.24	FUSINITE	238
F.25	SPORINITE	239
F.26	VITRINITE	240
F.27	AMBER (Resinite)	241
F.28	FOSSIL WOOD	242
F.29	FOSSIL CONIFER WOOD	243
GROUP G.	OTHER BIOCHEMICALLY IMPORTANT COMPOUNDS	245
G.1	DIGITOXIN	247
G.2	DIGOXIN	248
G.3	DIGITONIN	249
G.4	STREPTOMYCIN SULPHATE	250
G.5	KANAMYCIN SULPHATE	251
G.6	PENICILLIN G	252
G.7	AMPICILLIN	253
G.8	CANNABIDIOL	254
G.8a	CANNABIDIOL	255
G.9	CYANOCOBALAMIN	256
G.10	BILIRUBIN	257
G.11	ETIOPORPHYRIN I	258
GROUP H.	POLYMERS OF NON-BIOLOGICAL ORIGIN	259
H.1	POLYETHYLENE	261
H.2	POLYBUTENE	262

H.3	POLYSTYRENE	263
H.4	POLYETHYLENEGLYCOL (Carbowax 20M)	264
H.5	POLYCAPROLACTAM (Nylon 6)	265
H.6	POLYVINYLCHLORIDE	266
H.7	POLYDIMETHYLSILICONE (OV-1)	267
H.8	POLYISOPRENE/POLY(<i>cis</i>)BUTADIENE	268
H.9	DOWEX 50 WX8	269
H.10	DOWEX 1X2	270
H.11	DOWEX 2X8	271
H.12	DIETHYLAMINOETHYL-DEXTRAN	272
H.13	ETHYLCELLULOSE	273

1. INTRODUCTION

1.1. GENERAL REMARKS

This Atlas contains Curie-point pyrolysis mass spectra of a selection of biomaterials. As outlined in the Preface, this collection of spectra is primarily intended to aid in the evaluation of spectra of complex materials and unknowns and to give an impression of the typical fragment series that are obtained from various groups of biomolecular compounds. Thus, a subdivision into the following groups is made:

- Group A. Carbohydrates and glycoconjugates (Spectra A.1 - A.27).
- Group B. Peptides and proteins (Spectra B.1 - B.13).
- Group C. Nucleotides and nucleic acids (Spectra C.1 - C.9).
- Group D. Lipids (Spectra D.1 - D.12a).
- Group E. Natural products (Spectra E.1 - E.16).
- Group F. Humic materials and geopolymers (Spectra F.1 - F.29).
- Group G. Other biochemically important compounds (drugs, vitamins, metabolites, etc.) (Spectra G.1 - G.11).
- Group H. Polymers of non-biological origin (plastics, resins, etc.) (Spectra H.1 - H.13).

Synthetic polymers (Group H) are included since these may be present as contaminants in biochemical samples or may serve as model compounds for some biomaterials.

1.2. SAMPLE PREPARATION

In most cases the compounds were applied to the Curie-point wires from fine suspensions in methanol, prepared by sonication. To our experience methanol is the most generally applicable (ref. 101) and inert solvent and produces few residual fragment peaks. As mentioned already in Part I (Sections 2.3 and 4.1), changing the suspension or solution medium (solvent, ionic strength, pH, etc.) may drastically influence the constitution of the pyrolysate of a particular compound. In order to give an impression of the influence of the medium, some of the compounds were also analysed in phosphate-buffered saline solution (PBS; 0.01 M phosphate, 0.145 M Cl^- and 0.17 M Na^+ , pH 7.2), a frequently used solvent in biochemistry, biology and medicine. In many of our applications of Py-MS to the analysis of biochemical fractions and cells, this solvent was used to standardise ionic strength and pH conditions (refs. 49, 96, 158, 165).

Unless otherwise stated, solution or suspension concentrations were in the range of 0.1-0.3%. All commercial products analysed were used without further purification. Solvents were of analytical reagent grade. Generally, evaporation of the solvent from the Curie-point wires was carried out at reduced pressure under constant rotation of the wires.

1.3. ANALYTICAL CONDITIONS

Most spectra were run under conditions chosen on the basis of our previous studies on the influence of instrumental parameters (refs. 100, 101). These conditions are listed in Table 11.

Table 11

Standard conditions used in the Py-MS analysis of most samples listed in the Atlas.

Experimental Parameter	Selected Value or Mode
wire cleaning	reductive heating
equilibrium temp (T_{eq})	510°C
temperature rise-time (t_T)	0.1 s
total heating time (t_z)	0.9 s
inlet temperature	150°C
electron energy (E_{e1})	14 eV
scanning speed	10 spectra/s
mass range	m/z 15-162
total number of scans accumulated	150

The temperature/time profiles specified in Table 11 were achieved with a Fischer Labortechnik 1.5 kW, 1.1 MHz high frequency generator and ferromagnetic wires with a diameter of 0.5 mm. Occasionally, e.g. with relatively volatile compounds, samples were pyrolysed in ferromagnetic tubes ("oven pyrolysis") as indicated in the Atlas. Such oven pyrolysis was performed with pure iron tubes (Curie-point temperature 770°C), with an outer diameter of 1.5 mm, a length of 13 mm and a wall thickness of 0.1 mm. Temperature-rise times achieved are slightly faster than these of the corresponding ferromagnetic wires.

1.4. SPECTRUM PRESENTATION FORMAT

Because of the occurrence of prominent series of homologous ions in the pyrolysis mass spectra of some groups of compounds (e.g. "Lipids", Group D, "Humic materials and geopolymers", Group F), the authors have endeavoured to mark such ion series in the spectra. In order to achieve some degree of uniformity, thereby facilitating quick comparisons between spectra, the following ion series have been marked in many spectra regardless of their relative importance in each spectrum:

- m/z 42, 56, 70, 84, 98, 112
- m/z 54, 68, 82, 96, 110, 124
- m/z 66, 80, 94, 108, 122, 136
- m/z 78, 92, 106, 120, 134, 148

In addition, other ion series have occasionally been marked in the spectra. It should be stressed, however, that the use of ion series markings does not constitute an attempt at full chemical identification of the homologous ion series involved.

Notwithstanding their limited chemical significance, the authors have found ion series markings very useful in performing a first rapid qualitative evaluation of pyrolysis mass spectra.

Finally peaks and/or peak series pointing to certain chemical components have sometimes been marked using the following symbols:

- A uronic acid fragment
- L lignin fragment
- N N-acetylamino sugar fragment
- P protein fragment
- S sulphur-containing fragment
- * impurity
- ↙ special feature; discussed under "Remarks".

1.5. SPECTRUM CONTRIBUTIONS FROM INORGANIC CONSTITUENTS

It should be noted that the use of PBS buffer generally gives rise to intense peaks at m/z 36 and 38 representing $H^{35}Cl$ and $H^{37}Cl$, respectively. These and other ions of possible inorganic origin frequently encountered in pyrolysis mass spectra are listed in Table 12.

Table 12

Possible inorganic origins of some ions frequently observed in pyrolysis mass spectra of complex samples.

m/z	ion	possible inorganic origin
17	$NH_3^{+\bullet}$	ammonium salt
18	$H_2O^{+\bullet}$	crystal water, adsorbed water, residual gas
28	$N_2^{+\bullet}(1)$	residual gas
30	$NO^{+\bullet}$	nitrates
32	$O_2^{+\bullet}(1)$	residual gas
36/38	$HCl^{+\bullet}$	chlorides
43	CH_3CO^+	acetates (fragment ion)
44	$CO_2^{+\bullet}(1)$	carbonates
44	$N_2O^{+\bullet}$	nitrates
46	$NO_2^{+\bullet}$	nitrates
50/52	$CH_3Cl^{+\bullet}$	chlorides
60	$CH_3COOH^{+\bullet}$	acetates
64	$SO_2^{+\bullet}$	sulphates
64	$S_2^{+\bullet}(2)$	elemental sulphur

(1) at the very low electron impact energy used (14 eV) these ions do not contribute markedly to the spectra;

(2) a member of the homologous ion series S^+ up to S_8^+ .

Table 13

Amino acid composition of Peptides and Proteins shown in this Atlas

Spectrum	Compounds Analysed	Ala	Arg	Asn	Asp	Cys*	Gln	Glu	Gly	His	Ile	Leu	Lys*	Met	Phe	Pro*	Ser	Thr	Trp	Tyr	Val	Number of Residues
		A	R	N	D	C	Q	E	G	H	I	L	K	M	F	P	S	T	W	Y	V	
B.1	ACTH 1-24	-	12.5	-	-	-	-	4.2	8.3	4.2	-	-	16.6	4.2	4.2	12.5	8.3	-	4.2	8.3	12.5	24
B.2	ACTH 1-10	-	10.0	-	-	-	-	10.0	10.0	10.0	-	-	-	10.0	10.0	-	20.0	-	10.0	10.0	-	10
B.3	ACTH 11-24	-	14.2	-	-	-	-	-	7.1	-	-	-	28.6	-	-	21.4	-	-	-	7.1	21.4	14
B.4	Insulin, bov.	5.9	2.0	5.9	-	11.5	5.9	7.8	7.8	3.9	2.0	11.8	2.0	-	5.9	2.0	5.9	2.0	-	7.8	9.8	51
B.4a	Insulin, porc.	3.9	2.0	5.9	-	11.8	5.9	7.8	7.8	3.9	3.9	11.8	2.0	-	5.9	2.0	5.9	3.9	-	7.8	7.8	51
B.5	RNase A, bov.	9.7	3.2	8.0	4.0	6.5	5.6	4.0	2.4	3.2	2.4	1.6	8.0	3.2	2.4	3.2	12.0	8.0	-	4.8	7.3	124
B.6	DNase I, bov.	8.6	4.3	+12.5→	1.6	+7.4→	3.5	2.3	4.3	8.9	3.5	1.6	4.3	3.5	11.7	5.8	1.2	5.8	9.3	257		
B.7	Lysozyme	9.3	8.5	10.3	6.4	6.2	2.3	1.5	9.3	0.8	4.6	6.2	4.6	1.5	2.3	1.5	7.7	5.4	4.6	2.3	4.6	129
B.8	Hemoglobin, bov.	12.8	2.5	3.2	6.7	0.7	1.4	4.6	6.4	6.0	0.4	12.4	7.8	1.4	6.0	3.6	6.7	4.6	1.1	1.8	9.9	282
B.9	Cytochrome C, eq.	5.8	1.9	4.8	2.9	1.9	2.9	8.7	11.5	2.9	5.8	5.8	18.3	1.9	3.9	3.9	-	9.6	1.0	3.9	2.9	104
B.10	Myoglobin, eq.	9.8	1.3	1.3	4.6	-	3.9	8.5	9.8	7.2	5.9	11.1	13.1	1.3	4.6	2.6	3.3	4.6	1.3	1.3	4.6	153
B.11	Keratin, sheep	6.1	6.9	+6.9→	10.5	+10.7→	8.4	0.7	2.4	7.0	2.7	0.5	2.6	8.4	11.0	6.1	1.5	3.8	3.8	-		
B.12	Collagen, bov.	12.5	5.7	+5.1→	-	+8.6→	37.4	0.7	1.3	2.8	2.8	-	1.6	13.3	3.7	1.9	-	0.3	2.3	-		
B.13	Ceruloplasmin, porc.	5.0	3.5	+10.5→	-	+11.2→	7.3	3.3	4.6	6.9	6.4	1.9	5.5	5.9	7.2	7.1	1.5	5.5	6.6	1296		

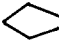
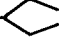
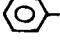
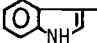
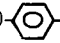
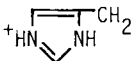
* values for Lys and Pro include possible hydroxylysine and hydroxyproline residues, respectively; values for Cys include cysteine residues.

1.6. PROTEIN SPECTRA (GROUP B)

A general discussion of prominent and characteristic peaks in protein spectra can be found in Part 1, Section 3.4. To aid in the evaluation of the spectra of Group B, Table 13 provides information on the amino acid composition of the various peptides and proteins analysed, whereas Table 14 lists the most prominent fragment peaks in the pyrolysis mass spectra of a number of poly(amino acids) purchased from Sigma Chem. Corp., St. Louis, USA. To a certain extent these poly(amino acids) may be regarded as model compounds for the more complex proteins and peptides.

Table 14

Prominent fragment peaks in the pyrolysis mass spectra of poly(amino acids)^a

Monomer	Monomer side chain	10 most intense peaks (above m/z 18) ^b											MW of monomer
Ala	CH ₃ -	28	42	43	55	<u>56</u>	57	81	97*	<u>124*</u>	<u>125</u>	89	
Val	(CH ₃) ₂ CH -	42	43	<u>56</u>	69	70	<u>71</u>	82	<u>84</u>	110*	125	117	
Leu	(CH ₃) ₂ CH-CH ₂ -	28	42	<u>43</u>	55	<u>56</u>	69	70	<u>98</u>	124*	166*	131	
Pro		41	42	43	60	<u>67</u>	<u>68</u>	<u>69</u>	70	97	99	115	
Hyp	HO- 	41	42	43	44	59	<u>67</u>	<u>68</u>	<u>69</u>	81	95	131	
Phe	 -CH ₂ -	43	78	<u>91</u>	<u>92</u>	104	<u>106</u>	117	119	129	131	165	
Trp	 -CH ₂ -	31	43	45	<u>58</u>	59	74	<u>117</u>	118	130	<u>131</u>	204	
Met	CH ₃ -S-CH ₂ -CH ₂ -	28	43	45	<u>47</u>	<u>48</u>	60	<u>61</u>	62	74	98	149	
Gly	H -	28	<u>41</u>	42	<u>43</u>	<u>44</u>	55	56	59	60	97*	75	
Ser	HO-CH ₂ -	28	<u>30</u>	42	<u>43</u>	<u>44</u>	56	60	69	95*	97*	105	
Tyr	HO-  -CH ₂ -	43	66	<u>94</u>	95	106	107	<u>108</u>	109	<u>120</u>	122	181	
Asn	H ₂ NOC-CH ₂ -	28	<u>43</u>	44	45	54	56	59	<u>69</u>	<u>97</u>	99	132	
Asp	⁻ OOC-CH ₂ -	28	<u>43</u>	44	45	54	56	59	69	<u>97</u>	<u>99</u>	133	
Glu	⁻ OOC-CH ₂ -CH ₂ -	42	43	44	<u>55</u>	67	79	<u>83</u>	95	97	<u>108</u>	147	
Lys	⁺ H ₃ N-CH ₂ -CH ₂ -CH ₂ -CH ₂ -	28	41	42	43	<u>55</u>	68	<u>69</u>	79	82	<u>83</u>	146	
Arg	H ₂ N-C(=NH)-CH ₂ -CH ₂ -CH ₂ -	30	<u>42</u>	<u>43</u>	67	68	69	79	91	107	<u>108</u>	174	
His	⁺ NH ₂  -CH ₂ -	28	41	42	<u>43</u>	<u>44</u>	45	60	<u>68</u>	82	94	155	

^a Spectra from suspensions of the compounds in PBS buffer, pH 7.

^b The three most intense peaks are underlined. It should be noted that the fragments marked with * must have been formed dimeric units of the polypeptide chain, or else represent products of recombination reactions.

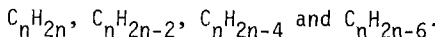
1.7. NUCLEOTIDE AND NUCLEIC ACID SPECTRA (GROUP C)

In view of the complete loss of signals derived from the base moieties in regular Curie-point Py-MS, as discussed in Part I, Section 3.3, it is worth mentioning that special methods can be used to obtain mass spectra of the tarry residue condensed on the wall of the glass reaction chamber during the Curie-point pyrolysis procedure. One approach is taking the used wire out of the reaction chamber after pyrolysis, heating the h.f. coil area up to 225°C (by means of a tungsten wire heater) and reinserting the reaction chamber into the heated h.f. coil zone (ref. 204). Another method involves the application of a thin ferromagnetic metal foil surrounding the sample wire and heated simultaneously with the wire by the h.f. field (ref. 205). The spectra produced are qualitatively similar to those obtained by direct probe Py-MS techniques (refs. 15-17) and by laser pyrolysis-MS (see Part I, Figure 5) and show relatively large purine and pyrimidine base signals. In contrast to direct probe and laser Py-MS techniques, however, the actual pyrolysis step is performed under well-defined Curie-point Py-MS conditions.

1.8. LIPID SPECTRA (GROUP D)

Because of the relatively high volatility of many of the lipid compounds analysed, pyrolysis was mostly carried out in ferromagnetic tubes. Attempts to pyrolyse lipids on ferromagnetic wires often fail to produce peaks of sufficient intensity because the large pyrolysis products formed are lost by condensation on the relatively cold walls of the reaction chamber. Alternatively, the whole lipid may escape from the pyrolysis wire intact and subsequently condense on the reaction chamber wall.

Such condensation losses may be prevented by (a) oven pyrolysis, which degrades the compound into smaller, more volatile products or (b) special pre-heating or post-heating of the reaction chamber, such as used in the analysis of nucleic acids (ref. 205). An important question is, of course, whether relatively volatile compounds such as lipids should be analysed by pyrolysis mass spectrometry when many of these compounds can directly be analysed by other MS techniques. However, the mass spectra of many hydrocarbons, especially aliphatic compounds, differ very little whereas pyrolysis techniques are capable of greater distinction between these compound series. Therefore it was decided to include a selection of pyrolysis mass spectra of lipids. Different homologous ion series, as presented in Section 1.4. of this Introduction, have been marked. In many cases, these series will represent hydrocarbon molecular ions with different degrees of unsaturation, i.e. the series:



1.9. SPECTRA OF HUMIC MATERIALS AND GEOPOLYMERS (GROUP F)

Compared with most other groups of compounds analysed for this Atlas, humic materials and geopolymers are usually ill-defined with regard to chemical composition

and structure. Therefore, when examining the pyrolysis mass spectra three important facts should be kept in mind:

1. The high degree of heterogeneity even in apparently closely related samples, e.g. coals of the same rank, implies that the spectra shown are not necessarily representative for other samples of the same type.
2. A given ion series does not necessarily represent one class of molecules only, e.g. the series at m/z 78, 92, etc. may represent benzenes as well as benzthiophenes (refs. 73, 196).
3. The yield of pyrolysis products obtained with the Curie-point Py-MS techniques used decreases rapidly with increasing degree of geochemical transformation. For instance, whereas lignites may produce pyrolysis yields of 50% or more, anthracites may yield as little as 10% or less. Thus conclusions drawn about the chemical composition of the sample on the basis of pyrolysis mass spectra pertain only to the relative composition of those pyrolysis products produced and detected by the technique used.

1.10. SPECTRA OF OTHER BIOCHEMICALLY IMPORTANT COMPOUNDS (GROUP G)

This group includes a number of relatively small molecules, mostly drugs, which are difficult or impossible to analyse by conventional MS techniques because of a lack of adequate volatility. A second reason for including this group of spectra in the Atlas is the fact that drugs and their metabolites sometimes show up in complex biological materials such as tissues and body fluids. In fact the Py-MS pattern of some drugs, e.g. penicillin, in human urine (ref. 159) is so easily recognizable that Py-MS techniques may offer a potentially new and fast approach to drug assays in urine.

This Page Intentionally Left Blank

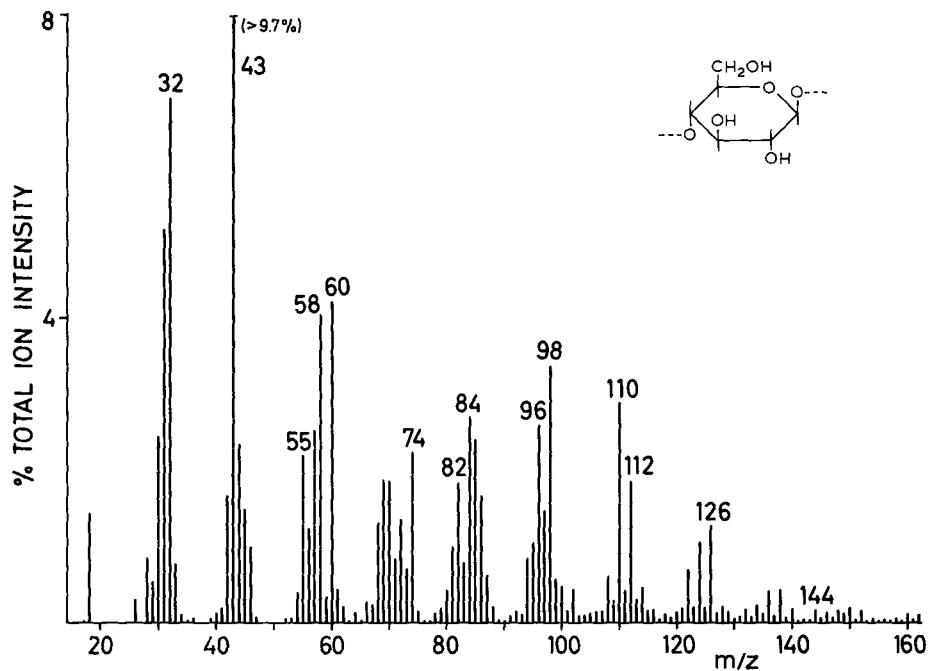
2. PYROLYSIS MASS SPECTRA

GROUP A

CARBOHYDRATES AND GLYCOCONJUGATES

This Page Intentionally Left Blank

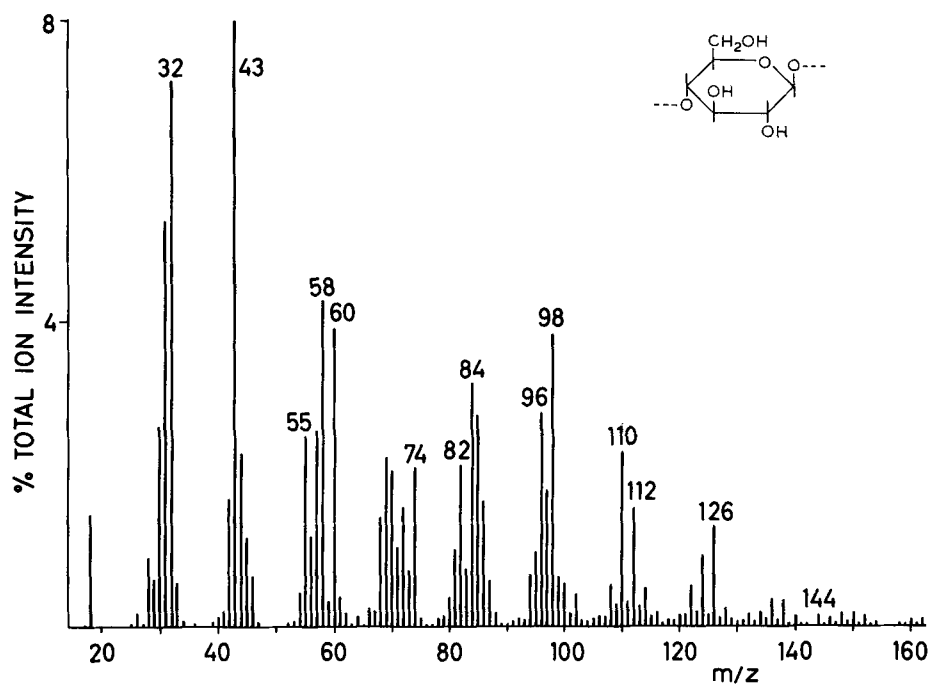
SPECTRUM A.1



SAMPLE : CELLULOSE
 CHEMICAL DETAILS : poly[(1→4)DGlCβ]; see insert in spectrum
 SAMPLE ORIGIN : Merck AG, Darmstadt, GFR
 SAMPLE PREP./SIZE : suspension in methanol; 10 μg
 PYROL. CONDITIONS : standard
 TOTAL ION COUNTS : 1.75 X 10⁵

REMARKS - For a discussion on pyrolysis mechanisms and the identity of pyrolysis products, see Part I, Section 3.2., and refs. 53, 90, 91, 92.

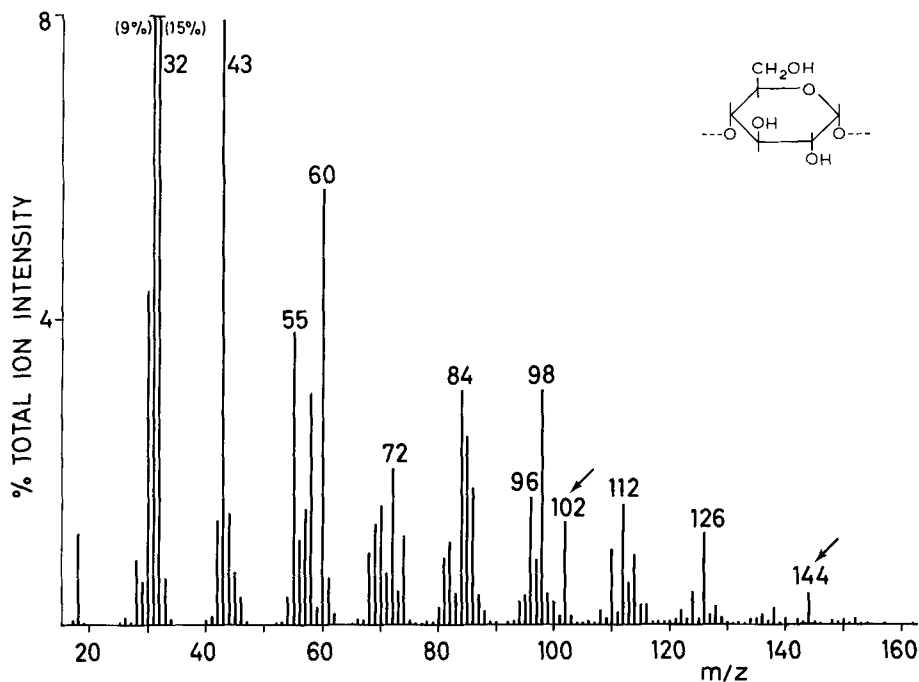
SPECTRUM A.1A



SAMPLE : CELLULOSE
 CHEMICAL DETAILS : poly[(1→4)DGlCβ]; see insert in spectrum
 SAMPLE ORIGIN : Whatman Chromedia, W. & R. Balston Ltd., UK
 SAMPLE PREP./SIZE : suspension in methanol; 10 μg
 PYROL. CONDITIONS : standard
 TOTAL ION COUNTS : 2.5 × 10⁵

REMARKS - Note the high degree of correspondence with Spectrum A.1. As demonstrated by Weijman (ref. 169), well purified celluloses from widely different origins (e.g. cotton wool, fungal cell walls) exhibit identical Py-MS patterns.

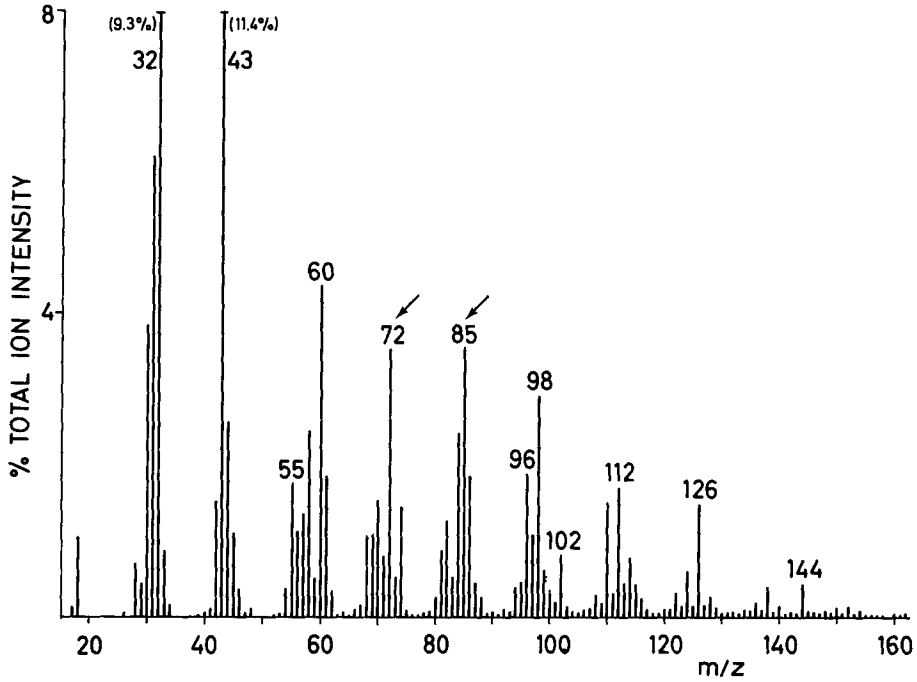
SPECTRUM A.2



SAMPLE : AMYLOSE
 CHEMICAL DETAILS : poly[(1→4)DGlα]; see insert in spectrum
 SAMPLE ORIGIN : Merck AG, Darmstadt, GFR
 SAMPLE PREP./SIZE : suspension in methanol; 10 μg
 PYROL. CONDITIONS : standard
 TOTAL ION COUNTS : 1 × 10⁵

REMARKS - Note the relatively high peak intensities at m/z 55, 72, 102 and 144, and the relatively low intensities at m/z 58, 74, 82, 96, 110 and 124 compared with the spectra of the β(1→4)-linked analogue (Spectra A.1 and A.1a). Similar characteristic differences are exhibited by the other glucans containing α-glycosidic linkages (Spectra A.3 and A.4).

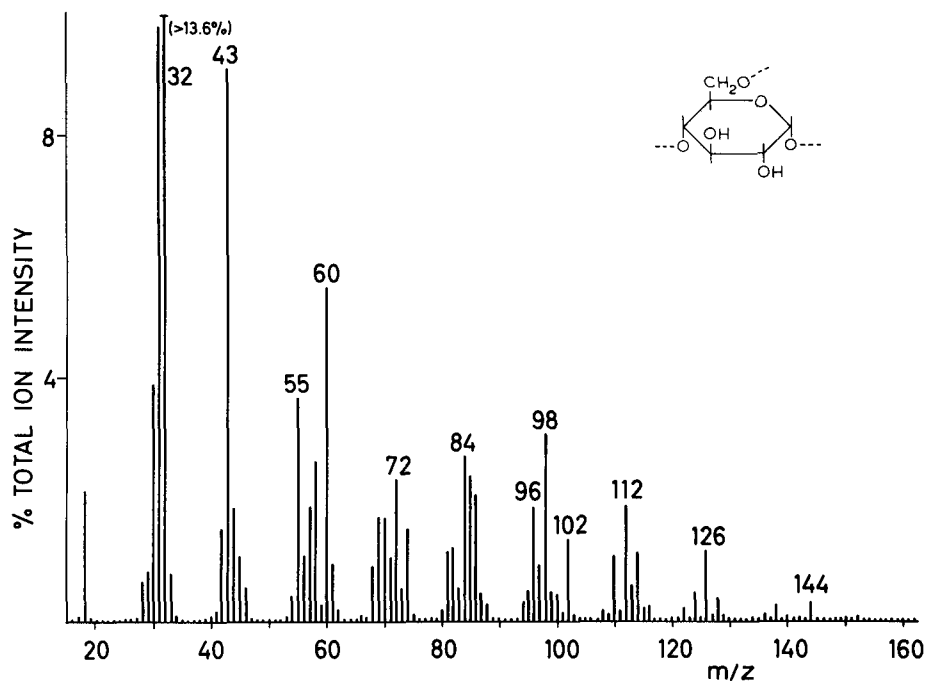
SPECTRUM A.3



SAMPLE : NIGERAN (from *Aspergillus niger*)
 CHEMICAL DETAILS : poly[(1→3),(1→4)DGlα]
 SAMPLE ORIGIN : Koch-Light Ltd., Colnbrook, Bucks., UK
 SAMPLE PREP./SIZE : suspension in methanol; 10 μg
 PYROL. CONDITIONS : standard
 TOTAL ION COUNTS : 1.4×10^5

REMARKS - Compared with Spectrum A.2 [amylose, containing only α(1→4) linkages] this spectrum shows relatively high intensities at m/z 72 and 85, and lower intensities at m/z 55. See also remarks on Spectrum A.2.

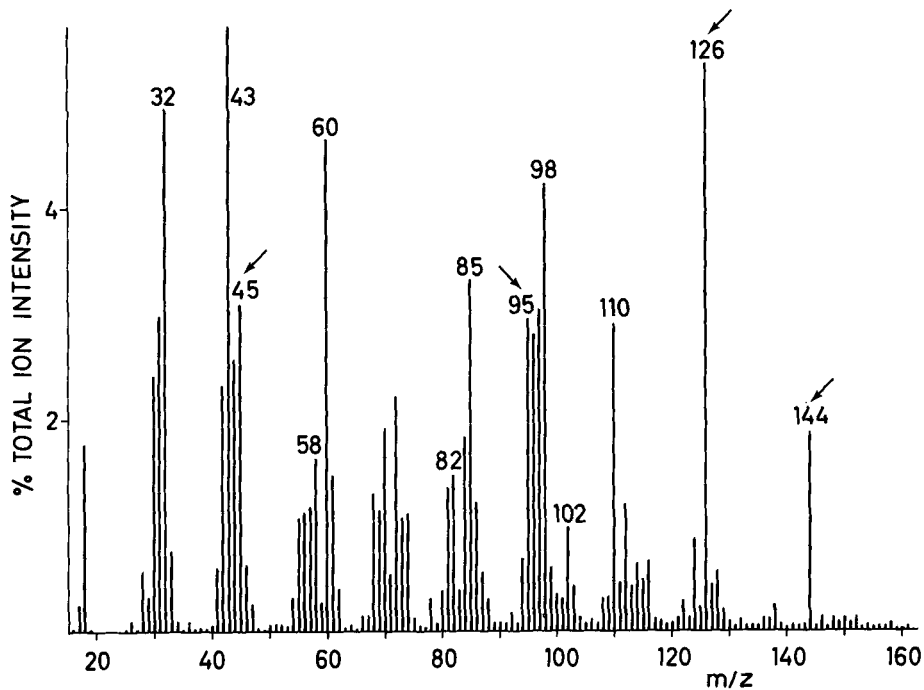
SPECTRUM A.4



SAMPLE : GLYCOGEN (from rabbit liver)
 CHEMICAL DETAILS : poly[(1→4)*D*Glcα] with α(1→6) branches; see insert in spectrum
 SAMPLE ORIGIN : BDH Chemicals Ltd., Poole, UK
 SAMPLE PREP./SIZE : suspension in methanol; 10 μg
 PYROL. CONDITIONS : standard
 TOTAL ION COUNTS : 2.2 × 10⁵

REMARKS - Note the high degree of correspondence with Spectrum A.2 [amylose, containing only α(1→4) linkages] either indicating the absence of strong effects of branching on the pyrolytic cleavages, or a relatively low degree of branching. See also Remarks on Spectrum A.2.

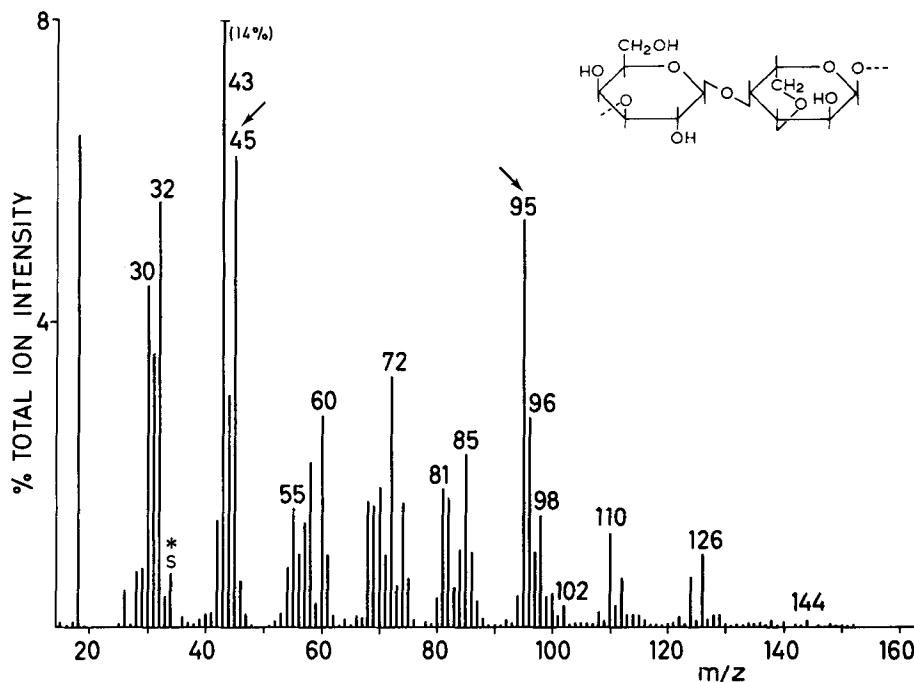
SPECTRUM A.5



SAMPLE : CARRAGHEENAN
 CHEMICAL DETAILS : poly[(1→3)DGalβ(1→4)DGalα]; containing sulphate substituents and 3,6-anhydride bridges
 SAMPLE ORIGIN : Sigma Chemical Corp., St. Louis, USA
 SAMPLE PREP./SIZE : suspension in methanol; 10 μg
 PYROL. CONDITIONS : standard
 TOTAL ION COUNTS : 6×10^4

REMARKS - Note the strong difference with the patterns of glucans (Spectra A.1-A.4). High peaks at m/z 45 and 95 may be indicative of 3,6-anhydrohexose moieties, whereas the high intensities at m/z 126 and 144 may represent degradation of the polymer backbone by 1,3-elimination ("peeling"). The low relative intensity of m/z 64 indicates a low degree of O-sulphation. Compare also with Spectrum A.6 (Agarose).

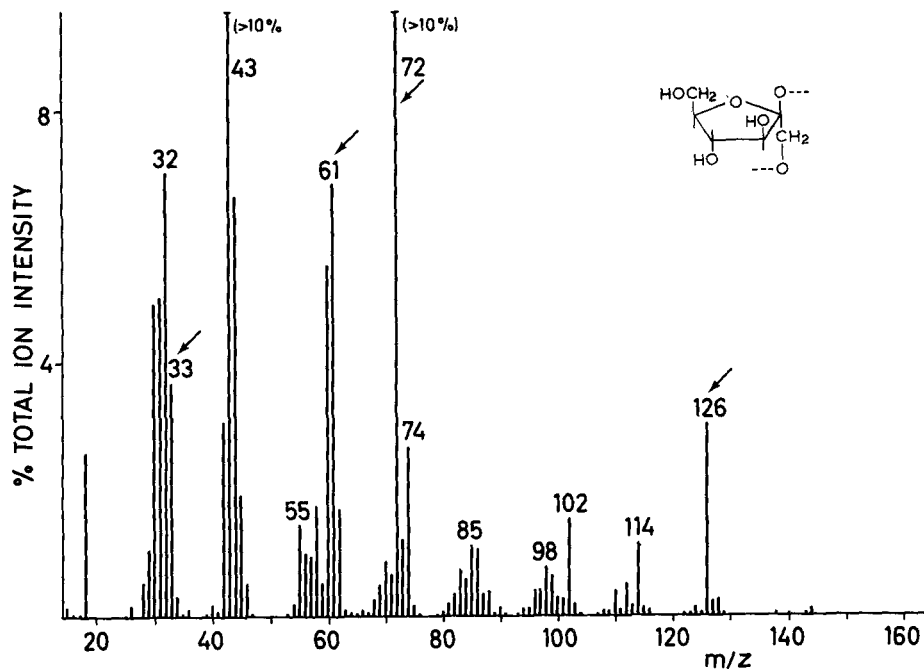
SPECTRUM A.6



SAMPLE : AGAROSE
 CHEMICAL DETAILS : poly[(1→3)*D*Galβ(1→4)3,6 anhydro*L*Galα]; partially sulphated; see insert in spectrum
 SAMPLE ORIGIN : Koch-Light Ltd., Colnbrook, Bucks., UK
 SAMPLE PREP./SIZE : suspension in methanol; 10 μg
 PYROL. CONDITIONS : standard
 TOTAL ION COUNTS : 1×10^5

REMARKS - Note the extremely high relative intensities at m/z 45 and 95, thought to be representative of the 3,6-anhydrohexose moieties (see also Spectrum A.5).

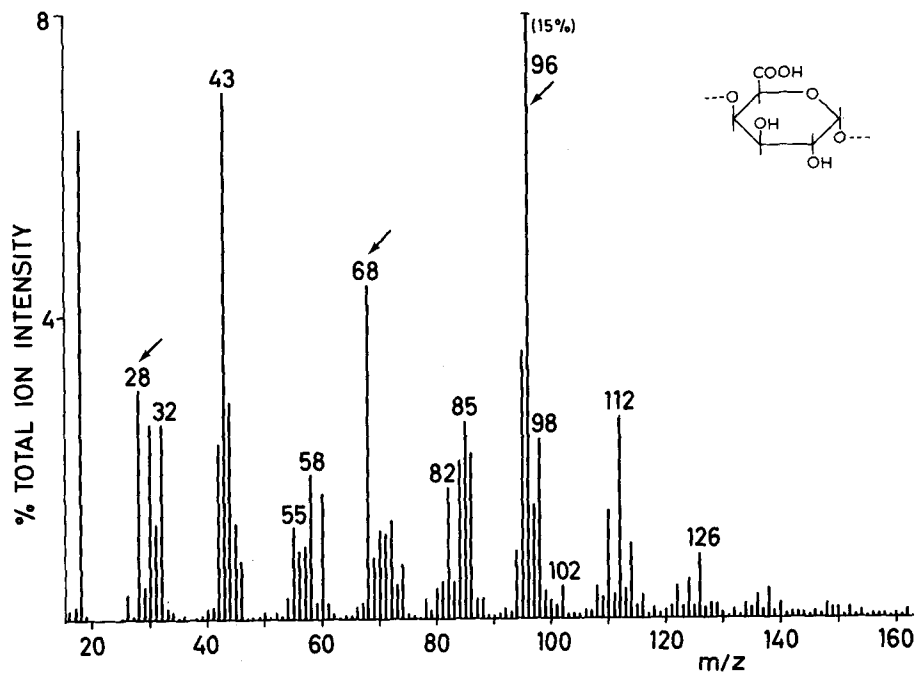
SPECTRUM A.7



SAMPLE : INULIN
 CHEMICAL DETAILS : poly[(2→1)DFruβ]; see insert in spectrum
 SAMPLE ORIGIN : Merck AG, Darmstadt, GFR
 SAMPLE PREP./SIZE : suspension in methanol; 10 μg
 PYROL. CONDITIONS : standard
 TOTAL ION COUNTS : 4 × 10⁵

REMARKS - Note the strong relative intensities at m/z 72 and 126 compared with the aldohexosyl polymers (Spectra A.1-A.4), and the occurrence of characteristic peaks at m/z 33 and 61. The latter peak is also prominent in Spectrum A.22 (Teichoic acid) and may represent a glycerol-type fragment.

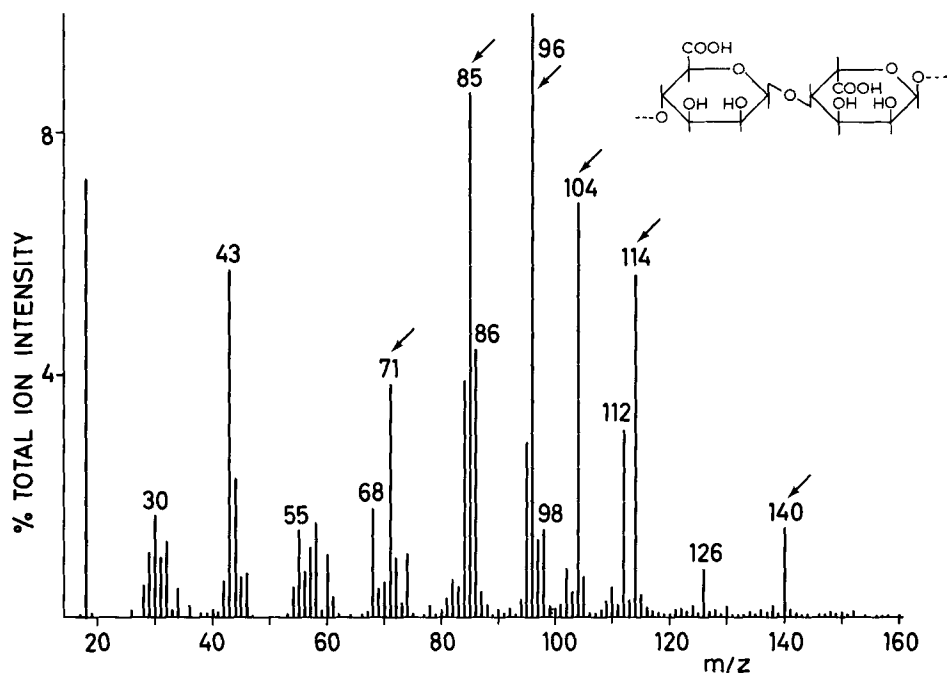
SPECTRUM A.8



SAMPLE : POLYGALACTURONIC ACID
 CHEMICAL DETAILS : poly[(1→4)DGalA_α]; see insert in spectrum
 SAMPLE ORIGIN : Fluka AG, Buchs, Switzerland
 SAMPLE PREP./SIZE : suspension in methanol; 10 μg
 PYROL. CONDITIONS : standard
 TOTAL ION COUNTS : 5 × 10⁴

REMARKS - Note the high relative intensities at m/z 28, 68 and 96 compared with the neutral hexose polymers (Spectra A.1-A.4). See also Part I, Figure 11.

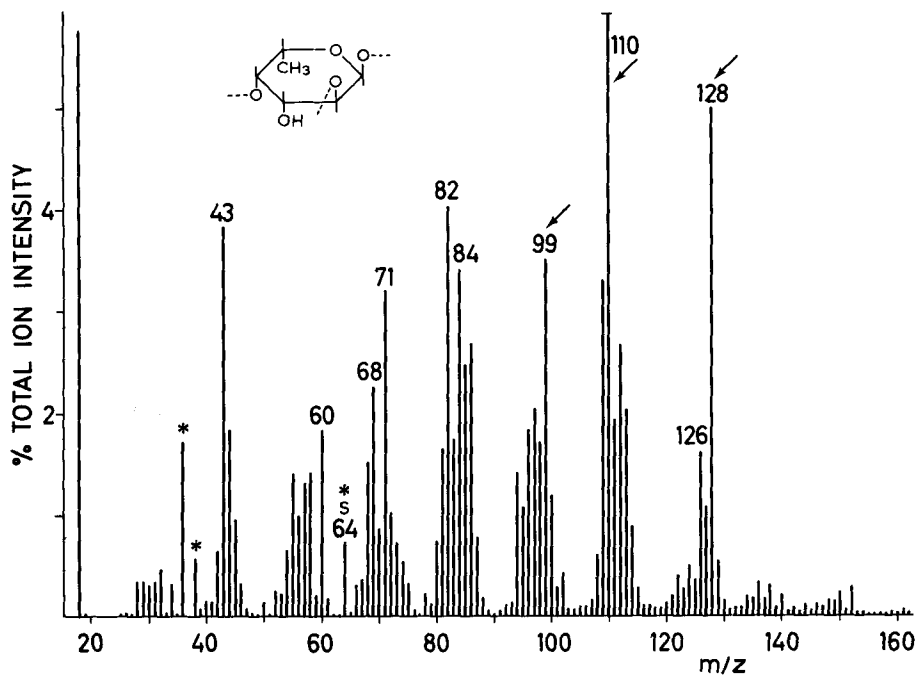
SPECTRUM A.9



SAMPLE : ALGINIC ACID
 CHEMICAL DETAILS : poly[(1->4)DManAβ(1->4)αGulAα]; see insert in spectrum;
 MW ~ 10⁵
 SAMPLE ORIGIN : Serva, Heidelberg, GFR
 SAMPLE PREP./SIZE : suspension in methanol; 10 μg
 PYROL. CONDITIONS : standard
 TOTAL ION COUNTS : 3.5 x 10⁵

REMARKS - Note the unusual peaks at m/z 71, 104 and 140, and the relatively high peaks at m/z 85, 96 and 114. The latter two peaks probably originate from acid decarboxylation-dehydration of hexuronic acid residues. The possibility that m/z 104 represents a polystyrene impurity (see Part I, Figure 1) cannot be excluded. Compare with the spectrum of polygalacturonic acid (Part I, Figure 11; spectrum A.8).

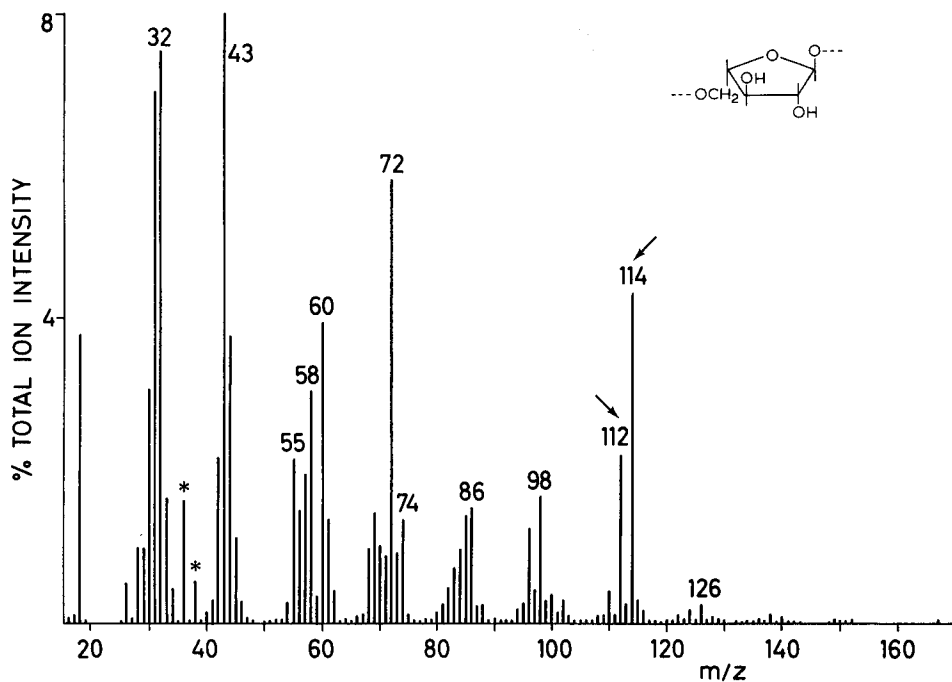
SPECTRUM A.10



SAMPLE : FUCOIDAN (from *Fucus vesiculosus*)
 CHEMICAL DETAILS : poly[(1→2),(1→4)LFuca]; containing sulphate substituents;
 see insert in spectrum
 SAMPLE ORIGIN : Koch-Light Ltd., Colnbrook, Bucks., UK
 SAMPLE PREP./SIZE : suspension in PBS buffer; 10 μg
 PYROL. CONDITIONS : standard
 TOTAL ION COUNTS : 4 × 10⁴

REMARKS - The pronounced peak set at m/z 99, 110 and 128 is typical for 6-deoxyhexose polymers, m/z 110 and 128 representing the monomeric building blocks minus one or two molecules of water. The presence of sulphate groups becomes evident from the peak at m/z 64 (SO₂⁺). The peak at m/z 126 may point to small amounts of hexose residues. In the spectrum obtained from a methanol suspension the peak at m/z 99 is less pronounced.

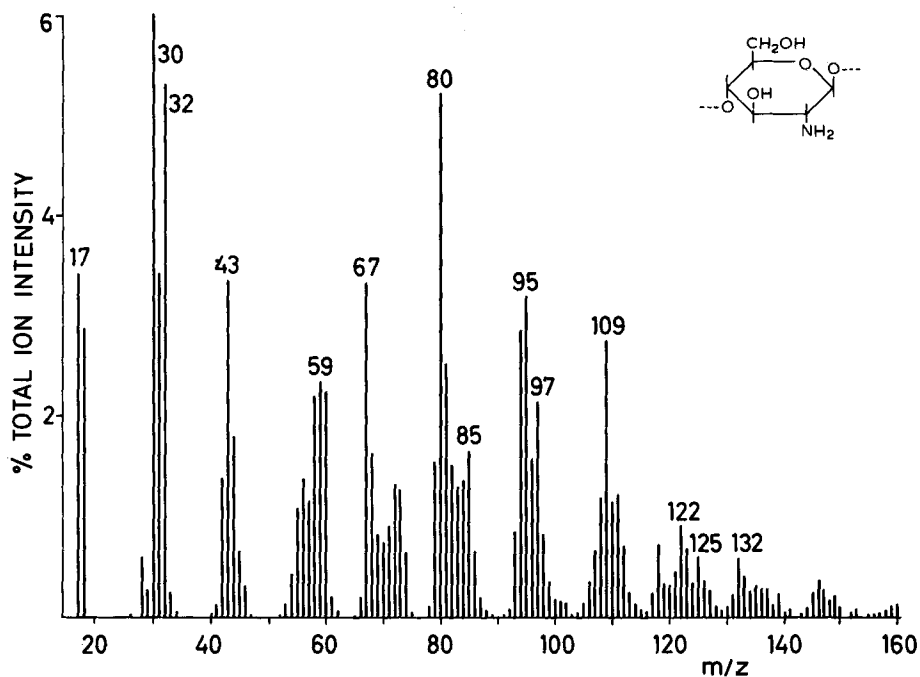
SPECTRUM A.11



SAMPLE : ARABINAN (from apple juice)
 CHEMICAL DETAILS : poly[(1→5)Ara α]; see insert in spectrum
 SAMPLE ORIGIN : gift from Dr. A.G.J. Voragen, Agricult. Univ. Wageningen,
 The Netherlands
 SAMPLE PREP./SIZE : suspension in methanol, 10 μ g
 PYROL. CONDITIONS : standard
 TOTAL ION COUNTS : 2.2×10^5

REMARKS - Note the high relative intensities of the peaks at m/z 112 and 114. Especially m/z 114 appears to be characteristic of pentose residues (e.g. compare with Spectrum C.1 (RNA)).

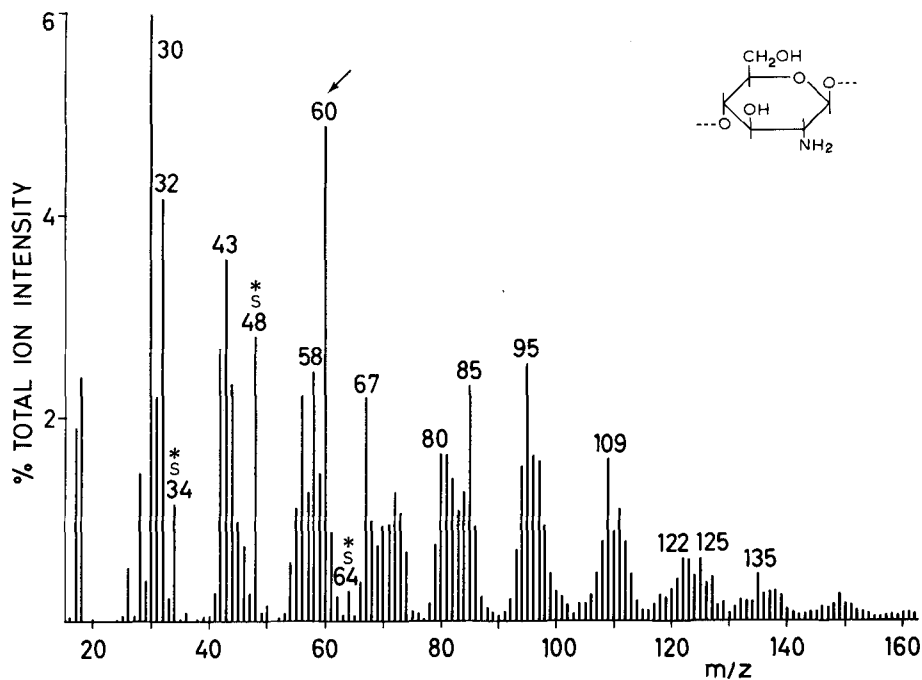
SPECTRUM A.12



SAMPLE : CHITOSAN
 CHEMICAL STRUCTURE : poly[(1→4)DGlCN_β]; see insert in spectrum
 SAMPLE ORIGIN : Polysciences Inc., Warrington, PA, USA
 SAMPLE PREP./SIZE : suspension in methanol; 10 μg
 PYROL. CONDITIONS : standard
 TOTAL ION COUNTS : 3 X 10⁴

REMARKS - Chitosan is a semi-synthetic compound obtained on de-acetylation of chitin. The structure and composition of chitosan is less well defined than that of the parent compound (compare Spectra A.12 and A.12a, representing chitosan preparations from different manufacturers). The spectrum shows a rather complex pattern of mainly odd-numbered peaks (N-containing pyrolysis products) which is significantly different from that of chitin (Spectrum A.13).

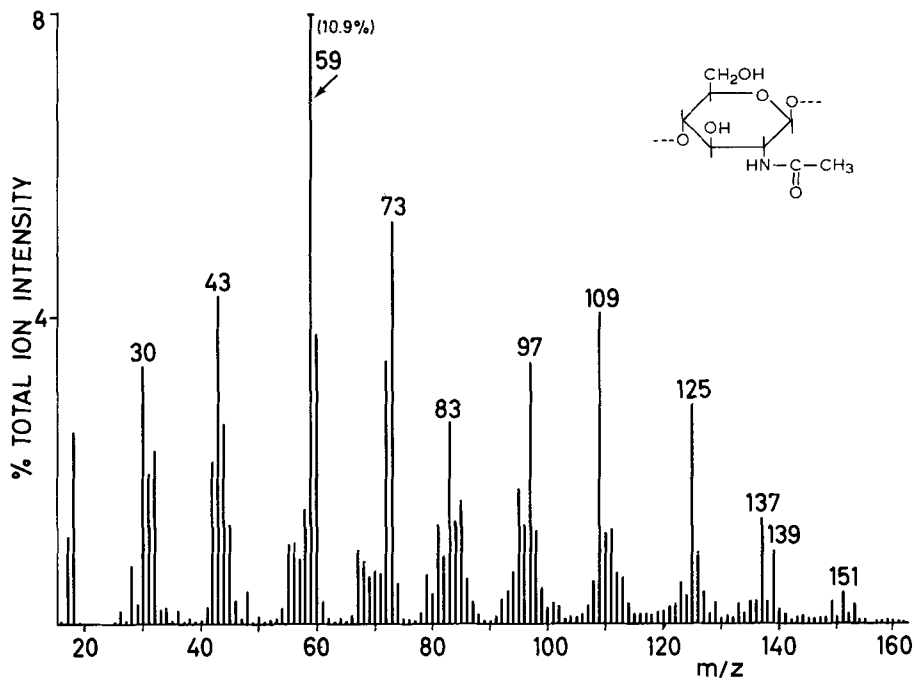
SPECTRUM A.12A



SAMPLE : CHITOSAN
 CHEMICAL DETAILS : poly[(1-4)DGlcn₆]; see insert in spectrum
 SAMPLE ORIGIN : Koch-Light Ltd., Colnbrook, Bucks., UK
 SAMPLE PREP./SIZE : suspension in methanol; 10 µg
 PYROL. CONDITIONS : standard
 TOTAL ION COUNTS : 2×10^5

REMARKS - Compare with Spectrum A.12. The intense peak at m/z 60 may point to the presence of acetate counter ions at the amine groups. Note the sulphur-containing ion signals at m/z 34 (H₂S⁺), 48 (CH₃SH⁺ and/or SO⁺) and 64 (SO₂⁺ and/or S₂⁺ and/or CH₃SOH⁺) indicating the presence of noncarbohydrate contaminants.

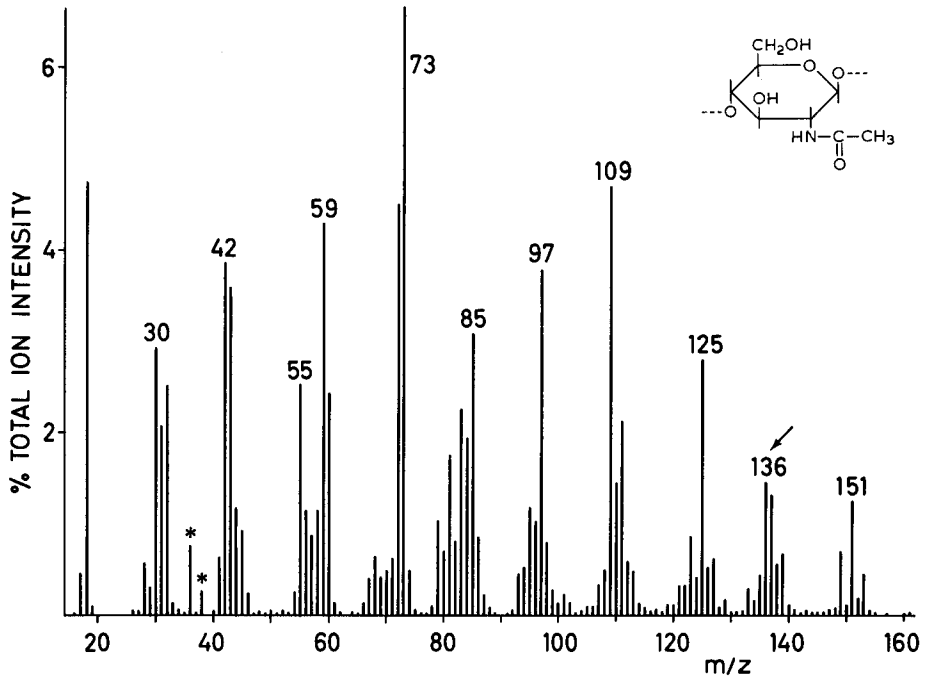
SPECTRUM A.13



SAMPLE : CHITIN
 CHEMICAL DETAILS : poly[(1→4)DGlcnAcβ]; see insert in spectrum
 SAMPLE ORIGIN : BDH Chemicals Ltd., Poole, UK
 SAMPLE PREP./SIZE : suspension in methanol; 10 μg
 PYROL. CONDITIONS : standard
 TOTAL ION COUNTS : 7.3 × 10⁴

REMARKS - This spectrum should be compared with that of the glucan analogue, cellulose (Spectrum A.1; see also Part 1, Figure 2) which shows similar characteristic series of ions at mass values differing by 1 or 41 amu, apparently representing the presence of NH₂ or NHAc groups instead of an OH function at C₂ in the respective pyrolysis fragments. This would seem to point to a strong similarity between the pyrolysis pathways of both polymers. The abundant fragment at m/z 59, as also found for other N-acetylamino sugars (see Spectra A.14-A.20, A.23, A.25), was identified as acetamide (ref. 80); it is much less pronounced in the chitosan pattern (Spectrum A.12).

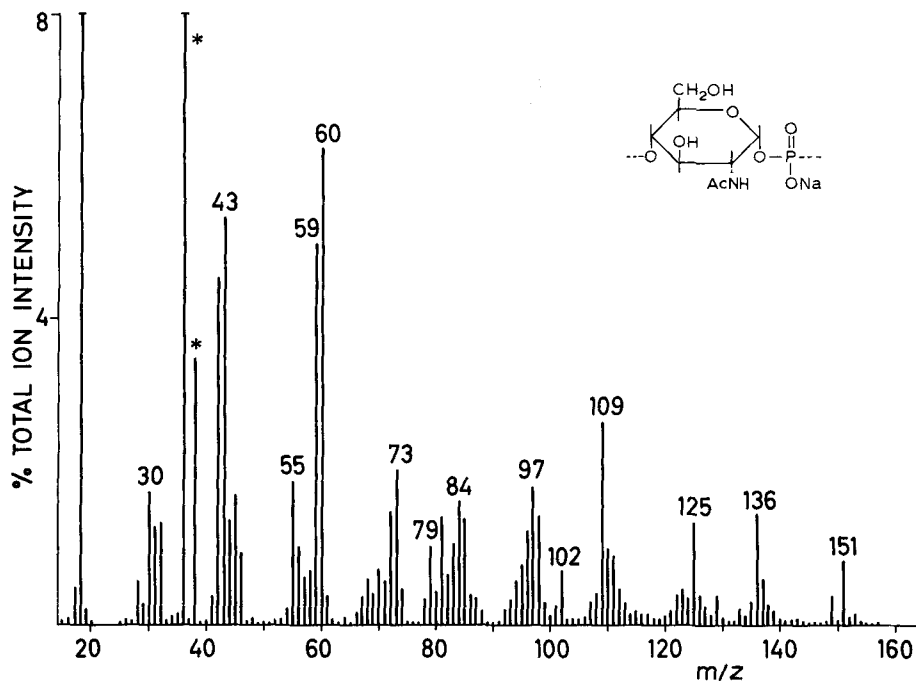
SPECTRUM A.13A



SAMPLE : CHITIN
 CHEMICAL DETAILS : poly[(1->4)DGlcnAcβ]; see insert in spectrum
 SAMPLE ORIGIN : BDH Chemicals Ltd., Poole, UK
 SAMPLE PREP./SIZE : suspension in PBS buffer; 10 μg
 PYROL. CONDITIONS : standard
 TOTAL ION COUNTS : 4.3×10^5

REMARKS - Compare with Spectrum A.13. Note the quantitative differences in the typical nitrogen-containing fragment series (odd mass values) and the increase in intensity at m/z 136 (structure unknown). Peaks at m/z 36, 38 represent HCl^+ (PBS buffer).

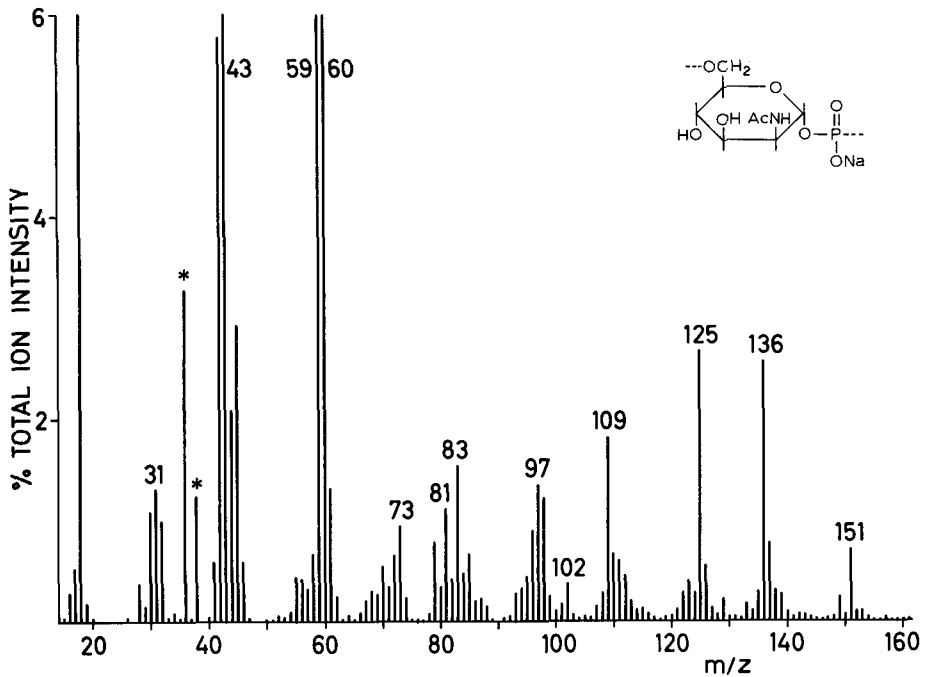
SPECTRUM A.14



SAMPLE : CAPSULAR POLYSACCHARIDE (from *Neisseria meningitidis*, group X)
 CHEMICAL DETAILS : poly[4DGlCNac α -1-phosphate]; see insert in spectrum
 SAMPLE ORIGIN : gift from Dr. E.C. Beuvery, Natl. Inst. Publ. Health, Bilthoven, The Netherlands
 SAMPLE PREP./SIZE : suspension in PBS buffer; 20 μ g
 PYROL. CONDITIONS : standard
 TOTAL ION COUNTS : 1.5×10^5

REMARKS - Sample prepared following ref. 49. Note the qualitative correspondence with the spectrum of other phosphate-bridged (Spectrum A.15) and non-phosphate-bridged (Spectrum A.13a) N-acetylhexosamine polymers. Peaks at m/z 36, 38 represent HCl⁺ (PBS buffer).

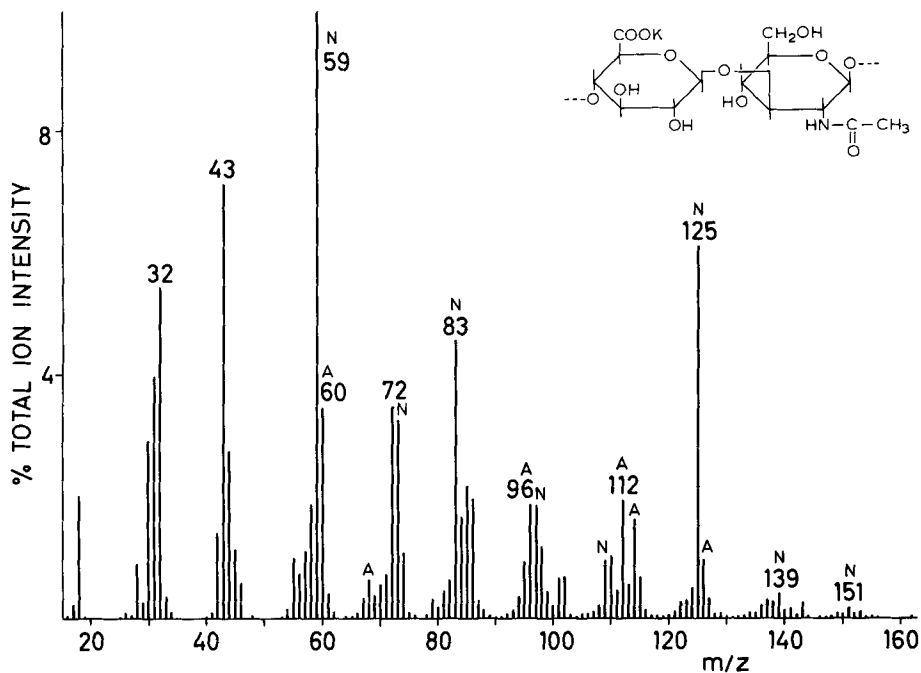
SPECTRUM A.15



SAMPLE : CAPSULAR POLYSACCHARIDE (from *Neisseria meningitidis*, Group A)
 CHEMICAL DETAILS : poly[6DManNAc α -1-phosphate]; see insert in spectrum
 SAMPLE ORIGIN : gift from Dr. E.C. Beuvery, Natl. Inst. Publ. Health, Bilthoven, The Netherlands
 SAMPLE PREP./SIZE : suspension in PBS buffer; 20 μ g
 PYROL. CONDITIONS : standard
 TOTAL ION COUNTS : 1 X 10⁵

REMARKS - Sample prepared following ref. 49. See Remarks on spectrum A.14.

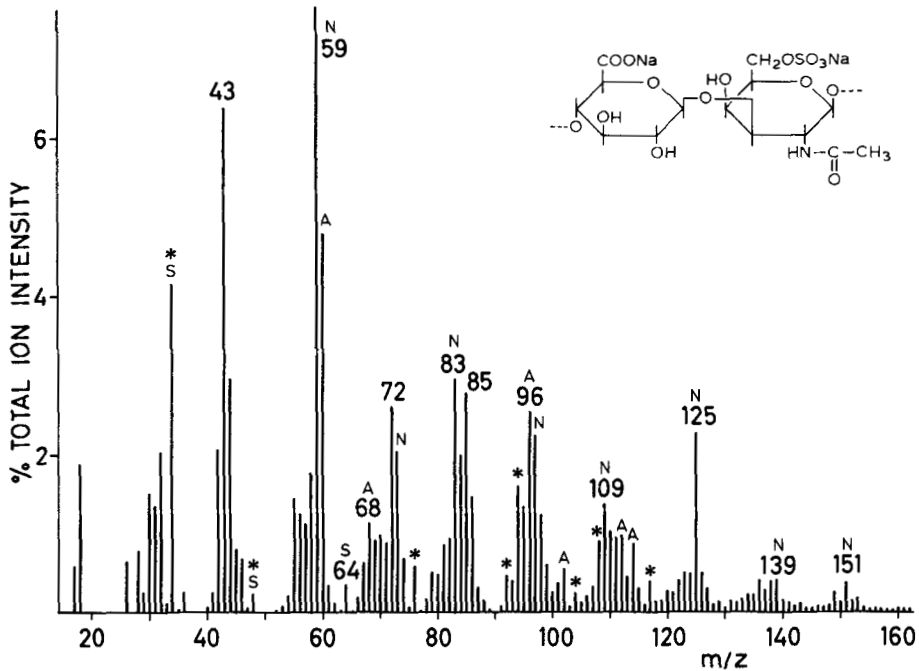
SPECTRUM A.16



SAMPLE : HYALURONIC ACID, K-salt
 CHEMICAL DETAILS : poly[(1→4)DGlcAβ(1→3)DGlcNAcβ]; see insert in spectrum
 SAMPLE ORIGIN : Boehringer, Mannheim, GFR
 SAMPLE PREP./SIZE : suspension in methanol; 10 μg
 PYROL. CONDITIONS : standard
 TOTAL ION COUNTS : 1.7 × 10⁵

REMARKS - Note the presence of the even-numbered mass peaks at m/z 60, 68, 96, 112, 114 and 126 apparently derived from the GlcA moieties (see Spectrum A.8) and the odd-numbered mass peaks at m/z 59, 73, 83, 97, 109, 125, 137, 139 and 151 derived from the GlcNAc moieties (see Spectrum A.13). The fragment at m/z 59 can be interpreted as acetamide derived from the NAC groups.

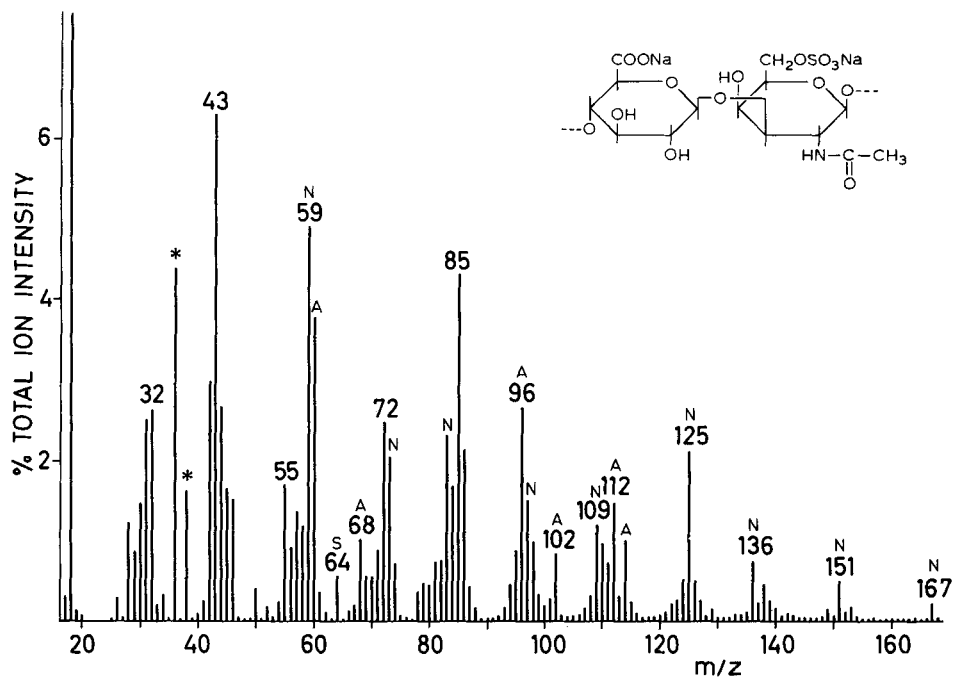
SPECTRUM A.17



SAMPLE : CHONDROITIN SULPHATE C, Na-salt
 CHEMICAL DETAILS : poly[(1+4)DGlCA β (1+3)DGalNAc β]; 0-sulphated at position 6 of GalNAc; see insert in spectrum
 SAMPLE ORIGIN : Seikagaku Kogyo Co. Ltd., Tokyo, Japan
 SAMPLE PREP./SIZE : suspension in methanol; 10 μ g
 PYROL. CONDITIONS : standard
 TOTAL ION COUNTS : 1.2×10^5

REMARKS - As is to be expected, this spectrum resembles that of hyaluronic acid (Spectrum A.16). Peaks at m/z 96, 112 and 114 indicate the GlcA residues; the peaks at m/z 59 (acetamide) and 125 are indicative of the GalNAc residues. The signal at m/z 64 (SO_2^{+}) apparently represents the sulphate moieties, the relatively low intensity might be connected with the fact that the compound is analysed in the salt form. The presence of ion signals at m/z 34, 48, 76, 92, 94, 108 and 117 probably indicates proteinaceous contaminants. Compare also with Spectrum A.18, showing the 4-sulphated analogue.

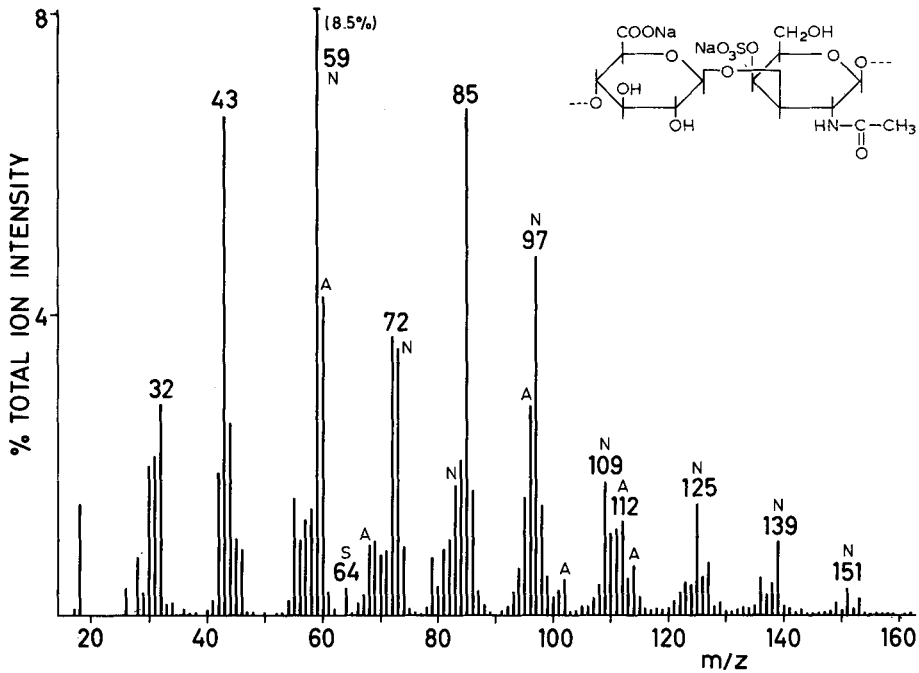
SPECTRUM A.17A



SAMPLE : CHONDROITIN SULPHATE C, Na-salt
 CHEMICAL DETAILS : poly[(1→4)DGlcAβ(1→3)DGalNAcβ]; 0-sulphated at position 6 of GalNAc; see insert in spectrum
 SAMPLE ORIGIN : Seikagaku Kogyo Co. Ltd., Tokyo, Japan
 SAMPLE PREP./SIZE : suspension in PBS buffer; 10 μg
 PYROL. CONDITIONS : standard
 TOTAL ION COUNTS : 4.5 × 10⁵

REMARKS - Peaks at m/z 36, 38 represent HCl⁺ (PBS buffer). Compare with Spectrum A.17 (methanol suspension).

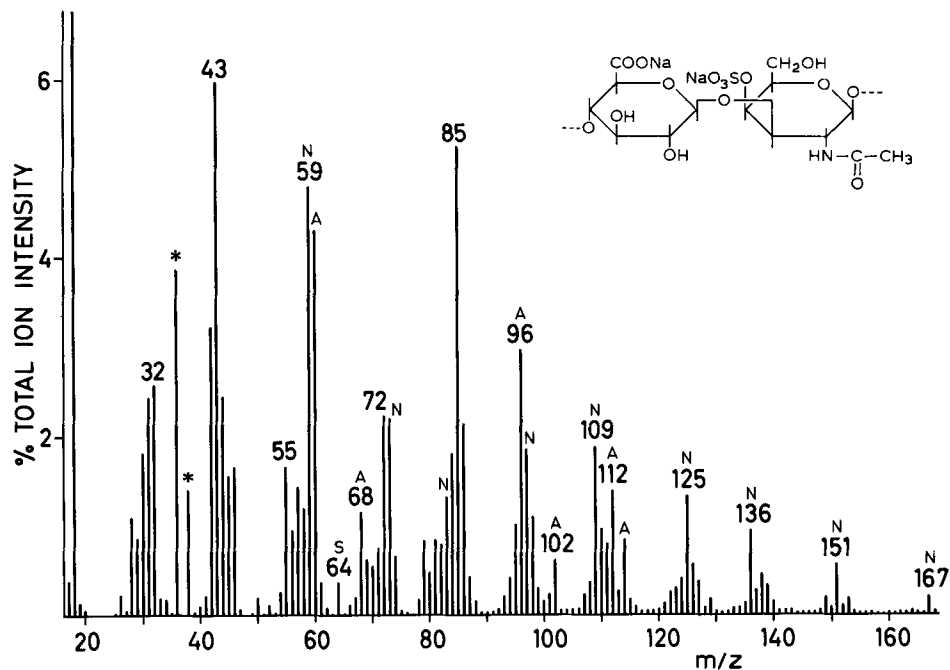
SPECTRUM A.18



SAMPLE : CHONDROITIN SULPHATE A, Na-salt
 CHEMICAL DETAILS : poly[(1→4)*D*GlcAβ(1→3)*D*GalNAcβ]; O-sulphated at position 4 of GalNAc; see insert in spectrum
 SAMPLE ORIGIN : Seikagaku Kogyo Co. Ltd., Tokyo, Japan
 SAMPLE PREP./SIZE : suspension in methanol; 10 μg
 PYROL. CONDITIONS : standard
 TOTAL ION COUNTS : 1.3 × 10⁵

REMARKS - The relatively large difference between this spectrum and that of the 6-sulphate analogue (Spectrum A.17) is remarkable. Probably this difference is attributable to differences in the ionic state or purity of the samples (the above spectrum shows much fewer protein fragment peaks than Spectrum A.17) rather than to the difference in the position of the sulphate substituents. These differences are less pronounced in the spectra obtained from PBS suspensions of the compounds (Spectra A.17a, A.18a).

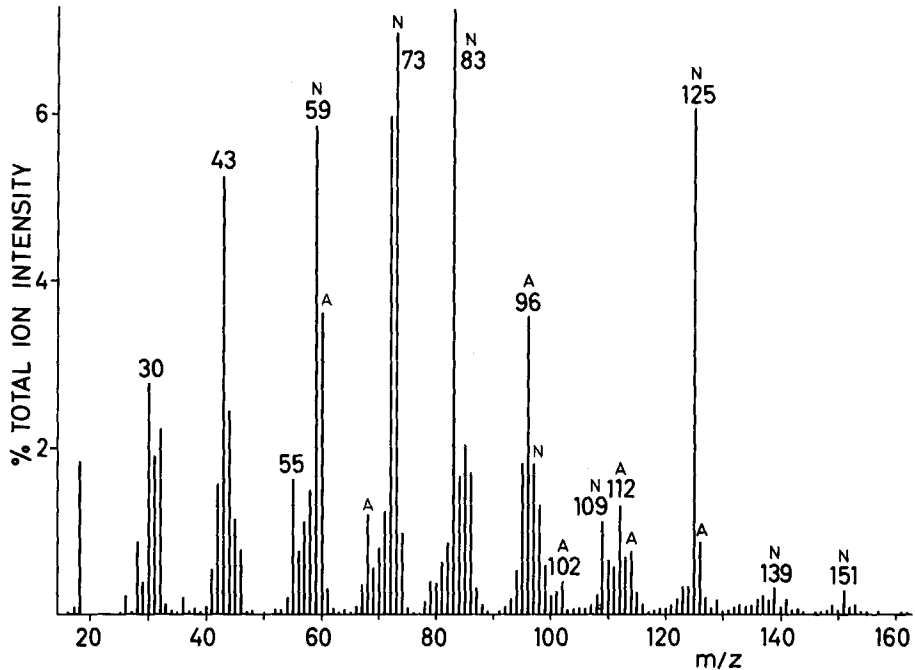
SPECTRUM A.18A



SAMPLE : CHONDROITIN SULPHATE A, Na-salt
 CHEMICAL DETAILS : poly[(1→4)DGlcAβ(1→3)DGalNAcβ]; 0-sulphated at position 4 of GalNAc; see insert in spectrum
 SAMPLE ORIGIN : Seikagaku Kogyo Co. Ltd., Tokyo, Japan
 SAMPLE PREP./SIZE : suspension in PBS buffer; 10 μg
 PYROL. CONDITIONS : standard
 TOTAL ION COUNTS : 3.6 X 10⁵

REMARKS - Peaks at m/z 36, 38 represent HCl⁺ (PBS buffer). Compare with Spectrum A.18 (methanol suspension).

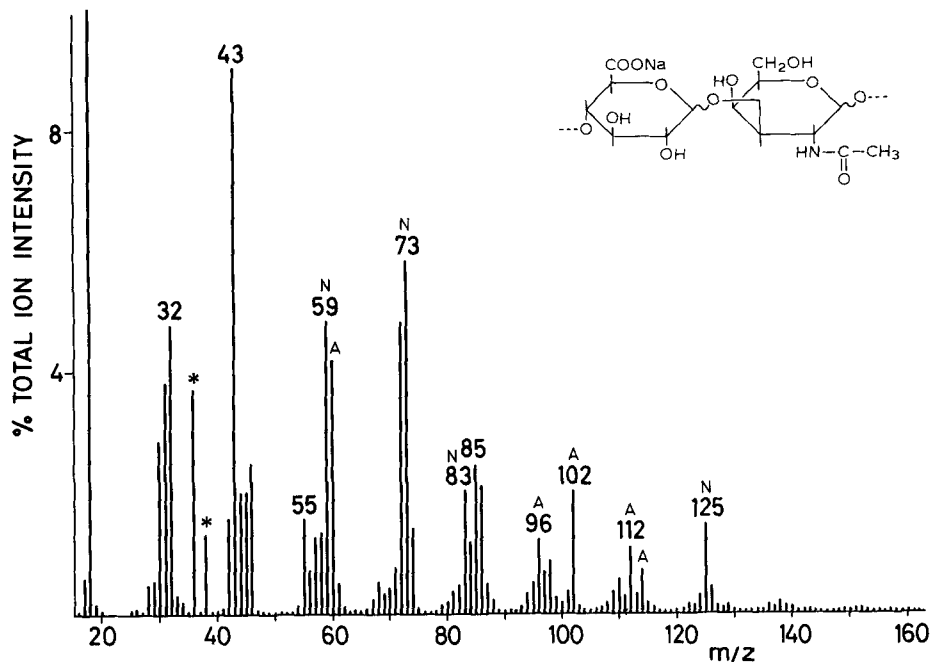
SPECTRUM A.19



SAMPLE : TEICHURONIC ACID (from *Bacillus subtilis*)
 CHEMICAL DETAILS : poly[(1→4)DGlcA_{α,β}(1→3)DGalNac_{α,β}]; see insert in Spectrum A.19a
 SAMPLE ORIGIN : gift from Dr. J.T.M. Wouters, Lab. of Microbiology, Univ. of Amsterdam, The Netherlands
 SAMPLE PREP./SIZE : suspension in methanol; 10 μg
 PYROL. CONDITIONS : standard
 TOTAL ION COUNTS : 3×10^5

REMARKS - Sample prepared following ref. 172. Abundant fragment ions at m/z 59, 73, 83, 109, 125, 139 and 151 indicate the GalNac moieties and the peaks at m/z 96, 102, 112, 114 and 126 the GlcA moieties. Note the large difference between this fragment pattern and that obtained for the neutral PBS solution (Spectrum A.19a).

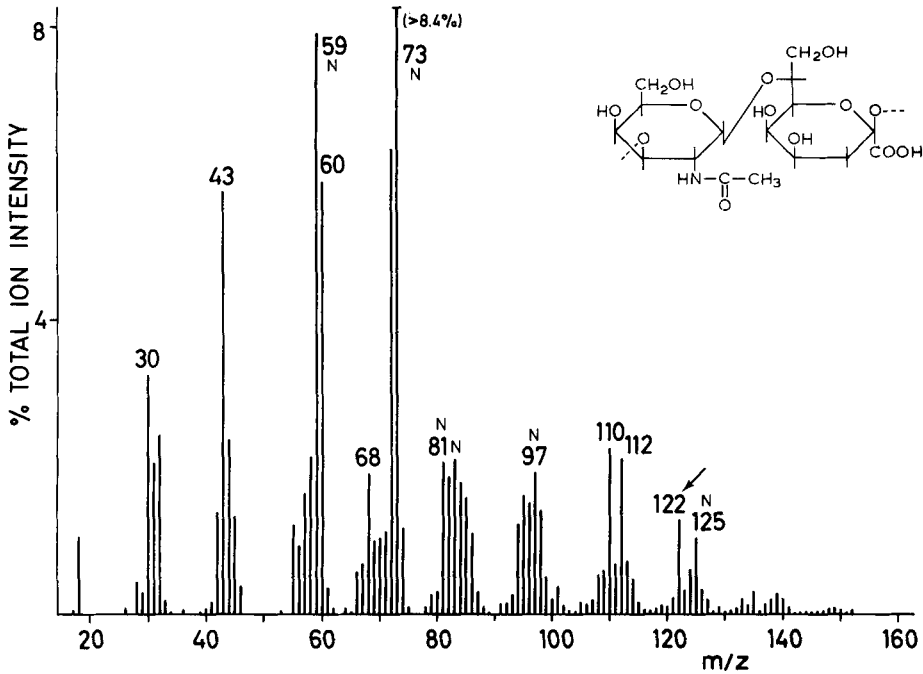
SPECTRUM A.19A



SAMPLE : TEICHURONIC ACID (from *Bacillus subtilis*)
 CHEMICAL DETAILS : poly[(1->4)D-GlcA_α,β-(1->3)D-GalNAc_α,β]; see insert in spectrum
 SAMPLE ORIGIN : gift from Dr. J.T.M. Wouters, Lab. of Microbiology, Univ. of Amsterdam, The Netherlands
 SAMPLE PREP./SIZE : suspension in PBS buffer; 10 μg
 PYROL. CONDITIONS : standard
 TOTAL ION COUNTS : 2 × 10⁵

REMARKS - Sample prepared following ref. 172. This spectrum shows a marked decrease in intensity at m/z 83, 96, 109 and 125 and an increase at m/z 102 with respect to Spectrum A.19. The identities of these fragments have not yet been established. Peaks at m/z 36, 38 represent HCl⁺ (PBS buffer).

SPECTRUM A.20



SAMPLE : CAPSULAR POLYSACCHARIDE (from *Neisseria meningitidis*, Group 29E)

CHEMICAL DETAILS : poly[(2->3)DGalNAc(1->7)KDO]_n; see insert in spectrum

SAMPLE ORIGIN : gift from Dr. E.C. Beuvery, Natl. Inst. Publ. Health, Bilthoven, The Netherlands

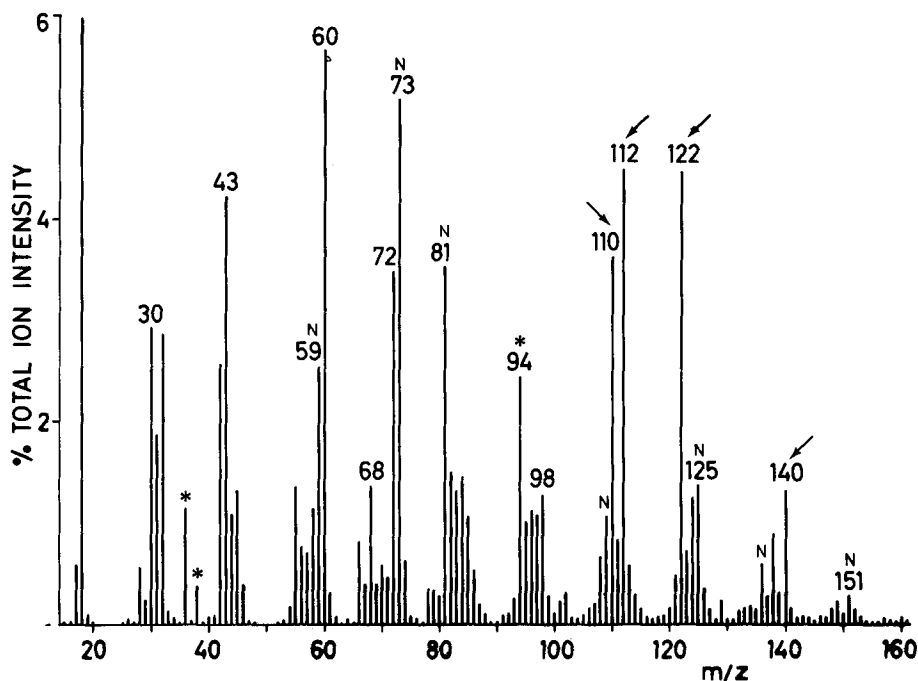
SAMPLE PREP./SIZE : suspension in methanol; 10 μg

PYROL. CONDITIONS : standard

TOTAL ION COUNTS : 2.2 × 10⁵

REMARKS - Sample prepared following ref. 49. Ion series at m/z 59, 73, 95, 97, 109 and 125 are characteristic of hexNAC residues (see Spectrum A.13). The peaks at m/z 110, 112, 122 are indicative of the KDO (ketodeoxyoctonate) residues (see Spectrum A.21) but are much more pronounced in a phosphate buffer environment (compare with Spectrum A.20a).

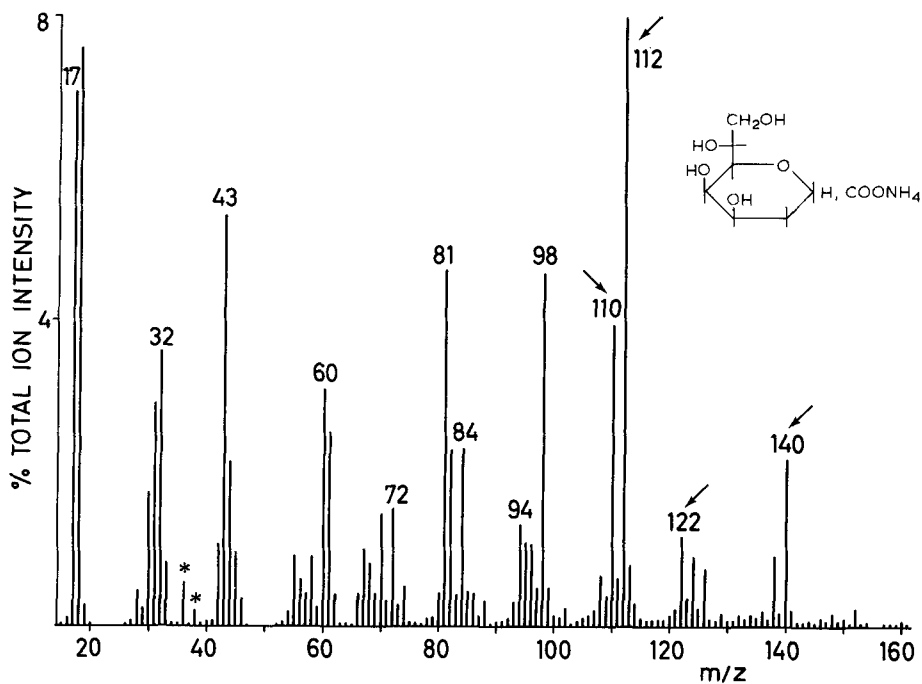
SPECTRUM A.20A



SAMPLE : CAPSULAR POLYSACCHARIDE (from *Neisseria meningitidis*, Group 29E)
 CHEMICAL DETAILS : poly[(2→3)DGalNAcα(1→7)KDOβ]
 SAMPLE ORIGIN : gift from Dr. E.C. Beuvery, Natl. Inst. Publ. Health, Bilthoven, The Netherlands
 SAMPLE PREP./SIZE : suspension in PBS buffer; 10 μg
 PYROL. CONDITIONS : standard
 TOTAL ION COUNTS : 1 X 10⁵

REMARKS - Compare with Spectra A.20 and A.21. The characteristic KDO peak series at m/z 110, 112, 122 and 140 is much more pronounced here. The peak at m/z 94 may be attributable to residual phenol used in the isolation procedure although it is also present in the KDO spectrum (A.21).

SPECTRUM A.21



SAMPLE : 2-KETO-3-DEOXYOCTONATE (KDO), NH₄⁺-salt (3-deoxy-*manno*-octulosonic acid)

CHEMICAL DETAILS : see insert in spectrum; C₈H₁₄O₇, MW=222

SAMPLE ORIGIN : Sigma Chemical Corp., St. Louis, USA

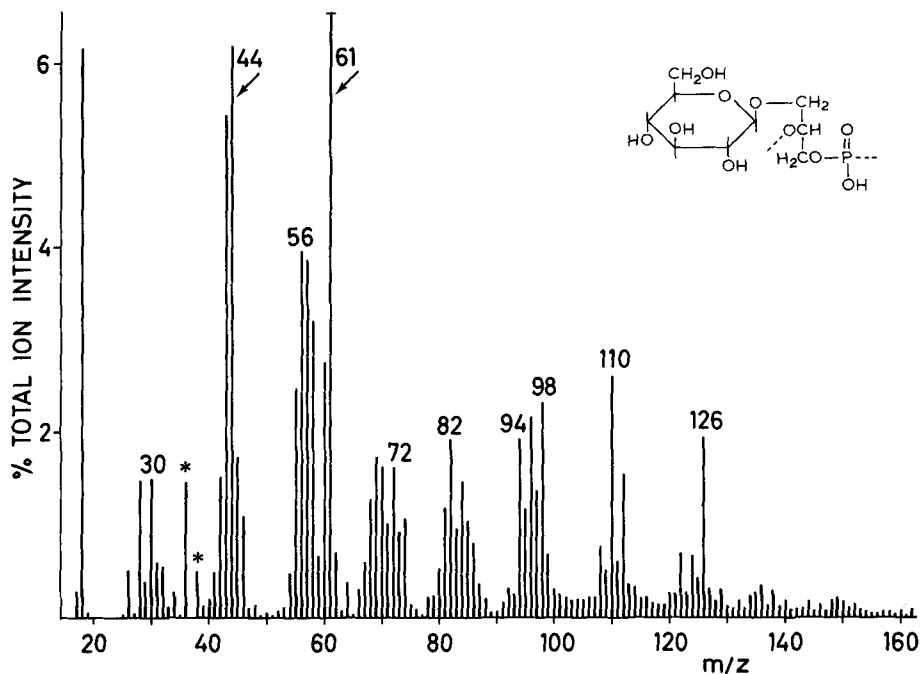
SAMPLE PREP./SIZE : solution in PBS buffer; 10 μg

PYROL. CONDITIONS : standard

TOTAL ION COUNTS : 6 × 10⁴

REMARKS - Note the characteristic peak series at m/z 110, 112, 122 and 140 (see also Spectra A.20 and A.20a). The high m/z 17 originates from the ammonium ions.

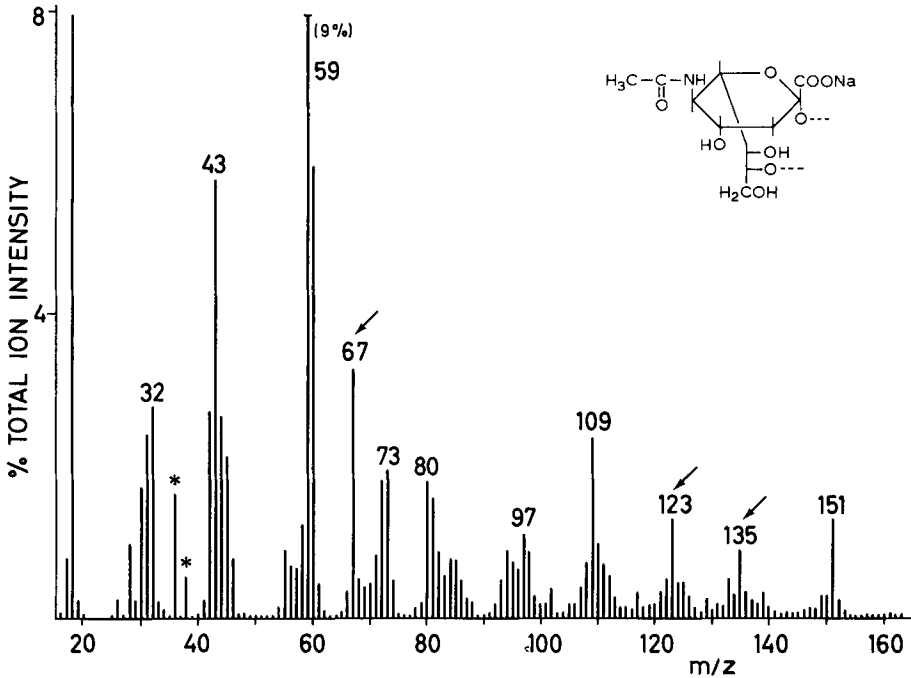
SPECTRUM A.22



SAMPLE : TEICHOIC ACID (from *Bacillus subtilis*)
 CHEMICAL DETAILS : poly[2,3-glycerol-phosphate] with *D*Glc β -units linked to position 1 of glycerol; see insert in spectrum
 SAMPLE ORIGIN : gift from Dr. J.T.M. Wouters, Lab. of Microbiology, Univ. of Amsterdam, The Netherlands
 SAMPLE PREP./SIZE : suspension in methanol; 10 μ g
 PYROL. CONDITIONS : standard
 TOTAL ION COUNTS : 1.2×10^5

REMARKS - Sample prepared following ref. 172. The terminal side chain glucose units appear to give rise to peaks at m/z 96, 98, 110 and 126 (see Spectra A.1-A.4), whereas the most pronounced fragments from the glycerol moieties are thought to be m/z 61 (probably an EI fragment) and m/z 44. Peaks at m/z 36, 38 (HCl^{+}) indicate the presence of chloride in the sample.

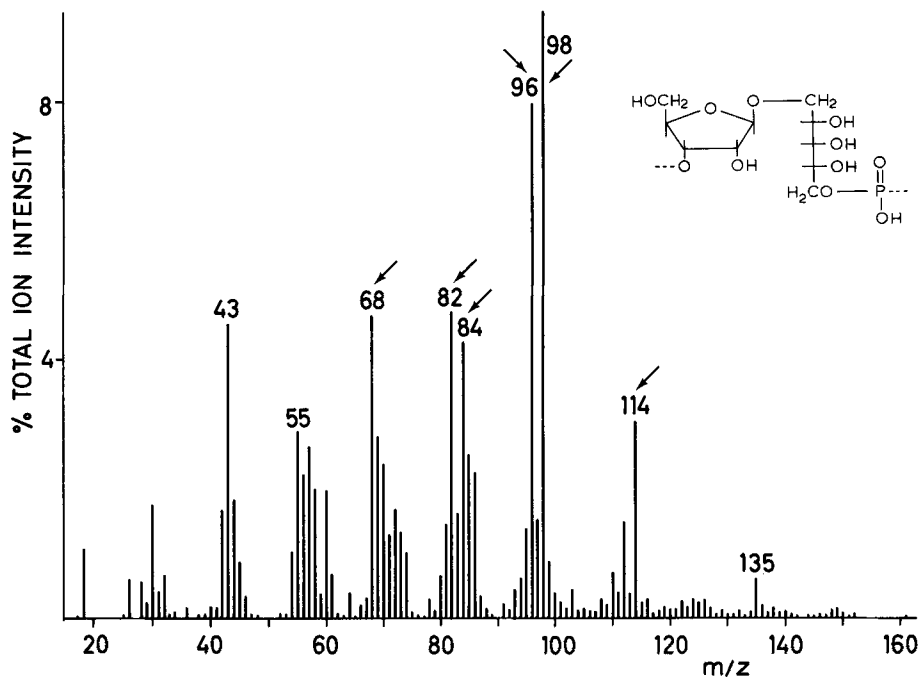
SPECTRUM A.23



SAMPLE : CAPSULAR POLYSACCHARIDE (from *Neisseria meningitidis*, group B)
 CHEMICAL DETAILS : poly[(2->8)-alpha-N-acetylneuraminic acid]; see insert in spectrum
 SAMPLE ORIGIN : gift from Dr. E.C. Beuvery, Natl. Inst. Publ. Health, Bilthoven, The Netherlands
 SAMPLE PREP./SIZE : solution in PBS buffer; 10 μ g
 PYROL. CONDITIONS : standard
 TOTAL ION COUNTS : 1×10^5

REMARKS - Sample prepared following ref. 49. The characteristic, odd-numbered peak series at m/z 59, 67, 73, 97, 109, 123, 135 and 151 is related to that observed for hexNAc-polymers. Marked differences, e.g. with the spectrum of chitin (Spectrum A.13a), are observed at m/z 67 and in the peak group around m/z 81, 123, 125 and 135. The spectrum of this acidic polysaccharide (and also that of the alpha(2->9)-linked analogue) is considerably influenced by the ionic strength and pH of the starting solutions (see also Part I, Figure 11). A comparison of Py-mass spectra of alpha(2->8) and alpha(2->9)-linked poly-N-acetylneuraminic acids and O-acetylated derivatives is made in ref. 49.

SPECTRUM A.24



SAMPLE : CAPSULAR POLYSACCHARIDE (from *Haemophilus influenzae*, type B)

CHEMICAL DETAILS : poly[3DRibβ(1→1)Ribitol-5-phosphate]; see insert in spectrum

SAMPLE ORIGIN : gift from Dr. E.C. Beuvery, Natl. Inst. Publ. Health, Bilthoven, The Netherlands

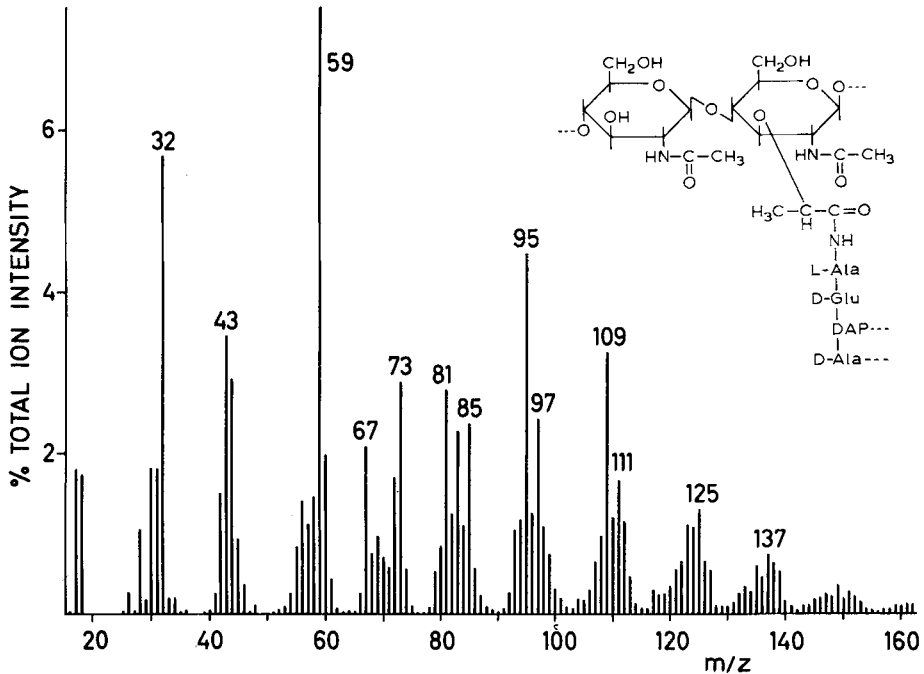
SAMPLE PREP./SIZE : suspension in methanol; 10 μg

PYROL. CONDITIONS : standard

TOTAL ION COUNTS : 5×10^4

REMARKS - The series of ions at m/z 68, 82, 84, 96, 98 and 114 is indicative of pentose polymers; compare with Spectrum C.1 (RNA).

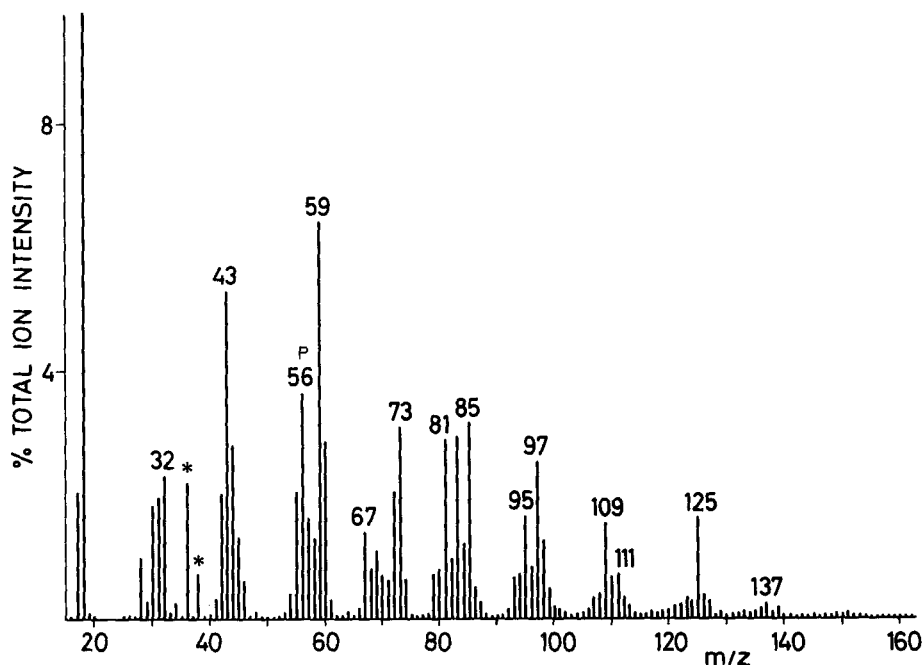
SPECTRUM A.25



SAMPLE : PEPTIDOLYCAN (from *Bacillus subtilis*)
 CHEMICAL DETAILS : poly[(1→4)DGlcNAcβ(1→4)MurNAcβ] with Ala-Glu-diaminopimelic acid-Ala cross-links bound to the polysaccharide chain via the muramic acid carbonyl groups; see insert in spectrum
 SAMPLE ORIGIN : gift from Dr. J.T.M. Wouters, Lab. of Microbiology, Univ. of Amsterdam, The Netherlands
 SAMPLE PREP./SIZE : suspension in methanol; 10 μg
 PYROL. CONDITIONS : standard
 TOTAL ION COUNTS : 5.5 X 10⁴

REMARKS - Sample prepared following ref. 172. The polysaccharide part of this glycoconjugate can be regarded as a chitin chain with D-lactic acid substituents on alternating monomeric residues. The spectrum is dominated by N-acetyl sugar fragments from the GlcNAc and MurNAc residues (compare with chitin Spectrum A.13). No strong signals are found which can be unambiguously ascribed to the amino acid residues. Apparently the small N-containing pyrolysis fragments of these aliphatic amino acids contribute to the same mass values as the amino sugars.

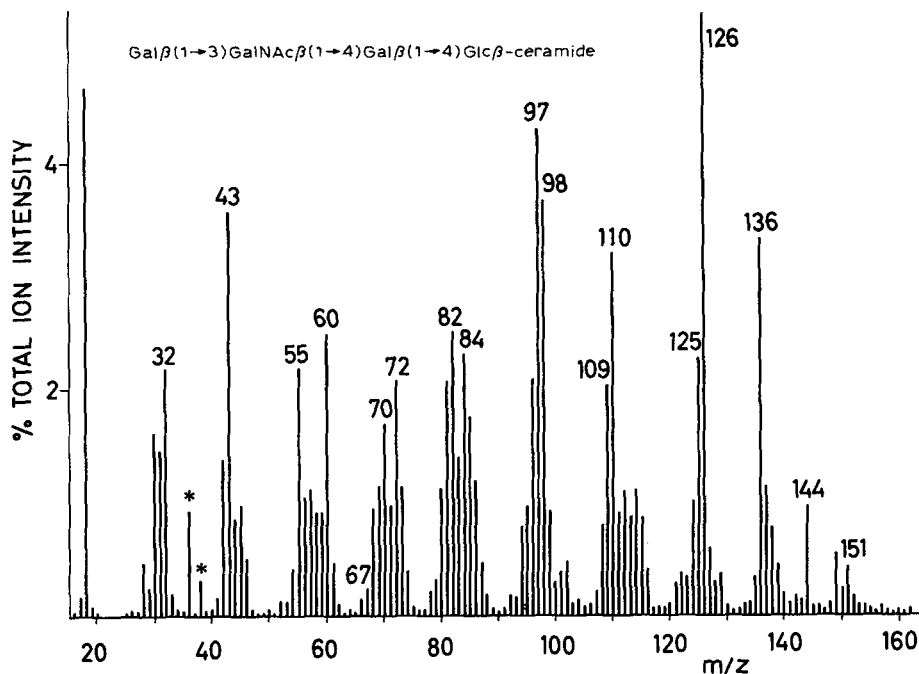
SPECTRUM A.25A



SAMPLE : PEPTIDOGLYCAN (from *Bacillus subtilis*)
 CHEMICAL DETAILS : poly[(1-4)DGlcNAc β (1-4)MurNAc β] with Ala-Glu-diaminopimelic acid-Ala cross-links, bound to the polysaccharide chains via the muramic acid carbonyl groups; see insert in spectrum A.25
 SAMPLE ORIGIN : gift from Dr. J.T.M. Wouters, Lab. of Microbiology, Univ. of Amsterdam, The Netherlands
 SAMPLE PREP./SIZE : suspension in PBS buffer; 10 μ g
 PYROL. CONDITIONS : standard
 TOTAL ION COUNTS : 1×10^5

REMARKS - Sample prepared following ref. 172. In comparison with the spectrum of the methanol suspension (Spectrum A.25) this spectrum shows a marked peak at m/z 56 possibly derived from the aliphatic amino acid and/or the Mur-lactic acid moieties. Also note the increased intensity at m/z 125 as well as the decreased intensities at m/z 95 and 109 as compared to Spectrum A.25. Peaks at m/z 36, 38 represent HCl⁺ (PBS buffer).

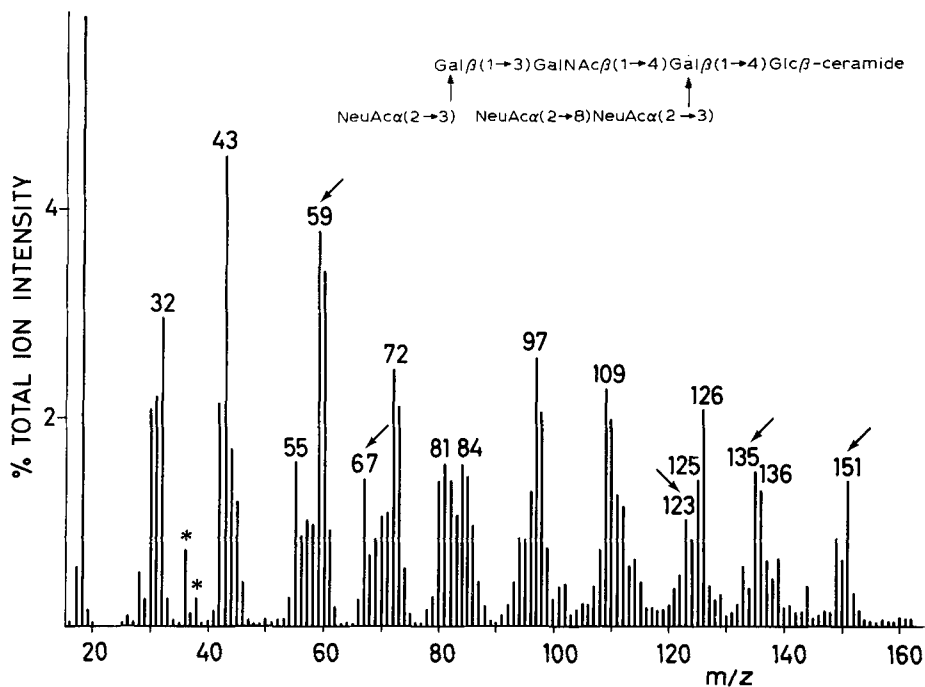
SPECTRUM A.26



SAMPLE : TETRAHEXOSYLCERAMIDE (glycosphingolipid)
 CHEMICAL DETAILS : see insert in spectrum
 SAMPLE ORIGIN : gift from Dr. R.W. Veh, Ruhr Universität, Bochum, GFR
 SAMPLE PREP./SIZE : suspension in PBS buffer; 10 μ g
 PYROL. CONDITIONS : standard
 TOTAL ION COUNTS : 2×10^5

REMARKS - Sample prepared from bovine brain. This glycolipid spectrum is dominated by large peaks at m/z 97, 98, 110 and 126, all of which appear to be derived from the hexose and N-acetylhexosamine moieties. The origin of the unusually large peak at m/z 136 is yet unknown. Although contributions from the lipid moiety might be expected to appear, e.g. at m/z 28, 42, 56, 70 and 84 (alkene fragments), such mass peaks are not pronounced.

SPECTRUM A.27



SAMPLE : GANGLIOSIDE G_{T1b} (Trisialosyl-tetraglycosylceramide)
 CHEMICAL DETAILS : see insert in spectrum
 SAMPLE ORIGIN : gift from Dr. R.W. Veh, Ruhr Universität, Bochum, GFR
 SAMPLE PREP./SIZE : suspension in PBS buffer; 10 µg
 PYROL. CONDITIONS : standard
 TOTAL ION COUNTS : 3×10^5

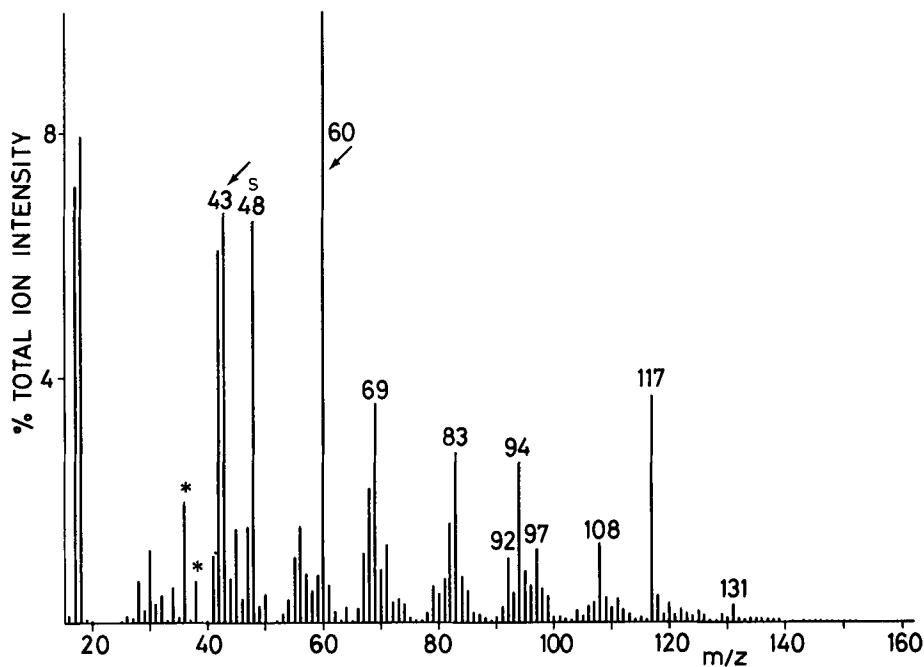
REMARKS - Sample prepared from bovine brain. Compared with the pattern of the asialo-analogue (Spectrum A.26) the spectrum of this ganglioside shows strongly increased signal intensities at m/z 59, 67, 123, 135 and 151. This appears to reflect the presence of the N-acetylneuraminic acid (sialic acid) residues (see Spectrum A.23). Furthermore, the lower intensities at m/z 97, 98, 110, 125 and 126 reflect the decreased percentage of hexose and N-acetylhexosamine residues. As in the case of Spectrum A.26 the lipid moiety is hardly expressed in the spectrum.

This Page Intentionally Left Blank

GROUP B
PEPTIDES AND PROTEINS

This Page Intentionally Left Blank

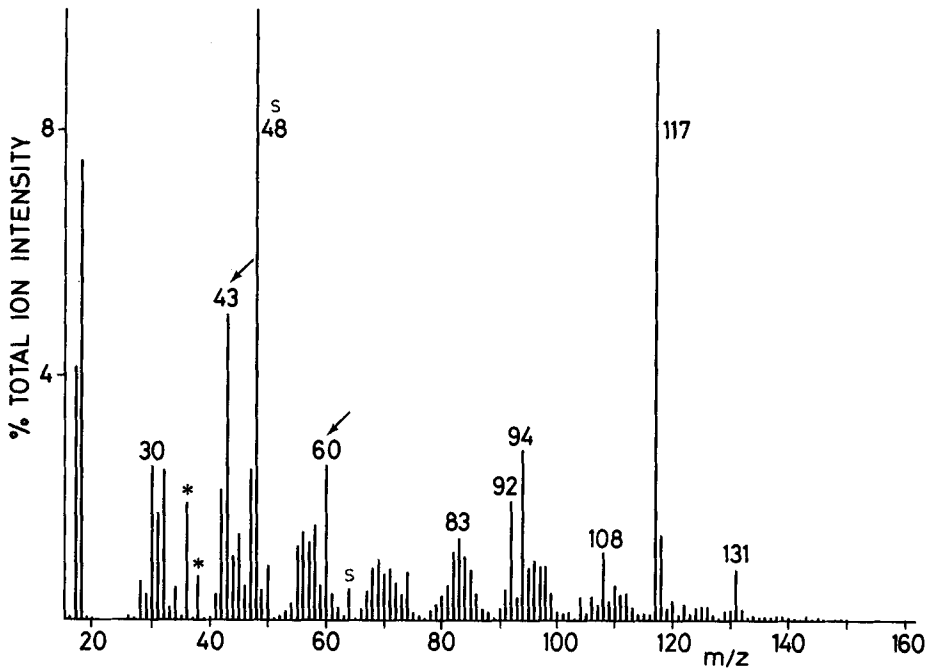
SPECTRUM B.1



SAMPLE : ADRENOCORTICOTROPIC HORMONE, fragment ACTH 1-24
 CHEMICAL DETAILS : H-Ser-Tyr-Ser-Met-Glu-His-Phe-Arg-Trp-Gly-Lys-Pro-Val-Gly-Lys-Lys-Arg-Arg-Pro-Val-Lys-Val-Tyr-Pro-OH
 SAMPLE ORIGIN : gift from Dr. H.M. Greven, Organon, Oss, The Netherlands
 SAMPLE PREP./SIZE : suspension in PBS; 10 μ g
 PYROL. CONDITIONS : standard
 TOTAL ION COUNTS : 2×10^5

REMARKS - The almost complete absence of a peak at m/z 34 (H_2S^{+}) is due to the lack of Cys residues. The relatively small amount of H_2S is formed from Met residues (ref. 58) which mainly yields CH_3SH^{+} (m/z 48). The prominent peak at m/z 69 points to the high Lys and Pro contents. The peak at m/z 60 (in combination with m/z 43) is thought to represent acetic acid derived from the acetate counter ions on the NH_2 -functions of the Lys and Arg residues. The relatively intense peak at m/z 117 in combination with the peak at m/z 131 is mainly due to (methyl)indole derived from the Trp residue.

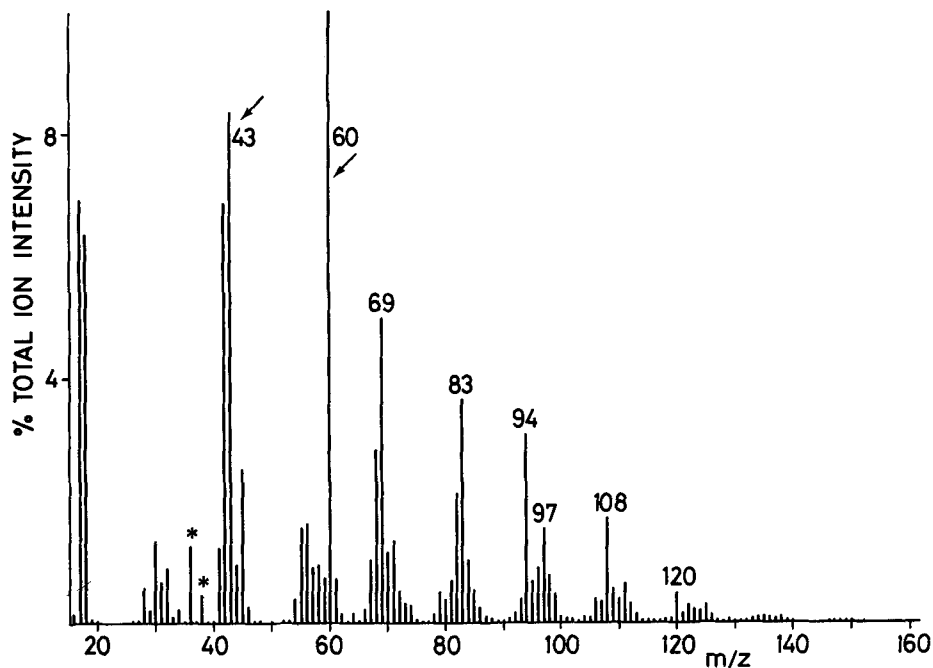
SPECTRUM B.2



SAMPLE : ADRENOCORTICOTROPIC HORMONE, fragment ACTH 1-10
 CHEMICAL DETAILS : H-Ser-Tyr-Ser-Met-Glu-His-Phe-Arg-Trp-Gly-OH
 SAMPLE ORIGIN : gift from Dr. H.M. Greven, Organon, Oss, The Netherlands
 SAMPLE PREP./SIZE : suspension in PBS; 10 μ g
 PYROL. CONDITIONS : standard
 TOTAL ION COUNTS : 2×10^5

REMARKS - Compare with Spectra B.1 and B.3. This spectrum is now entirely dominated by massive Met and Trp fragment peaks at m/z 48 (methanethiol) and m/z 117 (indole), respectively. The acetic acid peaks (m/z 60, 43) are reduced with respect to Spectrum B.1 due to the absence of Lys and the lower Arg content. The small peak at m/z 64 may point to slight oxidation of Met residues (ref. 96).

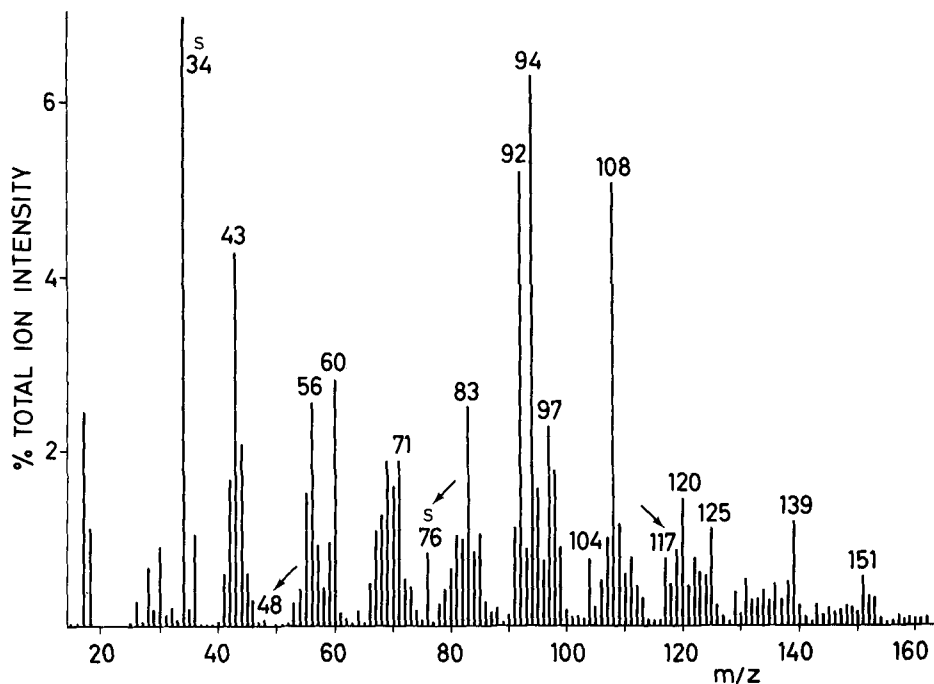
SPECTRUM B.3



SAMPLE : ADRENOCORTICOTROPHIC HORMONE, fragment ACTH 11-24
 CHEMICAL DETAILS : H-Lys-Pro-Val-Gly-Lys-Lys-Arg-Arg-Pro-Val-Lys-Val-Tyr-Pro-OH
 SAMPLE ORIGIN : gift from Dr. H.M. Greven, Organon, Oss, The Netherlands
 SAMPLE PREP./SIZE : suspension in PBS; 10 μ g
 PYROL. CONDITIONS : standard
 TOTAL ION COUNTS : 2.1×10^5

REMARKS - Compare with Spectra B.1 and B.2. For dominant peaks at m/z 60, 43 see remarks on Spectrum B.1. Spectra B.2 and B.3 when compared with Spectrum B.1 show a high degree of additivity.

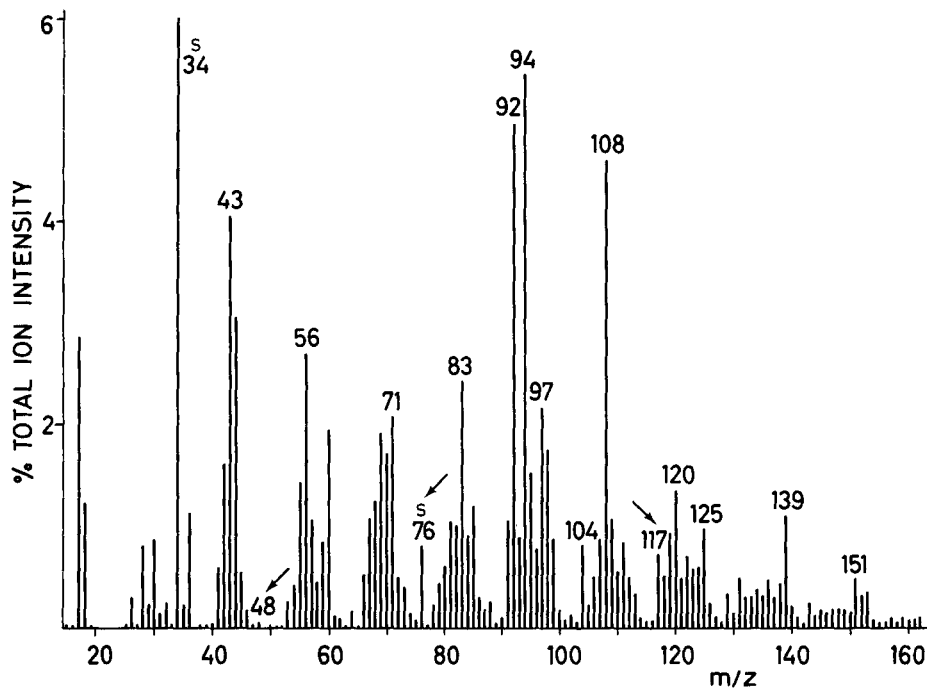
SPECTRUM B.4



SAMPLE : INSULIN (bovine)
 CHEMICAL DETAILS : for amino acid composition, see Table 13; proinsulin-like components ≤ 1 ppm; total salts $< 2\%$
 SAMPLE ORIGIN : Novo Res. Inst., Bagsvaerd, Denmark
 SAMPLE PREP./SIZE : suspension in methanol; 10 μ g
 PYROL. CONDITIONS : standard
 TOTAL ION COUNTS : 3×10^5

REMARKS - The pyrolysis pattern is dominated by fragments derived from the aromatic amino acids Phe and Tyr (m/z 92, toluene; m/z 94, phenol; m/z 108, cresol). The lack of Met residues explains the almost complete absence of a peak at m/z 48 (CH_3SH^+). The minor peak at m/z 117 should be interpreted as phenylacetonitrile from Phe, as Trp residues (yielding indole at this mass value) are absent (ref. 46). The marked peak at m/z 76, tentatively assigned to CS_2^+ probably involves the Cys-Cys-Cys tripeptide linkage region between the A and B chains.

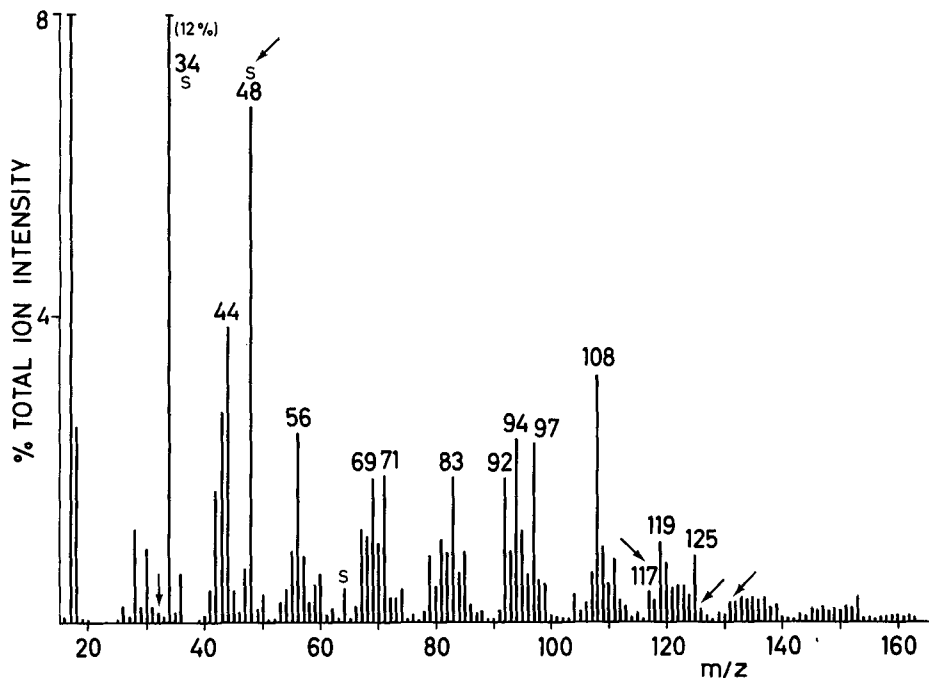
SPECTRUM B.4A



SAMPLE : INSULIN (porcine)
 CHEMICAL DETAILS : for amino acid composition see Table 13; proinsulin-like components ≤ 1 ppm; total salts $< 2\%$
 SAMPLE ORIGIN : Novo Res. Inst., Bagsvaerd, Denmark
 SAMPLE PREP./SIZE : suspension in methanol; 10 μ g
 PYROL. CONDITIONS : standard
 TOTAL ION COUNTS : 3.5×10^5

REMARKS - Note that this spectrum is virtually identical to that of bovine insulin (Spectrum B.4). The only significant differences in relative peak intensities are found at m/z 44, and 60 and are probably connected with the substitution of Thr and Ile residues for Ala and Val residues respectively in the A chain.

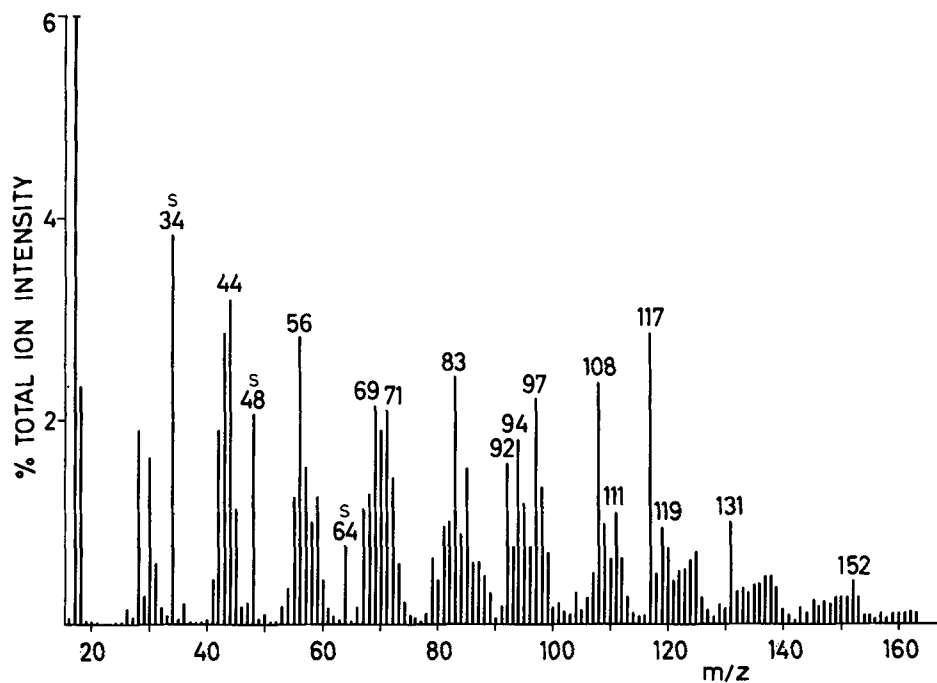
SPECTRUM B.5



SAMPLE : RIBONUCLEASE-A (from bovine pancreas)
 CHEMICAL DETAILS : for amino acid composition see Table 13
 SAMPLE ORIGIN : Boehringer, Mannheim, GFR
 SAMPLE PREP./SIZE : suspension in methanol; 10 μ g
 PYROL. CONDITIONS : standard
 TOTAL ION COUNTS : 1.1×10^5

REMARKS - The absence of Trp residues (producing indole and Me-indole) is indicated by the very low peaks at m/z 117 and 131, whereas the high abundance of Cys, and to a lesser extent Met residues, is evidenced by the high intensities at m/z 34 (H_2S^+) and 48 (CH_3SH^+). Although most RNase samples contain a few percent of hexose and N-acetylhexosamine residues, this carbohydrate content does not contribute significantly to the spectrum as judged by the absence of pronounced peaks at m/z 32 and 126.

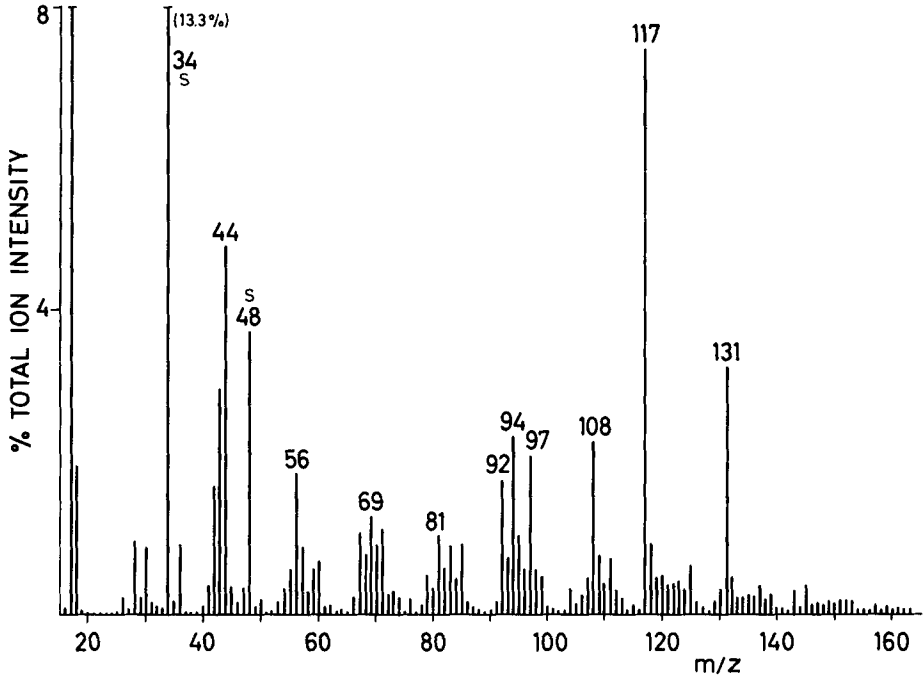
SPECTRUM B.6



SAMPLE : DEOXYRIBONUCLEASE I (from bovine pancreas)
 CHEMICAL DETAILS : for amino acid composition see Table 13
 SAMPLE ORIGIN : BDH Chemicals Ltd., Poole, UK
 SAMPLE PREP./SIZE : suspension in methanol; 10 μ g
 PYROL. CONDITIONS : standard
 TOTAL ION COUNTS : 1.7×10^5

REMARKS - In comparison with RNase (Spectrum B.5) the decrease in Cys and Met content as well as the appearance of Trp residues produce the expected changes at m/z 34, 48, 117 and 131. It should be noted, however, that the marked differences in the percentage contribution of some aliphatic amino acid residues, e.g. Leu, Ile, Val and Ala produce far less clearly defined differences in the spectrum. The peak at m/z 64 (SO_2^{+} and/or CH_3SOH^{+}) may point to slight oxidation of sulphur-containing amino acid residues.

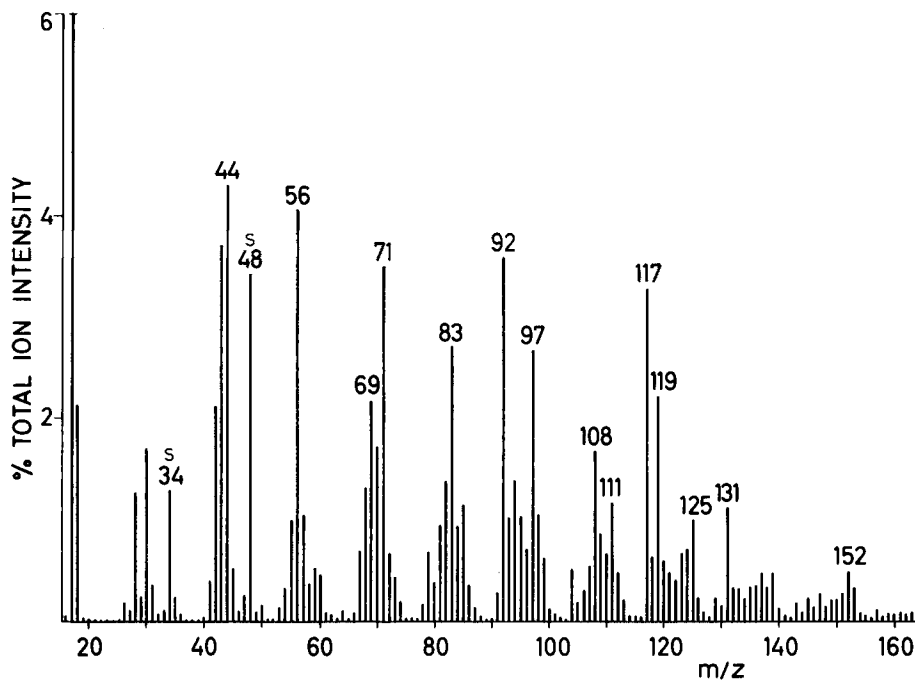
SPECTRUM B.7



SAMPLE : LYSOZYME (from chicken egg yolk)
 CHEMICAL DETAILS : for amino acid composition see Table 13
 SAMPLE ORIGIN : Boehringer, Mannheim, GFR
 SAMPLE PREP./SIZE : suspension in methanol; 10 μ g
 PYROL. CONDITIONS : standard
 TOTAL ION COUNTS : 1.2×10^5

REMARKS - Most notable are the very large peaks at m/z 34, 117 and 131 indicative of the high Cys and Trp content.

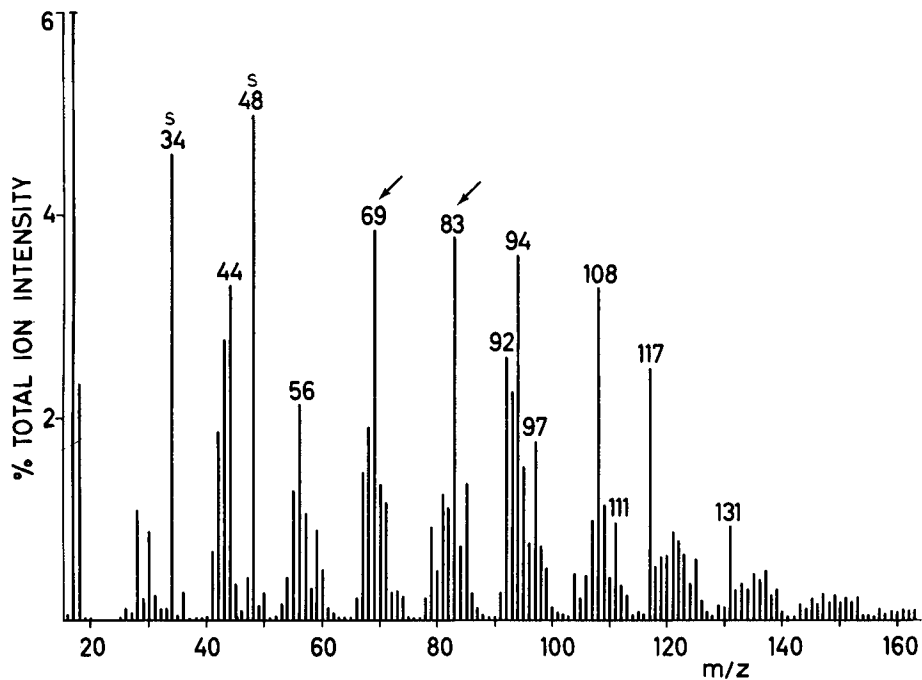
SPECTRUM B.8



SAMPLE : HEMOGLOBIN (from bovine erythrocytes)
 CHEMICAL DETAILS : for amino acid composition see Table 13
 SAMPLE ORIGIN : J.T. Baker Chemicals, Phillipsburg, NJ, USA
 SAMPLE PREP./SIZE : suspension in methanol; 10 μ g
 PYROL. CONDITIONS : standard
 TOTAL ION COUNTS : 1×10^5

REMARKS - This protein shows a rather balanced pattern. Specially noteworthy is the obvious absence of peaks which can be directly ascribed to the heme moiety. However, it should be realized that the porphyrin unit represents only about 1% by weight of the organic material. Moreover, the heme moiety tends not to give characteristic fragments, e.g. pyrrole and pyrroline derivatives, such as formed from bilirubin (Spectrum G.10).

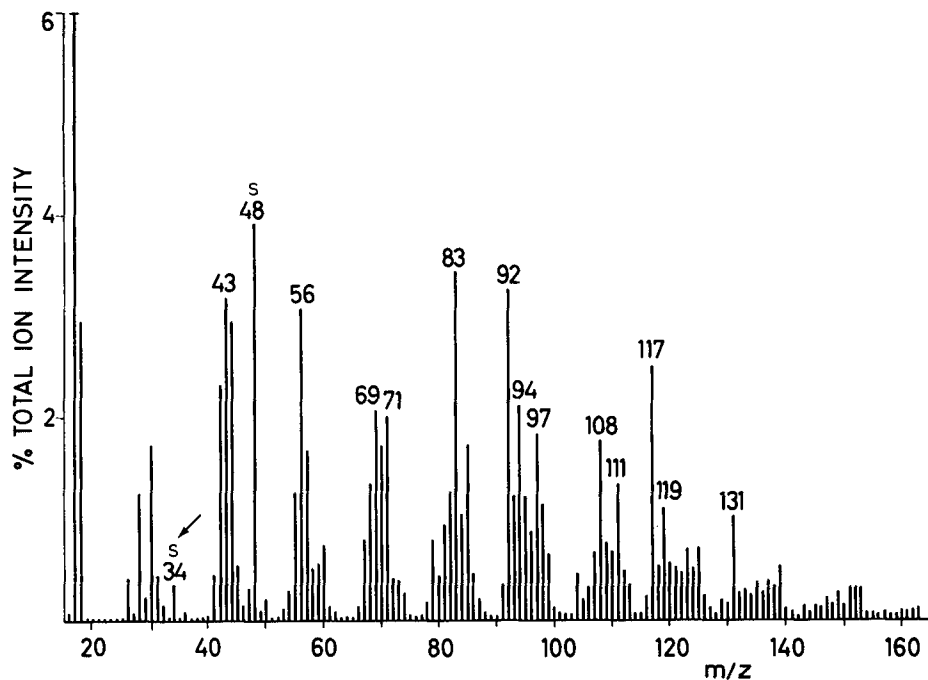
SPECTRUM B.9



SAMPLE : CYTOCHROME C (from equine heart)
 CHEMICAL DETAILS : for amino acid composition see Table 13
 SAMPLE ORIGIN : Boehringer, Mannheim, GFR
 SAMPLE PREP./SIZE : suspension in methanol; 10 μ g
 PYROL. CONDITIONS : standard
 TOTAL ION COUNTS : 1×10^5

REMARKS - High intensities at m/z 69, 83 with respect to hemoglobin (Spectrum B.8) may point to the high Lys content; the higher peaks at m/z 94, 108 to the higher Tyr content and the lower peak at m/z 119 to less Phe. As in the case of hemoglobin no marked contribution of the porphyrin group appears to be visible.

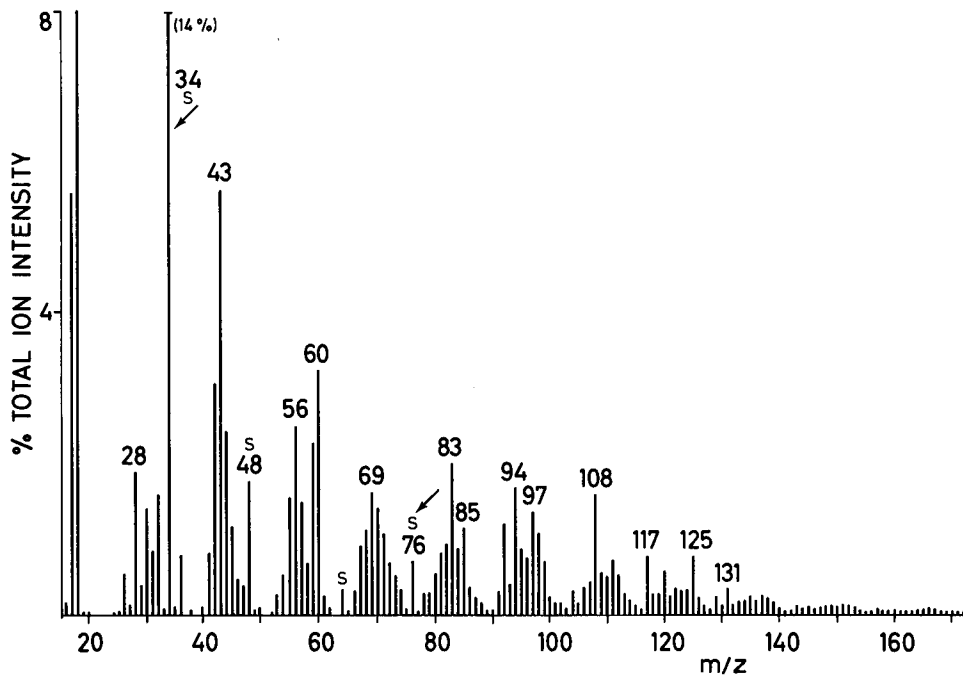
SPECTRUM B.10



SAMPLE : MYOGLOBIN, Type 1 (from equine skeletal muscle)
 CHEMICAL DETAILS : for amino acid composition see Table 13
 SAMPLE ORIGIN : Sigma Chemical Corp., St. Louis, USA
 SAMPLE PREP./SIZE : suspension in methanol; 10 μ g
 PYROL. CONDITIONS : standard
 TOTAL ION COUNTS : 4×10^4

REMARKS - The very low peak at m/z 34 indicates the absence of Cys residues and probably represents a minor fragment of Met (mainly producing methanethiol, m/z 48). As in the case of Cytochrome C (Spectrum B.9) the large peaks at m/z 69 and 83 probably represent the abundant Lys residues.

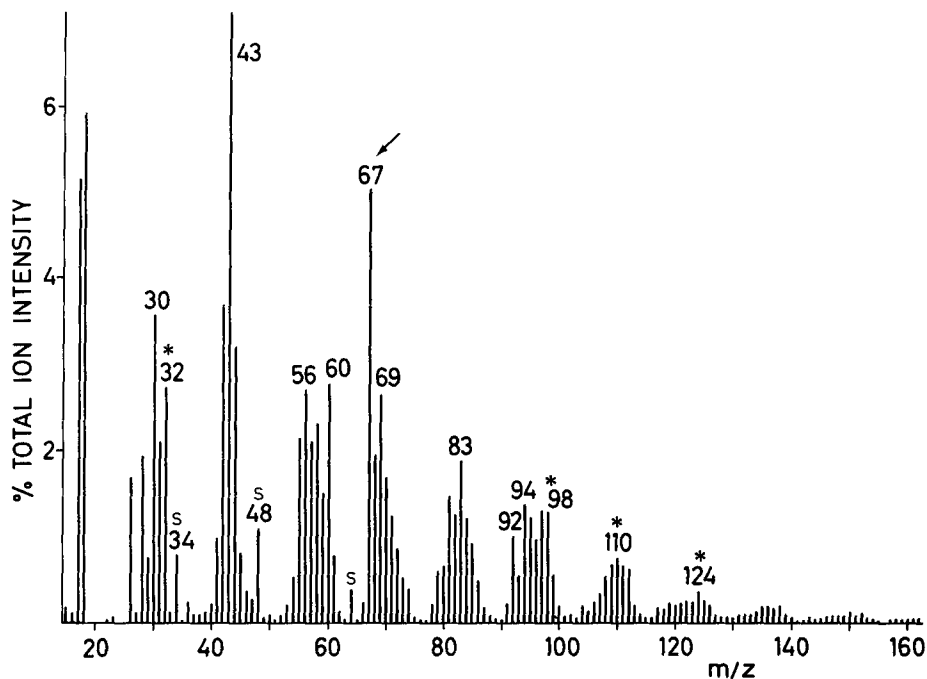
SPECTRUM B.11



SAMPLE : KERATIN
 CHEMICAL DETAILS : for amino acid composition see Table 13
 SAMPLE ORIGIN : Merck AG, Darmstadt, GFR
 SAMPLE PREP./SIZE : suspension in methanol; 10 μ g
 PYROL. CONDITIONS : standard
 TOTAL ION COUNTS : 1×10^5

REMARKS - This spectrum shows the extremely high H_2S^{+} peak at m/z 34 so characteristic for the abundant Cys residues in keratin. Although this peak is off-scale its actual height can be judged from the isotope peak at m/z 36 (5% ^{34}S abundance). The high Cys content also appears to be responsible for the marked peak at m/z 76 thought to represent CS_2^{+} .

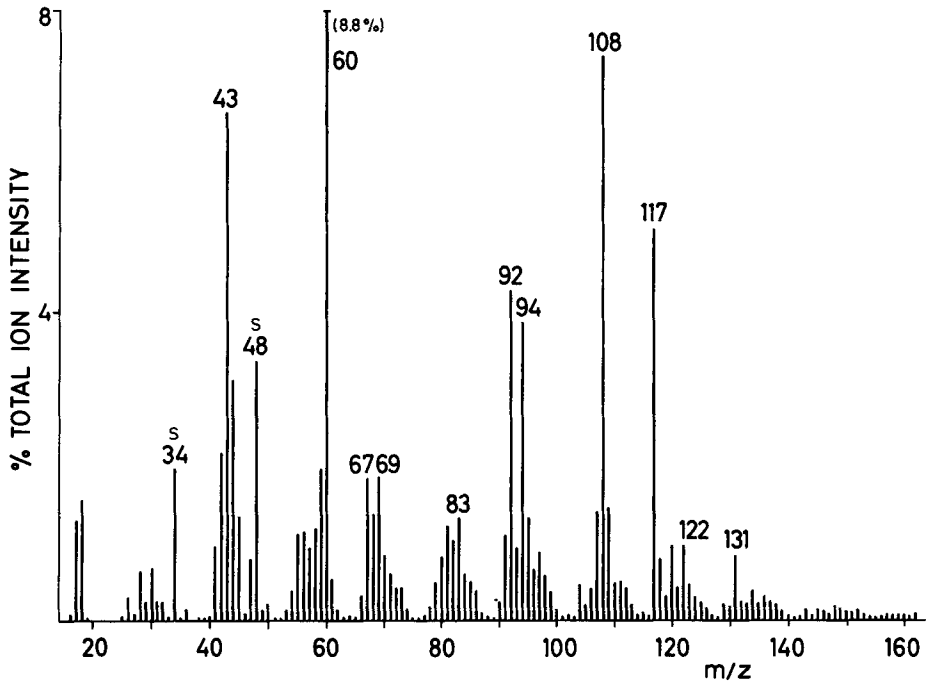
SPECTRUM B.12



SAMPLE : COLLAGEN (from bovine Achilles tendon)
 CHEMICAL DETAILS : for amino acid composition see Table 13
 SAMPLE ORIGIN : Koch-Light Ltd., Colnbrook, Bucks., UK
 SAMPLE PREP./SIZE : suspension in methanol; 10 μ g
 PYROLY. CONDITIONS : standard
 TOTAL ION COUNTS : 6×10^4

REMARKS - This spectral pattern is very unusual compared to those of most other proteins due to the extremely high content of Gly, Ala, Pro and Hyp residues, the complete absence of Trp and the very low contributions of aromatic and S-containing amino acid residues. The aliphatic character of this protein causes the dominance of small pyrolysis and EI fragments (with exception of the marked pyrrole and dihydropyrrole peaks at m/z 67, 69 and 83 from the Pro, Lys and Hyp moieties). Small amounts of carbohydrate are indicated by peaks at m/z 31, 32, 96, 98, 110 and 124.

SPECTRUM B.13



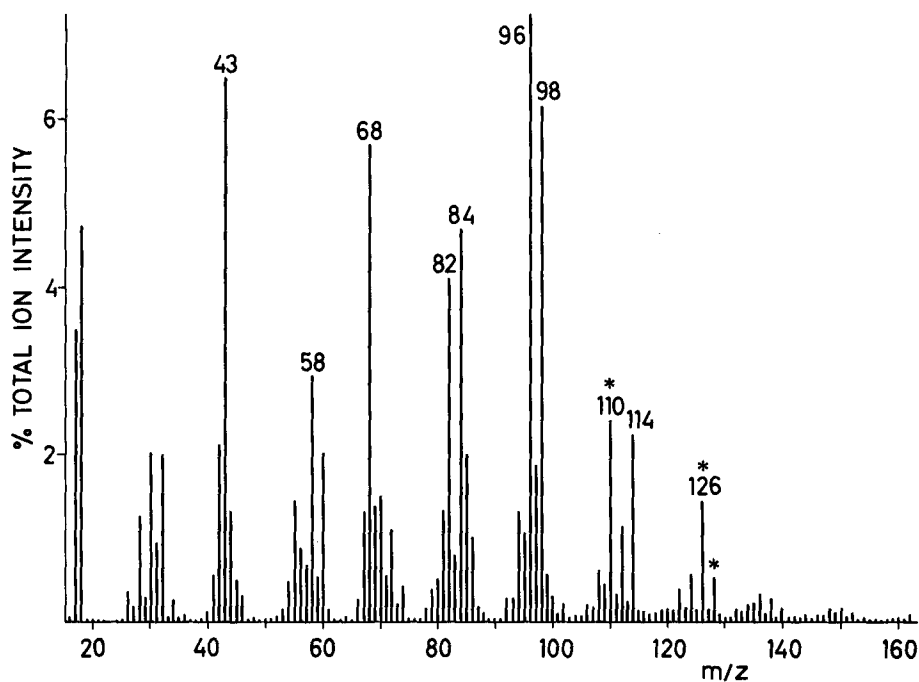
SAMPLE : CERULOPLASMIN (porcine)
 CHEMICAL DETAILS : for amino acid composition see Table 13
 SAMPLE ORIGIN : gift from Dr. R. Wever, Inst. of Biochemistry, Univ. of Amsterdam, The Netherlands
 SAMPLE PREP./SIZE : solution in H₂O, 10 µg
 PYROL. CONDITIONS : standard
 TOTAL ION COUNTS : 3.4×10^5

REMARKS - The aromatic character of this glycoprotein is expressed by the high peaks at m/z 92, 94, 108, 117 and 131. Although carbohydrate constitutes up to 7% by weight no obvious sugar signals are present. Peaks at m/z 43 and 60 are thought to stem mainly from acetate.

GROUP C
NUCLEOTIDES AND NUCLEIC ACIDS

This Page Intentionally Left Blank

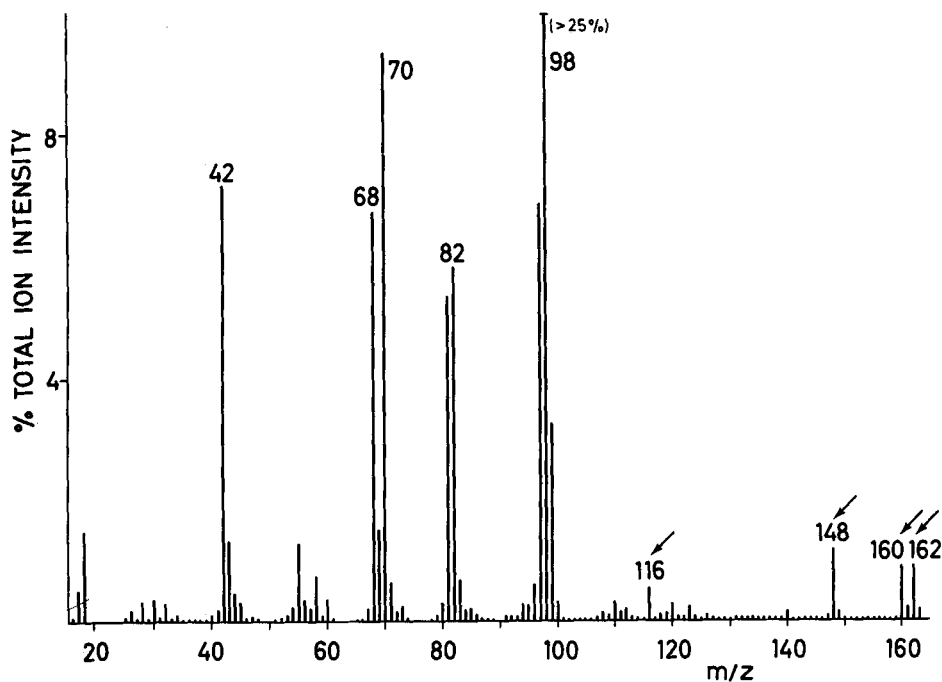
SPECTRUM C.1



SAMPLE : RIBONUCLEIC ACID (RNA) (from baker's yeast)
 CHEMICAL DETAILS : -
 SAMPLE ORIGIN : Aldrich Chem. Corp. Inc., Milwaukee, USA
 SAMPLE PREP./SIZE : suspension in methanol; 10 μ g
 PYROL. CONDITIONS : standard
 TOTAL ION COUNTS : 3.5×10^4

REMARKS - As discussed in Part I, Section 3.3, Curie-point pyrolysis mass spectra of RNA are completely dominated by ribose moiety fragments (compare also with Spectrum C.2 (DNA)). Signals which can be ascribed to complete base moieties or base moiety fragments are absent due to the loss of more or less intact base moieties by condensation on the wall of the reaction tube with an exception of the peak at m/z 17 which may result from deamination of base moieties. Such base fragments become more prominent when the entire pyrolysate transfer line is heated (ref. 205) indicating that in the present spectrum the absence of such fragments is due to condensation losses. The marked peaks at m/z 110, 126 and 128 point to the presence of residual hexose impurities in this sample.

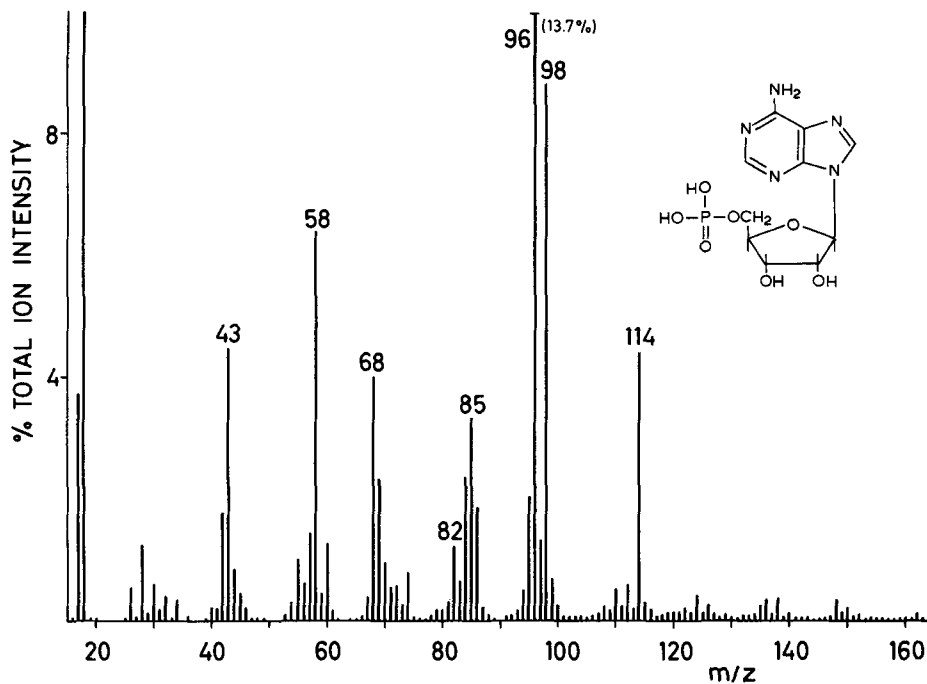
SPECTRUM C.2



SAMPLE : DEOXYRIBONUCLEIC ACID (DNA), Na-salt (from calf thymus)
 CHEMICAL DETAILS : -
 SAMPLE ORIGIN : Sigma Chemical Corp., St. Louis, USA
 SAMPLE PREP./SIZE : suspension in methanol; 10 μ g
 PYROL. CONDITIONS : standard
 TOTAL ION COUNTS : 1×10^5

REMARKS - The spectrum is dominated by deoxyribose moiety fragments, as discussed in Part I, Section 3.3 (compare also with Spectrum C.1 (RNA)). The peak at m/z 116 is often more pronounced in other DNA preparations. Note the characteristic (methyl)furan condensation products at m/z 148, 160 and 162, also described by Schulten *et al.* (ref. 62). At present it is not certain whether these products originate from recombination of (methyl)furan radicals or through successive eliminations of base and phosphate residues from the polymer chain.

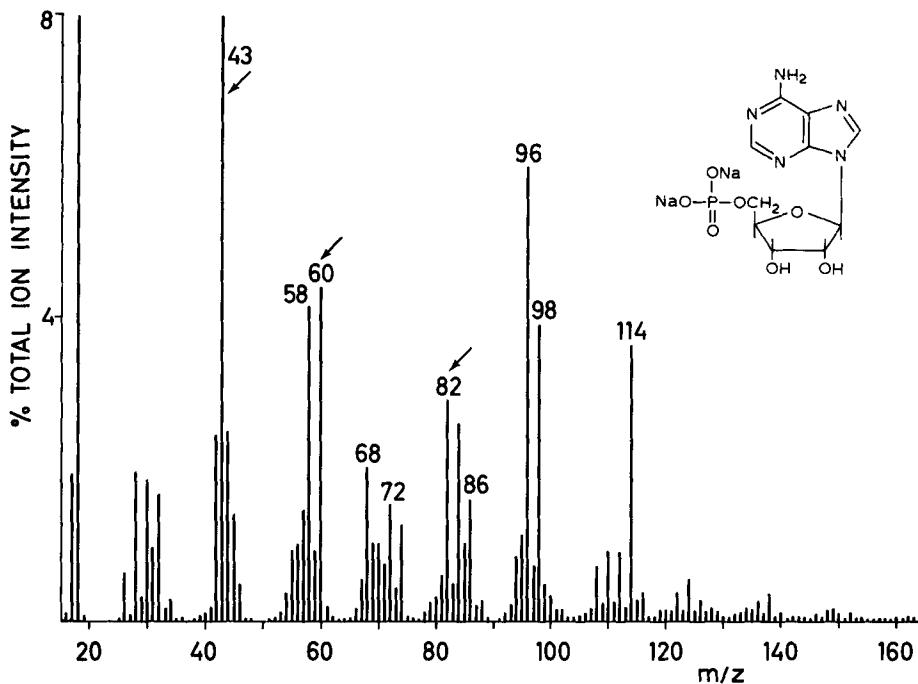
SPECTRUM C.3



SAMPLE : ADENOSINE-5'-PHOSPHATE (5'-AMP), free acid
 CHEMICAL DETAILS : see insert in spectrum; $C_{10}H_{14}N_5O_7P$; MW = 347
 SAMPLE ORIGIN : Serva, Heidelberg, GFR
 SAMPLE PREP./SIZE : suspension in methanol; 10 μ g
 PYROL. CONDITIONS : standard
 TOTAL ION COUNTS : 4×10^4

REMARKS - As in the spectrum of RNA (Spectrum C.1), ribose moiety fragments are almost exclusively present in this spectrum. The peak at m/z 114 can be rationalized as representing the loss of water from the ribose moiety. Compare also with the spectrum of the Na-salt of 5'-AMP (Spectrum C.4).

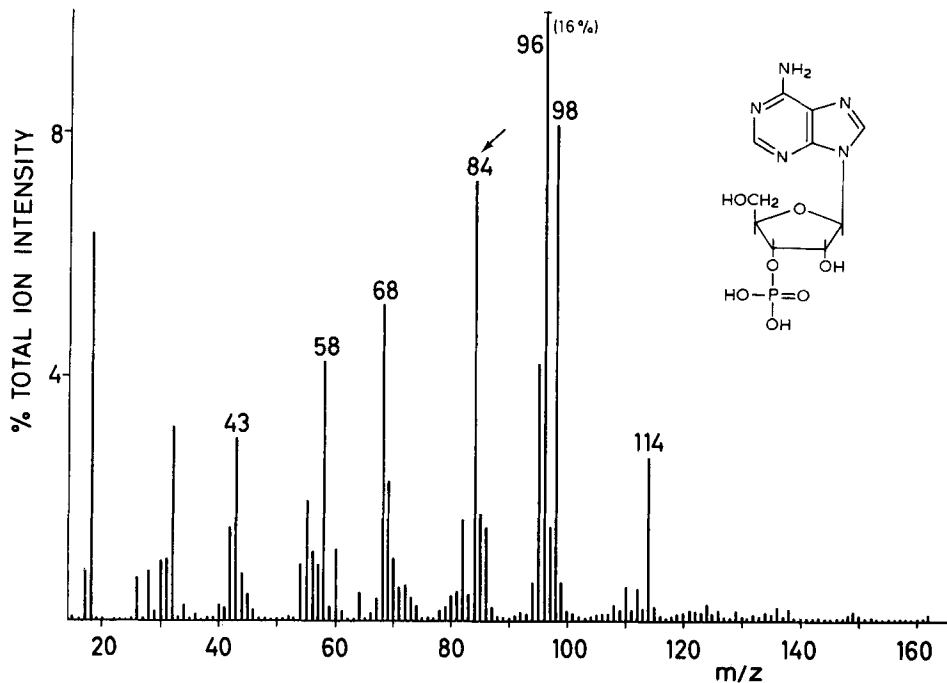
SPECTRUM C,4



SAMPLE : ADENOSINE-5'-PHOSPHATE (5'-AMP), Na-salt
 CHEMICAL DETAILS : see insert in spectrum; $C_{10}H_{12}N_5Na_2O_7P$; MW = 391
 SAMPLE ORIGIN : Serva, Heidelberg, GFR
 SAMPLE PREP./SIZE : suspension in methanol; 10 μ g
 PYROL. CONDITIONS : standard
 TOTAL ION COUNTS : 3.2×10^5

REMARKS - In comparison with the spectrum of the corresponding free acid (Spectrum C.3) marked quantitative changes are observed at m/z 43, 60, 72, 82, 85 indicating the importance of the ionic status of the compound.

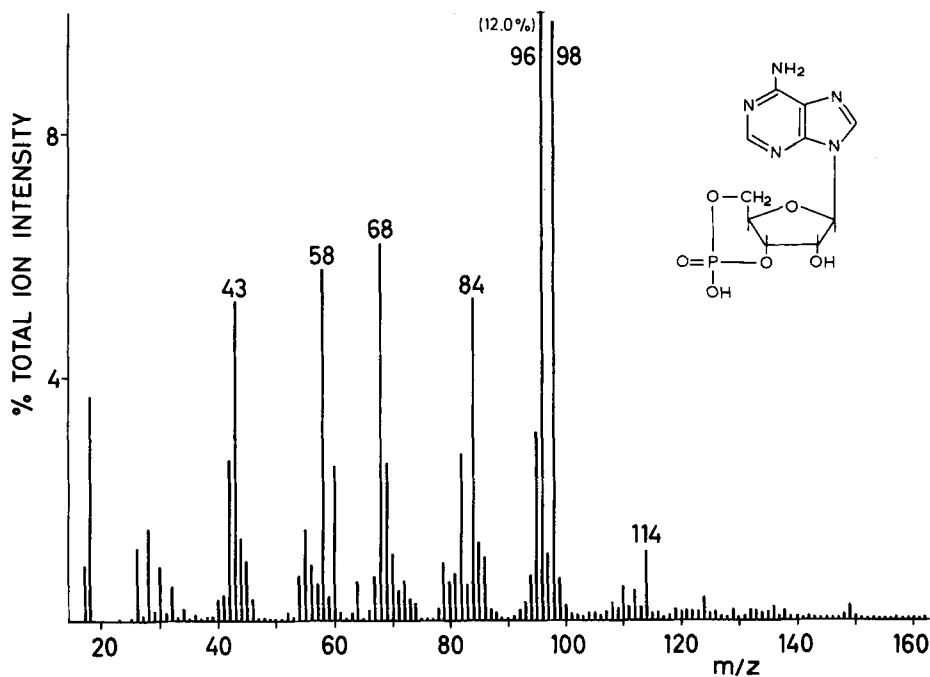
SPECTRUM C.5



SAMPLE : ADENOSINE-3'-PHOSPHATE (3'-AMP), free acid
 CHEMICAL DETAILS : see insert in spectrum; $C_{10}H_{14}N_5O_7P$; MW = 347
 SAMPLE ORIGIN : Serva, Heidelberg, GFR
 SAMPLE PREP./SIZE : suspension in methanol, 10 μ g
 PYROL. CONDITIONS : standard
 TOTAL ION COUNTS : 5×10^4

REMARKS - In comparison with the spectrum of 5'-AMP (Spectrum C.3) the intensity of the peaks at m/z 85 and 114 is reduced whereas a markedly higher peak is observed at m/z 84. This indicates the strong influence of the position of the phosphate group on the pyrolytic fragmentation pathways.

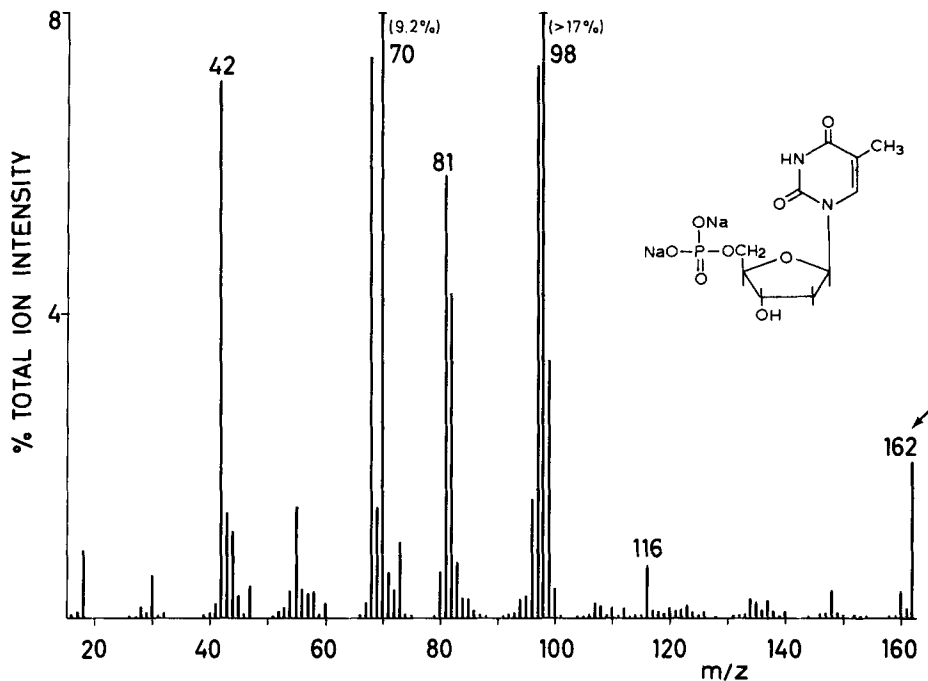
SPECTRUM C.6



SAMPLE : ADENOSINE-3',5'-PHOSPHATE (cyclic AMP), free acid
 CHEMICAL DETAILS : see insert in spectrum; $C_{10}H_{12}N_5O_6P$; MW = 329
 SAMPLE ORIGIN : Serva, Heidelberg, GFR
 SAMPLE PREP./SIZE : suspension in methanol, 10 μ g
 PYROL. CONDITIONS : standard
 TOTAL ION COUNTS : 4×10^4

REMARKS - This spectrum closely resembles that of 3'-AMP (Spectrum C.5), although the intensity of the peak at m/z 114 appears to be further reduced, possibly as a result of blocking of the elimination of the ribose moiety from the molecule described by Posthumus *et al.* (ref. 72).

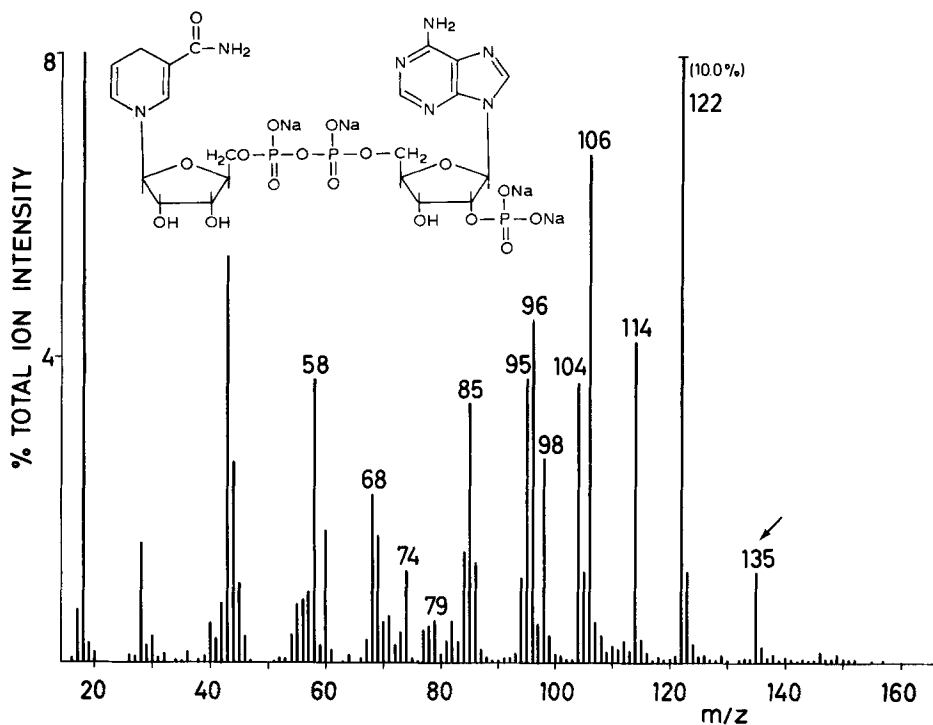
SPECTRUM C.7



SAMPLE : THYMIDINE-5'-PHOSPHATE (5'-TMP), Na-salt
 CHEMICAL DETAILS : see insert in spectrum; $C_{10}H_{13}N_2Na_2O_8P$; MW = 366
 SAMPLE ORIGIN : Serva, Heidelberg, GFR
 SAMPLE PREP./SIZE : suspension in methanol, 10 μ g
 PYROL. CONDITIONS : standard
 TOTAL ION COUNTS : 1.2×10^5

REMARKS - As is to be expected this pattern closely resembles that of DNA (see Spectrum C.2); both spectra are dominated by deoxyribose moiety fragments. Note the marked peak intensity at m/z 162 apparently caused by recombination of methylfuran radicals. Occurrence of such recombination reactions is rarely observed in filament pyrolysis and can be further reduced by using smaller sample amounts.

SPECTRUM C.8



SAMPLE : NICOTINAMIDE ADENINE DINUCLEOTIDE PHOSPHATE, reduced (NADPH)

CHEMICAL DETAILS : see insert in spectrum; $C_{21}H_{26}N_7Na_4O_{17}P_3$; MW = 833

SAMPLE ORIGIN : Boehringer, Mannheim, GFR

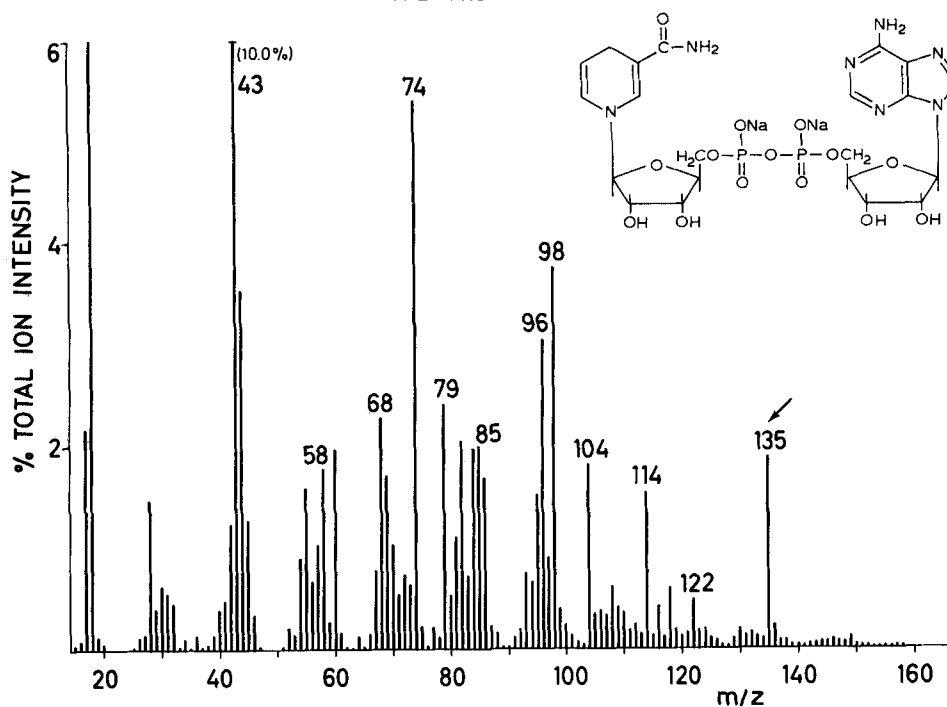
SAMPLE PREP./SIZE : suspension in methanol, 10 μ g

PYROL. CONDITIONS : standard

TOTAL ION COUNTS : 3×10^5

REMARKS - Apart from the typical ribose fragment series (compare Spectra C.1, C.3) this spectrum shows marked contributions from the nicotinamide (m/z 79, 95, 104, 106, 122) and adenine (m/z 135) moieties. The presence of adenine is especially noteworthy since no adenine signal is observed in Py-mass spectra of DNA or AMP (see Spectra C.2-C.4). Apparently, in the latter cases no free base moieties are produced as discussed in Part I, Section 3.3.

SPECTRUM C.9



SAMPLE : NICOTINAMIDE ADENINE DINUCLEOTIDE, reduced (NADH)
 CHEMICAL DETAILS : see insert in spectrum; $C_{21}H_{27}N_7Na_2O_{14}P_2$; MW = 709
 SAMPLE ORIGIN : Boehringer, Mannheim, GFR
 SAMPLE PREP./SIZE : suspension in methanol; 10 μ g
 PYROL. CONDITIONS : standard
 TOTAL ION COUNTS : 2×10^5

REMARKS - In comparison with the spectrum of NADPH (Spectrum C.8), the absence of the phosphate group in position 2' of the adenine-bearing ribose moiety causes marked quantitative differences in the relative intensities of the peak series of the ribose, adenine and nicotinamide moieties.

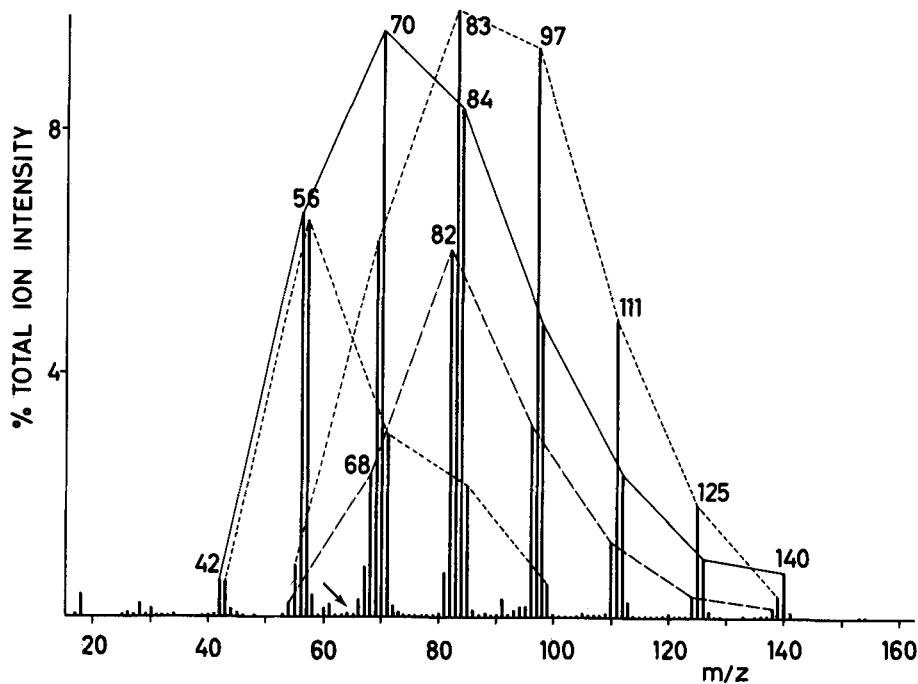
This Page Intentionally Left Blank

GROUP D

LIPIDS

This Page Intentionally Left Blank

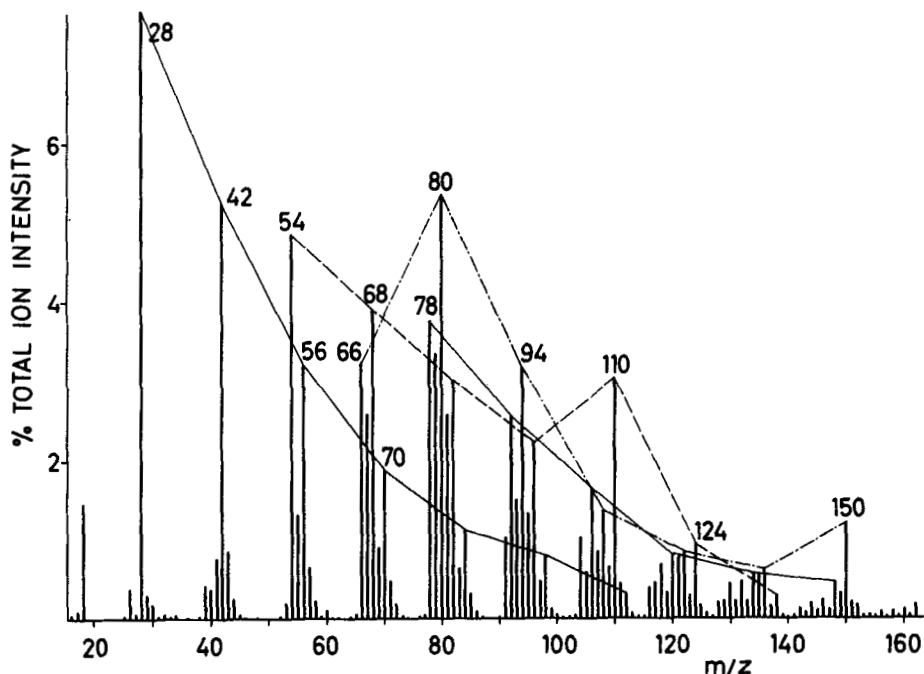
SPECTRUM D.1



SAMPLE : SODIUM LAURYL SULPHATE
 CHEMICAL DETAILS : $\text{CH}_3(\text{CH}_2)_{10}\text{CH}_2\text{OSO}_3\text{Na}$; MW = 288
 SAMPLE ORIGIN : Hahmes, Maastricht, The Netherlands
 SAMPLE PREP./SIZE : suspension in methanol; 20 μg
 PYROL. CONDITIONS : standard
 TOTAL ION COUNTS : 1×10^5

REMARKS - The spectrum is dominated by two homologous molecular ion series, namely at m/z 42, 56, etc. (alkenes) and at m/z 54, 68, etc. (alkadienes and/or alkynes) as well as two homologous fragment ion series at m/z 43, 57, etc. (alkyl fragments) and at m/z 55, 69, etc. (alkenyl fragments). Comparison with polyethylene (Spectrum H.1) shows that the alkenyl and alkadiene (alkyne) ion series are much more pronounced, probably as a result of unsaturation of the aliphatic hydrocarbon chain upon pyrolytic elimination of the sulphonate end group. Note the complete absence of obvious aromatic and sulphur-containing ion series.

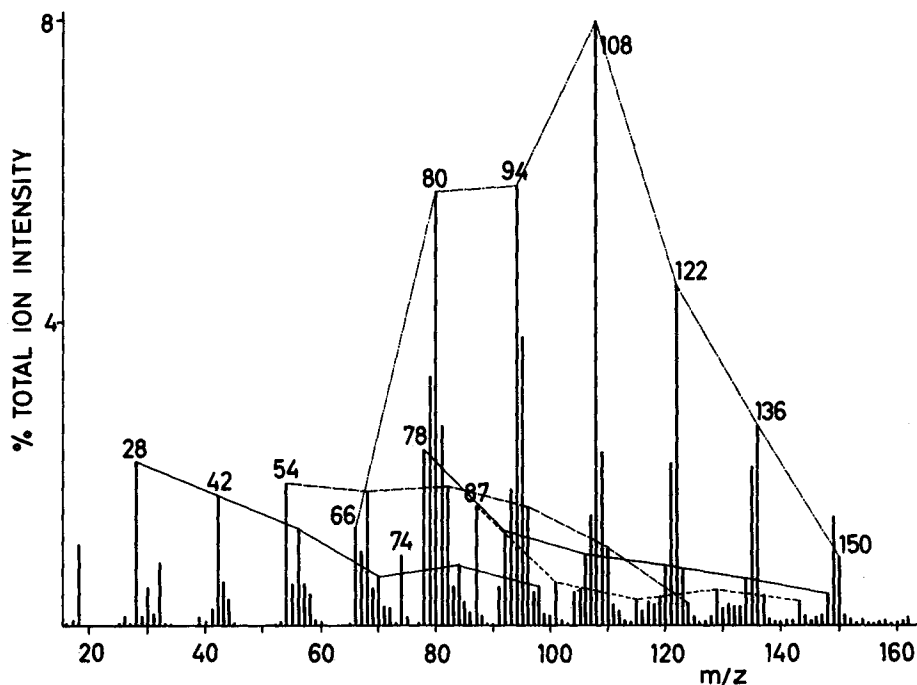
SPECTRUM D.2



SAMPLE : LINOLEIC ACID
 CHEMICAL DETAILS : *cis*-9, *cis*-12 octadecadienoic acid; $C_{18}H_{32}O_2$;
 MW = 280
 SAMPLE ORIGIN : Lipid Supplies, St. Andrews Univ., UK
 SAMPLE PREP./SIZE : solution in methanol; 10 μ g
 PYROL. CONDITIONS : ferromagnetic tube; T_{eq} 770°C
 TOTAL ION COUNTS : 2.6×10^5

REMARKS - Compared to sodium lauryl sulphate (Spectrum D.1), a saturated aliphatic acid, the linoleic acid pattern shows a higher abundance of relatively short chain polyunsaturated hydrocarbon ion series. To some extent this difference may be due to the effect of oven pyrolysis. Also noteworthy is the absence of prominent fragment ion series, apparently as a result of the low abundance of labile, saturated, long-chain hydrocarbons in the pyrolysate. Whether the ion series at m/z 78, 92, etc. represents aromatic or multiple unsaturated aliphatic ions cannot be decided from this spectrum.

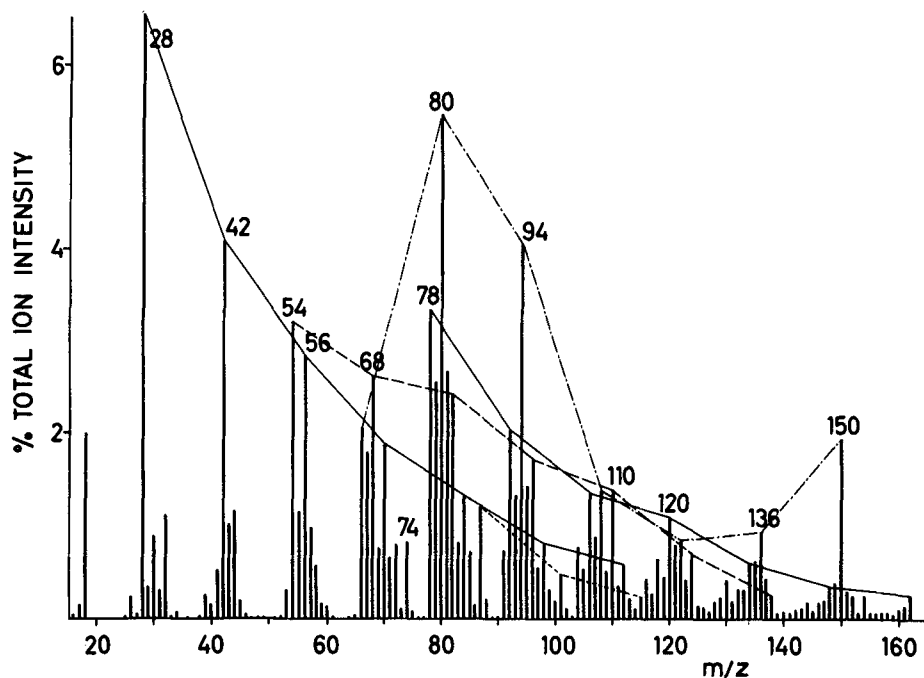
SPECTRUM D.3



SAMPLE : α -LINOLENIC ACID METHYL ESTER
 CHEMICAL DETAILS : *cis*-9, *cis*-12, *cis*-15 octadecatrienoic acid methyl ester;
 $C_{19}H_{32}O_2$; MW = 292
 SAMPLE ORIGIN : Unilever Res. Lab., Vlaardingen, The Netherlands
 SAMPLE PREP./SIZE : solution in methanol; 10 μ g
 PYROL. CONDITIONS : ferromagnetic tube; T_{eq} 770°C
 TOTAL ION COUNTS : 1.7×10^5

REMARKS - The strong homologous ion series at m/z 66, 80, etc. may well represent cyclic dienes and/or aliphatic trienes, especially in view of the multiple unsaturation in the parent molecule. A minor series of homologous ions at m/z 87, 101, etc., also observed in the spectrum of γ -linolenic acid methyl ester (Spectrum D.4), could be connected with the presence of the methyl ester function.

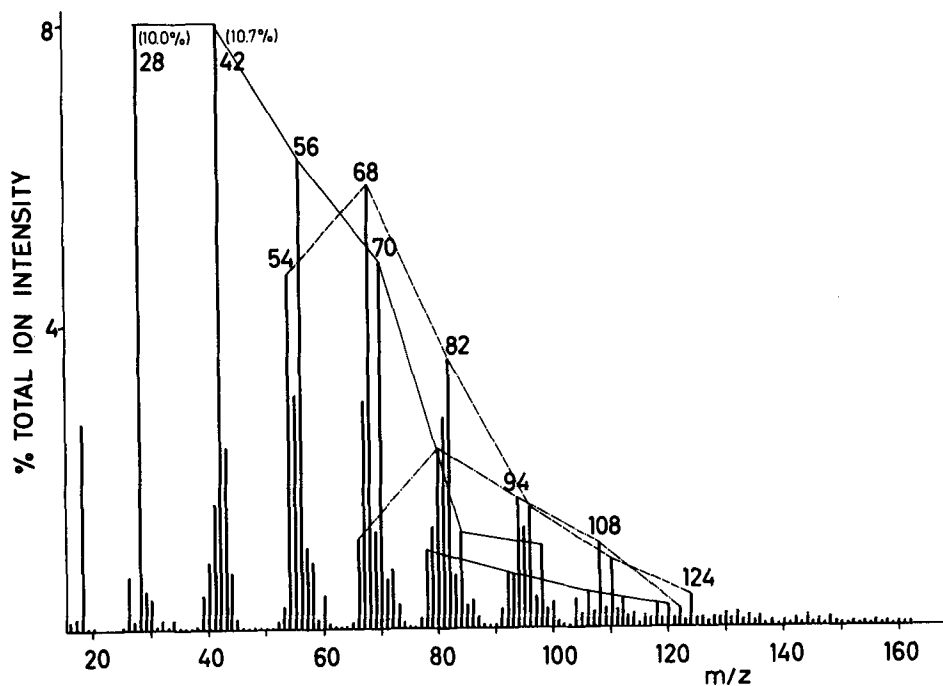
SPECTRUM D.4



SAMPLE : γ -LINOLENIC ACID METHYL ESTER
 CHEMICAL DETAILS : *cis*-6, *cis*-9, *cis*-12 octadecatrienoic acid methylester;
 $C_{19}H_{32}O_2$; MW = 292
 SAMPLE ORIGIN : Unilever Res. Lab., Vlaardingen, The Netherlands
 SAMPLE PREP./SIZE : solution in methanol; 10 μ g
 PYROL. CONDITIONS : ferromagnetic tube; T_{eq} 770°C
 TOTAL ION COUNTS : 1.5×10^5

REMARKS - Noteworthy is the strong difference of this spectrum and that of the α -linolenic acid analogue (Spectrum D.3) pointing to the strong influence of the position of the double bond on the pyrolytic fragmentation pathway.

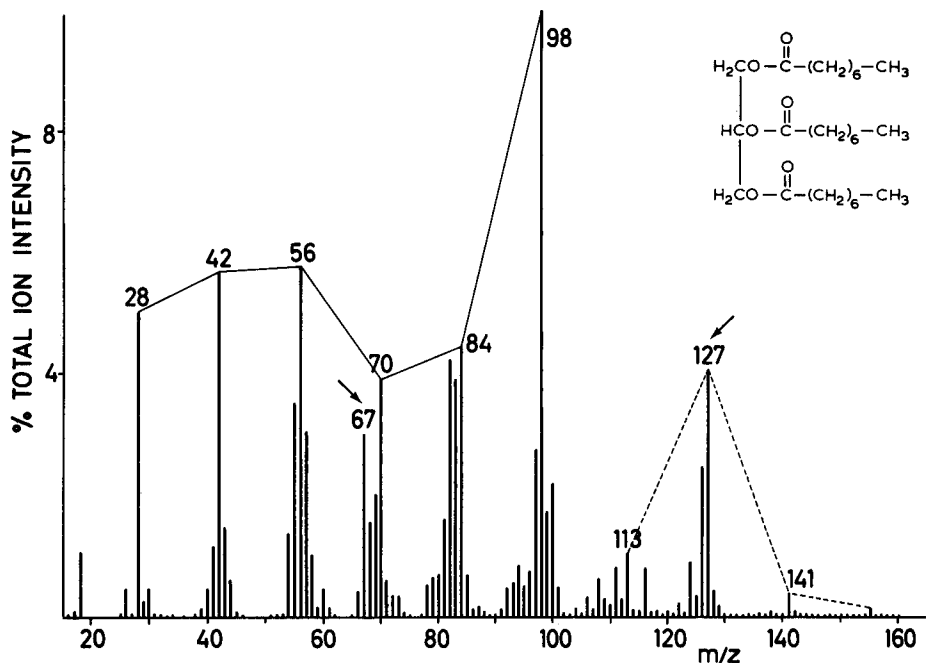
SPECTRUM D.5



SAMPLE : OCTADECADIYNOIC ACID
 CHEMICAL DETAILS : $\text{CH}_3-(\text{CH}_2)_7-\text{C}\equiv\text{C}-\text{CH}_2-\text{C}\equiv\text{C}-(\text{CH}_2)_4-\text{COOH}$; $\text{C}_{18}\text{H}_{28}\text{O}_2$;
 MW = 276
 SAMPLE ORIGIN : Unilever Res. Lab. Vlaardingen, The Netherlands
 SAMPLE PREP./SIZE : solution in methanol; 10 μg
 PYROL. CONDITIONS : ferromagnetic tube; $T_{\text{eq}} 770^\circ\text{C}$
 TOTAL ION COUNTS : 1.5×10^5

REMARKS - Surprisingly, multiply unsaturated homologous ion series are not as prominent as might be expected on the basis of the presence of the two triple bonds in the parent molecule.

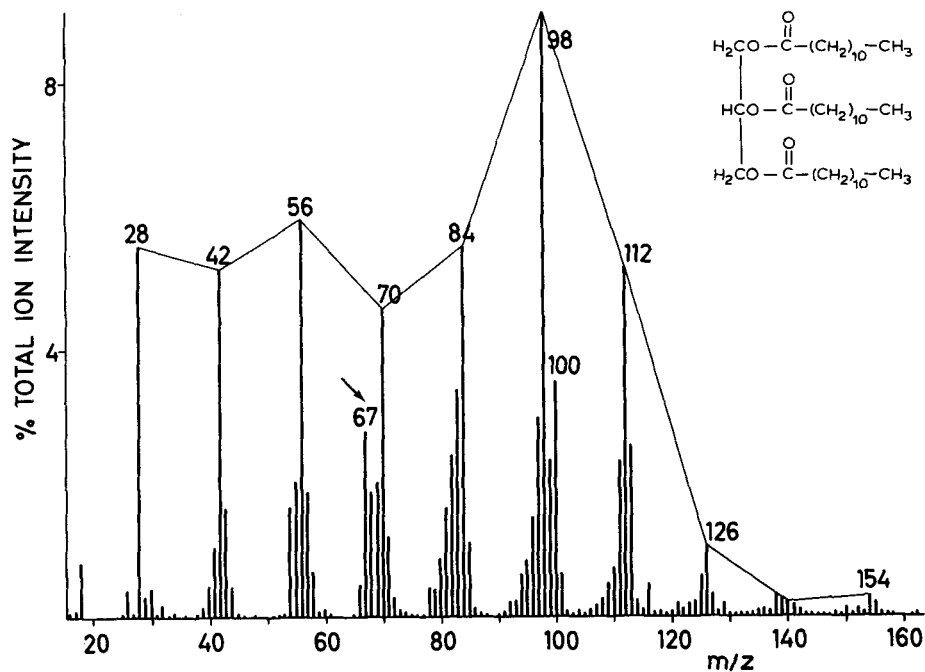
SPECTRUM D.6



SAMPLE : TRICAPRYLIN
 CHEMICAL STRUCTURE : see insert in spectrum; $(\text{C}_7\text{H}_{15}\text{COO})_3\text{C}_3\text{H}_5$; MW = 470
 SAMPLE ORIGIN : Serva, Heidelberg, GFR
 SAMPLE PREP./SIZE : solution in methanol; 10 μg
 PYROL. CONDITIONS : ferromagnetic tube; T_{eq} 770°C
 TOTAL ION COUNTS : 3.5×10^5

REMARKS - A prominent series of molecular ion peaks represents alkenes up to C_7H_{14} (m/z 98). In addition, marked EI fragments are observed at m/z 67 and 127. Note that the peak at m/z 67 is also present in the spectra of other glycerides (see Spectra D.7 and D.8). The peak at m/z 127 probably represents an EI fragment of the intact fatty acid moiety.

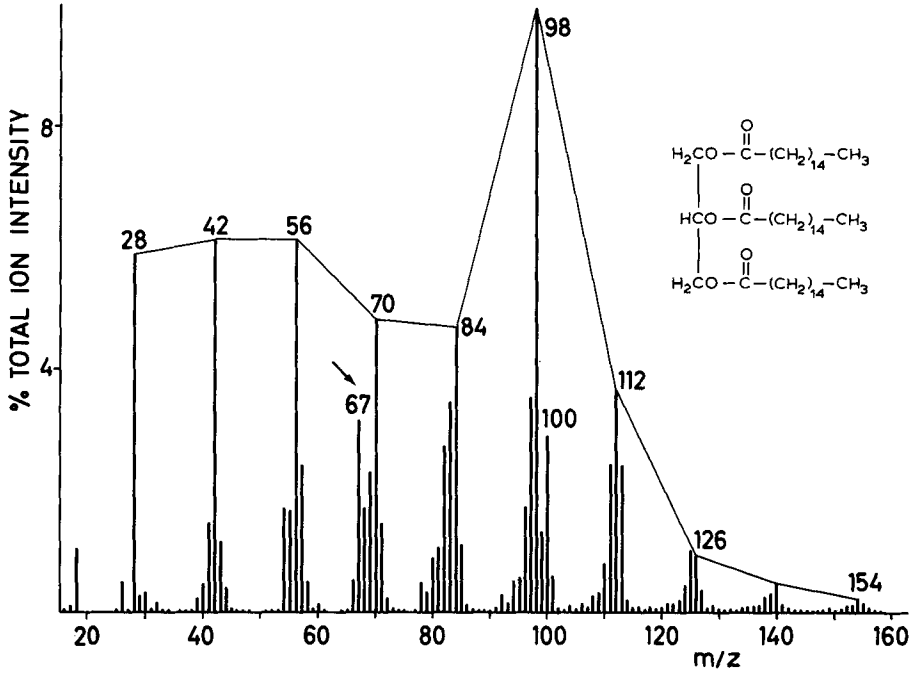
SPECTRUM D.7



SAMPLE : TRILAURIN
 CHEMICAL DETAILS : see insert in spectrum; $(\text{C}_{11}\text{H}_{23}\text{COO})_3\text{C}_3\text{H}_5$; MW = 638
 SAMPLE ORIGIN : Serva, Heidelberg, GFR
 SAMPLE PREP./SIZE : solution in methanol; 10 μg
 PYROL. CONDITIONS : ferromagnetic tube; $T_{\text{eq}} 770^\circ\text{C}$
 TOTAL ION COUNTS : 4×10^5

REMARKS - Up to m/z 100 the spectrum is very similar to that of tricapylin (Spectrum D.6). The alkene series of fragments, however, now appears to extend itself to $\text{C}_{11}\text{H}_{22}^+$ (m/z 154). Also the absence of the prominent fragment ion at m/z 127 is noteworthy.

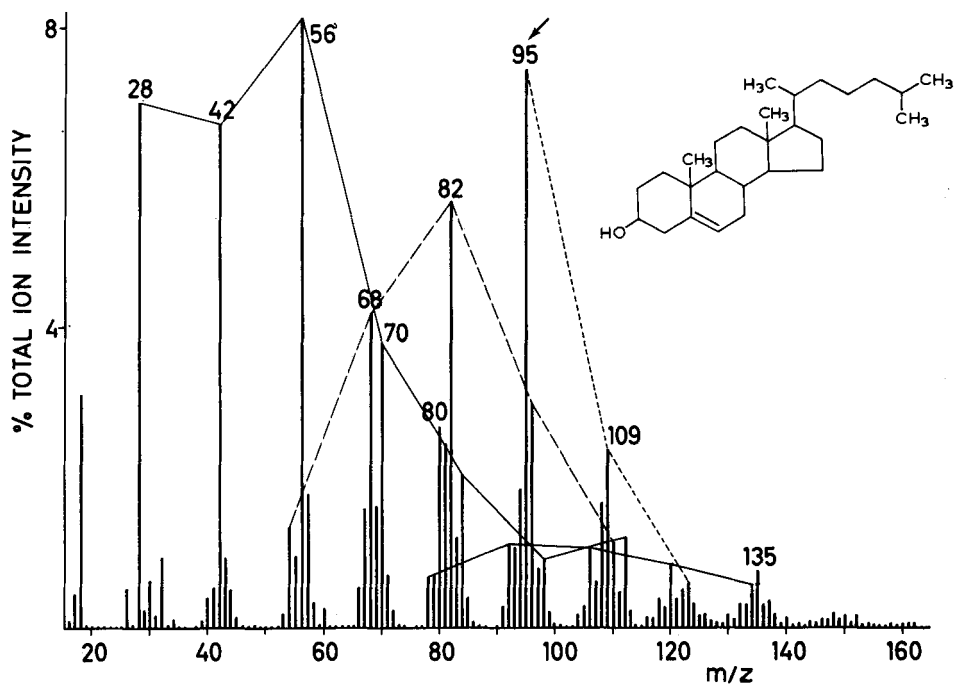
SPECTRUM D.8



SAMPLE : TRIPALMITIN
 CHEMICAL DETAILS : see insert in spectrum; $(\text{C}_{15}\text{H}_{31}\text{COO})_3\text{C}_3\text{H}_5$; MW = 806
 SAMPLE ORIGIN : Serva, Heidelberg, GFR
 SAMPLE PREP./SIZE : solution in methanol; 10 μg
 PYROL. CONDITIONS : ferromagnetic tube; T_{eq} 770°C
 TOTAL ION COUNTS : 2.7×10^5

REMARKS - This spectrum is virtually indistinguishable from that of trilaurein (Spectrum D.7) within the mass range scanned.

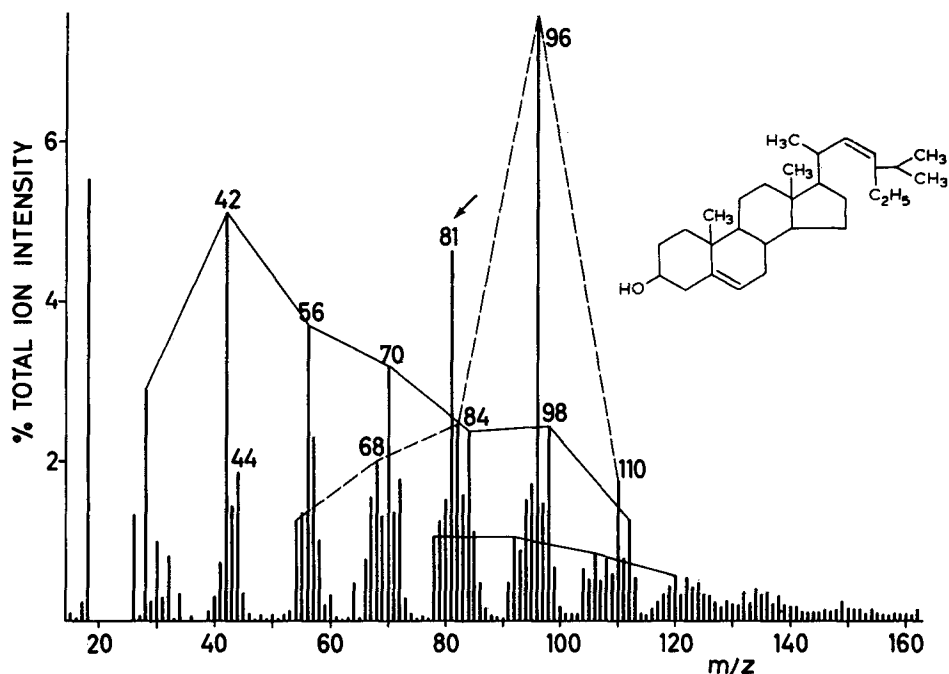
SPECTRUM D.9



SAMPLE : CHOLESTEROL
 CHEMICAL DETAILS : see insert in spectrum; cholest-5-en-3 β -ol; C₂₇H₄₆O;
 MW = 386
 SAMPLE ORIGIN : O.P.G., Utrecht, The Netherlands
 SAMPLE PREP./SIZE : solution in methanol; 10 μ g
 PYROL. CONDITIONS : ferromagnetic tube; T_{eq} 770°C
 TOTAL ION COUNTS : 5 x 10⁴

REMARKS - The prominent ion series at m/z 28, 42, etc. and at m/z 54, 68, etc. (apparently representing alkene and alkadiene series of pyrolysis fragments with up to 8 C atoms), are probably derived from the hydrocarbon side-chain of the molecule, whereas the peaks at m/z 95, 109 and 123 may well represent EI fragments from the more or less intact parent molecule.

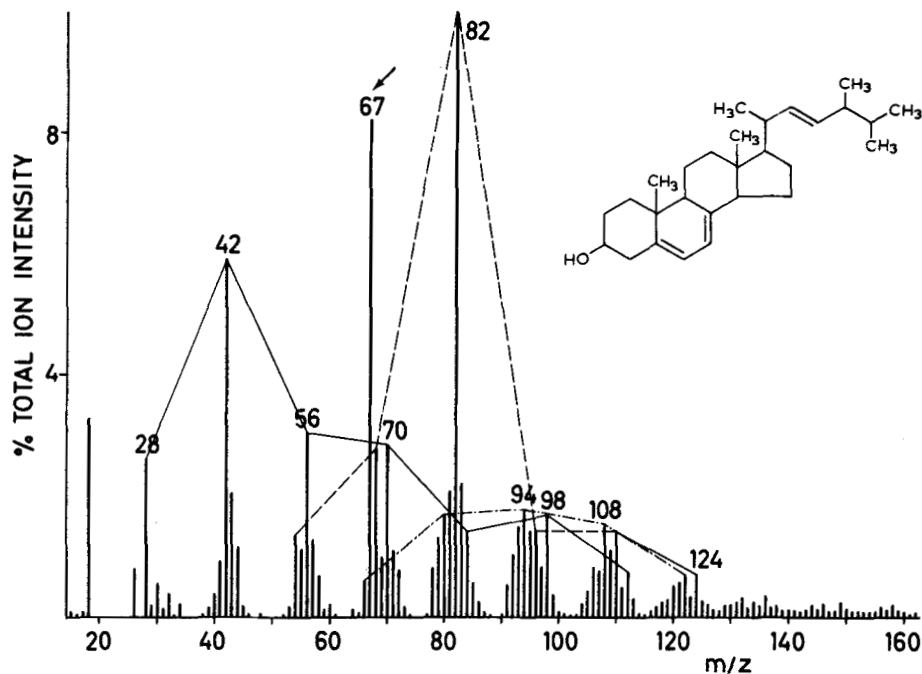
SPECTRUM D.10



SAMPLE : STIGMASTEROL
 CHEMICAL DETAILS : see insert in spectrum; stigmasterol; $C_{29}H_{48}O$; MW = 412
 SAMPLE ORIGIN : Sigma Chemical Corp., St. Louis, USA
 SAMPLE PREP./SIZE : solution in methanol; 10 μ g
 PYROL. CONDITIONS : ferromagnetic tube; T_{eq} 770°C
 TOTAL ION COUNTS : 7.5×10^4

REMARKS - In comparison with cholesterol (Spectrum D.9) the homologous ion series at m/z 54, 68, etc. is now more pronounced, apparently reflecting the unsaturated nature of the aliphatic hydrocarbon side-chain. Also an EI fragment is now observed at m/z 81, probably derived from olefinic pyrolysis fragments, such as the molecular ion species at m/z 96 (compare with ergosterol (Spectrum D.11)).

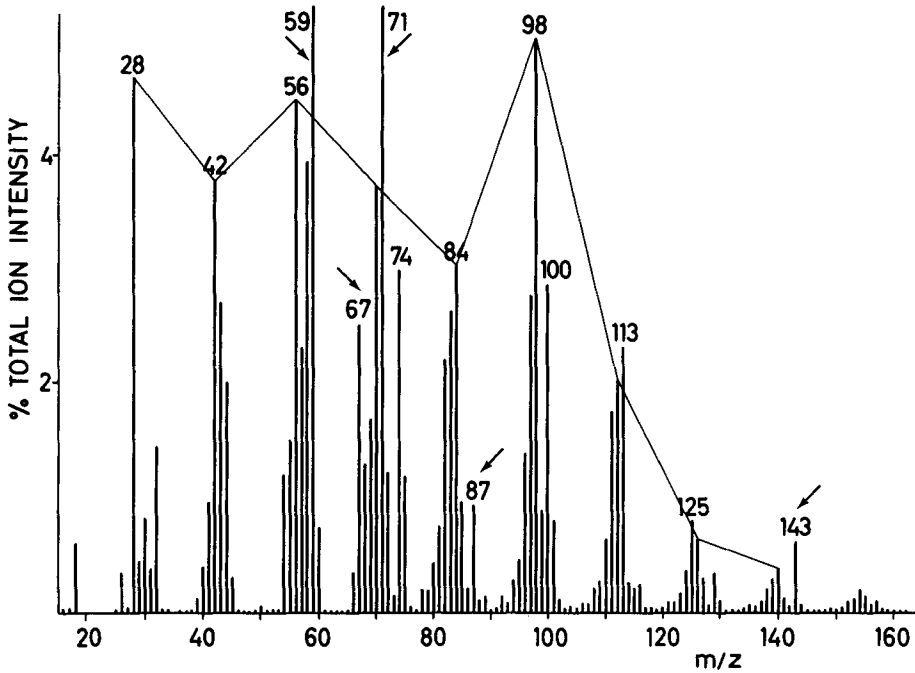
SPECTRUM D.11



SAMPLE : ERGOSTEROL
 CHEMICAL DETAILS : see insert in spectrum; ergosta-5,7,22-trien-3 β -ol;
 $C_{28}H_{44}O$; MW = 396
 SAMPLE ORIGIN : Sigma Chemical Corp., St. Louis, USA
 SAMPLE PREP./SIZE : solution in methanol; 10 μ g
 PYROL. CONDITIONS : ferromagnetic tube; T_{eq} 770°C
 TOTAL ION COUNTS : 1.2×10^5

REMARKS - Note the correspondence with stigmasterol (Spectrum D.10) with regard to the homologous ion series at m/z 28, 42, etc. However, the series at m/z 54, 68, etc. now attains its maximum intensity at m/z 82 instead of m/z 96, apparently reflecting the substitution of a methyl group for the ethyl group in the olefinic side-chain. A prominent fragment ion is observed at m/z 67, probably derived from the molecular ion species at m/z 82 (compare with stigmasterol (Spectrum D.10)).

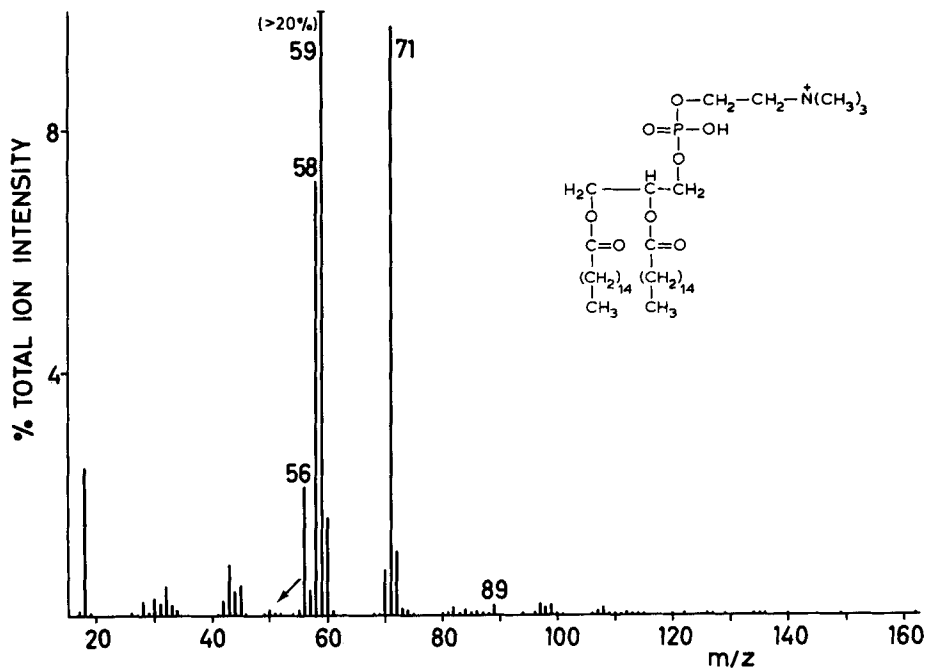
SPECTRUM D.12



SAMPLE : L- α -LECITHIN (dipalmitoyl)
 CHEMICAL DETAILS : C₄₀H₈₂O₉NP; MW = 792
 SAMPLE ORIGIN : Serva, Heidelberg, GFR
 SAMPLE PREP./SIZE : solution in methanol; 10 μ g
 PYROL. CONDITIONS : ferromagnetic tube; T_{eq} 770°C
 TOTAL ION COUNTS : 7 x 10⁵

REMARKS - Compared to tripalmitin (Spectrum D.8), a similar series of alkene molecular ions at m/z 28, 42, etc. is observed, as well as the characteristic fatty acid ester fragment ion at m/z 67. The prominent signals at m/z 58, 59 and 71 represent well-known pyrolysis fragments of the choline moiety (see Part I, Section 3.5, and Spectrum D.12a). Whether the odd-numbered ion signals at m/z 87 and 143 represent N-containing ions or hydrocarbon fragment ions is as yet unknown.

SPECTRUM D.12A



SAMPLE : L- α -LECITHIN (dipalmitoyl)
 CHEMICAL DETAILS : see insert in spectrum; $C_{40}H_{82}O_9NP$; MW = 792
 SAMPLE ORIGIN : Serva, Heidelberg, GFR
 SAMPLE PREP./SIZE : solution in methanol; 10 μ g
 PYROL. CONDITIONS : standard
 TOTAL ION COUNTS : 1.6×10^5

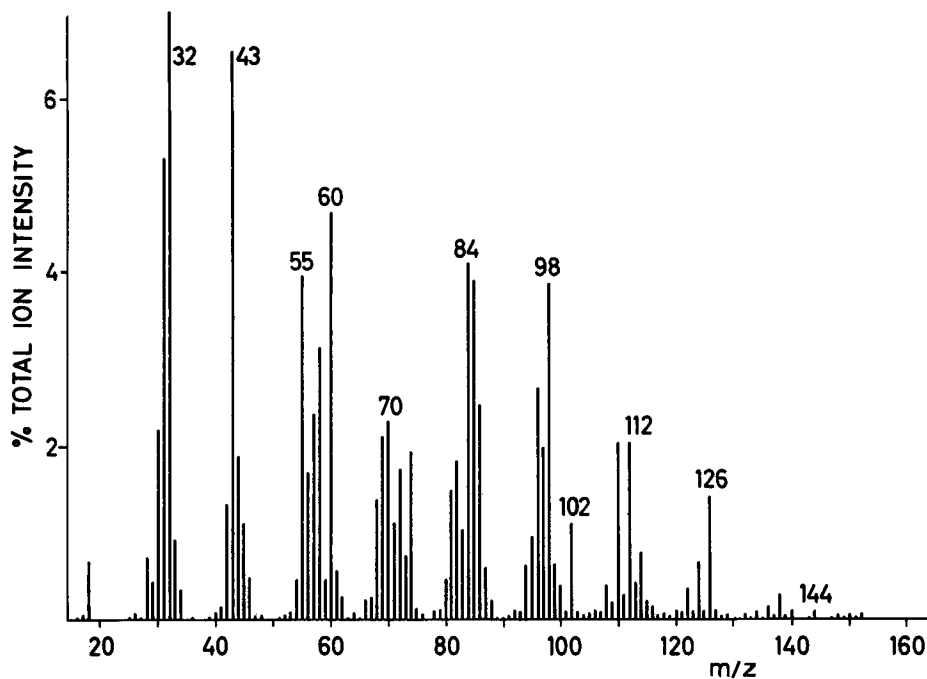
REMARKS - Comparison with the oven pyrolysis pattern (Spectrum D.12) shows the complete absence of aliphatic hydrocarbon series, apparently as a result of condensation losses. Instead, this spectrum is entirely dominated by the choline-derived fragments at m/z 58, 59 and 71 thought to represent $C_3H_8N^+$, trimethylamine and dimethylvinylamine respectively (see Part I, Section 3.5). The absence of marked peaks at m/z 50, 52 (CH_3Cl^+) and at m/z 89 (N,N-dimethylethanolamine) often observed in Py-mass spectra of choline-containing phospholipids (see Part I, Figure 9) is probably due to differences in the ionic status of the sample.

This Page Intentionally Left Blank

GROUP E
NATURAL PRODUCTS

This Page Intentionally Left Blank

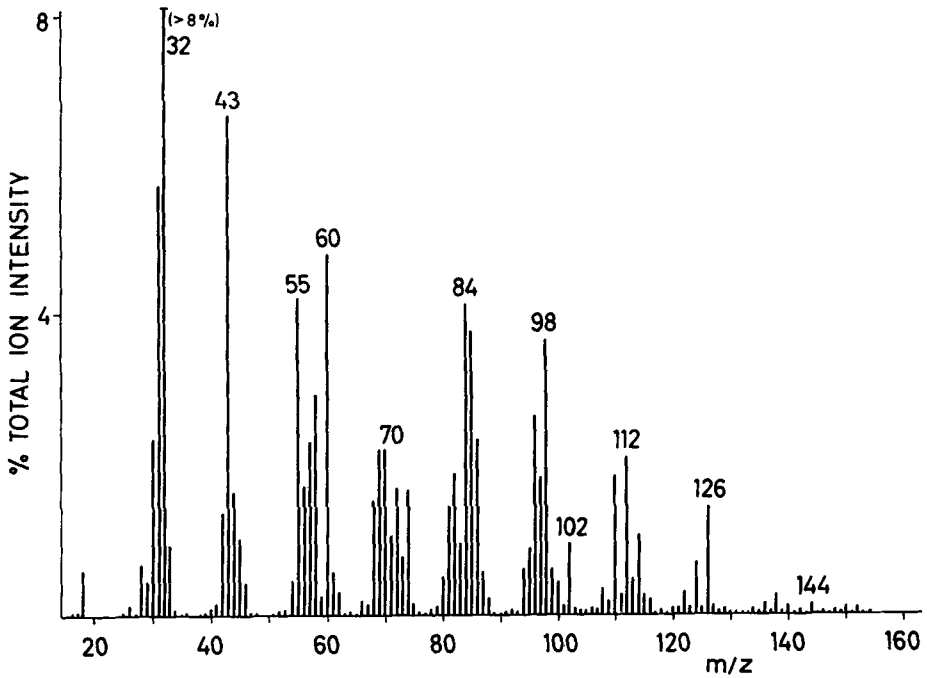
SPECTRUM E.1



SAMPLE : COTTON
 CHEMICAL DETAILS : almost pure cellulose
 SAMPLE ORIGIN : Fibre Institute, TNO, Delft, The Netherlands
 SAMPLE PREP./SIZE : ground in glass mortar with methanol; 10 µg
 PYROL. CONDITIIONS : standard
 TOTAL ION COUNTS : 4×10^5

REMARKS - The spectral pattern is entirely of a polysaccharidic nature without detectable contributions from other plant constituents such as proteins or lignins. The pattern strongly resembles that of cellulose (Spectra A.1, A.2). Compare also with flax (Spectrum E.2).

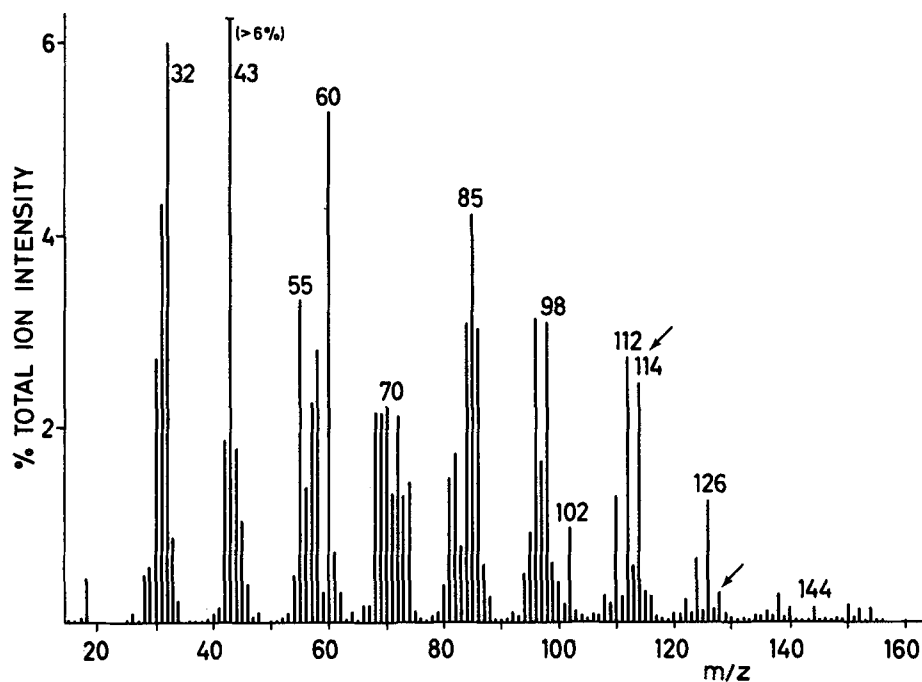
SPECTRUM E.2



SAMPLE : FLAX
 CHEMICAL DETAILS : largely cellulose
 SAMPLE ORIGIN : Fibre Institute, TNO, Delft, The Netherlands
 SAMPLE PREP./SIZE : ground in glass mortar with methanol; 10 µg
 PYROL. CONDITIONS : standard
 TOTAL ION COUNTS : 3×10^5

REMARKS - This spectrum shows a polysaccharide pattern virtually identical to that of cotton (Spectrum E.1), indicating a high degree of similarity in composition and structure between these two natural fibers.

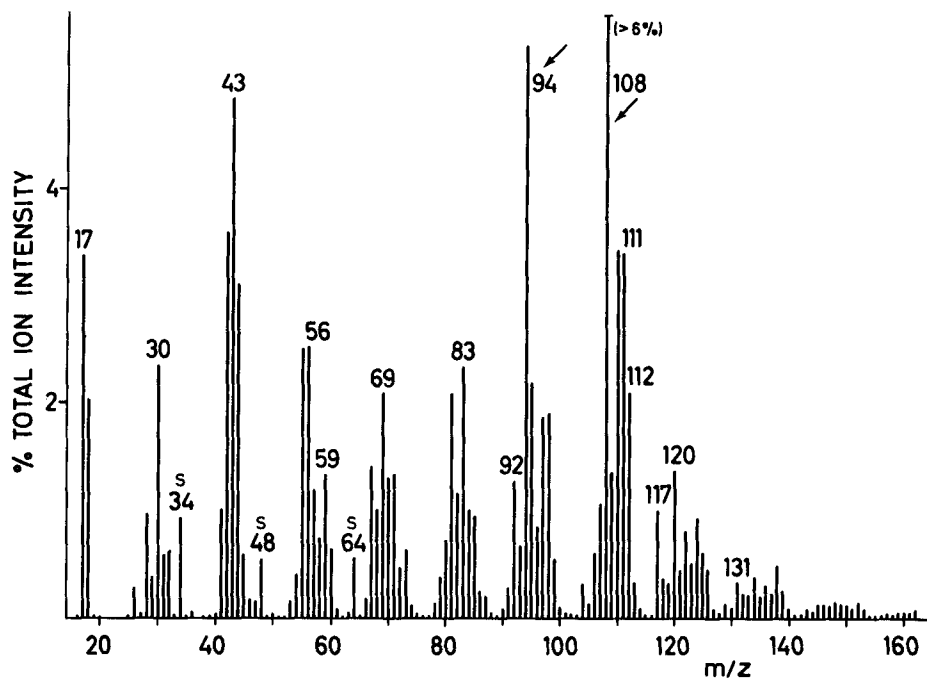
SPECTRUM E.3



SAMPLE : BURLAP
 CHEMICAL DETAILS : largely cellulose
 SAMPLE ORIGIN : Fibre Institute, TNO, Delft, The Netherlands
 SAMPLE PREP./SIZE : ground in glass mortar with methanol; 10 μ g
 PYROL. CONDITIONS : standard
 TOTAL ION COUNTS : 5×10^5

REMARKS - This spectrum also shows a typical polysaccharide pattern with only minor indications for the presence of other plant materials. However, this polysaccharide pattern appears to be somewhat more complex than that of cotton (Spectrum E.1) and flax (Spectrum E.2). For instance, the relatively high peak intensities at m/z 114 and 128 may well be derived from hemicellulose constituents (compare with the relatively high intensities of m/z 114 and 128 in the spectra of wood (Spectrum E.11) and cork (Spectrum E.12)).

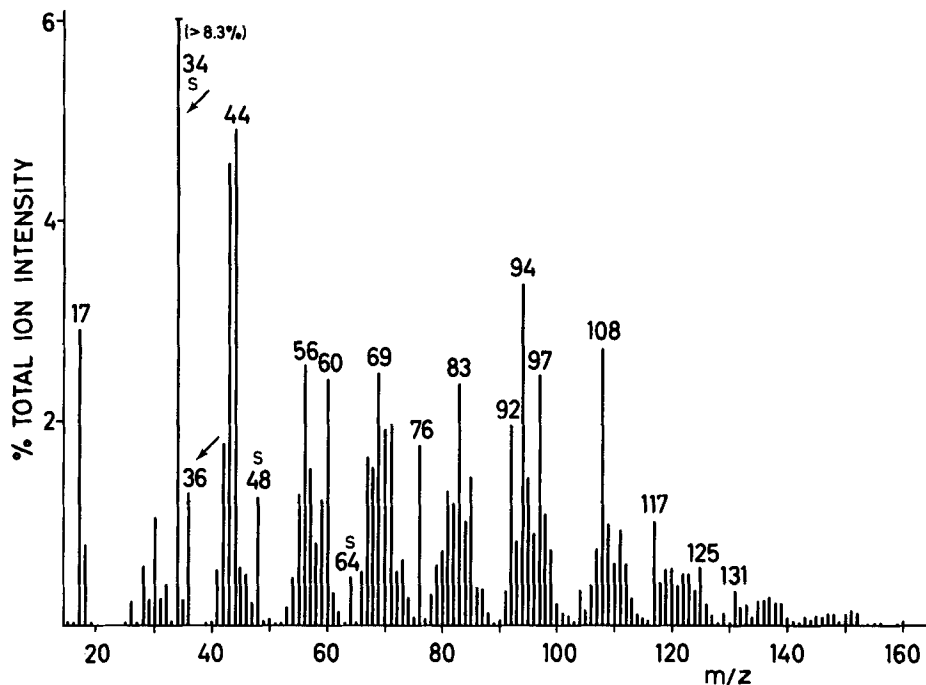
SPECTRUM E.4



SAMPLE : SILK
 CHEMICAL DETAILS : almost pure fibroin
 SAMPLE ORIGIN : Fibre Institute, TNO, Delft, The Netherlands
 SAMPLE PREP./SIZE : ground in glass mortar with methanol; 10 μ g
 PYROL. CONDITIONS : standard
 TOTAL ION COUNTS : 4×10^5

REMARKS - In contrast with the three previous spectra of natural fibers (Spectra E.1 - E.3) this spectrum shows a typical protein pattern with little or no indication of non-protein constituents. The marked intensity of peaks 94 and 108 represents the high abundance of tyrosine moieties in fibroin.

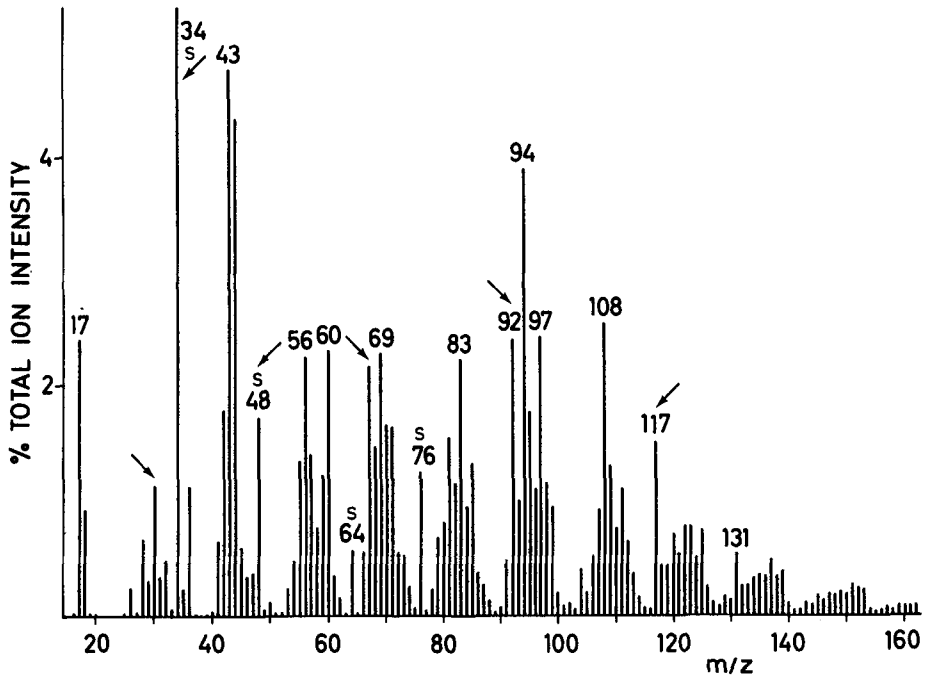
SPECTRUM E.5



SAMPLE : SHEEP WOOL
 CHEMICAL DETAILS : largely keratin
 SAMPLE ORIGIN : Fibre Institute, TNO, Delft, The Netherlands
 SAMPLE PREP./SIZE : ground in glass mortar with methanol; 10 μ g
 PYROL. CONDITIONS : standard
 TOTAL ION COUNTS : 2.4×10^5

REMARKS - The spectrum of sheep wool as well as of most other animal hairs, e.g. camel hair (Spectrum E.6) is completely dominated by the protein pattern of keratin (see Spectrum B.11). This is evidenced by the extremely high peak at m/z 34 ($H_2S^{+\cdot}$) derived from the cystein moieties which are unusually abundant in this protein. Although m/z 34 has gone off scale, its true intensity can be conveniently judged from the intensity of the 5% isotope peak at m/z 36 ($H_2^{34}S^{+\cdot}$).

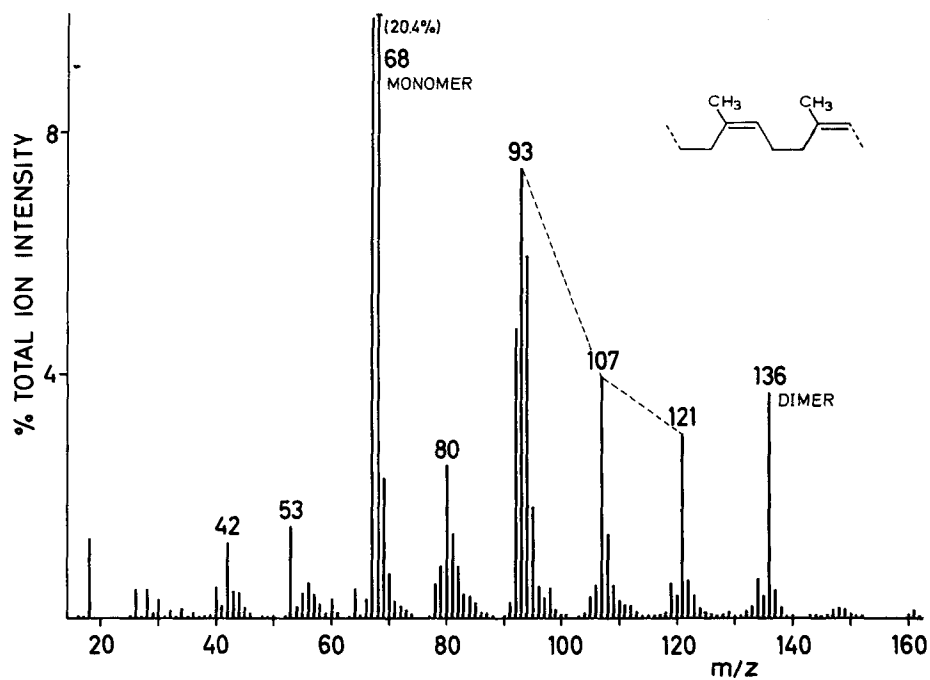
SPECTRUM E.6



SAMPLE : CAMEL HAIR
 CHEMICAL DETAILS : largely keratin
 SAMPLE ORIGIN : Fibre Institute, TNO, Delft, The Netherlands
 SAMPLE PREP./SIZE : ground in glass mortar with methanol; 10 μ g
 PYROL. CONDITIONS : standard
 TOTAL ION COUNTS : 5×10^5

REMARKS - This spectrum is highly similar to that of sheep wool (Spectrum E.5). However, small but significant increases in peak intensities at m/z 30, 48, 67, 92 and 117 may represent small amounts of non-keratin proteins, the presence of which is to be expected in animal hair.

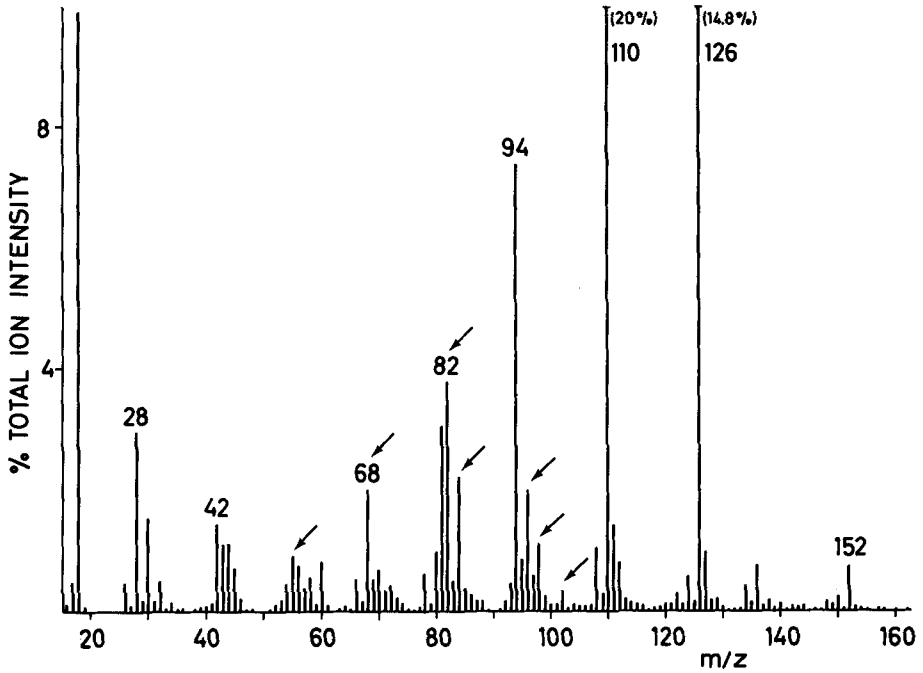
SPECTRUM E.7



SAMPLE : NATURAL RUBBER (pale crepe, I)
 CHEMICAL DETAILS : see insert in spectrum; *cis*-1,4-polyisoprene
 SAMPLE ORIGIN : KRI-TNO, Delft, The Netherlands
 SAMPLE PREP./SIZE : ground at minus 170°C in methanol; 10 µg
 PYROL. CONDITIONS : standard
 TOTAL ION COUNTS : 8.8×10^4

REMARKS - See Part I, Section 3.5. The spectrum shows no obvious protein and carbohydrate signals.

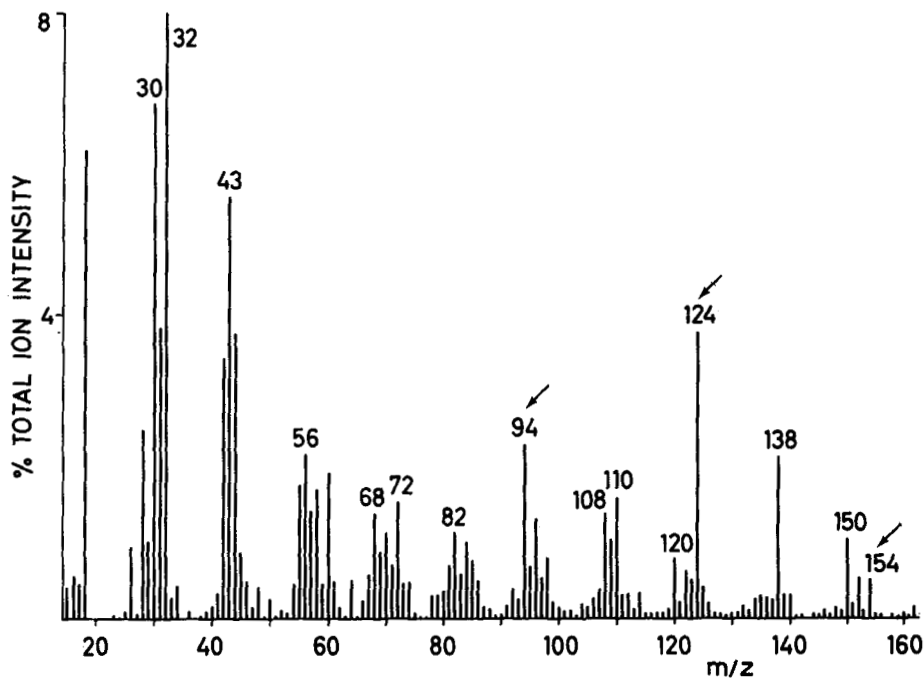
SPECTRUM E.8



SAMPLE : TANNIN
 CHEMICAL DETAILS : esters of hexoses and trihydroxybenzene carboxylic acids
 SAMPLE ORIGIN : Merck AG, Darmstadt, GFR
 SAMPLE PREP./SIZE : solution in methanol; 10 μ g
 PYROL. CONDITIONS : standard
 TOTAL ION COUNTS : 2.5×10^4

REMARKS - Although the structure of tannins is not well defined, the presence of hydroxybenzene moieties, e.g. gallic acid, is evidenced by the high peak intensities at m/z 94, 110 and 126 apparently representing phenol, dihydroxybenzenes and trihydroxybenzenes respectively. The ion series at m/z 55, 68, 82, 84, 96, 98, 102, 110 and 126 may represent (esterified) hexose moieties.

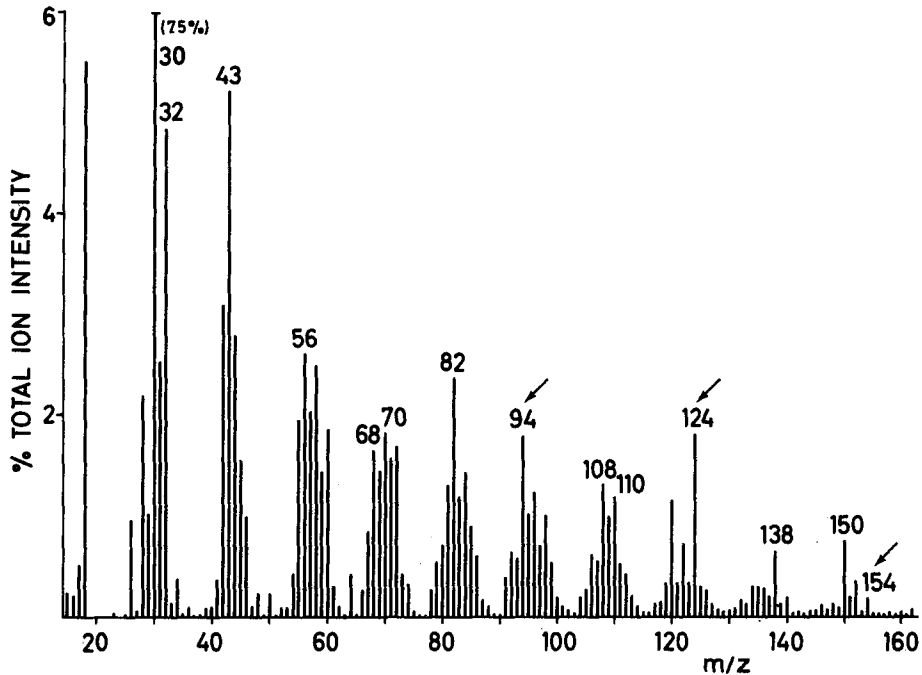
SPECTRUM E.9



SAMPLE : WHEAT STRAW LIGNIN
 CHEMICAL DETAILS : prepared according to the Bjørkman procedure
 SAMPLE ORIGIN : gift from Dr. K. Haider, F.A.L., Braunschweig, GFR
 SAMPLE PREP./SIZE : suspension in methanol; 10 μ g
 PYROL. CONDITIONS : standard
 TOTAL ION COUNTS : 1.5×10^5

REMARKS - The pyrolysis mass spectra of lignins are characterized by the presence of pyrolysis products derived from each of the main phenolic building blocks. In the case of grass lignins these are the parahydroxybenzoic, quaiacylic and syringylic acid moieties, giving rise to three discrete series of phenolic signals, namely m/z 94, 108, 120, 134, m/z 124, 138, 150, 164 and m/z 154, 168, 180, 194 respectively (signals beyond m/z 160 not shown). As confirmed by the Py-GC-MS studies of Bracewell *et al.* (ref. 186), the syringylic acid series is particularly prominent in hardwood lignins (e.g. beech lignin) but absent in softwood lignins (e.g. Douglas fir lignin). See also Part I, Section 3.6.

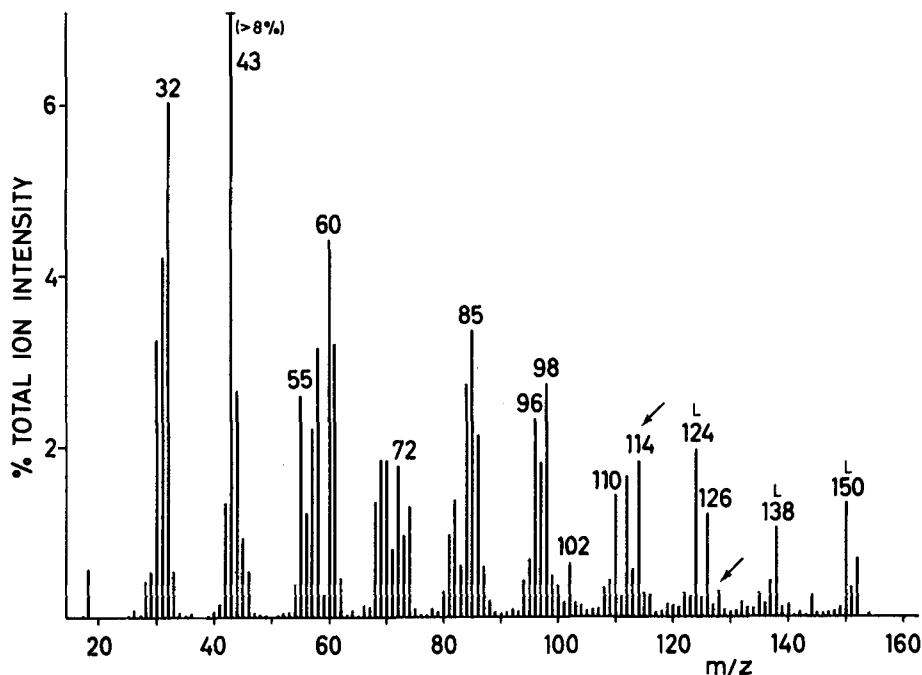
SPECTRUM E.10



SAMPLE : WHEAT STRAW LIGNIN
 CHEMICAL DETAILS : prepared according to the Brauns procedure
 SAMPLE ORIGIN : gift of Dr. K. Haider, F.A.L., Braunschweig, GFR
 SAMPLE PREP./SIZE : suspension in methanol; 10 μ g
 PYROL. CONDITIONS : standard
 TOTAL ION COUNTS : 1.2×10^5

REMARKS - Comparison of this spectrum with that of Björkman lignin (Spectrum E.9) shows the strong influence of the preparation procedure on composition and structure of the lignin obtained. This reflects a basic problem in obtaining pure, undegraded lignin samples as the lignin moieties in plant matter are intricately connected to the hemicellulose fraction (ref. 85). As shown in the spectrum of Douglas fir (Spectrum E.11), however, characteristic lignin patterns are easily obtained from whole wood samples by Py-MS. This should enable fast characterization of lignins without lengthy and risky separation procedures as well as provide a practical guide to comparing the effectiveness and reliability of various extraction and separation techniques for lignins.

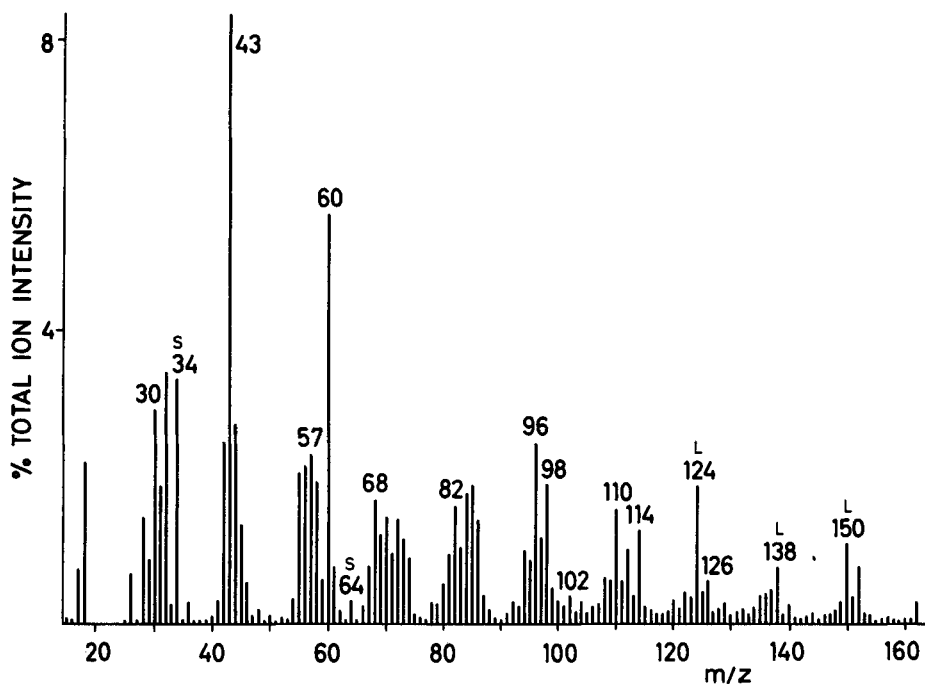
SPECTRUM E.11



SAMPLE : DOUGLAS FIR WOOD
 CHEMICAL DETAILS : -
 SAMPLE ORIGIN : gift from Flammability Research Center, Salt Lake City, USA
 SAMPLE PREP./SIZE : suspension in methanol; 10 μ g
 PYROL. CONDITIONS : standard
 TOTAL ION COUNTS : 2.5×10^5

REMARKS - The overall pyrolysis mass spectrometry patterns of whole wood samples can be explained to a large extent by adding the pattern of cellulose (Spectrum A.1) to a typical lignin pattern (Spectra E.9, E.10), taking into account the softwood or hardwood nature of the sample (see Remarks on Spectrum E.9). The major peak intensities not explained by this procedure, usually found at m/z 114 and 128, apparently represent hemicellulose fragments. Comparison with spectra of whole wood samples representing different types of wood shows characteristic differences with regard to lignin and hemicellulose patterns which should be of considerable practical value in industrial applications and technical uses of wood and wood products.

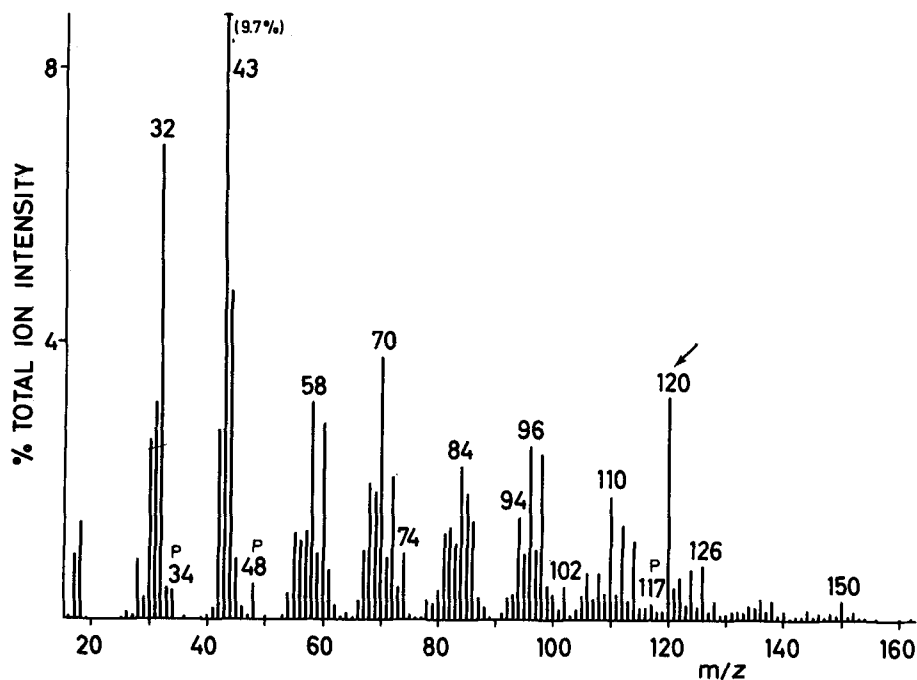
SPECTRUM E.12



SAMPLE : CORK
 CHEMICAL DETAILS : -
 SAMPLE ORIGIN : bottle stopper
 SAMPLE PREP./SIZE : suspension in methanol; 10 µg
 PYROL. CONDITIONS : standard
 TOTAL ION COUNTS : 1×10^5

REMARKS - The overall character of this spectrum appears to be similar to that of whole wood (see Spectrum E.11). A more close inspection, however, shows the presence of sulphur containing signals at m/z 34, 48, and 64 which could be derived from sulphur containing plant constituents, e.g. proteins. Alternatively, these signals might point to some form of chemical pretreatment of the sample. The low intensities of the peaks at m/z 102 and 126 is also noteworthy since this indicates a much lower cellulose content than in whole wood samples such as Douglas fir (Spectrum E.11). Finally the characteristic ion series at m/z 124, 138, and 150 appears to point to the presence of quaiacylic acid type lignin components. According to some views, however, "true lignins" are generally not found in bark (ref. 85).

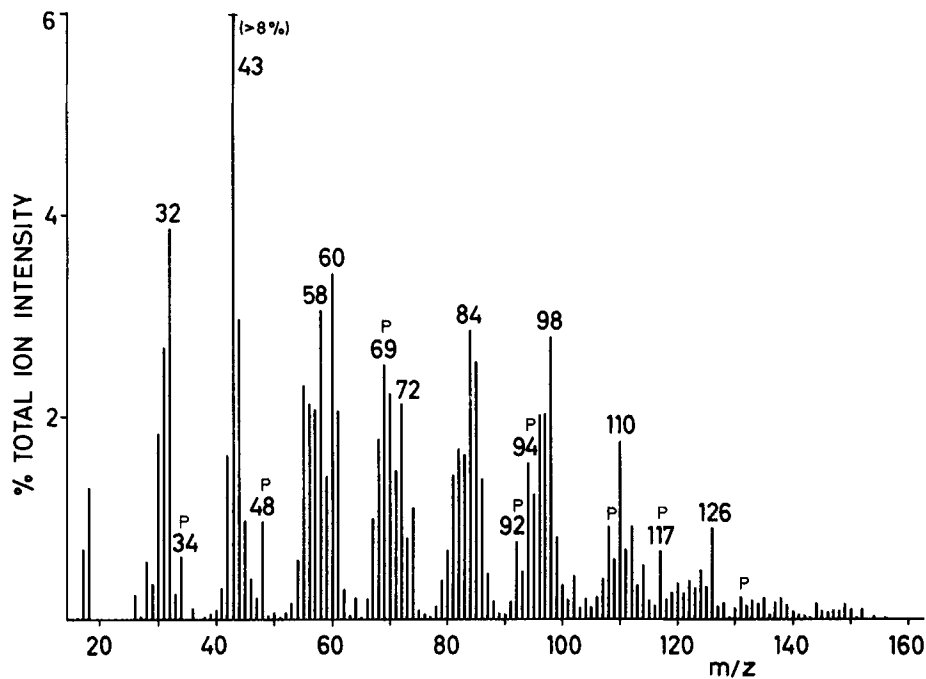
SPECTRUM E.13



SAMPLE : POLLEN (from *Pinus sylvestris*)
 CHEMICAL DETAILS : -
 SAMPLE ORIGIN : collected in The Netherlands
 SAMPLE PREP./SIZE : suspension in methanol; 20 μ g
 PYROL. CONDITIONS : standard
 TOTAL ION COUNTS : 7.2×10^4

REMARKS - Although dominated by signals typical of carbohydrate products, e.g. at m/z 32, 43, 72, 74, 84, 96, 98, 102, 110, 112, 114, 126, there are small but definite ion series which can be attributed to proteins e.g. at m/z 34, 43, 92, 94 and 117. Strong aromatic signals are present at m/z 94, 106, 108 and 120. Especially the large peak at m/z 120 is noteworthy since it is also found in some sporopollenin preparations (not shown in this Atlas) and therefore might be representative for this rather ill-defined type of biopolymer (ref. 74).

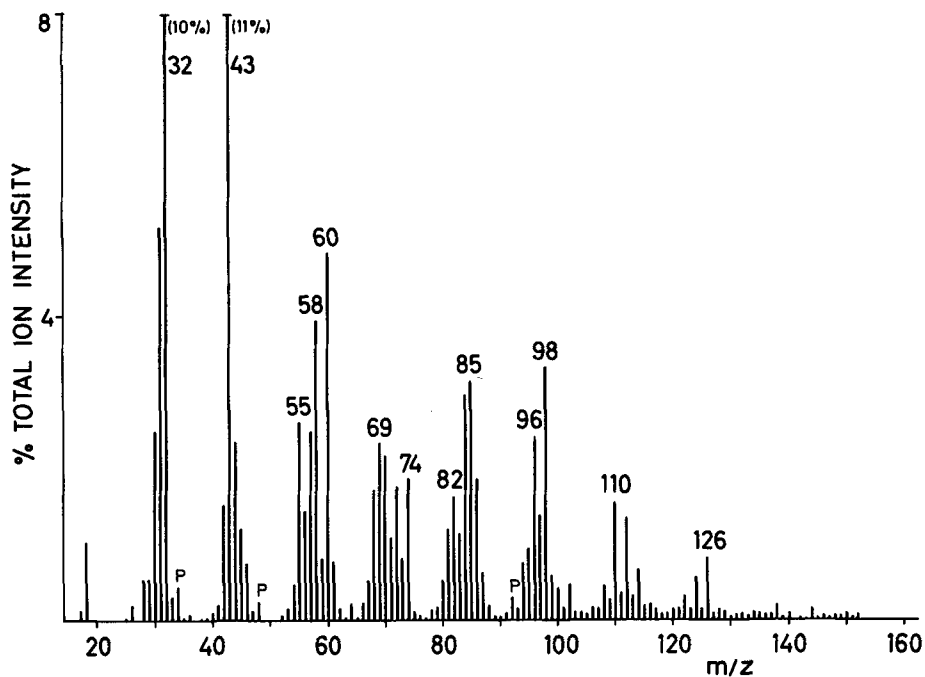
SPECTRUM E.14



SAMPLE : BREWER'S YEAST (*Saccharomyces cerevisiae*)
 CHEMICAL DETAILS : see NBS publications
 SAMPLE ORIGIN : Natl. Bureau of Standards (SRM 1569), Washington, USA
 SAMPLE PREP./SIZE : suspension in methanol; 10 μ g
 PYROL. CONDITIONS : standard
 TOTAL ION COUNTS : 8.3×10^4

REMARKS - As in the case of pollen (Spectrum E.13) carbohydrate signals dominate, e.g. at m/z 32, 43, 55, 60, 72, 74, 84, 96, 98, 110, 112, 126, but protein signals are also well represented e.g. at m/z 34, 48, 69, 92, 94, 108, 117. It should be realized that some of the carbohydrate signals may be derived from the ribose and deoxyribose moieties of RNA and DNA respectively (see Spectra C.1 and C.2). Under the Py-MS conditions employed these classes of compounds fail to produce detectable signals of the more characteristic base moieties (see Part I, Section 3.3). Also signals representing lipid moieties will tend to be underrepresented in these spectra (see Part I, Section 3.5).

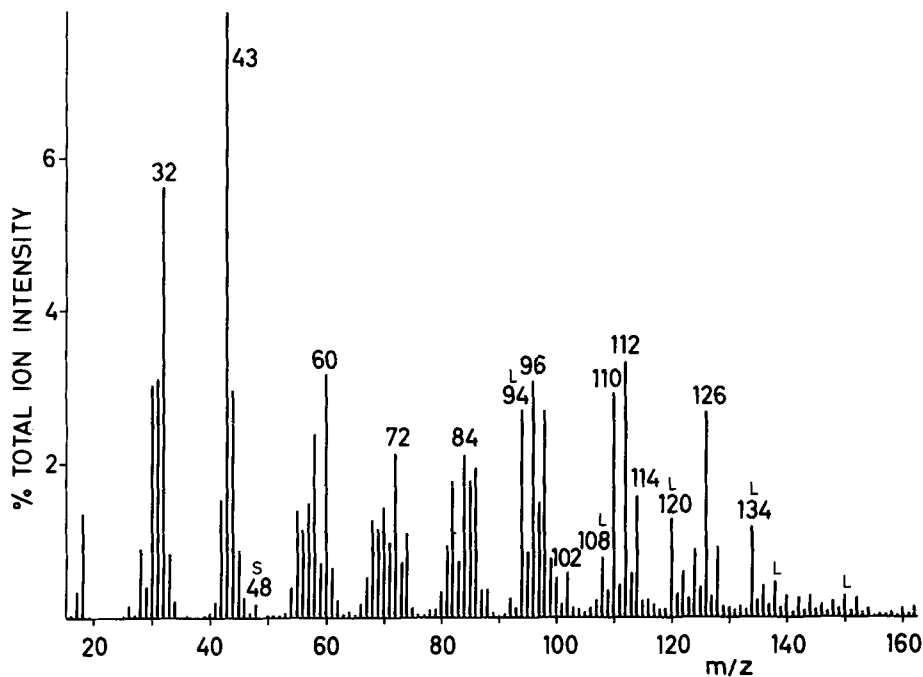
SPECTRUM E.15



SAMPLE : WHEAT FLOUR
 CHEMICAL DETAILS : see NBS publications
 SAMPLE ORIGIN : Natl. Bureau of Standards (SRM 1567), Washington, USA
 SAMPLE PREP./SIZE : suspension in methanol; 10 μ g
 PYROL. CONDITIONS : standard
 TOTAL ION COUNTS : 9×10^4

REMARKS - Somewhat surprisingly, this spectrum is more similar to that of cellulose (Spectrum A.1) than that of amylose (Spectrum A.2). No explanation for this finding can be given yet. In addition, relatively weak protein signals appear at m/z 34, 48, 92.

SPECTRUM E.16



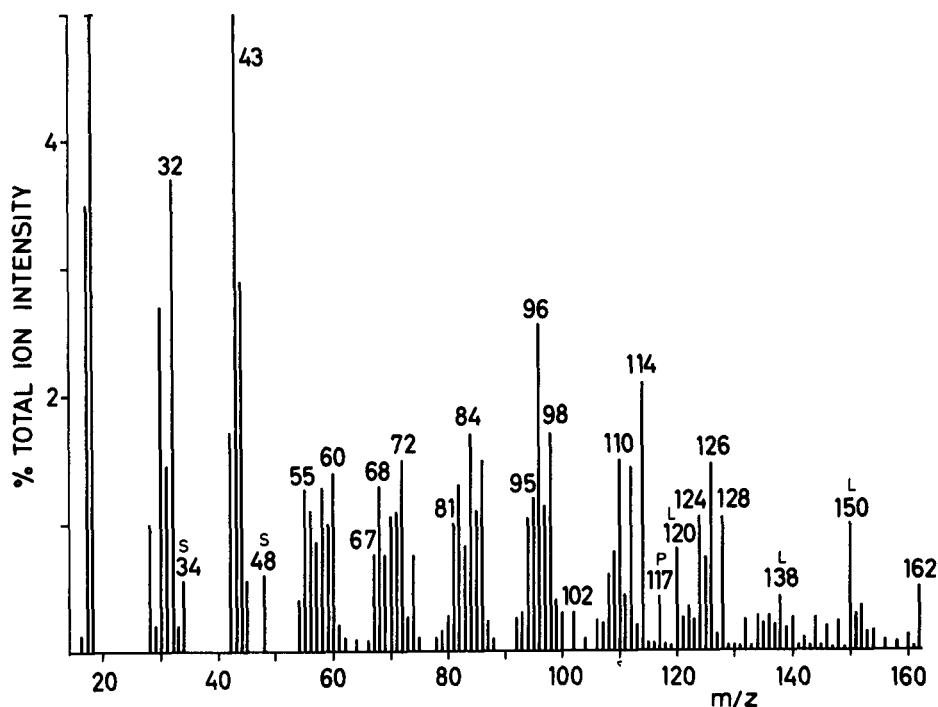
SAMPLE : SPHAGNUM MOSS
 CHEMICAL DETAILS : -
 SAMPLE ORIGIN : Marsh by Leiferde, GFR
 SAMPLE PREP./SIZE : suspension in methanol; 10 µg
 PYROL. CONDITIONS : standard
 TOTAL ION COUNTS : 7.3×10^4

REMARKS - This plant is of considerable interest as a major source and constituent of the extensive sphagnum peat deposits in some parts of the world. As in most plant samples, we find a dominant complex carbohydrate pattern pointing to the presence of cellulose as well as hemicellulose constituents. Most remarkable however are the large signals at m/z 120 and 134. These appear to represent fragments of sphagnol, a primitive type of lignin characterized by the absence of methoxylated phenol moieties (ref. 85). Accordingly, para-hydroxybenzoic acid moieties are the only lignin building blocks present, yielding a fragment series at m/z 94, 108, 120, 134 (see also Remarks on lignin Spectra E.9 and E.10 and on sphagnum peat (Spectrum F.15)).

GROUP F
HUMIC MATERIALS AND GEOPOLYMERS

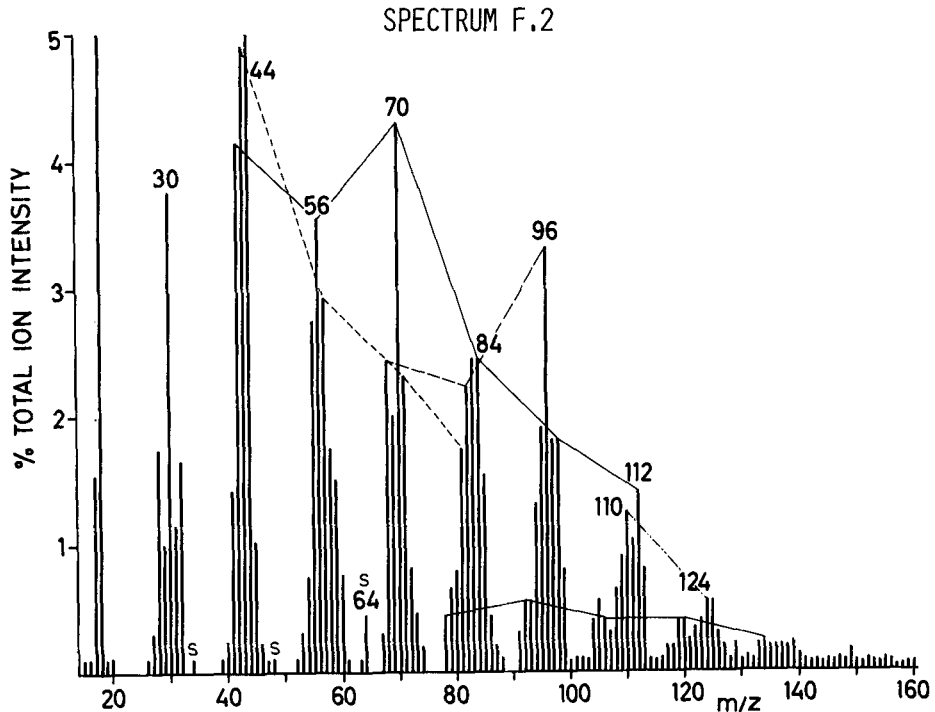
This Page Intentionally Left Blank

SPECTRUM F.1



SAMPLE : GRANITE BROWN SOIL, A-1 horizon (typic Xerochrept)
 CHEMICAL DETAILS : see ref. 188; carbon content 3.5%; nitrogen content 0.4%;
 pH 5.6 in H₂O
 SAMPLE ORIGIN : Huelva, SW Spain
 SAMPLE PREP./SIZE : suspension in methanol; approx. 50 µg
 PYROL. CONDITIONS : standard
 TOTAL ION COUNTS : not determined

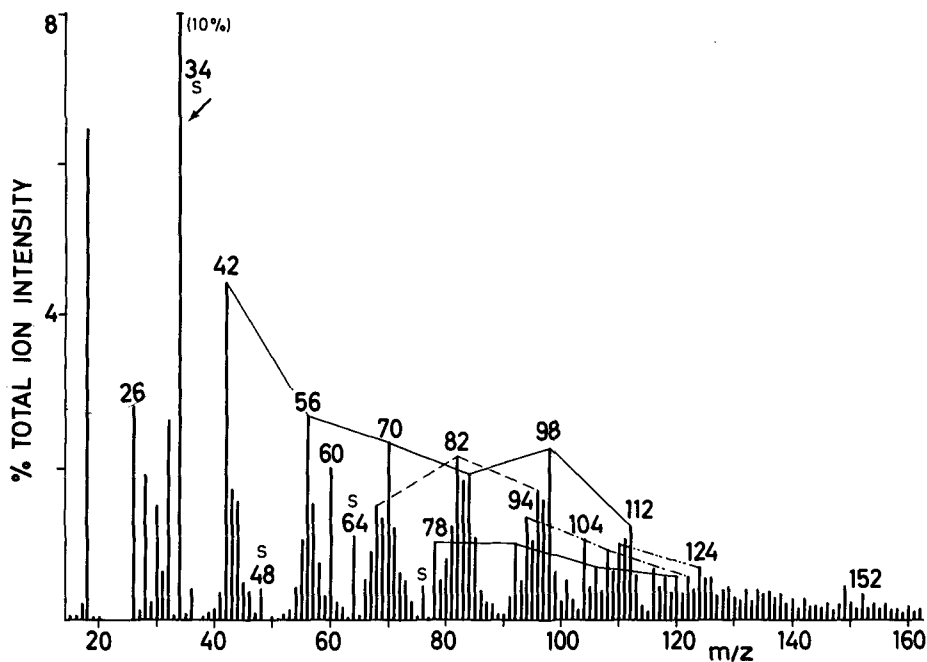
REMARKS - Typical of a soil of this type is the extremely rich mixture of organic compounds comprising carbohydrate (e.g. m/z 43, 72, 74, 84, 86, 96, 98, 102, 112, 114, 126, 128, 144) as well as proteinaceous (e.g. m/z 34, 48, 117) and lignin-type (e.g. m/z 120, 124, 134, 138, 150) compounds. Compare also to bog peat (Spectrum F.14) and to river clay (Spectrum F.2).



SAMPLE : RIVER CLAY (Holocene)
 CHEMICAL DETAILS : see ref. 51; 30.6% clay minerals; 0.45% organic C
 SAMPLE ORIGIN : Lienden, Marspolder, The Netherlands
 SAMPLE PREP./SIZE : suspension in methanol; 50 μ g
 PYROL. CONDITIONS : standard
 TOTAL ION COUNTS : not determined

REMARKS - In contrast to the humus-rich brown soil (carbon content 3.5%) (Spectrum F.1), the river clay shown here is very low in organic materials (0.45% C). Moreover, the organic matter appears to be composed primarily of aliphatic and aromatic hydrocarbons. The main heteroatom constituents appear to be found in the relatively low peaks at m/z 17 (NH_3^+), m/z 64 (SO_2^+ and/or S_2^+) and, possibly, in the ion series at m/z 68, 82, 96, 110, 124 which may represent compounds with oxygen functional groups.

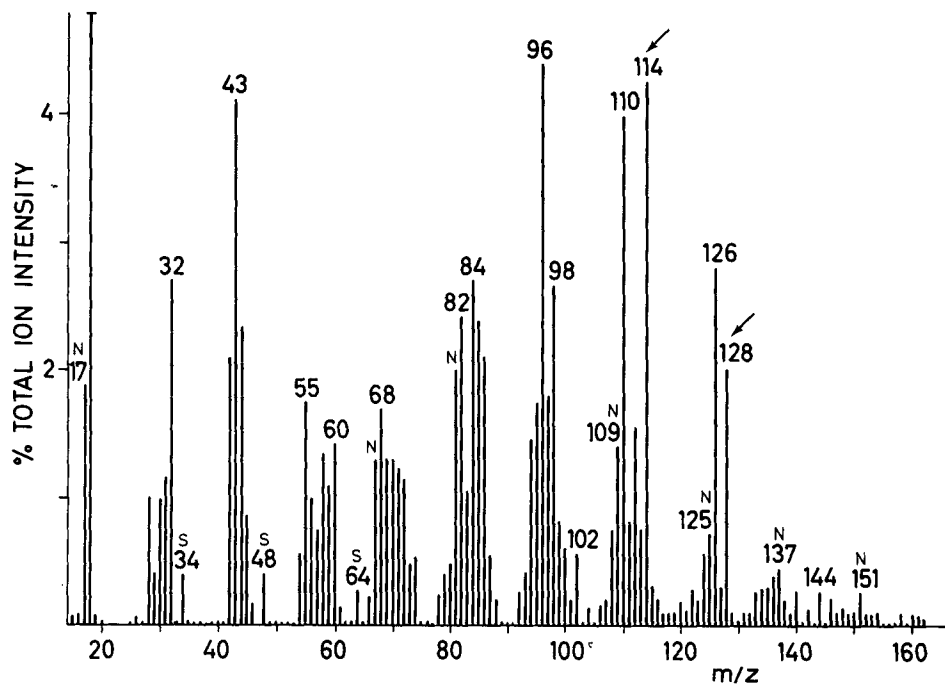
SPECTRUM F.3



SAMPLE : RIVER SEDIMENT (recent)
 CHEMICAL DETAILS : SiO₂ 51%; MgO 4%; Al₂O₃ 4%; CaO 4%; Kjeldahl nitrogen 0.08%; phosphorus 0.05%; freon solubles 1.7%
 SAMPLE ORIGIN : Natl. Bureau of Standards (SRM 1645), Washington, USA
 SAMPLE PREP./SIZE : suspension in methanol; 25 µg
 PYROL. CONDITIONS : standard
 TOTAL ION COUNTS : 4×10^4

REMARKS - The relatively strong intensities of sulphur-containing ion signals at m/z 34, 48, 64 and 76 are typical of organic materials exposed to aqueous environments. Note the relative monotony of the marked ion series, thus presenting a pattern not unlike some kerogen patterns (e.g. Spectrum F.12).

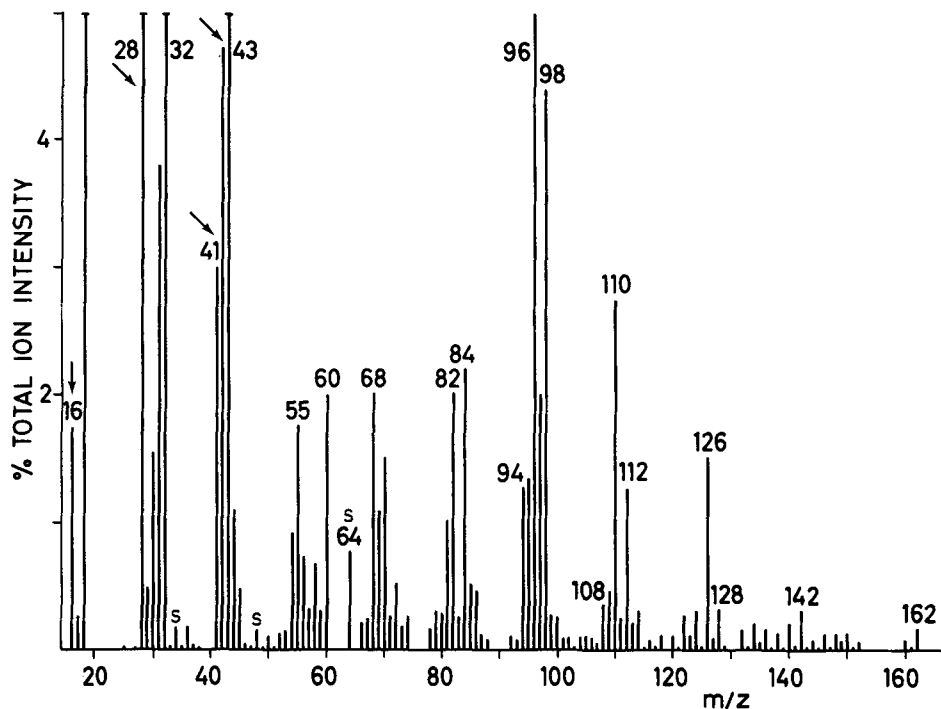
SPECTRUM F.4



SAMPLE : SOIL POLYSACCHARIDE (water extractable fraction from Granite Brown Soil; see Spectrum F.1).
 CHEMICAL DETAILS : see ref. 188; C 37.8%; H 6.8%; N 2.1%; O 53.3%; ash 22%
 SAMPLE ORIGIN : Huelva, SW Spain
 SAMPLE PREP./SIZE : suspension in methanol; approx. 20 µg
 PYROL. CONDITIONS : standard
 TOTAL ION COUNTS : not determined

REMARKS - The spectrum shows a pattern consistent with a relatively pure, but highly complex carbohydrate fraction containing neutral sugar residues as well as N-acetyl aminosugars. The presence of the latter is evidenced by ion series at m/z 17, 67, 81, 109, 125, 137 and 151. High signals at m/z 114 and 128 appear to indicate the presence of pentose and deoxyhexose residues respectively. Note the relatively low intensity of sulphur-containing ion signals at m/z 34, 48 and 64.

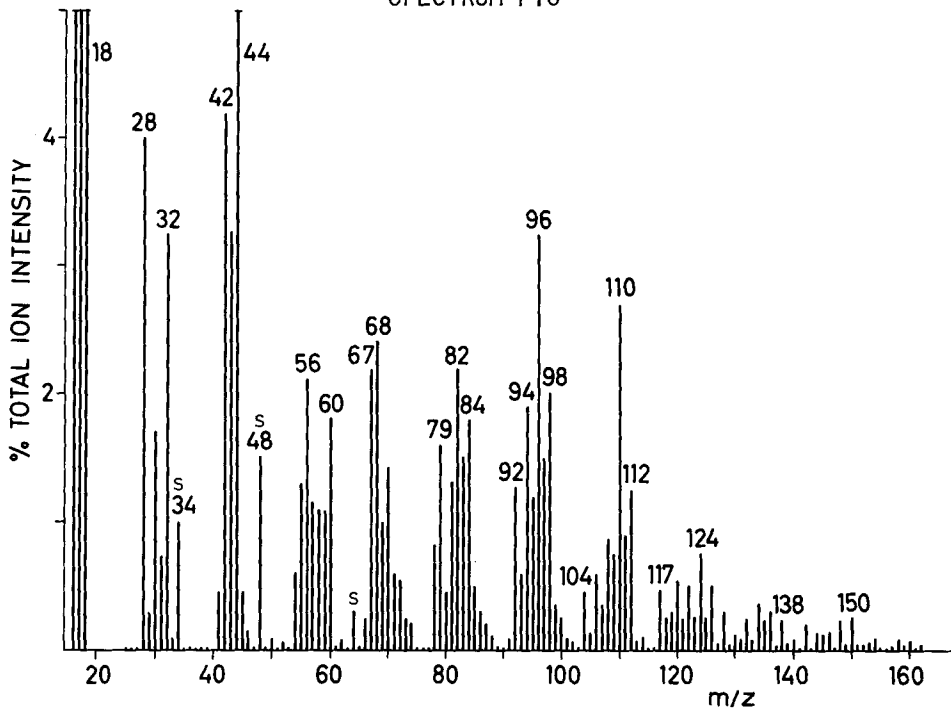
SPECTRUM F.5



SAMPLE : FULVIC ACID (from a Podzol)
 CHEMICAL DETAILS : see ref. 185
 SAMPLE ORIGIN : NW Spain
 SAMPLE PREP./SIZE : suspension in methanol; approx. 25 μ g
 PYROL. CONDITIONS : standard
 TOTAL ION COUNTS : not determined

REMARKS - The overall pattern is that of a carbohydrate material. Compared with the soil polysaccharide (Spectrum F.4), however, this spectrum is far more simple since it lacks ion series indicative of N-acetyl aminosugars and pentose or deoxyhexose residues. Moreover, the absence of a well marked peak at m/z 102 warns that we may not be dealing with a simple hexose polymer. Also, major peaks at m/z 16, 28, 41, 42, apparently indicating the presence of aliphatic hydrocarbon moieties, are unusual for polysaccharide patterns. Although varying amounts of carbohydrate material are often found in fulvic acids, depending on the preparation techniques used, the "core" of fulvic acids may be made up of polycarboxylic, e.g. polymaleic, acids rather than carbohydrates as shown by recent Py-GC/MS studies (ref. 181).

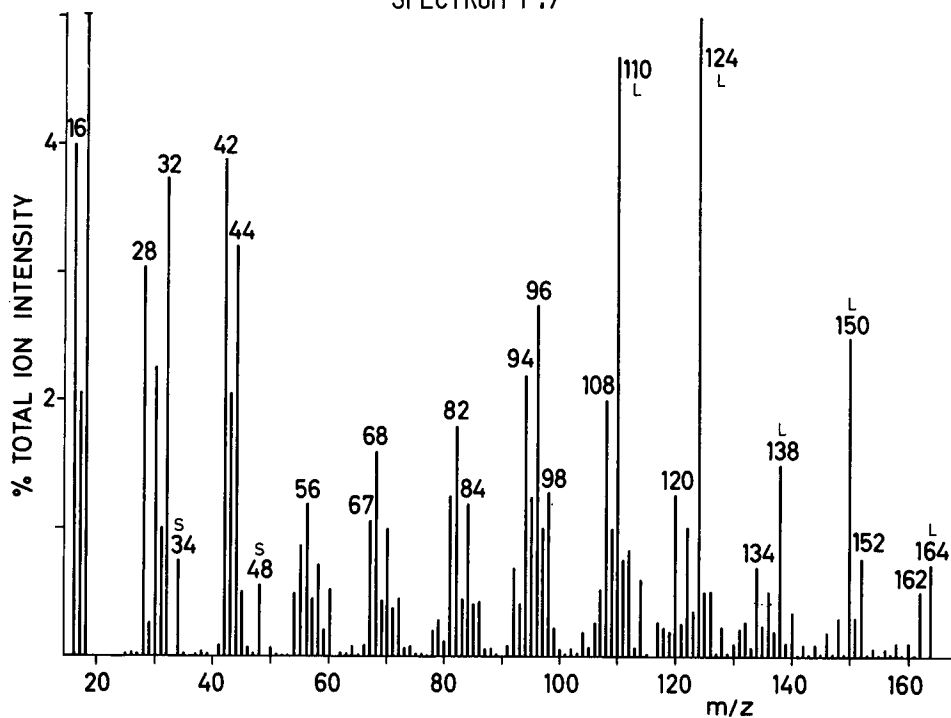
SPECTRUM F.6



SAMPLE : HUMIC ACID (from a Podzol)
 CHEMICAL DETAILS : see ref. 185
 SAMPLE ORIGIN : NW Spain
 SAMPLE PREP./SIZE : suspension in methanol; approx. 25 µg
 PYROL. CONDITIONS : standard
 TOTAL ION COUNTS : not determined

REMARKS - Although superficially rather similar to fulvic acid (Spectrum F.5), this humic acid spectrum shows much higher peak series indicating the presence of nitrogen-containing (m/z 17, 67, 79, 117), sulphur-containing (m/z 34, 48) and aromatic (m/z 78, 92, 94, 104, 106, 124) fragments. As most of these signals are also encountered in pyrolysis mass spectra of proteins this suggests a significant contribution of proteinaceous compounds.

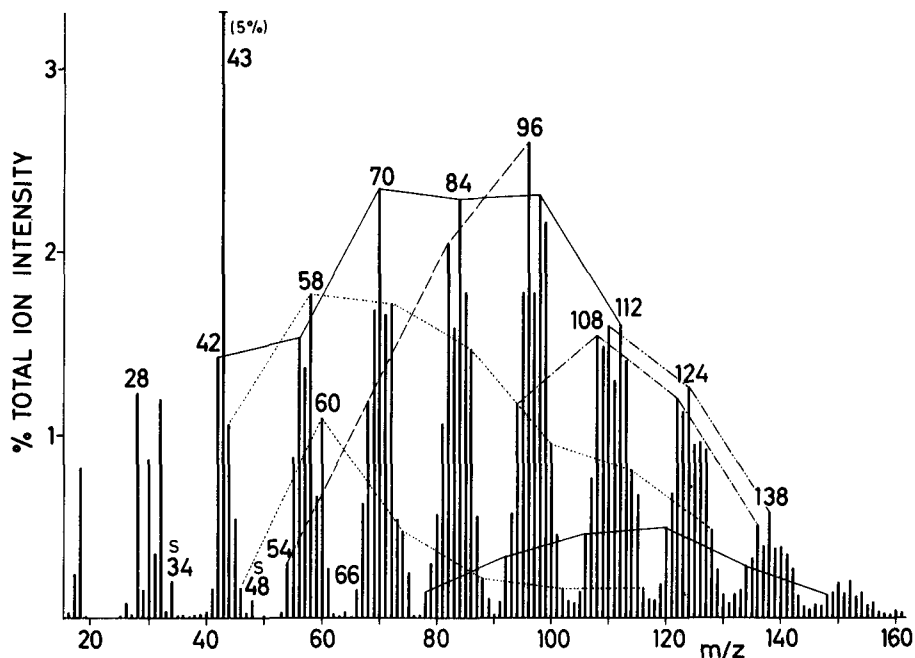
SPECTRUM F.7



SAMPLE : HUMIC ACID (from a forest soil)
 CHEMICAL DETAILS : see ref. 185
 SAMPLE ORIGIN : Canada
 SAMPLE PREP./SIZE : suspension in methanol; approx. 25 µg
 PYROL. CONDITIONS : standard
 TOTAL ION COUNTS : not determined

REMARKS - In spite of the strong qualitative resemblance to humic acid from Podzol (Spectrum F.6) a marked series of intense peaks at m/z 124, 138, 150, 164 easily distinguishes the two spectra. These signals appear to be derived from guaiacylic lignin moieties, obviously corresponding to the presence of sizeable amounts of incompletely degraded plant material in the upper horizons of the forest soil.

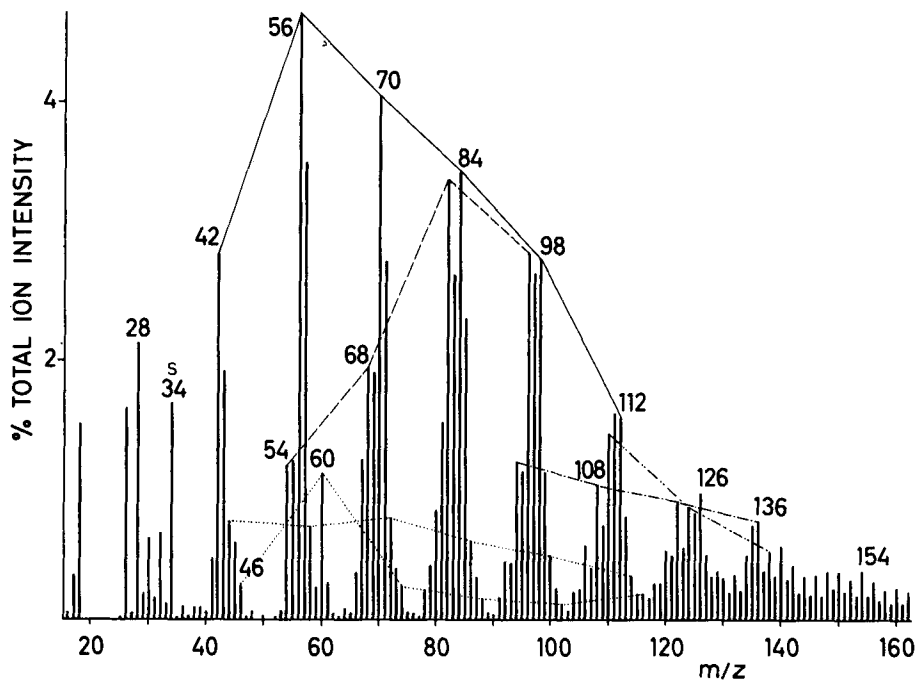
SPECTRUM F.8



SAMPLE : COORONGITE
 CHEMICAL DETAILS : possibly formed through oxidative polymerisation of three
 alkadienes with the structure $\text{CH}_2=\text{CH}(\text{CH}_2)_n\text{CH}=\text{CH}(\text{CH}_2)_7-\text{CH}_3$
 ($n=15, 17$ and 19) produced by *Botryococcus braunii*
 (ref. 206)
 SAMPLE ORIGIN : Coolaway, Australia
 SAMPLE PREP./SIZE : suspension in methanol; 20 μg
 PYROL. CONDITIONS : standard
 TOTAL ION COUNTS : 2.6×10^5

REMARKS - Coorongite, related to but probably not a direct precursor of Torbanite, shows a pattern rather similar to that of Torbanite (Spectrum F.9). However, compared to Torbanite the maxima of each homologous ion series have shifted to a higher mass range, indicating longer average aliphatic chain lengths. Also the ion series at m/z 44, 58, 72, 86 and at m/z 46, 60, 74 are much more pronounced than in Torbanite, apparently indicating a higher abundance of oxygen-containing aliphatic compounds.

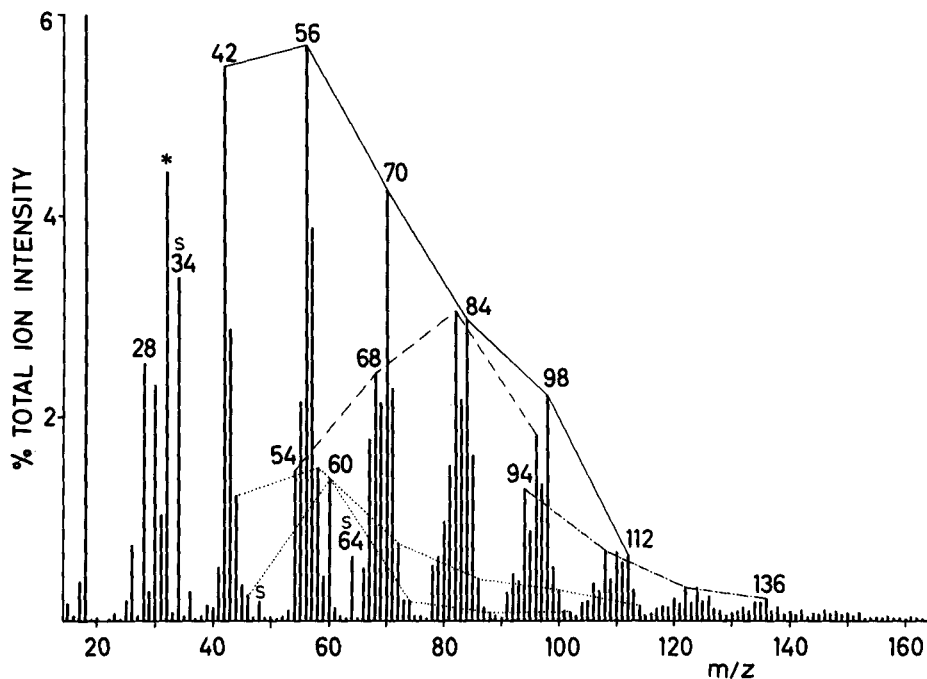
SPECTRUM F.9



SAMPLE : TORBANITE (*Botryococcus braunii* alginite)
 CHEMICAL DETAILS : see ref. 206
 SAMPLE ORIGIN : Coolaway, Australia
 SAMPLE PREP./SIZE : suspension in methanol; 20 μ g
 PYROL. CONDITIONS : standard
 TOTAL ION COUNTS : 1×10^5

REMARKS - In comparison with its "peat stage", Coorongite (Spectrum F.8) this Torbanite spectrum shows shorter average aliphatic chain lengths and less pronounced oxygen-containing compound series. Furthermore the alkene series at m/z 42, 56, etc. is relatively more pronounced in Torbanite, possibly indicating a more saturated nature of the carbon skeleton.

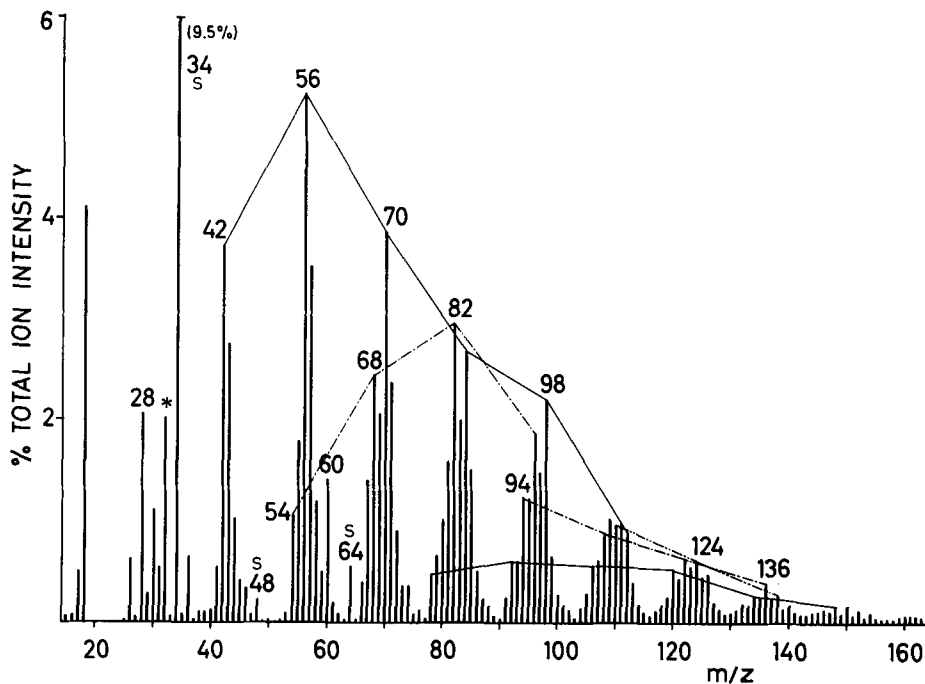
SPECTRUM F.10



SAMPLE : TORBANITE
 CHEMICAL DETAILS : see ref. 206
 SAMPLE ORIGIN : Ermelo, S. Africa
 SAMPLE PREP./SIZE : suspension in methanol; 20 μ g
 PYROL. CONDITIONS : standard
 TOTAL ION COUNTS : 2.5×10^4

REMARKS - This spectrum is highly similar to that of the Coolaway Torbanite (Spectrum F.9) in spite of the enormous geographic distance. The major difference appears to be a stronger preponderance of sulphur-containing products at m/z 34, 48 and 64 as well as of short chain aliphatic fragments.

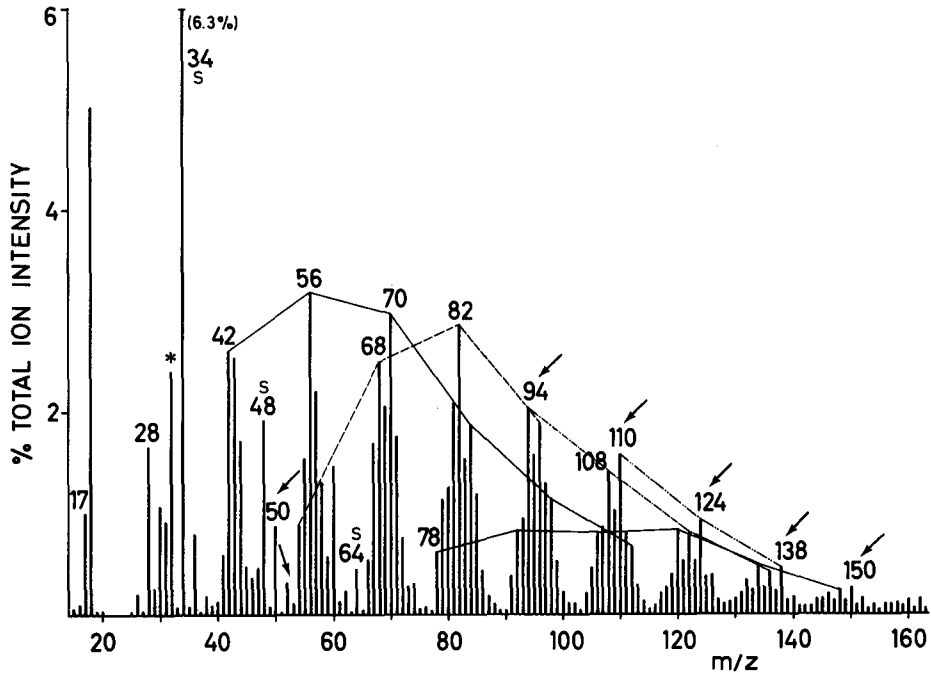
SPECTRUM F.11



SAMPLE : GREEN RIVER SHALE
 CHEMICAL DETAILS : 40% organic matter; C 64.5%; H 8.5%; O 6.8%; N 2.3%
 SAMPLE ORIGIN : Wyoming, USA
 SAMPLE PREP./SIZE : suspension in methanol; 20 μ g
 PYROL. CONDITIONS : standard
 TOTAL ION COUNTS : 6.3×10^4

REMARKS - The pyrolysis pattern of this shale is almost identical to that of the Coolaway Torbanite (Spectrum F.9). Apparently the lacustrine origin of both samples prevails over differences in age, etc. Also, this confirms the dominantly algal origin of the organic matter in Green River shale. Note, however, the much higher intensity of the sulphur-containing products at m/z 34, 48 and 64 compared to Torbanite (Spectrum F.9).

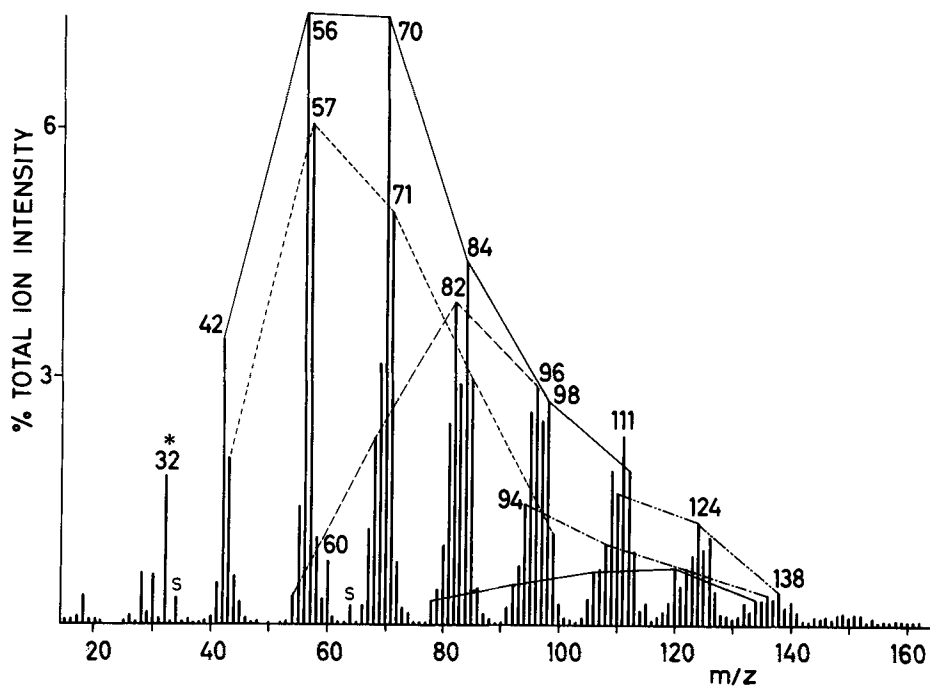
SPECTRUM F.12



SAMPLE : MESSEL SHALE
 CHEMICAL DETAILS : 50% organic matter; C 68.5%; H 7.9%; O 17.5%; N 2.4%
 SAMPLE ORIGIN : Darmstadt, GFR
 SAMPLE PREP./SIZE : suspension in methanol; 20 μ g
 PYROL. CONDITIONS : standard
 TOTAL ION COUNTS : 3×10^5

REMARKS - In comparison to Torbanite (Spectra F.9, F.10) and Green River Shale (Spectrum F.11), Messel shale shows relatively high peak intensities at m/z 94, 110, 124, 138 and 150. These signals can be explained by phenols and methoxyphenols (ref. 52). Most likely, these compounds are derived from lignin moieties present in terrestrial plant materials which are known to contribute to the organic matter in Messel shale. In fact, similar ion series are observed in lignite (Spectrum F.16). Another interesting phenomenon is the marked abundance of CH_3Cl^+ ions at m/z 50 and 52, indicative of the presence of methylating functional groups.

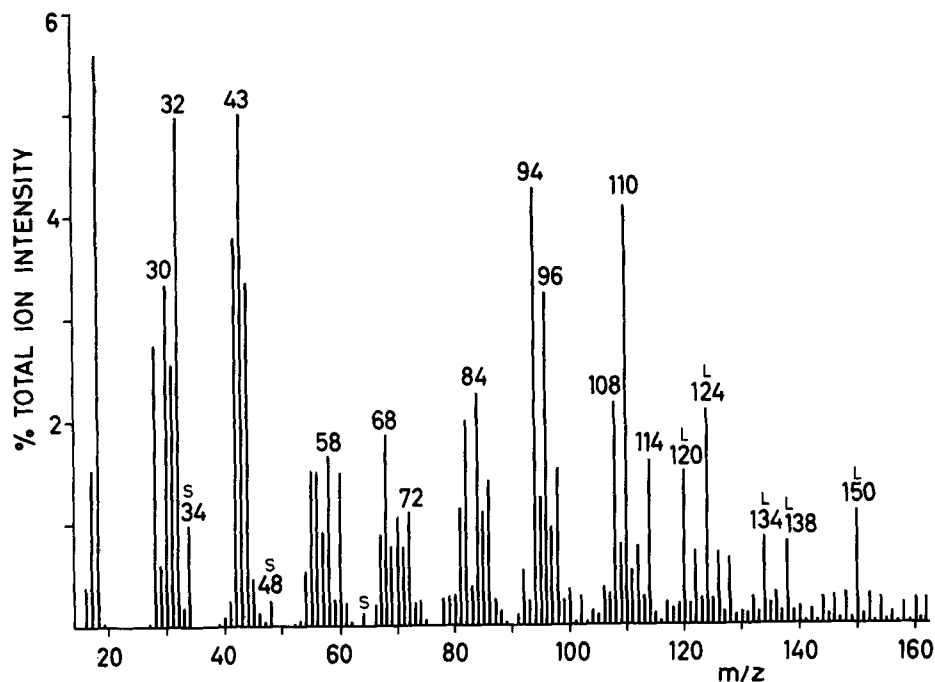
SPECTRUM F.13



SAMPLE : GILSONITE
 CHEMICAL DETAILS : largely long chain paraffins
 SAMPLE ORIGIN : Utah, USA
 SAMPLE PREP./SIZE : suspension in methanol; 20 μ g
 PYROL. CONDITIONS : standard
 TOTAL ION COUNTS : 6×10^4

REMARKS - The saturated aliphatic hydrocarbon nature of Gilsonite is reflected in the dominant ion series at m/z 42, 56, etc., apparently representing alkenes, and at m/z 43, 57, etc., thought to represent EI fragments of alkanes. The contribution of heteroatom compounds appears to be negligible as indicated by the very low peaks at m/z 17 (NH_3^+) and m/z 34 (H_2S^+) and the absence of prominent oxygen-containing ion series.

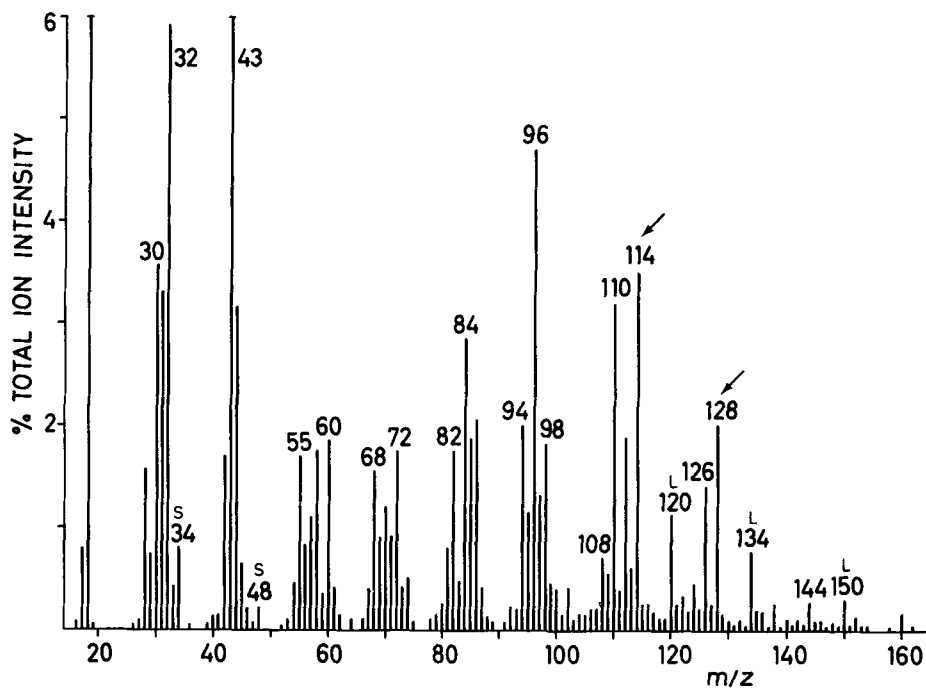
SPECTRUM F.14



SAMPLE : BOG PEAT
 CHEMICAL DETAILS : see ref. 50
 SAMPLE ORIGIN : Bad-Zwischenahn GFR; depth >250 cm
 SAMPLE PREP./SIZE : suspension in methanol; approx. 25 µg
 PYROL. CONDITIONS : standard
 TOTAL ION COUNTS : not determined

REMARKS - Bog peat is composed to a large extent of wool grass and other plant residues. Therefore it contains grass lignins characterised by the presence of methoxylated phenolic series derived from guaiacylic (m/z 124, 138, 150) as well as syringylic (weak signal at m/z 154) building blocks, in addition to the nonmethoxylated phenols (m/z 94, 108, 120, 134) also found in sphagnum peat (Spectrum F.15). Note also the characteristic methane peak (m/z 16) encountered in pyrolysis mass spectra of methoxylated lignins (Spectra E.9, E.10).

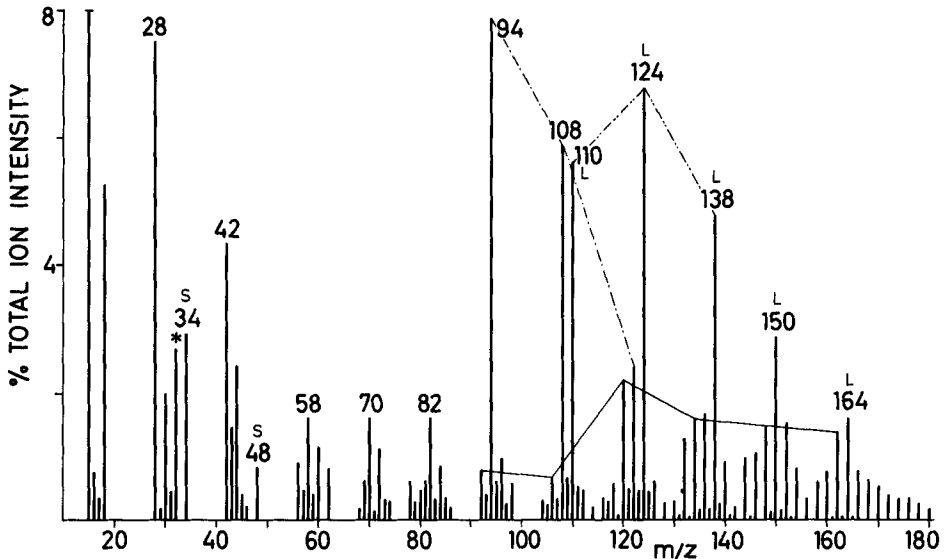
SPECTRUM F.15



SAMPLE : SPHAGNUM PEAT
 CHEMICAL DETAILS : see ref. 50
 SAMPLE ORIGIN : Bad-Zwischenahn, GFR; top 60 cm of profile
 SAMPLE PREP./SIZE : suspension in methanol; approx. 25 μ g
 PYROL. CONDITIONS : standard
 TOTAL ION COUNTS : not determined

REMARKS - In contrast to bog peat (Spectrum F.14), sphagnum peat exhibits an almost strictly polysaccharide pattern with strong peaks at m/z 114 and 128 indicating the presence of sugar residues other than hexose, e.g. pentose and deoxyhexose. The absence of a typical lignin pattern such as in bog peat is explained by the lack of true lignins in Sphagnum moss (Spectrum E.16). The only lignin-like constituent of Sphagnum moss, sphagnol (ref. 85), apparently gives rise to the nonmethoxylated (alkyl)phenol series at m/z 94, 108, 120 and 134. Also note the absence of pyrolytic methane (m/z 16).

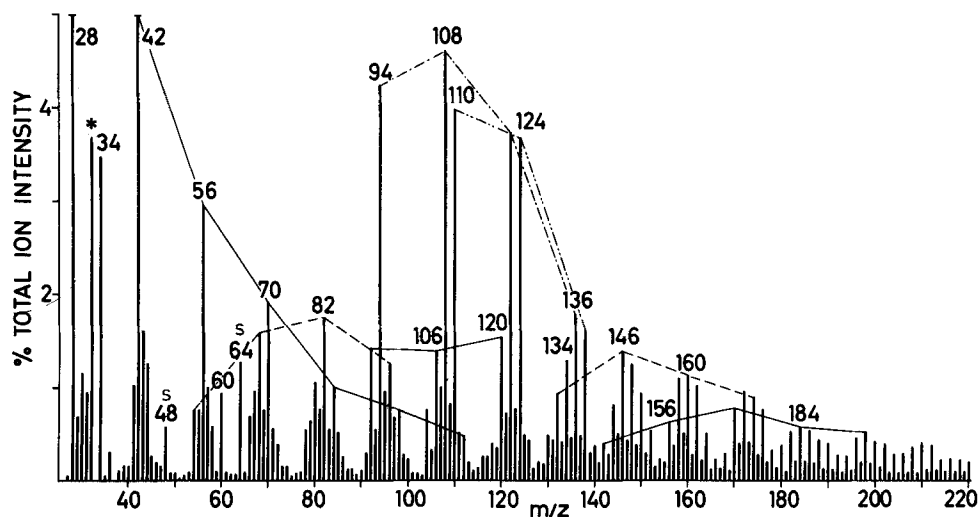
SPECTRUM F.16



SAMPLE : LIGNITE (Miocene)
 CHEMICAL DETAILS : see ref. 52; 90% organic material; C 61.6%; H 4.6%;
 O 32.4%; N 0.6%
 SAMPLE ORIGIN : Herzogenrath, GFR
 SAMPLE PREP./SIZE : suspension in methanol; 25 µg
 PYROL. CONDITIONS : standard
 TOTAL ION COUNTS : not determined

REMARKS - This lignite spectrum is dominated by phenolic peak series with signals at m/z 124, 138, 150, 164 apparently representing more or less unchanged guaiacylic building blocks (compare with lignin Spectra E.9 and E.10). However, the strong dihydroxybenzene peak at m/z 110 points to the loss of methoxy groups by demethylation. Also the multiple peaks at even mass numbers between the major "lignin" peaks in the high mass range provide evidence for a progressive chemical modification of the original biopolymer matrix. Note the complete absence of typical cellulosic fragments (compare with wood spectrum E.11) as a result of the more rapid degradation of the polysaccharide moieties of the original wood. Further note the low sulphur signals which confirms the non-marine origin of this lignite largely composed of redwood remains.

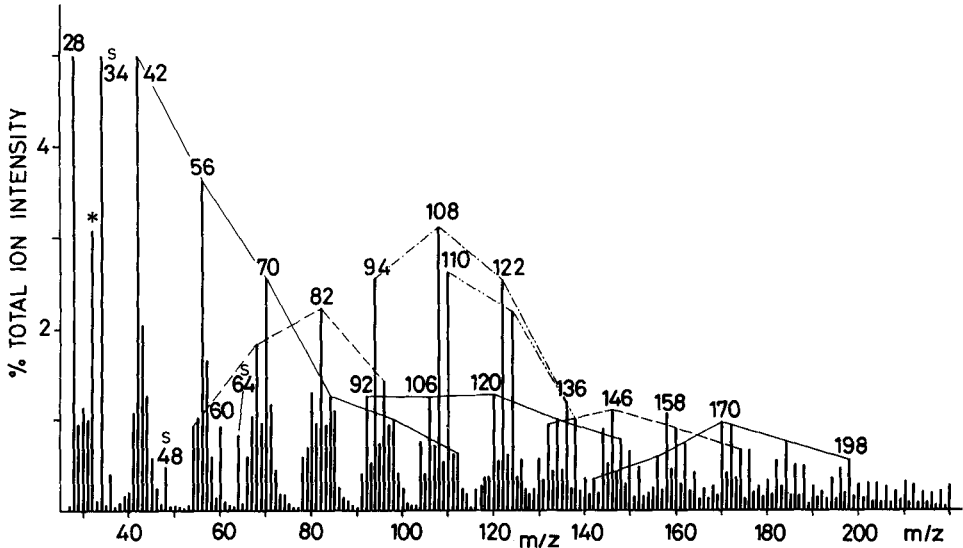
SPECTRUM F.17



SAMPLE : HIGH VOLATILE C BITUMINOUS COAL (from Hanna Bed #2)
 CHEMICAL DETAILS : C 78.8%; S 0.73%; mineral matter 20.4%; vitrinites 94.9%;
 exinites 2.1%; inertinites 3.0%
 SAMPLE ORIGIN : Wyoming, USA (Penn State Coal Sample Bank; PSOC 514)
 SAMPLE PREP./SIZE : suspension in methanol; 40 μ g
 PYROL. CONDITIONS : T_{eq} 610°C; t_T 5s; t_Z 10s; E_{e1} 15eV (Extranuclear 5000-1
 Py-MS system)
 TOTAL ION COUNTS : 1×10^5

REMARKS - Compared to Spectrum F.16 (lignite) the methoxyphenol series (at m/z 124, 138, 150, 164) appears to have been replaced by a dihydroxybenzene series with prominent peaks at m/z 110 and 124, apparently as a result of further demethylation. Moreover, aliphatic hydrocarbon series start appearing at m/z 42, 56, 70 etc. (alkenes) and 54, 68, 82 (dienes; perhaps mixed with furans). Note the relatively low sulphur-containing ion peaks at m/z 34, 48 and 64.

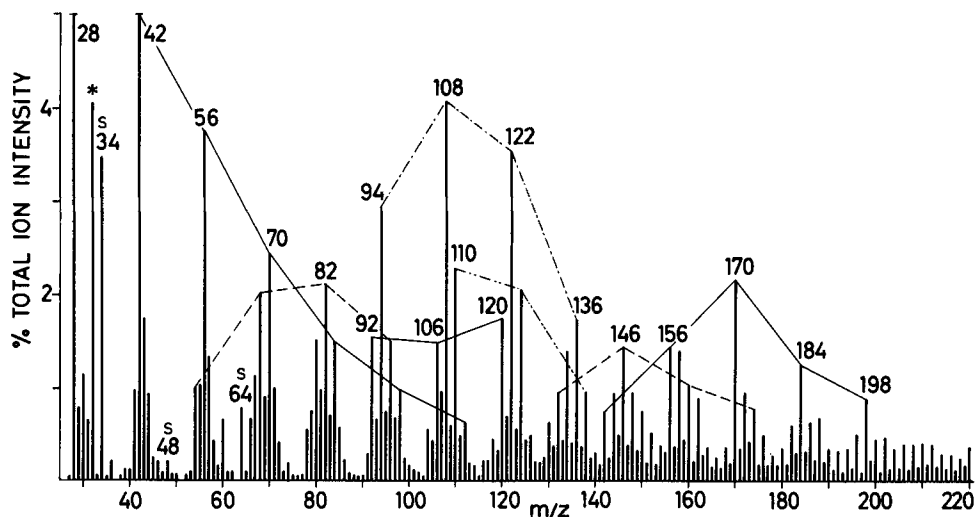
SPECTRUM F.18



SAMPLE : HIGH VOLATILE C BITUMINOUS COAL (from New Mexico Seam #7)
 CHEMICAL DETAILS : C 77.9%; S 0.92%; mineral matter 9.1%; vitrinites 83.5%;
 exinites 2.0%; inertinites 14.5%
 SAMPLE ORIGIN : New Mexico, USA (Penn State Coal Sample Bank; PSOC 310)
 SAMPLE PREP./SIZE : suspension in methanol; 40 μ g
 PYROL. CONDITIONS : T_{eq} 610°C; t_T 5s; t_Z 10s; E_{e1} 15eV (Extranuclear 5000-1
 Py-MS system)
 TOTAL ION COUNTS : 1×10^5

REMARKS - Compared to the Hanna Field coal of the same ASTM rank (Spectrum F.17)
 the phenolic series are less prominent whereas the aliphatic hydrocarbons series
 appear to be more pronounced.

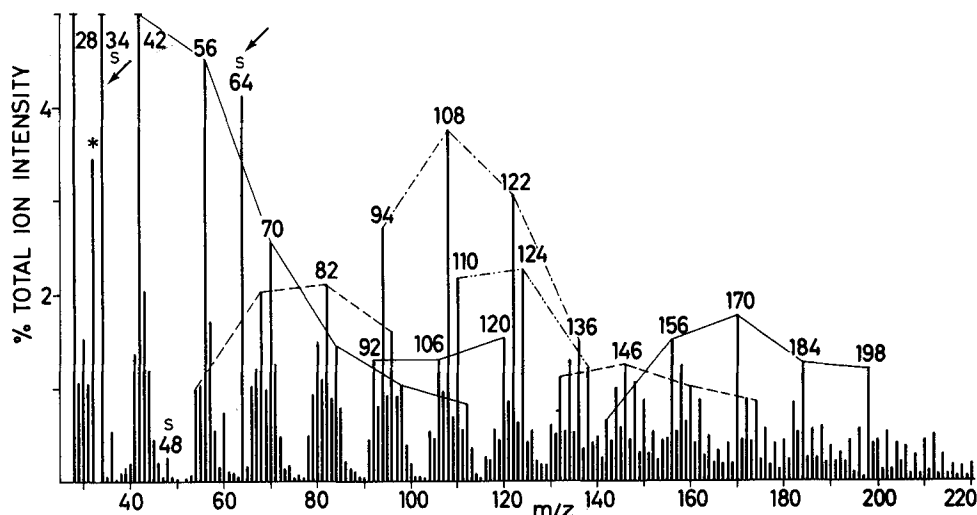
SPECTRUM F.19



SAMPLE : HIGH VOLATILE B BITUMINOUS COAL (from Blind Canyon Seam)
 CHEMICAL DETAILS : C 79.4%; S 0.76%; mineral matter 9.2%; vitrinite 82.3%;
 exinites 2.1%; inertinites 15.6%
 SAMPLE ORIGIN : Utah, USA (Penn State Coal Sample Bank; PSOC 238)
 SAMPLE PREP./SIZE : suspension in methanol; 40 μ g
 PYROL. CONDITIONS : T_{eq} 610°C; t_T 6s; t_C 10s; E_{e1} 15 eV (Extranuclear 5000-1
 Py-MS system)
 TOTAL ION COUNTS : 1×10^5

REMARKS - Compared to the High Volatile C Bituminous coal from the Rocky Mountain Coal Province (Spectrum F.18), the dihydroxybenzene peak series (m/z 110, 124, 138) is clearly reduced whereas the naphthalene series (m/z 142, 156, 170, 184, 198) starts to dominate the high mass region.

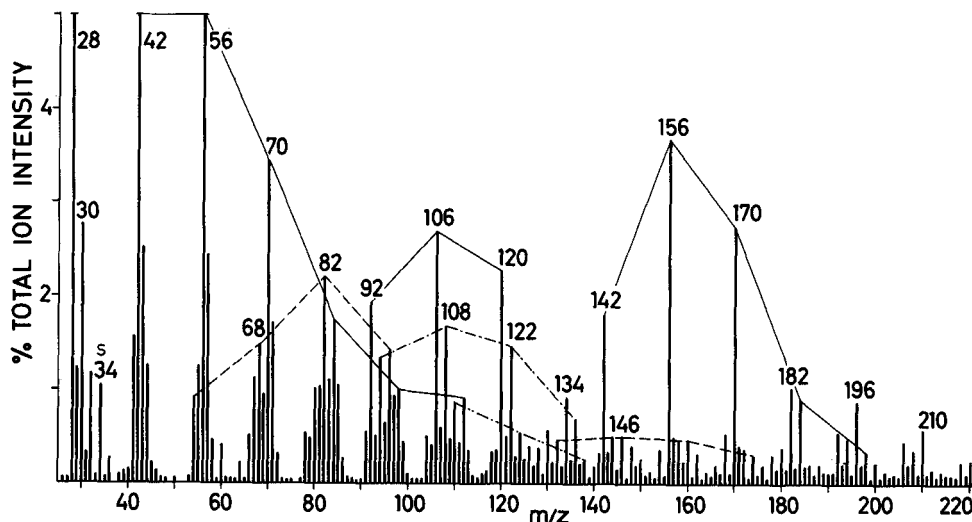
SPECTRUM F.20



SAMPLE : HIGH VOLATILE A BITUMINOUS COAL (from Utah A Seam)
 CHEMICAL DETAILS : C 80.5%; S 1.78%; mineral matter 10.8%; vitrinites 85.2%;
 exinites 2.9%; inertinites 11.9%
 SAMPLE ORIGIN : Utah, USA (Penn State Coal Sample Bank; PSOC 238)
 SAMPLE PREP./SIZE : suspension in methanol; 40 μ g
 PYROL. CONDITIONS : T_{eq} 610°C; t_f 6s; t_Σ 10s; E_e 15eV (Extranuclear 5000-1
 Py-MS system)
 TOTAL ION COUNTS : 1.3×10^5

REMARKS - This spectrum is very similar to that of the high volatile B bituminous coal of the same region (Utah Region of Rocky Mountain Coal Province) with the exception of the markedly higher sulphur-containing ion signals at m/z 34 and 64. This correlates with the much higher S content (1.78% vs. 0.76%). Note, however, that the peak at m/z 48 (CH_3SH^+) remains low. The absence of obvious rank-related differences between the pyrolysis mass spectra of high volatile B and A bituminous ranks is typical. Characteristic rank related changes occur most strongly between the HVCB and HVBB ranks and again between the HVAB and MVB ranks.

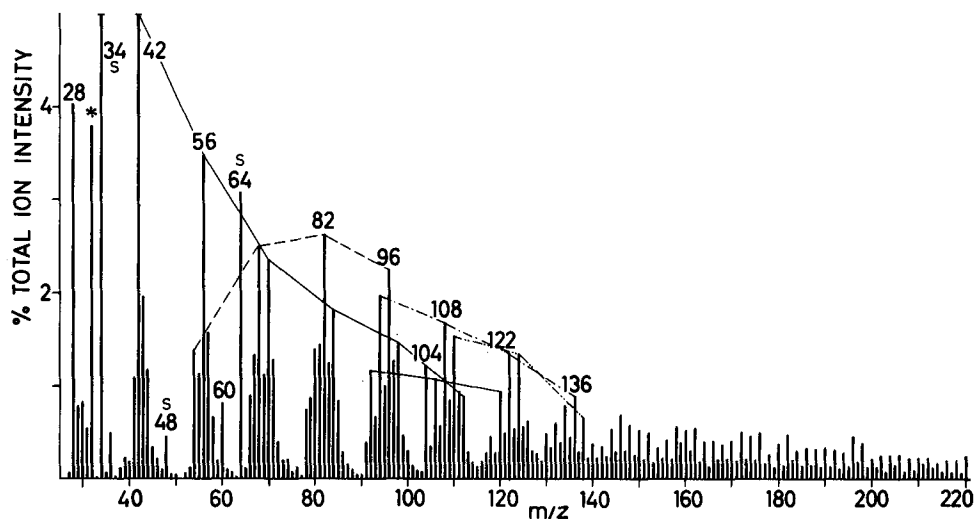
SPECTRUM F.21



SAMPLE : MEDIUM VOLATILE BITUMINOUS COAL (from Colorado B Seam)
 CHEMICAL DETAILS : C 89.9%; S 0.56%; O 2.07%; mineral matter 7.6%; vitrinites 92.0%; exinites 0.1%; inertinites 7.9%
 SAMPLE ORIGIN : Colorado, USA (Penn State Coal Sample Bank; PSOC 157)
 SAMPLE PREP./SIZE : suspension in methanol; 40 μ g
 PYROL. CONDITIONS : T_{eq} 610°C; t_T 6s; t_D 10s; E_e 15eV (Extranuclear 5000-1 Py-MS system)
 TOTAL ION COUNTS : 1×10^5

REMARKS - Compared to the high volatile bituminous coals in Spectra F.17-F.20, the phenolic series at m/z 94, 108, etc. and at m/z 110, 124, etc. are drastically decreased and the spectrum is now entirely dominated by aliphatic and aromatic hydrocarbons. Note especially the strong alkene (m/z 42, 56, etc.), benzene (m/z 92, 106, etc.) and naphthalene (m/z 142, 156, etc.) series. Further note the decrease in sulphur-containing ion peaks. Some of the differences with the high volatile bituminous coals may be exaggerated since the Colorado B Seam coals underwent accelerated maturation because of exposure to high geothermal gradients.

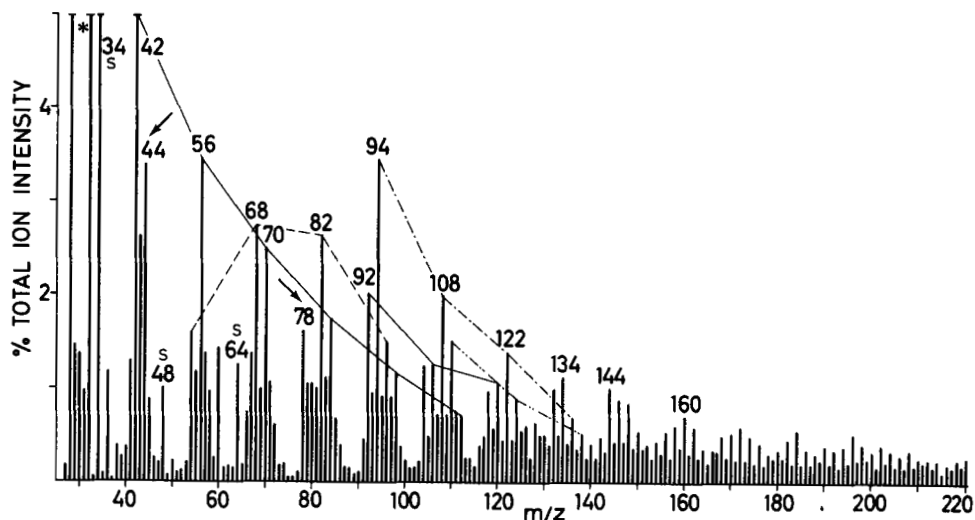
SPECTRUM F.22



SAMPLE : BOGHEAD COAL (from Cannel King Seam)
 CHEMICAL DETAILS : C 80.2%; S 1.82%; O 11.1%; mineral matter 29.1%;
 vitrinites 26.7%; exinites 69.1% (alginite!); inertinites
 3.9%
 SAMPLE ORIGIN : Utah, USA (Penn State Coal Sample Bank; PSOC 1109)
 SAMPLE PREP./SIZE : suspension in methanol; 40 μ g
 PYROL. CONDITIONS : T_{eq} 610°C; t_1 6s; t_2 10s; E_e 15eV (Extranuclear 5000-1
 Py-MS system)
 TOTAL ION COUNTS : 1.2×10^5

REMARKS - The spectrum of this alginite-rich coal is radically different from that of the vitrinite-rich coals shown in spectra F.16-F.21. Aliphatic hydrocarbon series dominate, e.g. alkenes (m/z 42, 56, etc.) and dienes (m/z 54, 68, etc.), whereas aromatic signals are inconspicuous. Note the high sulphur-containing ion peaks at m/z 34 and 64 which confirm the aquatic character of the depositional environment. In many respects this Boghead coal spectrum resembles that of the alginite-rich Torbanites (Spectra F.9, F.10) and shales (Spectra F.11, F.12).

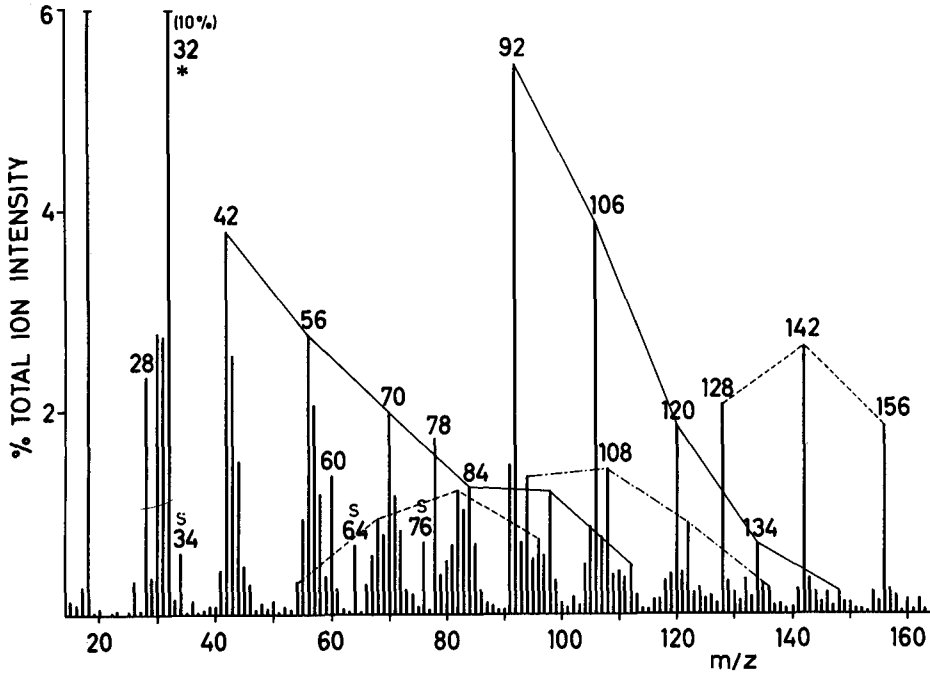
SPECTRUM F.23



SAMPLE : BOGHEAD COAL, severely weathered (from Cannel King Seam)
 CHEMICAL DETAILS : C 67.6%; S 2.39%; O 26.2%; mineral matter 32.7%
 SAMPLE ORIGIN : Utah, USA (Penn State Coal Sample Bank; PSOC 1108)
 SAMPLE PREP./SIZE : suspension in methanol; 40 μ g
 PYROL. CONDITIONS : T_{eq} 610°C; t_T 6s; t_Z 10s; E_e 15eV (Extranuclear 5000-1 Py-MS system)
 TOTAL ION COUNTS : 7×10^4

REMARKS - This spectrum is included to show the effects of severe weathering (oxidation). Comparison with the relatively non-weathered sample from the same seam (Spectrum F.22) shows a marked increase in the intensities of the peaks at m/z 44 (CO_2^{+}) and m/z 78 ($C_6H_6^{+}$). This is thought to indicate the presence of benzene carboxylic acids as a result of oxydation of aromatic rings. The relative increase in phenols (m/z 94, 108) may also reflect ring oxydation. Further note the higher peak at m/z 60, probably acetic acid, which may well represent oxidation of aliphatic moieties.

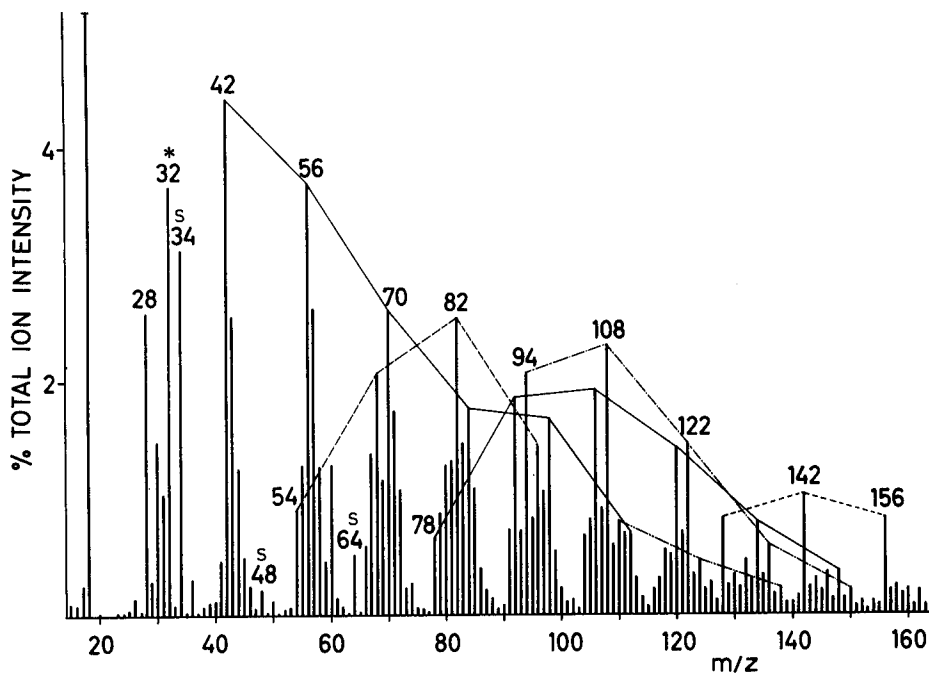
SPECTRUM F.24



SAMPLE : FUSINITE (from Westfield Fusain)
 CHEMICAL DETAILS : (see ref. 206)
 SAMPLE ORIGIN : Scotland
 SAMPLE PREP./SIZE : suspension in methanol; 20 μ g
 PYROL. CONDITIONS : standard
 TOTAL ION COUNTS : 3×10^4

REMARKS - This spectrum is dominated by (alkyl)benzenes, m/z 78, 92, etc. and (alkyl) naphthalenes, m/z 128, 142, etc.. This agrees well with a possible charcoal nature and origin of fusinite (ref. 194). Note further the relatively low sulphur-containing ion signals at m/z 34 and 48, although m/z 64 and 76 show well pronounced peaks.

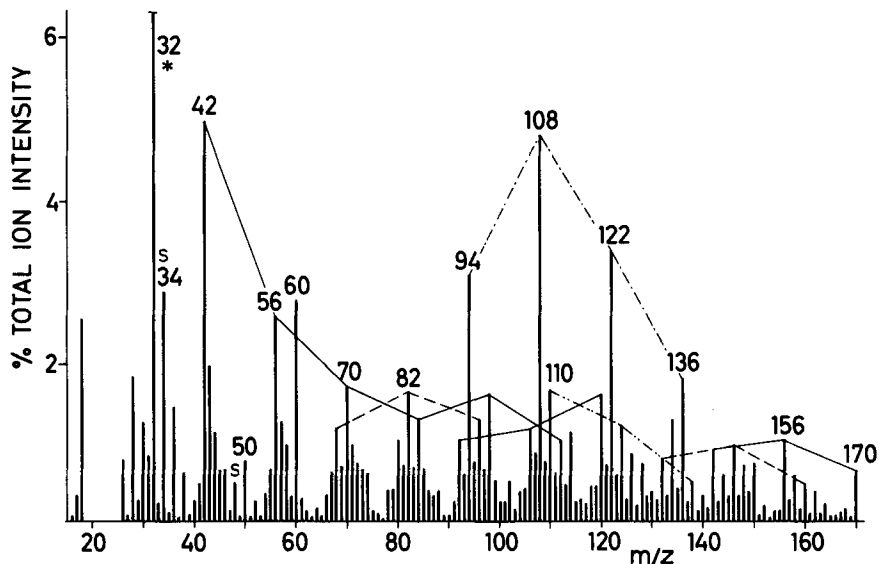
SPECTRUM F.25



SAMPLE : SPORINITE (from Deep Hard Seam)
 CHEMICAL DETAILS : H/C ratio 0.98; sporinite 93.0%; micrinite and fusinite 7.0% (see ref. 206)
 SAMPLE ORIGIN : England
 SAMPLE PREP./SIZE : suspension in methanol; 20 μ g
 PYROL. CONDITIONS : standard
 TOTAL ION COUNTS : 5×10^4

REMARKS - This pattern appears to be more or less intermediate between that of vitrinite (Spectrum F.26) and fusinite (Spectrum F.24). To some extent, this may reflect technical difficulties in obtaining sporinite fractions free of vitrinite and fusinite. Olefinic series at m/z 42, 56, etc. and m/z 54, 68, etc. appear to dominate the overall pattern as might be expected from a fraction rich in exinitic plant residues.

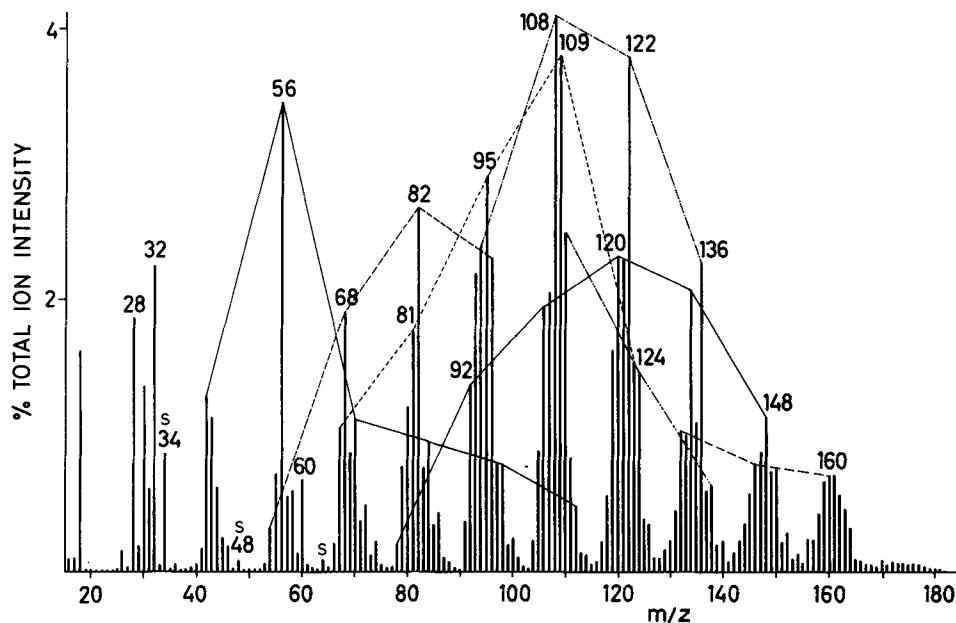
SPECTRUM F.26



SAMPLE : VITRINITE (from High Hazles Seam)
 CHEMICAL DETAILS : H/C ratio 0.80; vitrinite 97.0%; exinite 0.7%; inertinite 2.3% (see ref. 206)
 SAMPLE ORIGIN : England
 SAMPLE PREP./SIZE : suspension in methanol; 20 μ g
 PYROL. CONDITIONS : standard
 TOTAL ION COUNTS : not determined

REMARKS - Not surprisingly, this spectrum resembles that of a high volatile bituminous coal (e.g. Spectra F.19, F.20). Not only was this vitrinite prepared from a high volatile bituminous coal, but also vitrinites account for the bulk (e.g. up to 95%) of most coals.

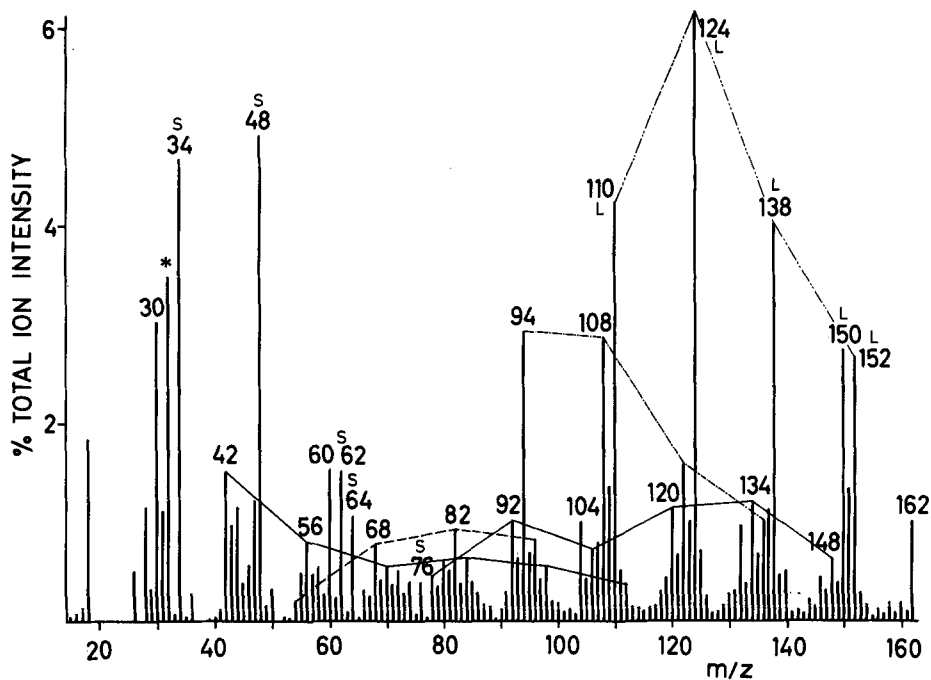
SPECTRUM F.27



SAMPLE : AMBER (resinite)
 CHEMICAL DETAILS : see ref. 207, 208
 SAMPLE ORIGIN : Baltic coast
 SAMPLE PREP./SIZE : suspension in methanol; 10 μ g
 PYROL. CONDITIONS : standard
 TOTAL ION COUNTS : 1.7×10^5

REMARKS - The original building blocks of this fossil natural resin are mainly terpenoids containing carboxylic acid, ester, aldehyde, keto and/or hydroxyl functional groups, which on fossilisation have been condensed and vinyl-polymerised. Further modifications may have been introduced by dehydration, decarboxylation and dehydrogenation. The complex Py-MS patterns of ambers (ref. 207) contain series of unsaturated hydrocarbon and aldehyde fragments. Prominent ion series at odd mass numbers (EI fragments) point to a mainly branched-aliphatic character of the pyrolysis fragments.

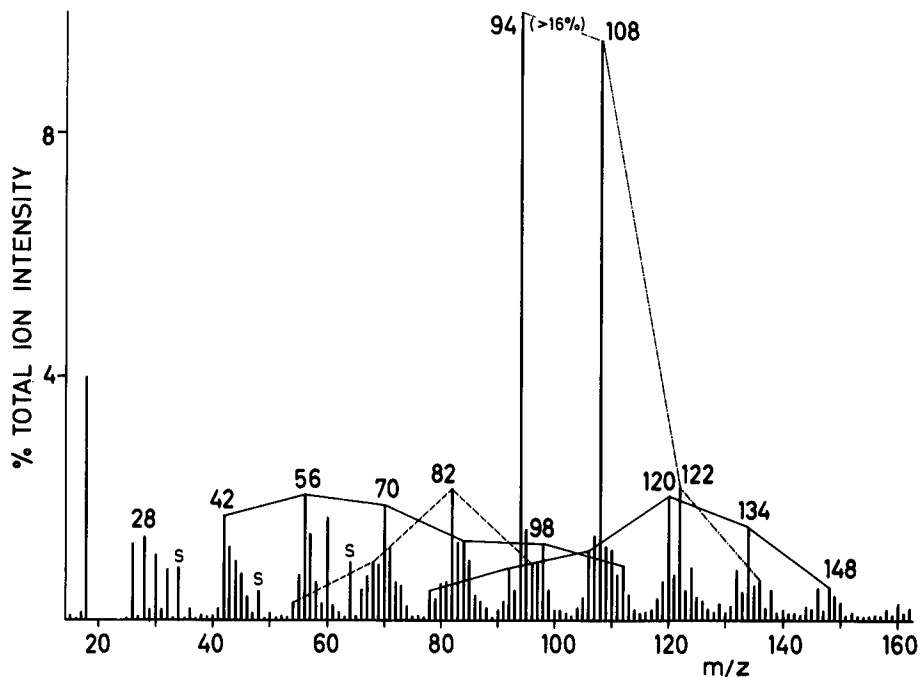
SPECTRUM F.28



SAMPLE : FOSSIL WOOD (Eocene)
 CHEMICAL DETAILS : carbonified
 SAMPLE ORIGIN : Hengelo, The Netherlands
 SAMPLE PREP./SIZE : suspension in methanol; 50 μ g
 PYROL. CONDITIONS : standard
 TOTAL ION COUNTS : 1.4×10^5

REMARKS - This pattern of carbonified wood is similar to that of many lignites (see Spectrum F.16) and is dominated by aromatic fragments obviously derived from lignin-like moieties. It differs from that of recent wood (see Spectrum E.11) by the almost complete absence of cellulose (Spectrum A.1) and hemicellulose fragments, as well as by the high sulphur-containing peaks at m/z 34, 48, 64, 76 and (possibly) 62.

SPECTRUM F.29



SAMPLE : FOSSIL CONIFER WOOD (Upper Cretaceous)
 CHEMICAL DETAILS : silicification phase: Opal CT
 SAMPLE ORIGIN : Aix-en-Provence, France; obtained from the Inst.
 Botanique et Palaeobotanique, Fac. des Sciences,
 Univ. Paris
 SAMPLE PREP./SIZE : suspension in methanol; 50 µg
 PYROL. CONDITIONS : standard
 TOTAL ION COUNTS : 2.2×10^4

REMARKS - This much older specimen of silicified wood shows a dominant (alkyl)-phenol pattern. The absence of more complex lignin-derived fragments, e.g. methoxyphenols, appears to indicate much higher degrees of chemical transformation. Also note relatively low signals for sulphur-containing ions.

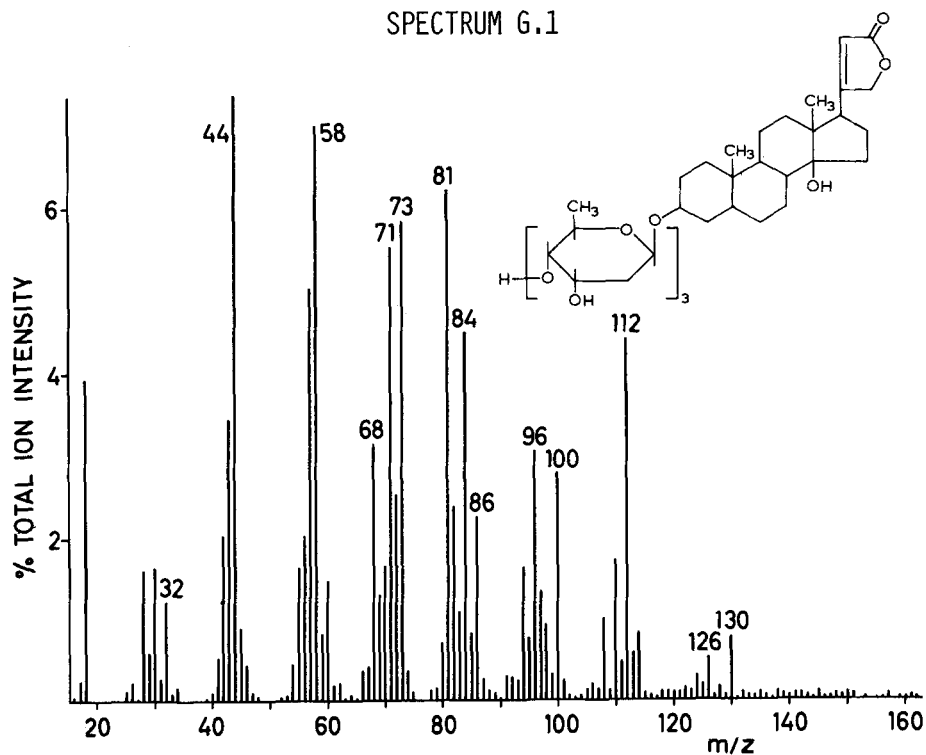
This Page Intentionally Left Blank

GROUP G

OTHER BIOCHEMICALLY IMPORTANT COMPOUNDS
(drugs, vitamins, metabolites, etc.)

This Page Intentionally Left Blank

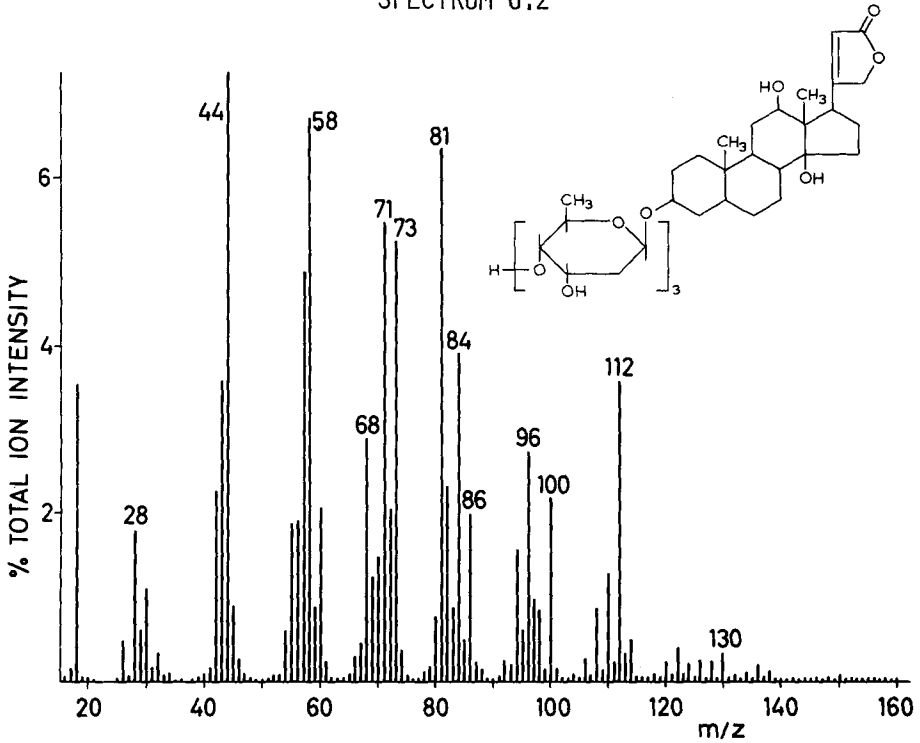
SPECTRUM G.1



SAMPLE : DIGITOXIN
 CHEMICAL DETAILS : see insert in spectrum; digitoxigenin-(digitoxose)₃;
 C₄₁H₆₄O₁₃; MW = 764
 SAMPLE ORIGIN : Serva, Heidelberg, GFR
 SAMPLE PREP./SIZE : suspension in methanol; 20 μg
 PYROL. CONDITIONS : standard
 TOTAL ION COUNTS : 1 × 10⁴

REMARKS - The spectrum is dominated by pyrolysis fragments of the sugar moieties (compare with polysaccharide patterns, Group A). The peak at m/z 130 may well represent a dideoxyhexose-minus-H₂O unit. No obvious pyrolysis products of the steroid skeleton are observed but note the high peak at m/z 44 (CO₂⁺?).

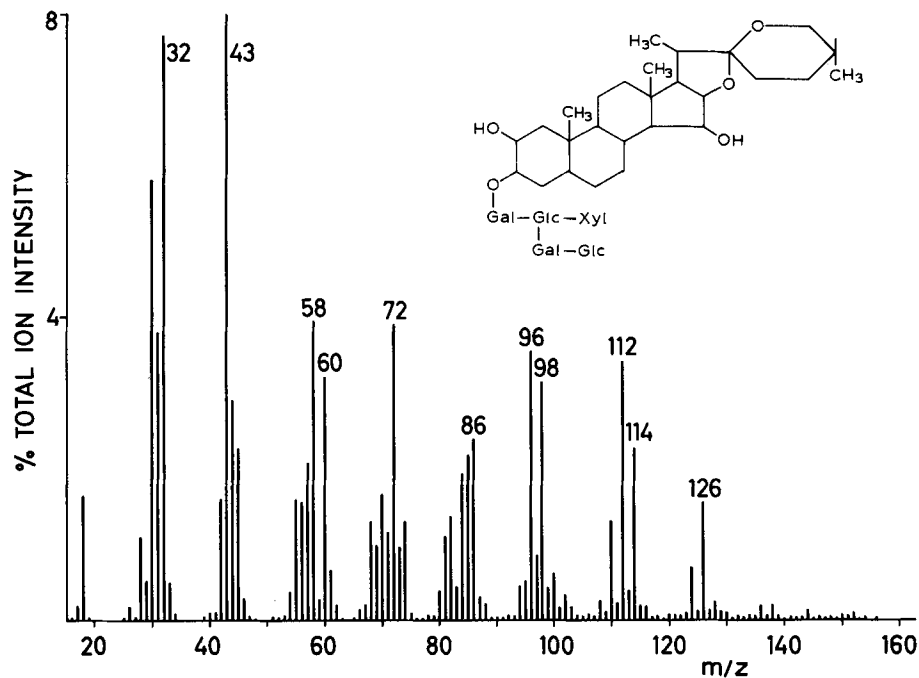
SPECTRUM G.2



SAMPLE : DIGOXIN
 CHEMICAL DETAILS : see insert in spectrum; digoxigenin-(digitoxose)₃;
 C₄₁H₆₄O₁₄; MW = 780
 SAMPLE ORIGIN : O.P.G., Utrecht, The Netherlands
 SAMPLE PREP./SIZE : suspension in methanol; 20 µg
 TOTAL ION COUNTS : 1 × 10⁴

REMARKS - Only minor quantitative differences are observed with digitoxin (Spectrum G.1), e.g. at m/z 112 and 130.

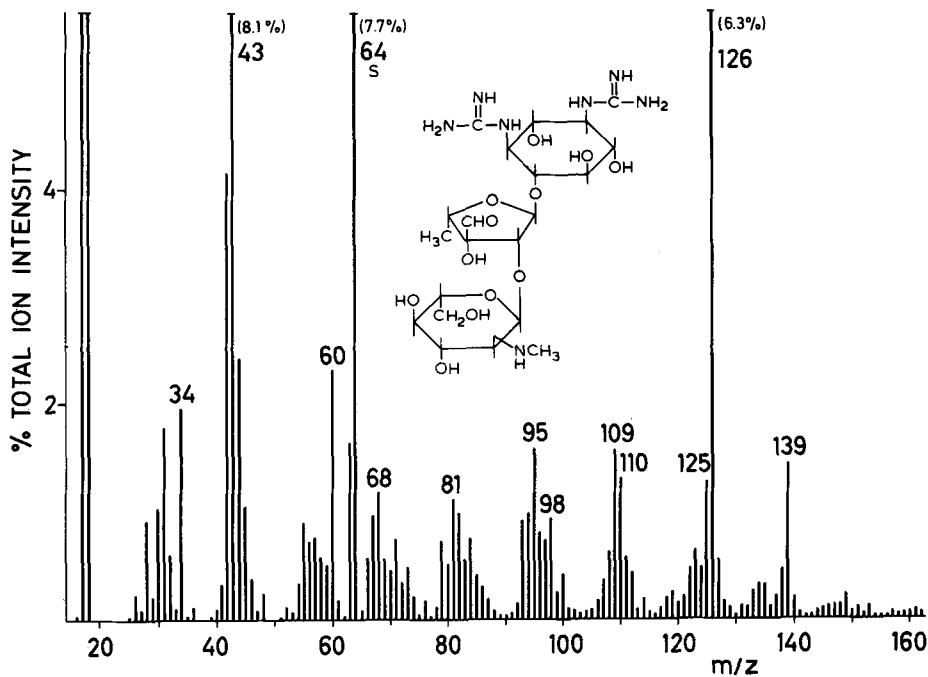
SPECTRUM G.3



SAMPLE : DIGITONIN
 CHEMICAL DETAILS : see insert in spectrum; Glc β (1 \rightarrow 3)Gal β (1 \rightarrow 2)[Xyl β -(1 \rightarrow 3)]Glc β (1 \rightarrow 4)Gal β -digitogenin; C₅₆H₉₂O₂₉; MW = 1229
 SAMPLE ORIGIN : Serva, Heidelberg, GFR
 SAMPLE PREP./SIZE : suspension in methanol; 20 μ g
 PYROL. CONDITIONS : standard
 TOTAL ION COUNTS : 2.5 \times 10⁴

REMARKS - This spectrum presents a typical hexose pattern (compare with polysaccharide patterns, Group A). No obvious pyrolysis fragments of the steroid skeleton are observed.

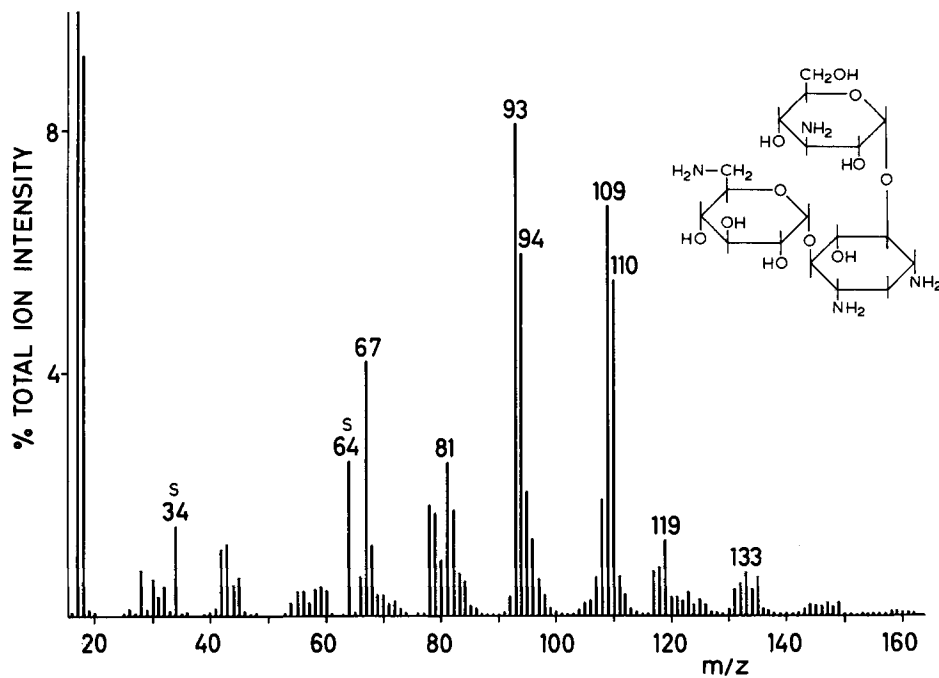
SPECTRUM G.4



SAMPLE : STREPTOMYCIN SULPHATE
 CHEMICAL DETAILS : see insert in spectrum; $C_{21}H_{39}N_7O_{12}(1.5 H_2SO_4)$; MW=728
 SAMPLE ORIGIN : Serva, Heidelberg, GFR
 SAMPLE PREP./SIZE : suspension in methanol; 20 μ g
 PYROL. CONDITIONS : standard
 TOTAL ION COUNTS : 1×10^5

REMARKS - The spectrum shows typical neutral sugar as well as aminosugar fragment series (compare with polysaccharide patterns, Group A). The high peak at m/z 64 must represent SO_2^+ derived from the sulphate group.

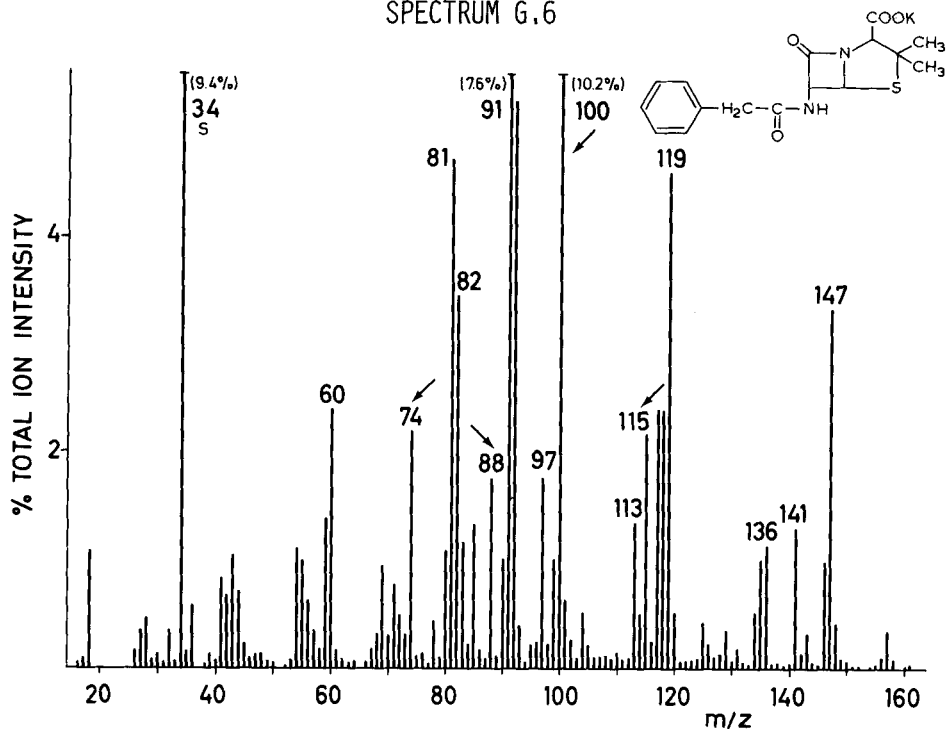
SPECTRUM G.5



SAMPLE : KANAMYCIN SULPHATE
 CHEMICAL DETAILS : see insert in spectrum; $C_{18}H_{36}N_4O_{11}(H_2SO_4)$; MW = 582
 SAMPLE ORIGIN : Serva, Heidelberg, GFR
 SAMPLE PREP./SIZE : suspension in methanol; 20 μ g
 PYROL. CONDITIONS : standard
 TOTAL ION COUNTS : 7×10^4

REMARKS - A highly characteristic spectrum with unusual peak series, obviously due to the exotic character of the sugar moieties. The peak at m/z 64 must represent SO_2^+ derived from the sulphate group. The identity of the "sugar fragments" is as yet unknown.

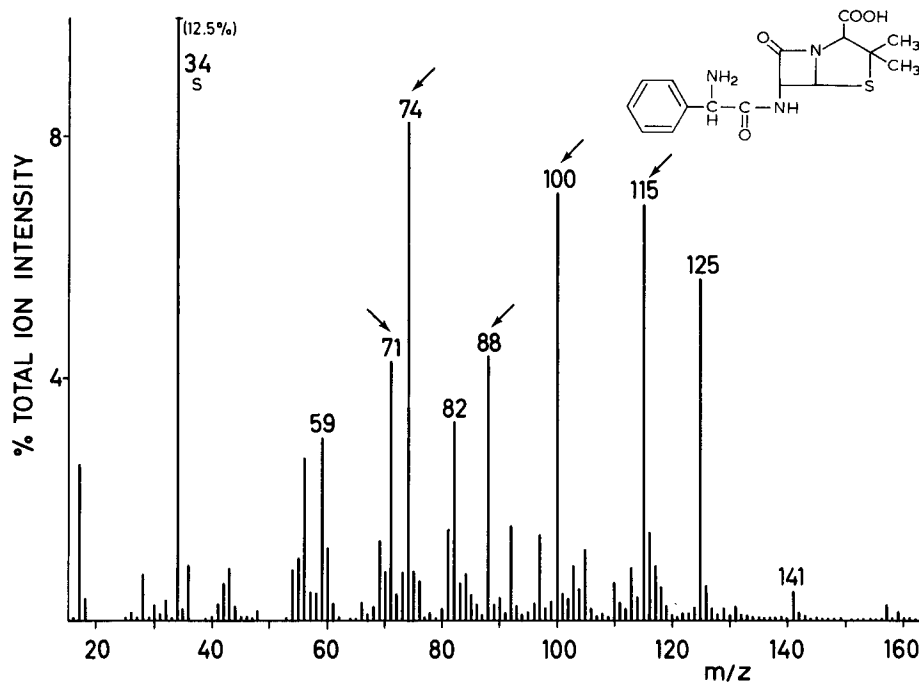
SPECTRUM G.6



SAMPLE : PENICILLIN G, K-salt (benzylpenicillin)
 CHEMICAL DETAILS : see insert in spectrum; $C_{16}H_{17}N_2O_4S(K)$; MW = 372
 SAMPLE ORIGIN : Serva, Heidelberg, GFR
 SAMPLE PREP./SIZE : suspension in methanol; 20 μ g
 PYROL. CONDITIONS : standard
 TOTAL ION COUNTS : 5×10^5

REMARKS - Considering the relatively small size of this molecule, the spectrum is unusually complex indicating the occurrence of complicated fragmentation pathways. With the exception of the H_2S^{+} ion at m/z 34 the identity and origin of most of the peaks is as yet unknown. Nevertheless the marked peak series at m/z 34, 71, 74, 88, 100 and 115 is highly characteristic for all penicillins thus far analysed.

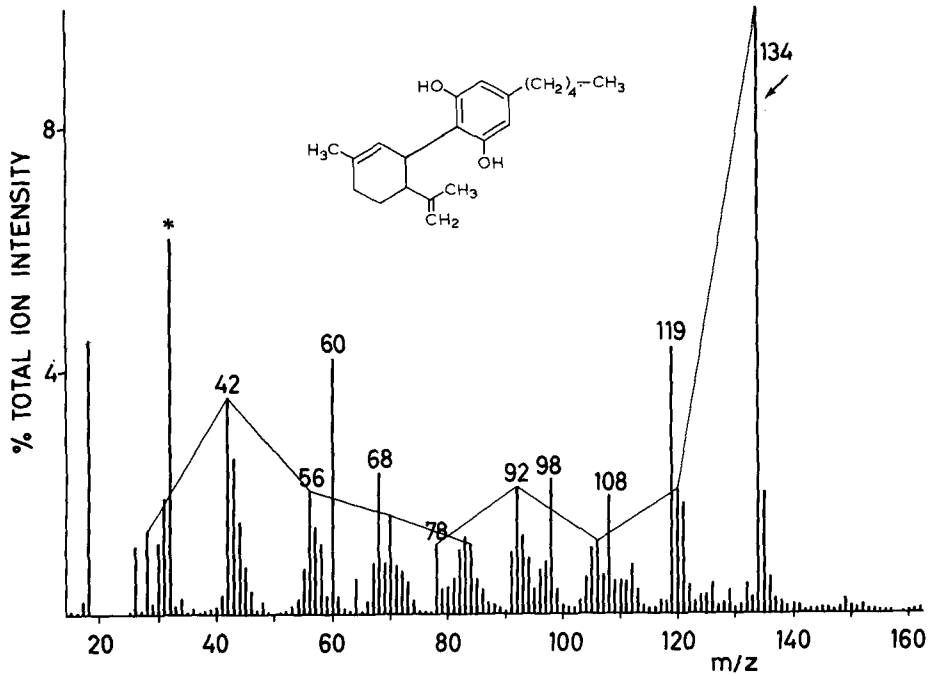
SPECTRUM G.7



SAMPLE : AMPICILLIN
 CHEMICAL DETAILS : see insert in spectrum; 6-[D- α -aminophenylacetamido]-penicillanic acid; $C_{16}H_{19}N_3O_4S(3H_2O)$; MW = 403
 SAMPLE ORIGIN : Serva, Heidelberg, GFR
 SAMPLE PREP./SIZE : suspension in methanol; 20 μ g
 PYROL. CONDITIONS : standard
 TOTAL ION COUNTS : 1.6×10^5

REMARKS - Compared to the spectrum of benzylpenicillin the characteristic penicillin peaks at m/z 100 and 115 are much more pronounced whereas no significant peaks at 147, 136, 119, 97, 91 and 81 are observed indicating a rather different pyrolysis mechanism. The strong peak at m/z 125 may well be characteristic for ampicillin.

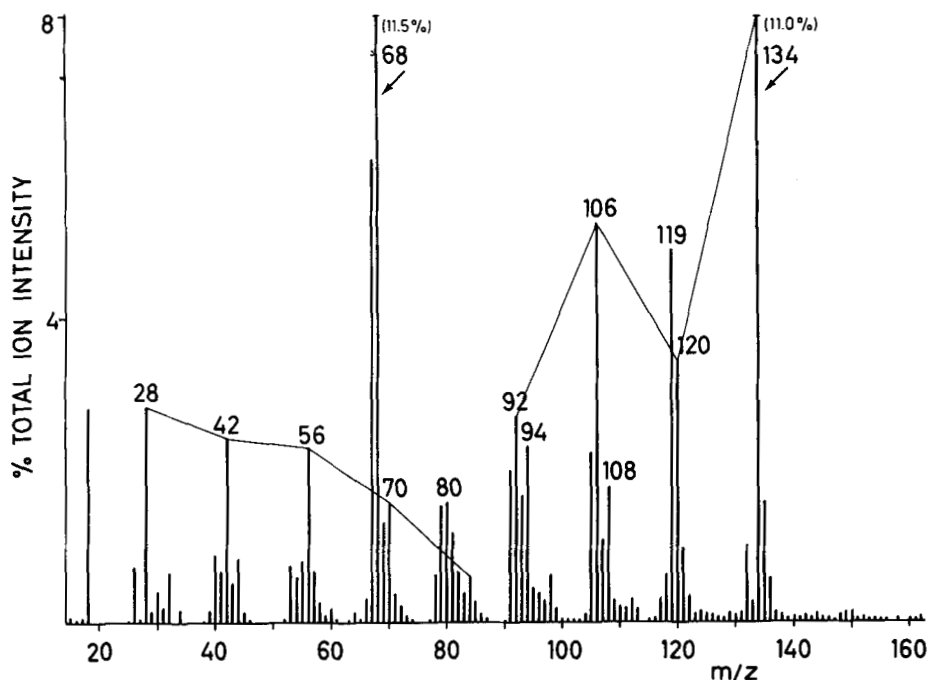
SPECTRUM G.8



SAMPLE : CANNABIDIOL
 CHEMICAL DETAILS : see insert in spectrum; $C_{21}H_{30}O_2$; MW = 314
 SAMPLE ORIGIN : UNO, Narcotics, Vienna
 SAMPLE PREP./SIZE : solution in methanol; 20 μ g
 PYROL. CONDITIONS : standard
 TOTAL ION COUNTS : 2×10^4

REMARKS - The strong peak at m/z 134 is thought to represent the eliminated cyclohexadienyl moiety ($C_{10}H_{14}^{+}$). Note the presence of the alkene series (m/z 28, 42, etc.). No obvious fragments of the pentyl-dihydroxybenzene moiety are observed in this mass range. For pyrolysis products of cannabidiol see ref. 209.

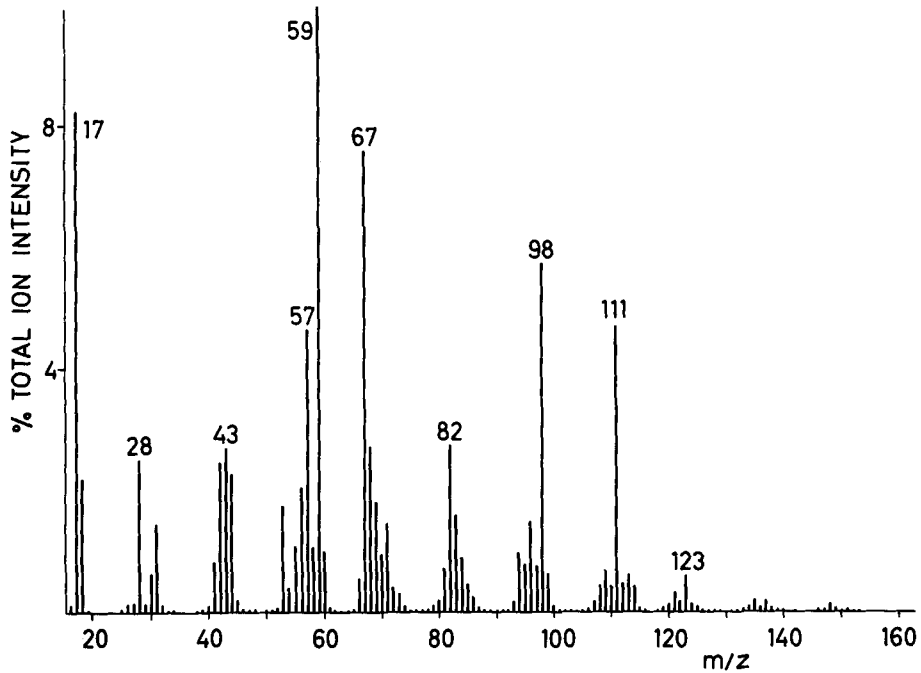
SPECTRUM G.8A



SAMPLE : CANNABIDIOL
 CHEMICAL DETAILS : $C_{21}H_{30}O_2$; MW = 314
 SAMPLE ORIGIN : UNO, Narcotics, Vienna
 SAMPLE PREP./SIZE : solution in methanol; 10 μ g
 PYROL. CONDITIONS : ferromagnetic tube; $T_{eq}=770^\circ C$
 TOTAL ION COUNTS : 2×10^5

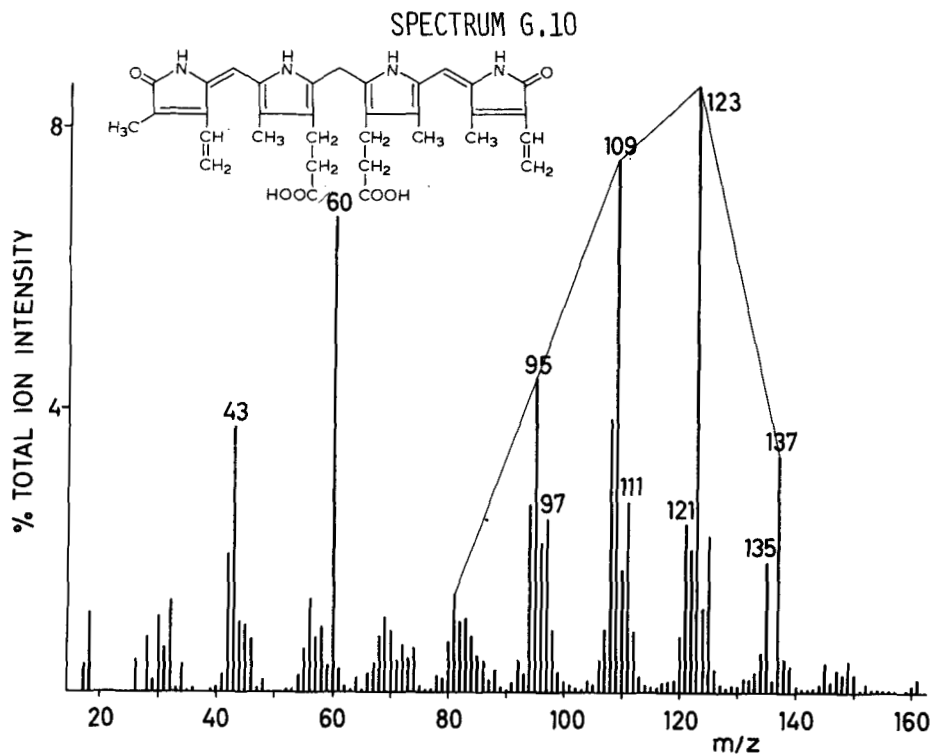
REMARKS - In comparison with the filament pyrolysis pattern (Spectrum G.8) this spectrum is dominated by a peak at m/z 68, possibly representing $C_5H_8^+$ and a stronger aromatic hydrocarbon series at m/z 92, 106 and 120. In addition, phenolic peaks at m/z 94 and 108 may represent pyrolysis fragments of the C_5 -alkyldihydroxybenzene moiety. The peak at m/z 134 is again thought to be the $C_{10}H_{14}^+$ (cyclohexadienyl) moiety.

SPECTRUM G.9



SAMPLE : CYANOCOBALAMIN (vitamin B₁₂)
 CHEMICAL DETAILS : C₆₃H₈₈CoN₁₄O₁₄P; MW = 1355
 SAMPLE ORIGIN : Merck AG, Darmstadt, GFR
 SAMPLE PREP./SIZE : suspension in methanol; 20 µg
 PYROL. CONDITIONS : standard
 TOTAL ION COUNTS : 5 × 10⁴

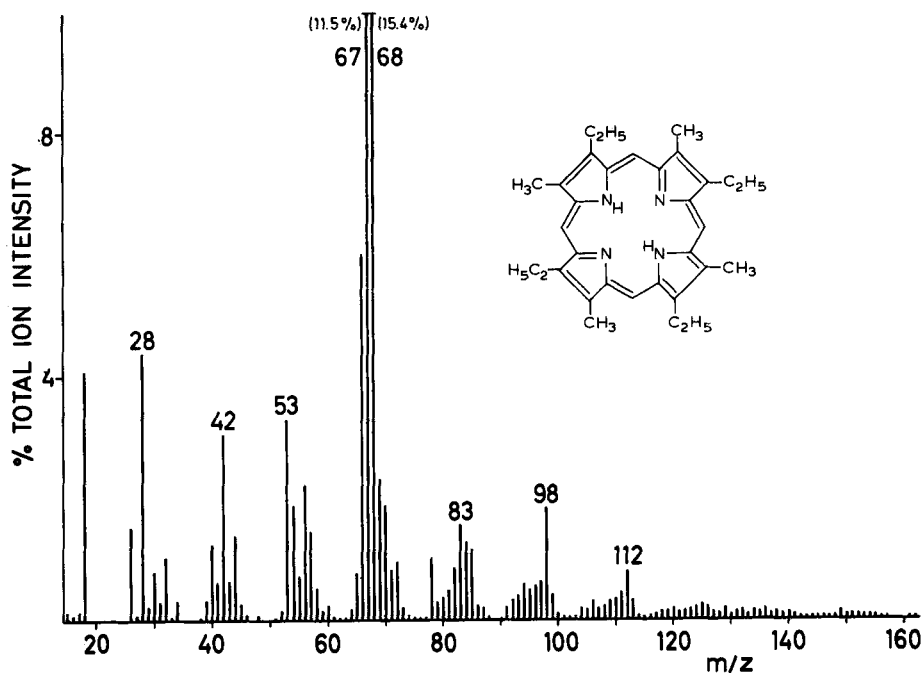
REMARKS - The amide substituents of the heterocyclic ring system may give rise to the formation of acetamide (m/z 59). The peak at m/z 67 probably represents pyrrole whereas the peak at m/z 98 may be derived from the ribofuranoside moiety. Note the high NH₃⁺ peak at m/z 17.



SAMPLE : BILIRUBIN
 CHEMICAL DETAILS : see insert in spectrum; $C_{33}H_{36}N_4O_6$; MW = 584
 SAMPLE ORIGIN : Serva, Heidelberg, GFR
 SAMPLE PREP./SIZE : suspension in methanol; 20 μ g
 PYROL. CONDITIONS : standard
 TOTAL ION COUNTS : 6×10^4

REMARKS - The dominant series of molecular ions at m/z 95, 109, 123 and 137 apparently represents alkylypyroles and related hetero-compounds. In addition the marked peak at m/z 60 probably represents acetic acid derived from the carboxyethyl groups.

SPECTRUM G.11



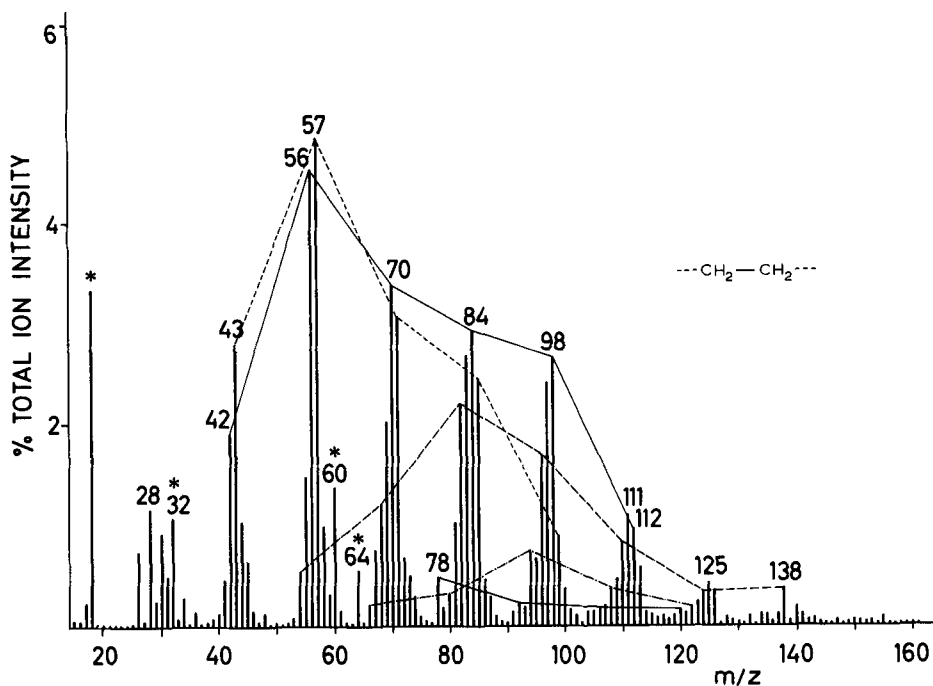
SAMPLE : ETIOPORPHYRIN I
 CHEMICAL DETAILS : see insert in spectrum; $C_{32}H_{38}N_4$; MW = 478
 SAMPLE ORIGIN : Phillips Petroleum Co., Bartlesville, OK, USA.
 SAMPLE PREP./SIZE : suspension in methanol; 10 μ g
 PYROL. CONDITIONS : ferromagnetic tube; T_{eq} 770°C
 TOTAL ION COUNTS : 1.3×10^5

REMARKS - The intense peak group at m/z 67, 68 is thought to represent C_5 -alkynes derived from the alkyl-substituted rings. This unusual pyrolysis mechanism may well be unique for this type of compound.

GROUP H
POLYMERS OF NON-BIOLOGICAL ORIGIN
(plastics, resins, etc.)

This Page Intentionally Left Blank

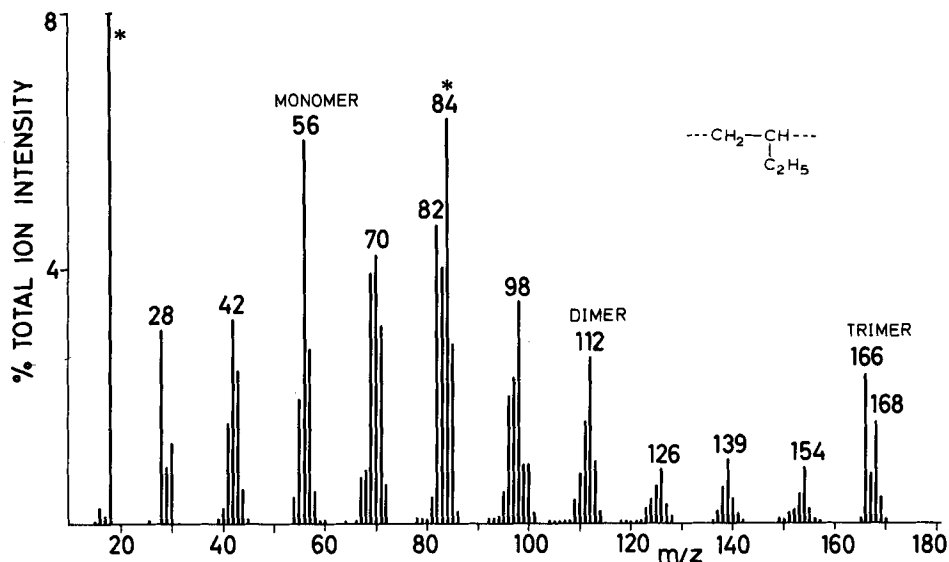
SPECTRUM H.1



SAMPLE : POLYETHYLENE (longitudinal fibrillar crystalline)
 CHEMICAL DETAILS : see insert in spectrum
 SAMPLE ORIGIN : gift from Dr. A.J. Pennings, Lab. for Polymer Chemistry,
 Univ. of Groningen, The Netherlands
 SAMPLE PREP./SIZE : suspension in methanol; 10 μg
 PYROL. CONDITIONS : standard
 TOTAL ION COUNTS : 4×10^4

REMARKS - The spectrum shows the absence of marked monomer and oligmer peaks due to a dominance of thermal degradation rather than depolymerisation reactions. Note the presence of homologous ion series representing increasingly unsaturated aliphatic hydrocarbons and even some degree of aromatisation (m/z 78!). Dotted lines connect alkane fragment ion series at m/z 43, 57, 71, 85, etc.. Heteroatom-containing ions at m/z 18 ($\text{H}_2\text{O}^{+\cdot}$), 32 ($\text{CH}_3\text{OH}^{+\cdot}$), 60 ($\text{C}_2\text{H}_4\text{O}_2^{+\cdot}$) and 64 ($\text{SO}_2^{+\cdot}$) must represent sample contaminants.

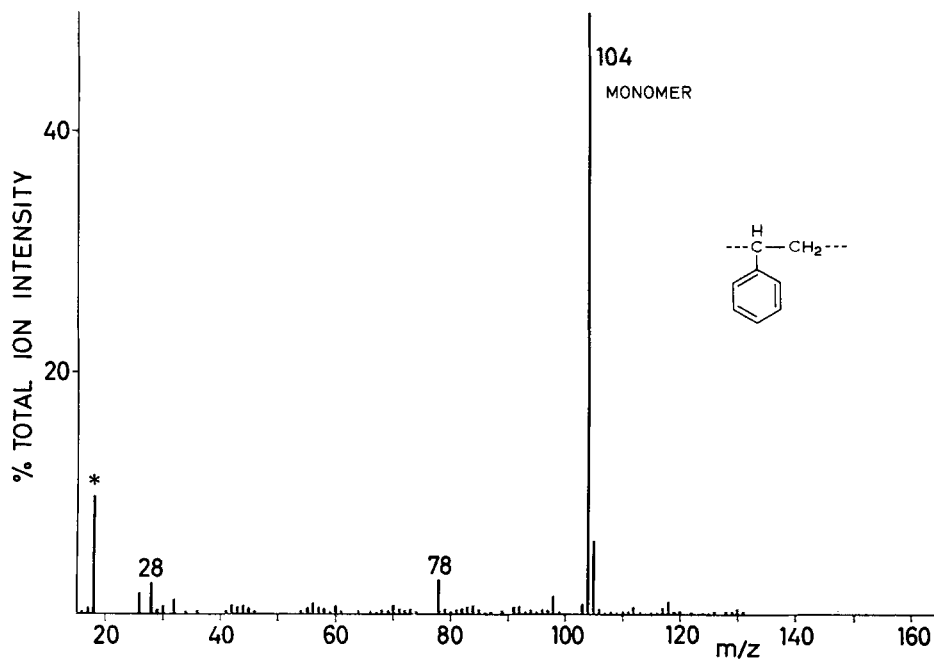
SPECTRUM H.2



SAMPLE : POLYBUTENE (isotactic)
 CHEMICAL DETAILS : see insert in spectrum; low molecular weight; density 0.91
 SAMPLE ORIGIN : Scientific Polymer Products; USA
 SAMPLE PREP./SIZE : solution in cyclohexane; 10 μg
 PYROL. CONDITIONS : T_{eq} 610°C; t_{I} 5s; t_{E} 10s; E_{e1} 12eV; (Extranuclear 5000-1 Py-MS system)
 TOTAL ION COUNTS : 1×10^5

REMARKS - In comparison with polyethylene (Spectrum H.1), polybutene shows a combination of thermal degradation and depolymerisation reactions. The thermal degradation reactions result in the formation of prominent alkene and alkadiene series. The depolymerisation reactions appear to proceed via unzipping, leading to the monomer peak at m/z 56, as well as via a backbiting mechanism, resulting in the marked trimer peak complex at m/z 166/168 (it should be interesting to study to what extent backbiting occurs in atactic and/or syndiotactic polybutene). Whether the peak at m/z 168 represents a linear or cyclic trimer is unknown, although the latter configuration would seem to be the most probable. The peak at m/z 166 must represent a dehydrogenated trimer, whereas the peak at m/z 139 is probably an electron impact fragment (M-29) of the trimer.

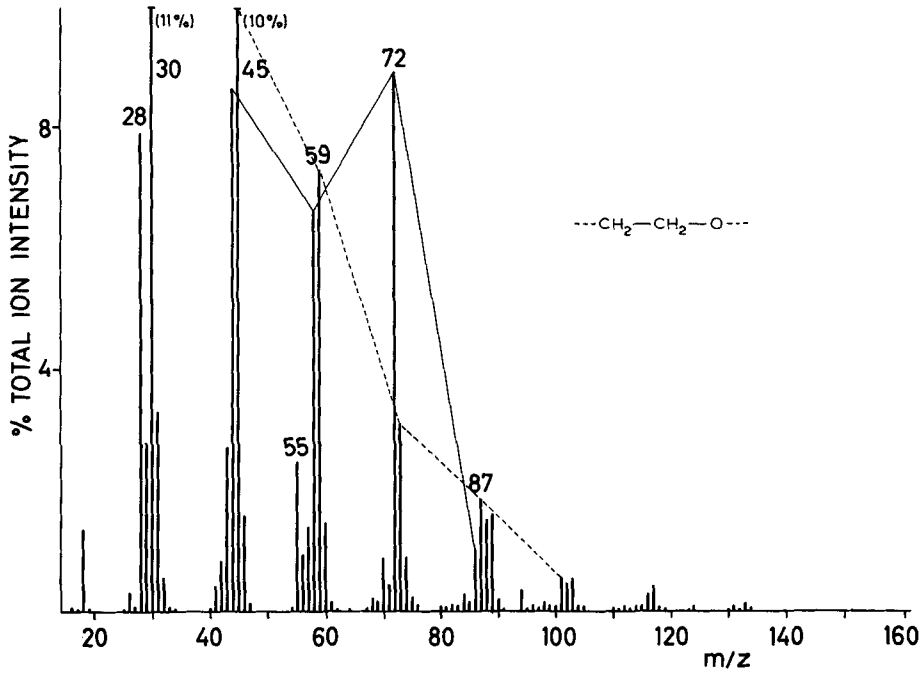
SPECTRUM H.3



SAMPLE : POLYSTYRENE
 CHEMICAL DETAILS : see insert in spectrum; MW = 270,000
 SAMPLE ORIGIN : Natl. Bureau of Standards (SRM 706), Washington, USA
 SAMPLE PREP./SIZE : solution in acetone; 2 μ g
 PYROL. CONDITIONS : standard
 TOTAL ION COUNTS : 3×10^4

REMARKS - This simple spectrum shows a dominant styrene monomer peak at m/z 104 as well as relatively minor benzene (m/z 78) and phenylpropene (m/z 118) peaks. A dimer peak appearing at m/z 208 is outside the mass range shown here.

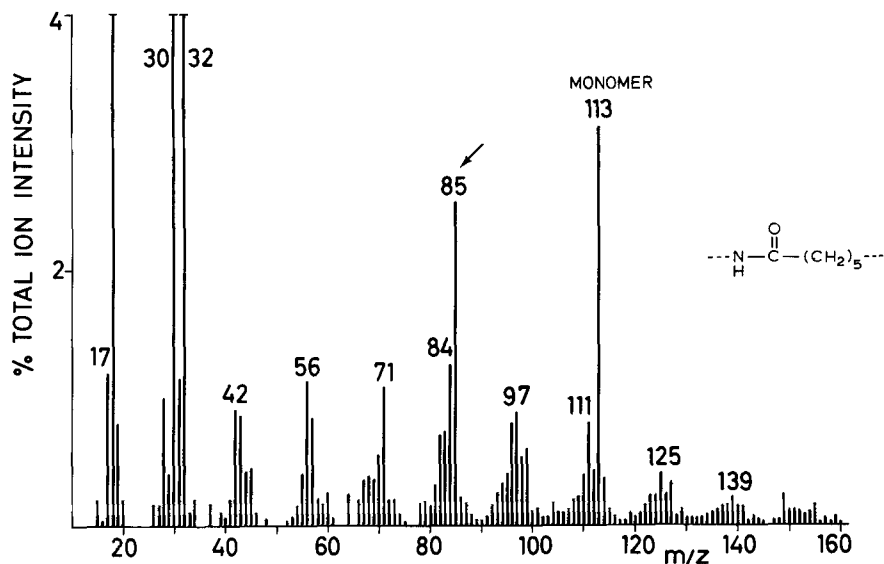
SPECTRUM H.4



SAMPLE : POLYETHYLENEGLYCOL (Carbowax 20M)
 CHEMICAL DETAILS : see insert in spectrum
 SAMPLE ORIGIN : Becker, Delft, The Netherlands
 SAMPLE PREP./SIZE : suspension in methanol; 10 μg
 PYROL. CONDITIONS : standard
 TOTAL ION COUNTS : 2.3×10^5

REMARKS - The pyrolysis mass spectrum of Carbowax 20M shows a relatively complex pattern due to thermal degradation mechanisms and EI fragmentation processes. The strong contribution of the latter results from the fact that the aliphatic CHO-fragments produced in the thermal degradation process apparently fail to produce stable molecular ions at 14eV electron energy, thus leading to intense fragment ion series (e.g. at m/z 45, 59, 73, 87, 101). The peak at m/z 44 may be thought to represent the basic repeating subunit $\text{C}_2\text{H}_4\text{O}$ (ethyleneglycol minus H_2O).

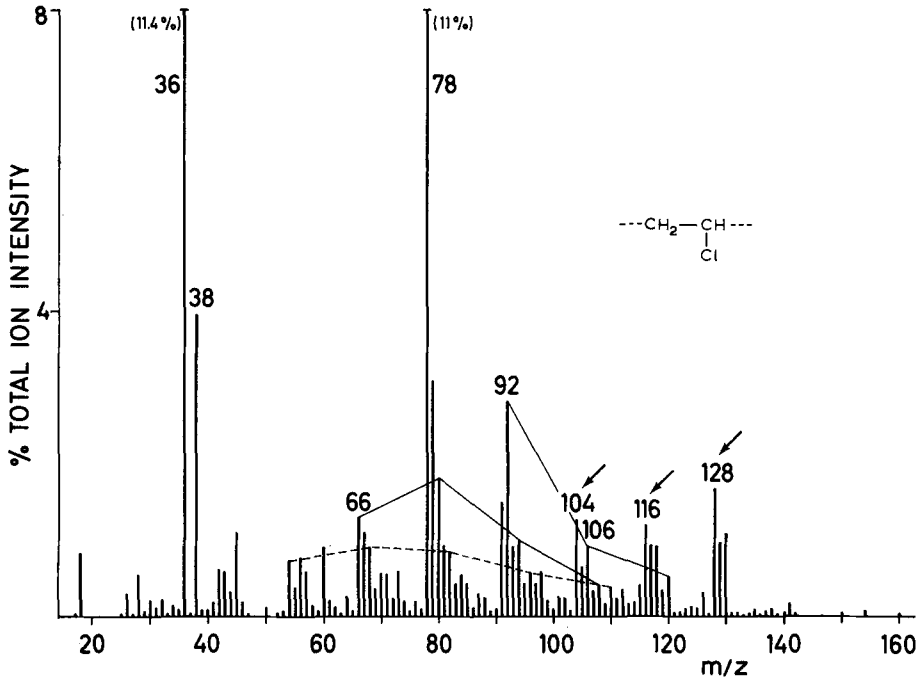
SPECTRUM H.5



SAMPLE : POLYCAPROLACTAM (Nylon 6)
 CHEMICAL DETAILS : see insert in spectrum
 SAMPLE ORIGIN : Scientific Polymer Products, USA
 SAMPLE PREP./SIZE : suspension in methanol; 10 μ g
 PYROL. CONDITIONS : T_{eq} 610°C, t_T 5s, t_Σ 10s, E_{el} 12eV, (Extranuclear 5000-1 Py-MS system)
 TOTAL ION COUNTS : 5×10^4

REMARKS - The marked monomer peak at m/z 113 points to a dominant unzipping mechanism although thermal degradation reactions are also evident, e.g. from peaks at m/z 17 (NH_3^+), 30 (CH_2O^+) and the small alkene series at m/z 42, 56, etc. The large peak at m/z 85 probably represents CO elimination from the monomer by electron impact or pyrolysis mechanisms. Although the mass spectrum was scanned up to m/z 240 no obvious dimer peak or other large fragments were observed.

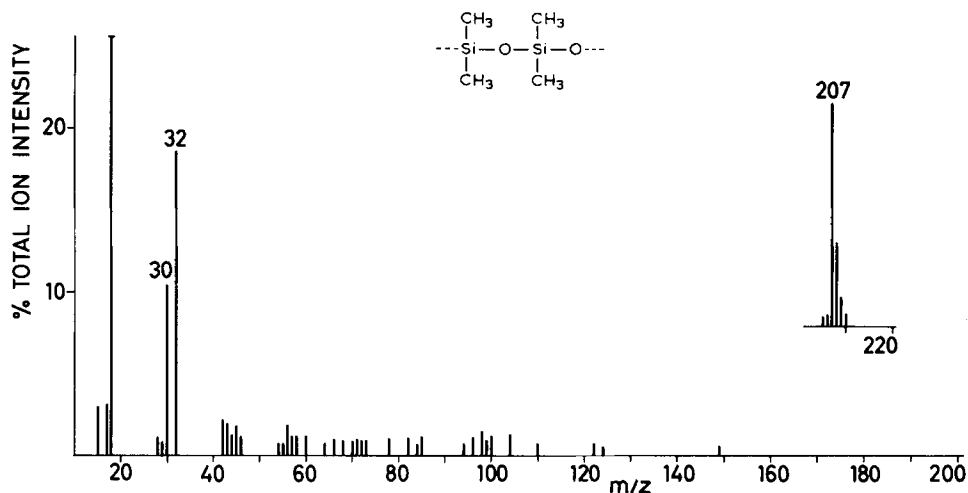
SPECTRUM H.6



SAMPLE : POLYVINYLCHLORIDE
 CHEMICAL DETAILS : see insert in spectrum
 SAMPLE ORIGIN : Solvic 239, Solvay, France
 SAMPLE PREP./SIZE : suspension in methanol; 10 μg
 PYROL. CONDITIONS : standard
 TOTAL ION COUNTS : 1.7×10^5

REMARKS - This spectrum shows dominant molecular ions for HCl (m/z 36 and 38) and benzene (m/z 78). Other aromatic and/or unsaturated hydrocarbon products are observed as relatively low signals at m/z 54, 68, etc., m/z 66, 80, etc. and m/z 92, 106, 120. The peaks at m/z 104, 116 and 128 probably represent C_8H_8 (styrene), C_9H_8 (indene) and C_{10}H_8 (naphthalene). Note the absence of an obvious vinylchloride monomer signal at m/z 62.

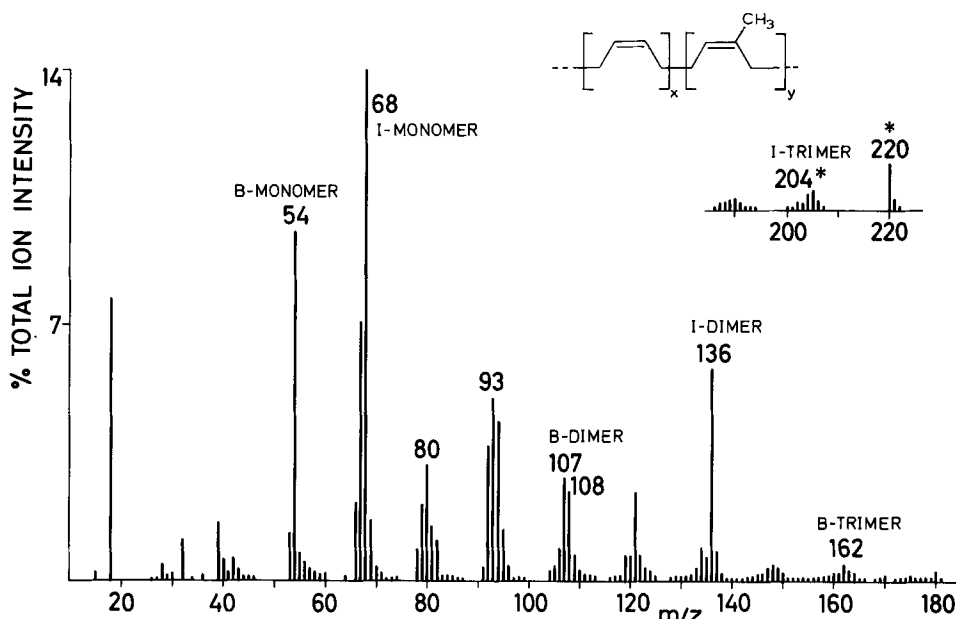
SPECTRUM H.7



SAMPLE : POLYDIMETHYLSILICONE (OV-1)
 CHEMICAL DETAILS : see insert in spectrum
 SAMPLE ORIGIN : Supelco, USA
 SAMPLE PREP./SIZE : solution in toluene; 10 μ g
 PYROL. CONDITIONS : T_{eq} 510°C; t_{r} 5s; t_{d} 10s; E_{el} 12eV; expansion chamber removed (Extranuclear 5000-1 Py-MS system)
 TOTAL ION COUNTS : 2×10^3

REMARKS - The low ion intensity may be caused by condensation losses of large fragments on the reaction chamber wall, by incomplete pyrolysis, by lower ion transmission in the high mass range or by a combination of these factors. The large peak at m/z 207 must represent the (M-15) electron impact fragment of the trimer although no trimer parent ion is observed at m/z 222. This is due to the presence of six methyl groups in the trimer, each of which has a significant chance of being lost in the electron impact ionisation process in spite of the low electron energy. Note the unusual isotope peak distribution around m/z 207, due to the presence of three Si atoms. The absence of obvious monomer or dimer peaks as well as of thermal degradation products indicates a strong dominance of backbiting mechanisms. A peak occurring at m/z 281 (not shown) points at the occurrence of tetramer formation.

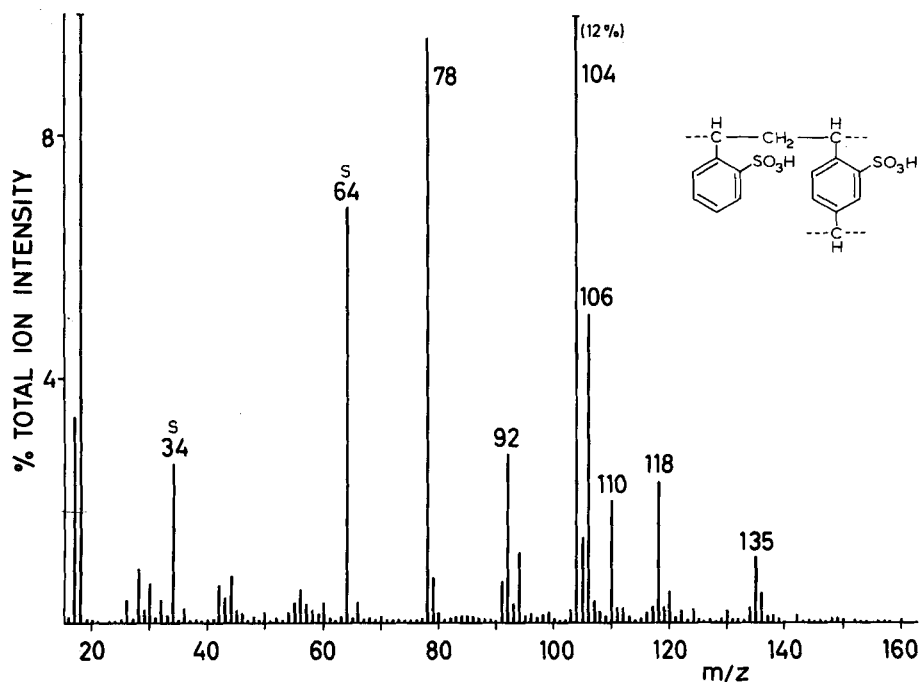
SPECTRUM H.8



SAMPLE : POLYISOPRENE/POLY(*cis*)BUTADIENE (50/50 copolymer)
 CHEMICAL DETAILS : see insert in spectrum (X and Y represent integers, the values of which may change throughout the polymer matrix)
 SAMPLE ORIGIN : B.F. Goodrich, USA
 SAMPLE PREP./SIZE : solution in tetrahydrofuran; 10 μ g
 PYROL. CONDITIONS : T_{eq} 510°C; t_T 5s; t_{Σ} 10s; E_e 12eV; expansion chamber removed (Extranuclear 5000-1 Py-MS system)
 TOTAL ION COUNTS : 5×10^4

REMARKS - The dominant pyrolysis mechanism appears to be depolymerisation resulting in the formation of large monomer, medium-sized dimer and small trimer peaks. Many of the other signals including all odd-numbered mass peaks, appear to be due to residual electron impact fragmentation (mainly loss of 15 daltons from the monomer and oligomer ions). In addition, some peaks may be due to thermal degradation reactions. The conspicuous peaks at m/z 220 and m/z 205 represent the molecular ion and (M-15) fragment ion of dibutylhydroxytoluene, a common stabilizer in tetrahydrofuran solvents. Note the relatively low abundance of mixed oligomer signals (e.g. the lack of a marked butadiene-isoprene dimer at m/z 122) indicating a block co-polymer structure.

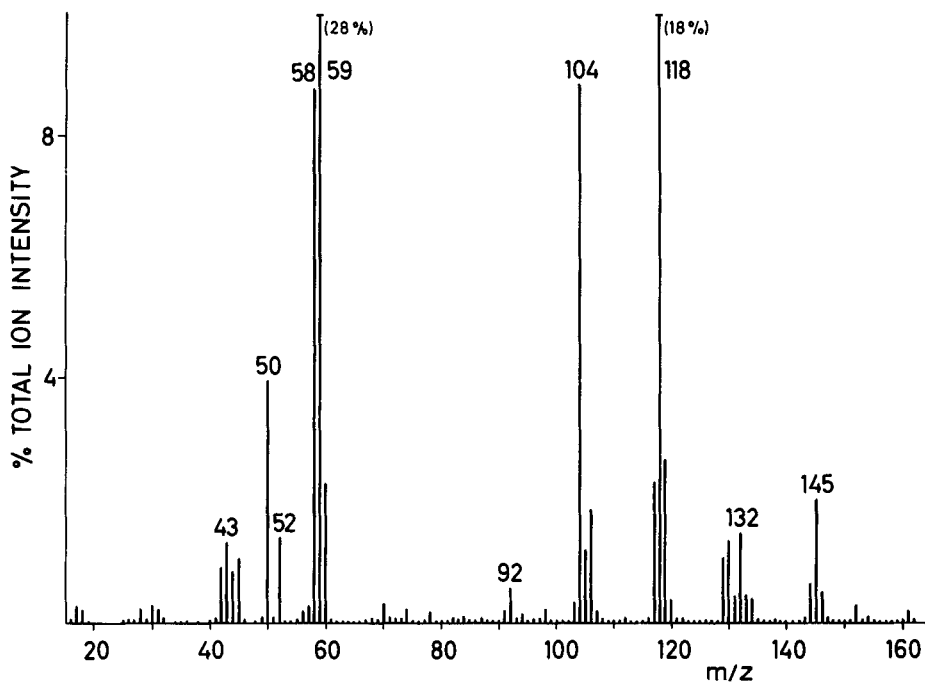
SPECTRUM H.9



SAMPLE : DOWEX 50 WX8, H⁺ (cation-exchange resin)
 CHEMICAL DETAILS : see insert in spectrum; styrene-divinylbenzene copolymer with sulphonic acid functional groups
 SAMPLE ORIGIN : Fluka AG, Buchs, Switzerland
 SAMPLE PREP./SIZE : suspension in water; 10 µg
 PYROL. CONDITIONS : standard
 TOTAL ION COUNTS : 2 x 10⁴

REMARKS - Compare with the spectra of other styrene-type polymers (Spectrum H.3, H.10, H.11). A styrene monomer peak shows up at m/z 104 but no clear divinylbenzene monomer (MW 130) is seen. The peaks at m/z 78, 92 and 118 must represent benzene, toluene and phenylpropene. The high peak at m/z 64 (SO₂⁺) is directly derived from the sulphonic acid substituents. The presence of a H₂S⁺ peak at m/z 34 and a probable thiobenzene peak at m/z 110 appear to indicate the influence of reductive processes on the sulphonic acid groups, either in the original polymer or during the pyrolysis process.

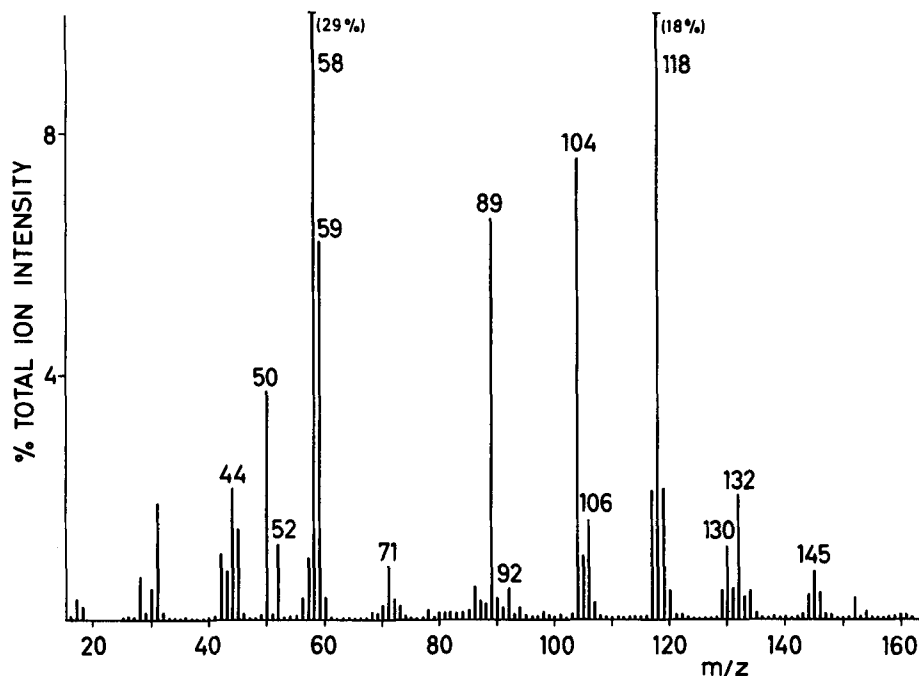
SPECTRUM H.10



SAMPLE : DOWEX 1X2, Cl⁻ (anion-exchange resin)
 CHEMICAL DETAILS : crosslinked styrene-type polymer with Phe-CH₂-N(Me)₃⁺Cl⁻ functional groups
 SAMPLE ORIGIN : Fluka AG, Buchs, Switzerland
 SAMPLE PREP./SIZE : suspension in water; 10 μg
 PYROL. CONDITIONS : standard
 TOTAL ION COUNTS : 1.7 × 10⁵

REMARKS - Compare with spectra of other styrene-type polymers (Spectra H.3, H.9, H.11). The polymer backbone is represented by the peaks at m/z 92, 104, 106, 118 (130) and 132 (alkylbenzenes). The peaks at m/z 50, 52 (CH₃Cl⁺), 58 (Me₂N=CH₂⁺) and 59 (Me₃N⁺) are derived from the alkylamine functional groups.

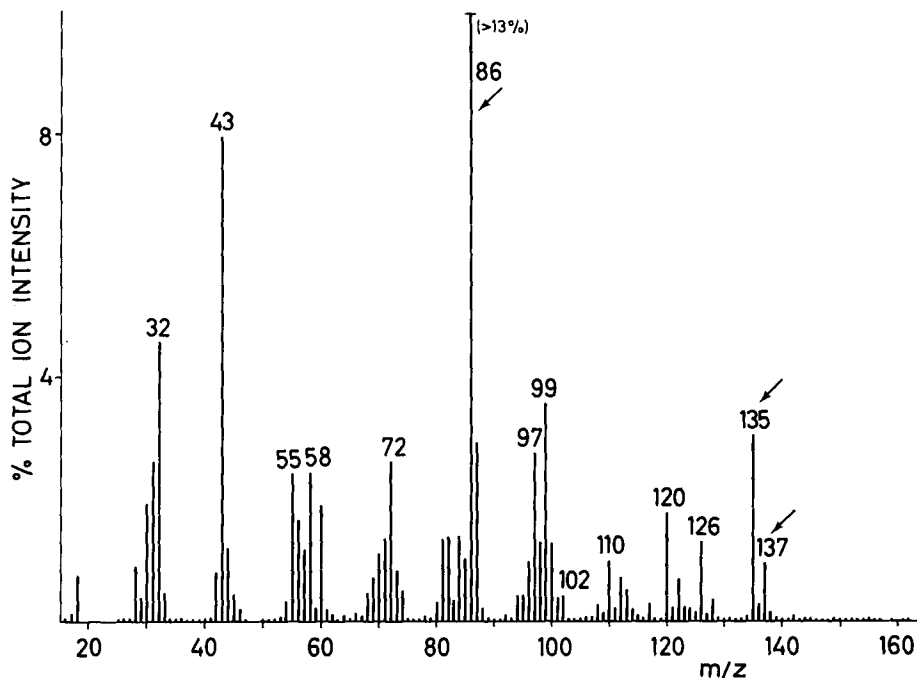
SPECTRUM H.11



SAMPLE : DOWEX 2X8, Cl⁻ (anion-exchange resin)
 CHEMICAL DETAILS : crosslinked styrene-type polymer with
 Phe-CH₂-N(Me₂,C₂H₄OH)⁺Cl⁻ functional groups
 SAMPLE ORIGIN : Fluka AG, Buchs, Switzerland
 SAMPLE PREP./SIZE : suspension in water; 10 μg
 PYROL. CONDITIONS : standard
 TOTAL ION COUNTS : 1.7 X 10⁵

REMARKS - Compare with spectra of other styrene-type polymers (Spectra H.3, H.9, H.10). The polymer backbone is represented by the peaks at m/z 92, 104, 106, 118 (130) and 132 (alkylbenzenes). The peaks at m/z 50, 52 (CH₃Cl⁺), 58 (Me₂N=CH₂⁺), 59 (Me₃N⁺), 71 (N,N-dimethylvinylamine) and 89 (N,N-dimethylamino-ethanol) are derived from the amino functional groups.

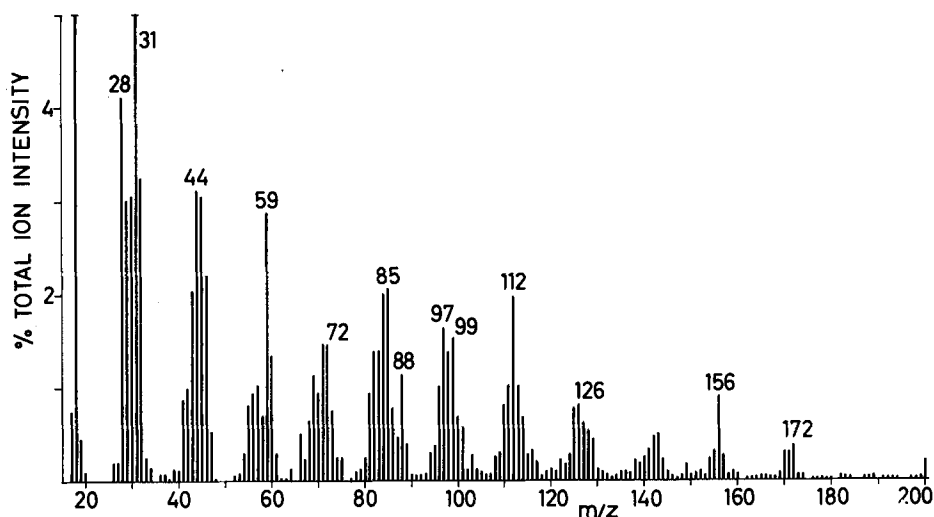
SPECTRUM H.12



SAMPLE : DIETHYLAMINOETHYL-DEXTRAN
 CHEMICAL DETAILS : glucan with ether-linked $-O-CH_2-CH_2-NH(C_2H_5)_2^+Cl^-$ groups;
 MW = 2×10^6
 SAMPLE ORIGIN : Pharmacia, Sweden
 SAMPLE PREP./SIZE : solution in H_2O ; 10 μg
 PYROL. CONDITIONS : standard
 TOTAL ION COUNTS : 1.5×10^5

REMARKS - The spectrum shows a carbohydrate fragment pattern of the dextran backbone (e.g. m/z 32, 43, 55, 58, 60, 72, 102, 110, 126) somewhat overshadowed by ion signals derived from the diethylaminoethyl units. The main molecular ions representing the latter group appear at m/z 135 and 137 and presumably represent a $(C_2H_5)_2NC_2H_4Cl$ organochlorine compound formed during the pyrolysis process. For a discussion of other organochlorine products formed by pyrolysis of quaternary ammonium compounds in the presence of Cl^- ions see Spectra D.10, D.11 and Part I, Section 3.5. The intense ion signals at m/z 86, 99, 120 appear to represent electron impact fragments of the molecular ion at m/z 135, formed by the loss of 15 (CH_3), 36 (HCl) and 49 (CH_2Cl) daltons, respectively. The high intensity fragment at m/z 86 has proven to be a useful marker for detecting small quantities of DEAE-dextrans in biological samples, e.g. virus preparations (ref. 63).

SPECTRUM H.13



SAMPLE : ETHYLCELLULOSE
 CHEMICAL DETAILS : ethoxyl content 49%
 SAMPLE ORIGIN : Scientific Polymer Products, USA
 SAMPLE PREP./SIZE : suspension in methanol; 10 μ g
 PYROL. CONDITIONS : T_{eq} 510°C; t_T 5s; t_D 10s; E_{e1} 12eV; expansion chamber removed (Extranuclear 5000-1 Py-MS system)
 TOTAL ION COUNTS : 1×10^5

REMARKS - At first sight this spectrum appears to be quite different from that of cellulose (Spectrum A.1) because of the dominance of odd numbered mass peaks and the prominent signals in the high mass range. Obviously many pyrolysis products now possess an ethoxyl group instead of a hydroxyl group. Also, the presence of the ethoxyl groups significantly reduces the otherwise dominant dehydration reactions. Therefore, the peaks at m/z 172 and 200 can be rationalised as the mono-ethylated and diethylated analogues of anhydrolevoglucosan (normally at m/z 144) respectively, whereas the peaks at m/z 143 and 171 may then represent the (M-29) fragments. Interestingly, ethylation (gain of 28 daltons) followed by the loss of an ethyl radical (29 daltons) results in the net loss of 1 dalton. Thus, some of the major odd mass peaks may well correspond to the next higher mass peak in the normal cellulose spectrum, e.g. m/z 31 vs. 32, m/z 59 vs. 60, m/z 97 vs. 98, m/z 125 vs. 126. Furthermore, pyrolytic degradation of the ethoxyl groups may result in the elimination of ethene (m/z 28) and ethanal (m/z 44) respectively. Such pyrolytic eliminations may explain the occurrence of the marked peaks at m/z 156 (m/z 200 - 44) and 112 (m/z 200 - 2 x 44).

This Page Intentionally Left Blank

REFERENCES

- 1 P.D. Zemaný, Identification of complex organic materials by mass spectrometric analysis of their pyrolysis products. *Anal. Chem.*, 24 (1952) 1709-1713.
- 2 W.H.T. Davison, S. Slaney and A.L. Wragg, A novel method of identification of polymers. *Chem. and Ind.*, (1954) 1356.
- 3 E.M. Wilson, V. Oyama and S.P. Vango, Design features of a lunar gas chromatograph, in N.B. Brenner (Ed.), *Proc. 3rd Int. Symp. on Gas Chromatography*, 1962, Acad. Press, New York, pp. 329-338.
- 4 V.J. Oyama, Use of gas chromatography for the detection of life on Mars. *Nature*, 200 (1963) 1058-1059.
- 5 E. Reiner, Identification of bacterial strains by pyrolysis-gas-liquid chromatography. *Nature*, 206 (1965) 1272-1274.
- 6 E. Reiner, R.E. Beam and G.P. Kubica, Pyrolysis-gas-chromatography studies for the classification of mycobacteria. *Am. Rev. Resp. Dis.*, 99 (1969) 750-759.
- 7 E. Reiner, J.J. Hicks, M.M. Ball and W.J. Martin, Rapid characterization of *Salmonella* organisms by means of pyrolysis-gas-liquid chromatography. *Anal. Chem.*, 44 (1972) 1058-1061.
- 8 D.O. Hummel and H.-D.R. Schüddemage, Thermischer Abbau von Polysulfonen I. Gaschromatographische Untersuchung der Pyrolyseprodukte von Polystyrolsulfonen. *Kolloid-Z. u. Z. Polymere*, 210 (1966) 97-102.
- 9 H.-D.R. Schüddemage, *Karakterisierung von Hochpolymeren durch Pyrolyse im Feldionen-Massenspektrometer*. Thesis, University of Cologne (1967).
- 10 R.L. Levy, Pyrolysis gas chromatography, review of the technique. *Chromatogr. Rev.*, 8 (1966) 48-89.
- 11 W.J. Irwin and J.A. Slack, Analytical pyrolysis in biomedical studies, a review. *The Analyst*, 103 (1978) 673-704.
- 12 W.J. Irwin, Analytical Pyrolysis - An overview. *J. Anal. Appl. Pyrol.*, 1 (1979) 1-25; 89-122.
- 13 H.G. Boettger and A.M. Kelly, Identification of products from nucleotide pyrolysis by high resolution mass spectrometry, in *Proc. 17th Annual ASMS Conf. on Mass Spectrometry and Allied Topics*, Dallas, U.S.A., 1969, p. 333.
- 14 G.A. Charnock and J.L. Loo, Mass spectral studies of deoxyribonucleic acid. *Anal. Biochem.*, 37 (1970) 81-84.
- 15 J.L. Wiebers, Sequence analysis of oligodeoxyribonucleotides by mass spectrometry. *Anal. Biochem.*, 51 (1973) 542-556.
- 16 J.L. Wiebers, Detection and identification of minor nucleotides in intact deoxyribonucleic acids by mass spectrometry. *Nucl. Acids Res.*, 3 (1976) 2959-2970.
- 17 J.L. Wiebers and J.A. Shapiro, Sequence analysis of oligodeoxyribonucleotides by means of mass spectrometry. I, Dinucleoside monophosphates. *Biochemistry*, 16 (1977) 1044-1050.
- 18 J.P. Anhalt and C. Fenselau, Identification of bacteria using mass spectrometry. *Anal. Chem.*, 47 (1975) 219-224.
- 19 T.H. Risby and A.L. Yergey, Identification of bacteria using linear programmed thermal degradation mass spectrometry. *J. Phys. Chem.*, 80 (1976) 2839-2845.
- 20 T.H. Risby and A.L. Yergey, Linear programmed thermal degradation mass spectrometry. *Anal. Chem.*, 50 (1978) 327A-334A.

- 21 G. Buchhorn, I. Lüderwald, H. Ringsdorf and H.-G. Willert, Mass spectrometrical detection of polymer particles in capsule tissue surrounding joint endoprotheses of polyethyleneterephthalate, in *Proc. Symp. on Mass Spectrometry and Combined Techniques in Medicine, Clinical Chemistry and Clinical Biochemistry*, Tübingen, W. Germany, 1977, pp. 319-329.
- 22 I. Lüderwald, Pyrolysis-electron impact mass spectrometry. in D.O. Hummel (Ed.), *Proc. 5th European Symp. on Polymer Spectroscopy*, Cologne, W. Germany, 1978, Verlag Chemie, Weinheim, W. Germany, 1979, pp. 218-255.
- 23 K.A. Lincoln, Flash-pyrolysis of solid-fuel materials by thermal radiation. *Pyrodynamics*, 2 (1965) 133-143.
- 24 F.J. Vastola, A.J. Pirone and B.E. Knox, The production of vapor species in a mass spectrometer ionization chamber, in *Proc. 14th Annual ASMS Conf. on Mass Spectrometry and Allied Topics*, Dallas, Texas, U.S.A., 1966, p. 78-81.
- 25 W.K. Joy, W.R. Ladner and E. Pritchard, Laser heating of coal particles in the source of "time-of-flight" mass spectrometer. *Nature*, 217 (1968) 640-641.
- 26 F.S. Karn, R.A. Friedel and A.G. Sharkey, Studies of the solid and gaseous products from laser pyrolysis of coal. *Fuel*, 51 (1972) 113-115.
- 27 N.E. Vanderborgh, M.A. Fletcher and C.E.R. Jones, Laser pyrolysis of carbonaceous rocks. *J. Anal. Appl. Pyrol.*, 1 (1979) 177-186.
- 28 P.G. Kistemaker, A.J.H. Boerboom and H.L.C. Meuzelaar, Laser pyrolysis mass spectrometry: Some aspects and applications to technical polymers. in D. Price and J.F.J. Todd (Eds.), *Dynamic Mass Spectrometry, Vol. 4*, Heyden and Son, London, 1975, pp. 139-152.
- 29 P.G. Kistemaker, H.H. Tuithof, A.J.H. Boerboom, B. Neering and H.L.C. Meuzelaar, Laser pyrolysis - mass spectrometry of biopolymers. in C.E.R. Jones and C.A. Cramers (Eds.), *Analytical Pyrolysis*, Elsevier, Amsterdam, 1977, pp. 420.
- 30 M.A. Posthumus, P.G. Kistemaker, H.L.C. Meuzelaar and M.C. Ten Noever de Brauw, Laser desorption - mass spectrometry of polar nonvolatile bio-organic molecules. *Anal. Chem.*, 50 (1978) 985-991.
- 31 A.J.H. Boerboom, P.G. Kistemaker, M.A. Posthumus and H.L.C. Meuzelaar, Simultaneous opto-electrical ion selection of sub-microsecond laser-induced desorption processes. in D. Price and J.F.J. Todd (Eds.) *Dynamic Mass Spectrometry, Vol. 5*, Heyden and Son, London, 1978, pp. 114-120.
- 32 R. Kaufmann, F. Hillenkamp and E. Remy, Die Lasermikrosonde (the Laser Microprobe). *Microscopica Acta*, 73 (1972) 1-18.
- 33 R. Wechsung, F. Hillenkamp, R. Kaufmann, R. Nitsche and H. Vogt, Laser-Mikrosonden-Massen-Analysator, LAMMA: Ein neues Analysenverfahren für Forschung und Technologie. *Mikroskopie*, 34 (1978) 47-54.
- 34 E. Unsöld, G. Renner, F. Hillenkamp and R. Nitsche, Investigations on organic materials using a laser microprobe mass analyzer, in N.R. Daley (Ed.), *Advances in Mass Spectrometry, Vol. 7*, Heyden and Son, London, 1978, pp. 1425-1428.
- 35 H.J. Heinen, S. Meier, H. Vogt and R. Wechsung, Laser induced mass spectrometry of organic and inorganic compounds with a laser microprobe mass analyzer, in A. Quayle (Ed.), *Advances in Mass Spectrometry, Vol. 8*, Heyden and Son, London, 1980, pp. 942-953.
- 36 U. Seydel and H.J. Heinen, First results on fingerprinting of single mycobacteria cells with LAMMA in *Proc. 6th Int. Symp. on Mass Spectrometry in Biochem. and Medicine*, Venice, Italy, 1979.
- 37 H.J. Heinen, R. Wechsung, H. Vogt, F. Hillenkamp, and R. Kaufmann, Laser-Mikrosonden-Massenanalysator LAMMA, *Acta Phys. Austr.*, 20 (1979) 257-272.

- 38 H.G. Boettger, Electro-optical multi-channel ion detector for a mass spectrometer, in *Proc. 21st Annual ASMS Conf. on Mass Spectrometry and Allied Topics*, San Francisco, U.S.A., 1973, pp. 440-443.
- 39 H.H. Tuithof, A.J.H. Boerboom and H.L.C. Meuzelaar, Simultaneous detection of a mass spectrum using a channeltron electron multiplier array. *Int. J. Mass Spectrom. Ion Phys.*, 17 (1975) 299-307.
- 40 R. Flückiger, Beitrag zur Strukturaufklärung organischer Verbindungen mit Hilfe der Curie-Punkt-Pyrolyse. Thesis, E.T.H., Zürich, Switzerland, 1970.
- 41 H. Giacobbo and W. Simon, Methodik zur Pyrolyse und anschließenden Gas-chromatographischen Analyse von Probenmengen unter einem Mikrogramm. *Pharmac. Acta Helv.*, 39 (1964) 162-167.
- 42 H.L.C. Meuzelaar, H.G. Ficke and H.C. den Harink, Fully automated Curie-point pyrolysis gas-liquid chromatography. *J. Chromatogr. Sci.*, 13 (1975) 12-17.
- 43 H.L.C. Meuzelaar, P.G. Kistemaker, W. Eshuis and A.J.H. Boerboom, Automated pyrolysis-mass spectrometry; Application to the differentiation of micro-organisms. in N.R. Daley (Ed.), *Advances in Mass Spectrometry, Vol. 7B*, Heyden and Son, London, 1978, pp. 1452-1456.
- 44 H.L.C. Meuzelaar and P.G. Kistemaker, A technique for fast and reproducible fingerprinting of bacteria by pyrolysis mass spectrometry. *Anal. Chem.*, 45 (1973) 587-590.
- 45 W. Eshuis, P.G. Kistemaker and H.L.C. Meuzelaar, Some numerical aspects of reproducibility and specificity, in C.E.R. Jones and C.A. Cramers (Eds.), *Analytical Pyrolysis*, Elsevier, Amsterdam, 1977, pp. 151-166.
- 46 H.L.C. Meuzelaar, M.A. Posthumus, P.G. Kistemaker and J. Kistemaker, Curie-point pyrolysis in direct combination with low voltage electron impact ionization mass spectrometry. *Anal. Chem.*, 45 (1973) 1546-1549.
- 47 M.A. Posthumus, A.J.H. Boerboom and H.L.C. Meuzelaar, Analysis of biopolymers by Curie-point pyrolysis in direct combination with low voltage electron impact ionization mass spectrometry. in A.R. West (Ed.), *Advances in Mass Spectrometry, Vol. 6*, Applied Science Publ. U.K., 1974, pp. 397-402.
- 48 H.L.C. Meuzelaar, P.G. Kistemaker and M.A. Posthumus. Recent advances in pyrolysis mass spectrometry of complex biological materials. *Biomed. Mass Spectrom.*, 1 (1974) 312-319.
- 49 J. Haverkamp, H.L.C. Meuzelaar, E.C. Beuvery, P.M. Boonekamp and R.H. Tiesjema, Characterization of *Neisseria meningitidis* capsular polysaccharides containing sialic acid by pyrolysis mass spectrometry. *Anal. Biochem.*, 104 (1980) 407-418.
- 50 H.L.C. Meuzelaar, K. Haider, B.R. Nagar and J.P. Martin, Comparative studies of pyrolysis - mass spectra of melanins, model phenolic polymers, and humic acid. *Geoderma*, 17 (1977) 239-252.
- 51 G. Halma, M.A. Posthumus, R. Miedema, W. van de Westeringh and H.L.C. Meuzelaar, Characterization of soil types by pyrolysis mass spectrometry, *Agrochimica*, 22 (1978) 372-382.
- 52 W.L. Maters, D. van de Meent, P.J.W. Schuyf, J.W. de Leeuw, P.A. Schenck and H.L.C. Meuzelaar, Curie-point pyrolysis in organic geochemistry, in C.E.R. Jones and C.A. Cramers (Eds.), *Analytical Pyrolysis*, Elsevier, Amsterdam, 1977, pp. 203-216.
- 53 H.-R. Schulten and W. Görtz, Curie-point pyrolysis and field ionization mass spectrometry of polysaccharides. *Anal. Chem.*, 50 (1978) 428-433.
- 54 F.D. Hileman, personal communication.
- 55 Ch. U. Oertli, *Beitrag zur Curie-Punkt-Pyrolyse/Massenspektrometrie organischer Verbindungen*, Thesis, E.T.H., Zürich, Switzerland, 1974.

- 56 P.P. Schmid and W. Simon, A technique for Curie-point pyrolysis mass spectrometry with a Knudsen reactor, *Anal. Chim. Acta*, 89 (1977) 1-8.
- 57 M.A. Posthumus, N.M.M. Nibbering and A.J.H. Boerboom, A comparative study of the pyrolytic and electron impact -induced fragmentations of 4-phenylbutanoic acid and some analogues. *Org. Mass Spectrom.*, 11 (1976) 907-919.
- 58 M.A. Posthumus and N.M.M. Nibbering, Pyrolysis mass spectrometry of methionine. *Org. Mass Spectrom.*, 12 (1977) 334-337.
- 59 M.A. Posthumus, Some aspects of pyrolysis mass spectrometry. Ph.D. Thesis, Univ. of Amsterdam, The Netherlands, 1976.
- 60 M.D. Müller and W. Simon, The identification of anthocyanins by pyrolysis mass spectrometry and pyrolysis-GC/MS. *Microchimica Acta*, (1979) 389-396.
- 61 M.D. Müller, J. Seibl and W. Simon, Characterization of some penicillins and cephalosporins by pyrolysis mass spectrometry. *Anal. Chim. Acta*, 100 (1978) 263-269.
- 62 H.-R. Schulten, H.D. Beckey, A.J.H. Boerboom and H.L.C. Meuzelaar, Pyrolysis field desorption mass spectrometry of deoxyribonucleic acid. *Anal. Chem.* 45 (1973) 2358-2362.
- 63 W. Windig, J. Haverkamp and A.L. van Wezel, Control on the absence of DEAE-polysaccharides in DEAE-Sephadex-purified poliovirus suspensions by pyrolysis mass spectrometry. *Develop. Biol. Standardization*, 47 (1981) 169-177.
- 64 M.A. Ratcliff, E.E. Medley and P.G. Simmonds, Pyrolysis of amino acids: Mechanistic considerations, *J. Org. Chem.*, 39 (1974) 1481-1490.
- 65 J. Haverkamp, W. Eshuis, A.J.H. Boerboom and P.A.M. Guinée, Pyrolysis mass spectrometry as a rapid screening method of biological materials. in A. Quayle (Ed.) *Advances in Mass Spectrometry*, Vol. 8, Heyden and Son, London, 1980, pp. 983-989.
- 66 P.G. Kistemaker, H.L.C. Meuzelaar and M.A. Posthumus, Rapid and automated identification of microorganisms by Curie-point pyrolysis techniques, II. Fast identification of microbiological samples by Curie-point pyrolysis mass spectrometry, in C.-G. Hedén and T. Illéni (Eds.), *New Approaches to the Identification of Microorganisms*, Wiley and Sons, New York, 1975, pp. 179-191.
- 67 F.D. Hileman, L.H. Wojcik, J.H. Futrell and I.N. Einhorn, Comparison of the thermal degradation products of α -cellulose and Douglas fir under inert and oxidative environments, in F. Shafizadeh, K.V. Sarkanen and D.A. Tillman (Eds.) *Thermal Uses and Properties of Carbohydrates and Lignins*, Academic Press, New York, 1976, pp. 49-71.
- 68 D. van de Meent, J.W. de Leeuw, P.A. Schenck, W. Windig and J. Haverkamp, Quantitative analysis of polymer mixtures by pyrolysis-mass spectrometry/-discriminant analysis. *J. Anal. Appl. Pyrol.*, (1982) in press.
- 69 P.I.A. Szilagy, J.P. Green, O. Monroe Brown and S. Margolis, The measurement of nanogram amounts of acetylcholine in tissues by pyrolysis gas chromatography. *J. Neurochem.*, 19 (1972) 2555-2566.
- 70 A.C.M. Weijman, The application of Curie-point pyrolysis mass spectrometry in fungal taxonomy. in C.E.R. Jones and C.A. Cramers (Eds.), *Analytical Pyrolysis*, Elsevier, Amsterdam, 1977, pp. 225-233.
- 71 H.-R. Schulten, H.D. Beckey, H.L.C. Meuzelaar and A.J.H. Boerboom, High resolution field ionization mass spectrometry of bacterial pyrolysis products. *Anal. Chem.*, 45 (1973) 191-195.
- 72 M.A. Posthumus, N.M.M. Nibbering, A.J.H. Boerboom and H.-R. Schulten, Pyrolysis mass spectrometric studies on nucleic acids. *Biomed. Mass Spectrom.*, 1 (1974) 352-357.

- 73 G. van Graas, J.W. de Leeuw and P.A. Schenck, Analysis of coals of different rank by Curie-point pyrolysis - mass spectrometry and Curie-point pyrolysis - gas chromatography - mass spectrometry. in A.G. Douglas and J.R. Maxwell (Eds.) *Adv. in Organic Geochemistry*, (1979), Pergamon Press, Oxford, 1980, pp. 485-494.
- 74 P.A. Schenck, J.W. de Leeuw, G. van Graas, J. Haverkamp and M. Bouman, Analysis of recent spores and pollen and of thermally altered sporopollenin by flash pyrolysis -mass spectrometry and flash pyrolysis - gas chromatography - mass spectrometry, in J. Brooks (Ed.), *Organic Maturation Studies and Fossil Fuel Exploration*, Acad. Press, Cambridge, 1981, pp. 225-237.
- 75 K. Levsen and H.-R. Schulten, Analysis of mixtures by collisional activation mass spectrometry: Pyrolysis products of deoxyribonucleic acid. *Biomed. Mass Spectrom.*, 3 (1976) 137-139.
- 76 H.H. Tuithof, A.J.H. Boerboom, P.G. Kistemaker and H.L.C. Meuzelaar, A magnetic mass spectrometer with simultaneous ion - detection and variable mass dispersion in laser pyrolysis and collision-induced dissociation studies. in N.R. Daley (Ed.), *Advances in Mass Spectrometry*, Vol. 7B, Heyden and Son, London, 1978, pp. 838-844.
- 77 F.W. McLafferty, An automated analytical system for complex mixtures utilizing separation by high-resolution mass spectrometry and identification by collisional activation mass spectrometry. in C.E.R. Jones and C.A. Cramers (Eds.), *Analytical Pyrolysis*, Elsevier, Amsterdam, 1977, pp. 39-48.
- 78 F.W. McLafferty, P.J. Todd, D.C. McGilvery, M.A. Baldwin, F.M. Bockhoff, G.J. Wendell, M.R. Wixom and T.E. Niemi, MSMS: A new separation/identification technique for complex organic mixtures, in A. Quayle (Ed.), *Advances in Mass Spectrometry*, Vol. 8B, Heyden and Son, London, 1980, pp. 1589-1596.
- 79 G.J. Louter, A.J.H. Boerboom, P.F.M. Stalmeier, H.H. Tuithof and J. Kistemaker, A tandem mass spectrometer for collision-induced dissociation. *Int. J. Mass Spectrom. Ion Phys.*, 33 (1980) 335-347.
- 80 G.J. Louter, P.F.M. Stalmeier, A.J.H. Boerboom, J. Haverkamp and J. Kistemaker, High sensitivity in CID mass spectrometry, structure analysis of pyrolysis fragments, *Z. Naturforsch.*;35C (1980) 6-11.
- 81 P.J. Todd, A tandem double focussing mass spectrometer for collisional activation studies. Thesis, Cornell Univ. Ithaca, New York, 1980.
- 82 National Bureau of Standards, Washington, D.C. 20234, Catalogue of Standard Reference Materials.
- 83 R. Alvarez, National Bureau of Standards, personal communication.
- 84 H.L.C. Meuzelaar and J. Haverkamp, unpublished results.
- 85 K.V. Sarkanen and C.H. Ludwig, *Lignins*, Wiley-Intersci., New York, 1971.
- 86 J. Freudenthal and L.G. Gramberg, Pulse counting techniques in organic mass spectrometry. *Anal. Chem.*, 49 (1977) 2205-2208.
- 87 R.A. Yost and C.G. Enke, Triple quadrupole mass spectrometry for direct mixture analysis and structure elucidation. *Anal. Chem.*, 51 (1979) 1251A-1264A.
- 88 M.W. Siegel, Collision-induced dissociation apparatus with quadrupole field collision cell for mass spectrometry - mass spectrometry. *Anal. Chem.*, 52 (1980) 1790-1792.
- 89 Finnigan triple quadrupole ms. Finnigan Corp., Sunnyvale, California, U.S.A.
- 90 G.A. Byrne, D. Gardiner and F.H. Holmes, The pyrolysis of cellulose and the action of flame-retardants. II. Further analysis and identification of products. *J. Appl. Chem.*, 16 (1966) 81-88.
- 91 F. Shafizadeh, Industrial pyrolysis of cellulosic materials. *Appl. Polymer Symp.*, 28 (1975) 153-174.

- 92 F. Shafizadeh and Y.L. Fu, Pyrolysis of cellulose. *Carbohydr. Res.*, 29 (1973) 113-122.
- 93 F. Shafizadeh, G.D. McGinnis, R.A. Susott and M.H. Meshreki, Thermolysis of derivatives of amino sugars. *Carbohydr. Res.*, 33 (1974) 191-202.
- 94 H.-R. Schulten, unpublished results.
- 95 W.R. Johnson, J.W. Nedlock and R.W. Hale, Mechanisms of the pyrolysis of poly-(amino acids). *Tobacco Sci.*, 17 (1973) 89-92.
- 96 P.M.M. van Haard, H.J. Hoenders, J. Wollensak and J. Haverkamp, Pyrolysis mass spectra, sulphhydryl and tryptophan content of the embryonic nuclei from adult human normal and nuclear-cataractous lenses. *Biochim. Biophys. Acta*, 631 (1980) 177-187.
- 97 F. Martin, C. Saiz-Jimenez and F.J. Gonzalez-Vila, Pyrolysis-gas chromatography-mass spectrometry of lignins, *Holzforschung*, 33 (1979) 210-212.
- 98 Committee of chemical Sciences of the National Research Council, "The Department of Energy", U.S.A. *Some Aspects of Basic Research in the Chemical Sciences*, Section I.2, Basic Research in Coal Chemistry, 1979.
- 99 H.L.C. Meuzelaar, R.E. Wood, J.H. Futrell and L.H. Wojcik, Rapid characterization of coal samples by pyrolysis mass spectrometry, in *Proc. 28th Annual ASMS Conf. on Mass Spectrometry and Allied Topics*, New York, U.S.A., 1980, pp. 460-461.
- 100 H.L.C. Meuzelaar, Pyrolysis mass spectrometry; prospects for interlaboratory standardization. in *Proc. 26th Annual ASMS Conf. on Mass Spectrometry and Allied Topics*, St. Louis, U.S.A., 1978, pp. 29-41.
- 101 W. Windig, P.G. Kistemaker, J. Haverkamp and H.L.C. Meuzelaar, The effects of sample preparation, pyrolysis and pyrolyzate transfer conditions on pyrolysis mass spectra. *J. Anal. Appl. Pyrol.*, 1 (1979) 39-52.
- 102 M.F. Kutter, P.P. Schmid and W. Simon, The formation of amines in the analytical pyrolysis of nitro and azo compounds, *Anal. Chim. Acta*, 118 (1980) 227-231.
- 103 H.L.C. Meuzelaar, P.G. Kistemaker and A. Tom, Rapid and automated identification of microorganisms by Curie-point pyrolysis techniques, I: Differentiation of bacterial strains by fully automated Curie-point pyrolysis gas liquid chromatography. in C.G. Hedén and T. Illéni (Eds.), *New Approaches to the Identification of Microorganisms*, Wiley and Sons, New York, 1975, pp. 165-178.
- 104 Ch. Bühler and W. Simon, Curie-point pyrolysis gas chromatography. *J. Chromatogr. Sci.*, 8 (1970) 323-329.
- 105 F. Farré-Rius and G. Guiochon, On the conditions of flash pyrolysis of polymers as used in pyrolysis gas chromatography. *Anal. Chem.*, 40 (1968) 998-1000.
- 106 W. Simon, P. Kriemler, J.A. Voellmin and H. Steiner, Elucidation of the structure of organic compounds by thermal fragmentation. *J. Gas Chromatogr.*, 5 (1967) 53-57.
- 107 C.J. Wolf, M.A. Grayson and D.L. Fanter, Pyrolysis gas chromatography of polymers. *Anal. Chem.*, 52 (1980) 349A-358A.
- 108 G.G. Meisels, R.H. Emmel, S.E. Scheppele, R.K. Mitchum, K.F. Kinneberg and J.H. Draeger. Evaluation and application of energy deposition functions in electron-impact mass spectrometry. in A.R. West (Ed.), *Advances in Mass Spectrometry*, Vol. 6, Applied Science, Publ., U.K., 1974, pp. 955-961.
- 109 W. Windig, P.G. Kistemaker, J. Haverkamp and H.L.C. Meuzelaar, Factor analysis of the influence of changes in experimental conditions in pyrolysis-mass spectrometry. *J. Anal. Appl. Pyrol.*, 2 (1980) 7-18.
- 110 H.L.C. Meuzelaar and S.M. Huff, Characterization of leukemic and normal white blood cells by Curie-point pyrolysis mass spectrometry; II, Biochemical interpretation of some of the differences in the pyrolysis patterns, *J. Anal. Appl. Pyrol.*, 3 (1981) 111-130.

- 111 D.F. Hunt, J.C. Stafford, F.W. Crow and J.W. Russell, Pulsed positive negative ion chemical ionization mass spectrometry. *Anal. Chem.*, 48 (1976) 2098-2105.
- 112 F.H. Field, Chemical ionization mass spectrometry, in J.L. Franklin (Ed.), *Ion-Molecule Reactions*, Plenum Press, New York, 1972, pp. 261-313.
- 113 L.W. Sieck, Fingerprinting and partial quantification of complex hydrocarbon mixtures by chemical ionization mass spectrometry, *Anal. Chem.*, 51 (1979) 128-132.
- 114 H.J. Heinen, U. Giessmann and F.W. Röllgen, Field desorption of electrolytic solutions using untreated wire emitters. *Org. Mass Spectrom.*, 12 (1977) 710-715.
- 115 S.E. Scheppele, P.L. Grizzle, G.I. Greenwood, T.D. Marriott and N.B. Perreira, Determination of field-ionization relative sensitivities for the analysis of coal derived liquids and their correlation with low-voltage electron-impact relative sensitivities. *Anal. Chem.*, 48 (1976) 2105-2113.
- 116 H.-R. Schulten, High resolution field ionization and field desorption mass spectrometry of pyrolysis products of complex organic materials, in C.G. Hedén and T. Illeni (Eds.), *New Approaches to the Identification of Microorganisms*, Wiley and Sons, New York, 1975, pp. 155-164.
- 117 C.L. Wilkins, Fourier transform mass spectrometry, *Anal. Chem.*, 50 (1978) 493A-500A.
- 118 E.M. Chait, W.N. Huse and C.W. Hull, A novel computer controlled GC/MS with applications oriented software, in *Proc. 26th Annual ASMS Conf. on Mass Spectrometry and Allied Topics*, St. Louis, U.S.A., 1978, p. 132.
- 119 OLFAX mass spectrometry system, Vitek Corporation, Pasadena, California, U.S.A.
- 120 Curie-point Py-MS system manufactured by (a) Extranuclear Laboratories, Inc. Pittsburgh, PA, USA and (b) VG Micromass, Winsford, Cheshire, U.K.
- 121 D.A. Hickman and I. Jane, Reproducibility of pyrolysis-mass spectrometry using three different pyrolysis systems. *The Analyst*, 104 (1979) 334-347.
- 122 T.A. Gough and C.E.R. Jones, Precision of the pyrolysis-gas chromatography of polymers, Part IV. Assessment of the results of the fourth correlation trial organized by the pyrolysis sub-group of the Chromatography Discussion Group (London). *Chromatographia*, 8 (1975) 696-698.
- 123 G. Wieten, J. Haverkamp, H.L.C. Meuzelaar, H.W.B. Engel and L.G. Berwald, Pyrolysis mass spectrometry: A new method to differentiate between the mycobacteria of the "Tuberculosis complex" and other mycobacteria, *J. Gen. Microbiol.* 122 (1981) 109-118.
- 124 G. Wieten, J. Haverkamp, H.W.B. Engel and L.G. Berwald, Application of pyrolysis mass spectrometry in mycobacterial classification and identification. *Rev. Infectious Diseases*, 3 (1981) 871-877.
- 125 G. Wieten, J. Haverkamp, H.W.B. Engel and I. Tarnok, Pyrolysis mass spectrometry in mycobacterial taxonomy and identification, in G.P. Kubica, L.G. Wayne and R.C. Good (Eds.), 1954-1979; *Twenty five Years of Mycobacterial Taxonomy*, (Proc. 6th Conf. on Systematics of the genus *Mycobacterium*, Atlanta, Georgia, USA, 1979) CDC Press, Atlanta, U.S.A. 1980, pp. 171-188.
- 126 D.R. Burgard, S.P. Perone and J.L. Wiebers, Sequence analysis of oligodeoxyribonucleotides by mass spectrometry 2. Application of computerized pattern recognition to sequence determination of di-, tri-, and tetranucleotides. *Biochemistry*, 16 (1977) 1051-1057.
- 127 D.R. Burgard, S.P. Perone and J.L. Wiebers, Factor analysis of the mass spectra of oligodeoxyribonucleotides. *Anal. Chem.*, 49 (1977) 1444-1446.

- 128 Statistical Package for the Social Sciences (SPSS). N.H. Nie, C.H. Hull, J.G. Jenkins, K. Steinbrenner and D.H. Bent (Eds.) McGraw Hill, New York, 1975, 2nd edition.
- 129 J.W. Frane, The BMD and BMDP series of statistical computer programs. *Communication of the ACM*, 19 (1976) 570-576.
- 130 B.R. Kowalski, Measurement analysis by pattern recognition. *Anal. Chem.*, 47 (1975) 1152A-1162A, Information about ARTHUR: Infometrix, P.O.B. 25888, Seattle, Washington, 98125, U.S.A.
- 131 CLUSTAN, 16 Kingsburgh Road, Edinburgh, EH12 6DZ, Scotland.
- 132 P.H.A. Sneath and R.R. Sokal, *Numerical Taxonomy: The principles and practice of Numerical Classification*, W.H. Freeman and Company, San Francisco, 1973.
- 133 P.C. Jurs and Th.L. Isenhour, *Chemical Applications of Pattern Recognition*, Wiley and Sons, New York, 1975.
- 134 J.B. Kruskal, Nonmetric multidimensional scaling; a numerical method, *Psychometrika*, 29 (1964) 115-129.
- 135 J.B. Kruskal, Multidimensional scaling by optimizing goodness of fit to a non-metric hypothesis. *Psychometrika*, 29 (1964) 1-27.
- 136 D.G. Whitten, K.E. Bentley, and D. Kuwada, Pyrolysis studies, controlled thermal degradation of mesoporphyrin, *J. Org. Chem.*, 31 (1966) 322-324.
- 137 M.V. Stack, Quantitative resolution of protein pyrolyzates by gas chromatography, *J. Gas Chromatog.*, 5 (1967) 22-24.
- 138 R.W. Rozett and E. McLaughlin Petersen, Methods of factor analysis of mass spectra. *Anal. Chem.*, 47 (1975) 1301-1308.
- 139 F.J. Knorr and J.H. Futrell, Separation of mass spectra of mixtures by factor analysis, *Anal. Chem.*, 51 (1979) 1236-1241.
- 140 W. Windig, P.G. Kistemaker and J. Haverkamp, Chemical interpretation of differences in pyrolysis-mass spectra of simulated mixtures of biopolymers by factor analysis with graphical rotation, *J. Anal. Appl. Pyrol.*, 3 (1982) 199-212.
- 141 E.R. Małinowski and M. McCue, Qualitative and quantitative determination of suspected components in mixtures by target transformation factor analysis of their mass spectra, *Anal. Chem.*, 49 (1977) 284-287.
- 142 F.W. McLafferty, R.H. Hertel and R.D. Villwock, Probability based matching of mass spectra. *Org. Mass Spectrom.*, 9 (1974) 690-702.
- 143 R.J. Rummel, *Applied factor analysis*, Northwestern University Press, Evanston, U.S.A., 4th Ed., 1970, p. 389.
- 144 G.L. Ritter, S.R. Lowry, Th.L. Isenhour and Ch.L. Wilkins, Factor analysis of the mass spectra of mixtures. *Anal. Chem.*, 48 (1976) 591-595.
- 145 G.L. Ritter and H.B. Woodruff, Dimensionality and the number of features in "Learning machine" classification methods. *Anal. Chem.*, 49 (1977) 2116-2118.
- 146 S. Wold and M. Sjöström, SIMCA: A method for analyzing chemical data in terms of similarity and analogy, in B.R. Kowalski (Ed.), *Chemometrics: Theory and Application*, Amer. Chem. Soc. Symp. Series No. 52, A.C.S., Washington, D.C., (1977) pp. 243-282.
- 147 G. Blomquist, E. Johansson, B. Söderström and S. Wold, Data analysis of pyrolysis-chromatograms by means of SIMCA pattern recognition. *J. Anal. Appl. Pyrol.*, 1 (1979) 53-65.
- 148 R. Saferstein and J.J. Manura, Pyrolysis mass spectrometry-A new forensic science technique. *J. Forensic Sci.*, 22 (1977) 748-756.
- 149 J.C. Hughes, B.B. Wheals and M.J. Whitehouse, Pyrolysis mass spectrometry of textile fibres. *The Analyst*, 103 (1978) 482-491.

- 150 C.S. Gutteridge and J.R. Norris, The application of pyrolysis techniques to the identification of micro-organisms. A review. *J. Appl. Bacteriol.*, 47 (1979) 5-43.
- 151 H.L.C. Meuzelaar, P.G. Kistemaker, W. Eshuis and H.W.B. Engel, Progress in automated and computerized characterization of microorganisms by pyrolysis mass spectrometry, in H.H. Johnston and S.W.B. Newsom (Eds.), *Rapid Methods and Automation in Microbiology*, Learned Information, Oxford, U.K., 1977, pp. 225-230.
- 152 R. Böhm and H.L.C. Meuzelaar, unpublished results.
- 153 J. Borst, A.C. van der Sneek-Enkelaar and H.L.C. Meuzelaar, Typing of *Neisseria gonorrhoeae* by pyrolysis mass spectrometry. *Antonie van Leeuwenhoek; J. Microbiol. Serol.*, 44 (1978) 253.
- 154 J. Haverkamp, P.G. Kistemaker and W. Eshuis, Pyrolysis mass spectrometry as an analytical tool in microbiology. *Antonie van Leeuwenhoek; J. Microbiol. Serol.*, 45 (1979) 627-629.
- 155 R.P. Rennie and I.B.R. Duncan, Combined biochemical and serological typing of clinical isolates of *Klebsiella*. *Appl. Microbiol.*, 28 (1974) 534-539.
- 156 R.F. Smith, C.L. Bettge, S.L. Dayton and J.H. Jorgensen, Characterization of *Staphylococcus aureus* in a pediatric burn unit. *Appl. Microbiol.*, 25 (1973) 15-20.
- 157 H.L.C. Meuzelaar, unpublished results.
- 158 J. Haverkamp, P.G. Kistemaker, A.J.H. Boerboom, W. Eshuis, G. Wieten and W. Windig, Toepassingen van pyrolyse massaspectrometrie in de Klinische chemie. *Mededelingen Nederl. Vereniging voor Klin. Chemie*, 4 (1979) 188-202.
- 159 H.L.C. Meuzelaar, P.G. Kistemaker, R.B.H. Schutgens, H.A. Veder, J.R. Cardinal, J.H. Bowers and A.G. Antoschekhin, Fast, quantitative profiling of urine, bile and fibroblast samples by pyrolysis mass spectrometry, in *Developments in the Clinical Applications of HPLC, GC and MS*, (Proc. Clin. Res. Centre Symp. No. 1, Harrow, U.K. 1979) Academic Press, London, 1980, pp. 209-231.
- 160 E. Jellum, Profiling of human body fluids in healthy and diseased states using gas chromatography and mass spectrometry with special reference to organic acids. *J. Chromatogr.*, 143 (1977) 427-462.
- 161 S.C. Gates and C.C. Sweeley, Quantitative metabolic profiling based on gas chromatography, *Clin. Chem.*, 24 (1978) 1663-1673.
- 162 H.L.C. Meuzelaar, J. Haverkamp and L.M.A. Akkermans, unpublished results.
- 163 T.A. Roy, Application of pyrolysis-gas chromatography-mass spectrometry to the study of metabolic disorders, *Anal. Letters*, B11 (1978) 175-182.
- 164 A.L. Yergey, T.H. Risby and H.M. Golomb, Monitoring normal and malignant human white blood cells by the use of linear programmed thermal degradation mass spectrometry. *Biomed. Mass Spectrom.*, 5 (1978) 47-51.
- 165 H.L.C. Meuzelaar, M. Jacobson, J. Haverkamp and D.L. Pope, The frog embryo as a model for cell and tissue characterization by pyrolysis mass spectrometry. in *Proc. 28th Annual ASMS Conf. on Mass Spectrometry and Allied Topics*, New York, U.S.A., 1980, p. 51
- 166 H.A. Laitinen, Automated identification of microbes. *Anal. Chem.*, 49 (1977) 193.
- 167 G.S. de Hoog, P. Hogeweg, H.L.C. Meuzelaar and A.C.M. Weijman, *Rhinocladiella* and allied genera. *Stud. Mycol.*, 15 (1977) 1-140.
- 168 A.C.M. Weijman, Carbohydrate composition and taxonomy of the genus *Dipodascus* *Antonie van Leeuwenhoek; J. Microbiol. Serol.*, 43 (1977) 323-331.
- 169 A.C.M. Weijman, Cell-wall composition and taxonomy of *Cephaloscybus fragrans* and some Ophiostomataceae, *Antonie van Leeuwenhoek; J. Microbiol. Serol.*, 42 (1976) 315-324.

- 170 A.C.M. Weijman and H.L.C. Meuzelaar, Biochemical contributions to the taxonomic status of the *Endogonaceae*, *Can. J. Botany*, 57 (1979) 284-291.
- 171 H.L.C. Meuzelaar, Potential application of pyrolysis mass spectrometry in coffee rust research. in German Agency for Technical Cooperation (GTZ), Eschborn, W. Germany (Ed.) *Coffee Rust Control*, TZ-Verlags GmbH, Rossdorf, W. Germany, 1979 pp. 181-198.
- 172 J.J. Boon, W.R. de Boer, F.J. Kruyssen and J.T.M. Wouters, Pyrolysis mass spectrometry of whole cells, cell walls and isolated cell wall polymers of *Bacillus subtilis* var. *niger* WM. *J. Gen. Microbiol.*, 122 (1981) 119-127.
- 173 J.J. Boon and J. Haverkamp, Pyrolysis mass spectrometry of a benthic marine ecosystem - The influence of *Arenicola marina* on the organic matter cycle. *Netherl. J. Sea Res.*, 13 (1979) 457-478.
- 174 A. Myers and L. Watson, Rapid diagnosis of viral and fungal diseases in plants by pyrolysis and gas-liquid chromatography, *Nature*, 223 (1969) 964-965.
- 175 L.J. Marais and J.M. Kotzé, Pyrolysis-gas-liquid chromatographic differentiation of plant virus strains *in situ*. *J. Plant Diseases and Protection*, 86 (1979) 569-576.
- 176 H.L.C. Meuzelaar, unpublished results.
- 177 B.R. Nagar, Examination of the structure of soil humic acids by pyrolysis-gas chromatography. *Nature*, 199 (1963) 1213-1214.
- 178 J.M. Bracewell and G.W. Robertson. A pyrolysis-gas chromatography method for discrimination of soil humus types. *J. Soil Sci.*, 27 (1976) 196-205.
- 179 B.R. Nagar, E.S. Waight, H.L.C. Meuzelaar and P.G. Kistemaker, Studies on the structure and origin of soil humic acids by Curie-point pyrolysis in direct combination with low-voltage mass spectrometry. *Plant and Soil*, 43 (1975) 681-685.
- 180 F. Martin, C. Saiz-Jimenez and A. Cert, Pyrolysis-gas chromatography-mass spectrometry of soil humic fractions. II. The high boiling point compounds. *Soil Sci.*, 43 (1979) 309-312.
- 181 J.M. Bracewell, G.W. Robertson and D.I. Welch, Polycarboxylic acids as the origin of some pyrolysis products characteristic of soil organic matter. *J. Anal. Appl. Pyrol.*, 2 (1980) 239-248.
- 182 J.M. Bracewell and G.W. Robertson, Pyrolysis studies on humus in freely drained Scottish soils, in C.E.R. Jones and C.A. Cramers (Eds.), *Analytical Pyrolysis*, Elsevier, Amsterdam, 1977, pp. 167-178.
- 183 J.M. Bracewell and G.W. Robertson, Humus type discrimination using pattern recognition of the mass spectra of volatile pyrolysis products. *J. Soil Sci.*, 24 (1973) 421-428.
- 184 K. Haider, B.R. Nagar, C. Saiz, H.L.C. Meuzelaar and J.P. Martin, Studies on soil humic compounds, fungal melanins and model polymers by pyrolysis mass spectrometry, in *Soil Organic Matter Studies, Vol. II*, I.A.E.A., Vienna, Austria, 1977, pp. 213-220.
- 185 C. Saiz-Jimenez, F. Martin, K. Haider and H.L.C. Meuzelaar, Comparison of humic and fulvic acids from different soils by pyrolysis mass spectrometry. *Agrochimica*, 22 (1978) 353-359.
- 186 J.M. Bracewell, G.W. Robertson and B.L. Williams, Pyrolysis mass spectrometry studies of humification in a peat and a peaty podzol. *J. Anal. Appl. Pyrol.*, 2 (1980) 53-62.
- 187 H. de Haan, G. Halma, T. de Boer and J. Haverkamp, Seasonal variations in the composition of fulvic acids in Tjeukemeer, The Netherlands, as studied by Curie-point pyrolysis-mass spectrometry, *Hydrobiologia*, 78 (1981) 87-95.

- 188 C. Saiz-Jimenez, K. Haider and H.L.C. Meuzelaar, Comparisons of soil organic matter and its fractions by pyrolysis mass spectrometry, *Geoderma*, 22 (1979) 25-37.
- 189 M. Schnitzer, Some observations on the chemistry of humic substances, *Agrochimica*, 22 (1978) 216-225.
- 190 D. van de Meent, J.W. de Leeuw and P.A. Schenck, Chemical characterization of non-volatile organics in suspended matter and sediments of the River Rhine delta. *J. Anal. Appl. Pyrol.*, 2 (1980) 249-263.
- 191 J.W. de Leeuw, personal communication, 1977.
- 192 K.J. Voorhees, F.D. Hileman, and S.M. Kunen, Pyrolysis-mass spectrometry studies of atmospheric particulates, in *Proc. 26th Annual ASMS Conf. on Mass Spectrometry and Allied Topics*, St. Louis, U.S.A., 1978, p. 437.
- 193 A.C. Siglio, Degraded lignin compounds identified in silicified wood 200 million years old. *Science*, 200 (1978) 1054-1056.
- 194 H.L.C. Meuzelaar, G.R. Hill, J.H. Futrell, A.M. Harper, D.J. Iwamoto, D.L. Pope, G.S. Metcalf and J.H. Tomlinson, Characterization of Rocky Mountain Coals and coal liquids by computerized analytical techniques, First Annual Progress Report (DOE contract number DE-FG22-80PC30242), 1981.
- 195 M. Teichmüller, R. Teichmüller, in E. Stach, G.H. Taylor, M-Th Mackowsky, D. Chandra, M. Teichmüller, R. Teichmüller (Eds.), *Stach's Textbook of Coal Petrology*, Gebrüder Borntraeger, Berlin, 1975, pp. 5-53.
- 196 G. van Graas, J.W. de Leeuw and P.A. Schenck, Characterization of coals and sedimentary organic matter by Curie-point pyrolysis mass spectrometry, Part I. *J. Anal. Appl. Pyrol.*, 2 (1980) 265-276.
- 197 L.H. Wojcik, D.L. Pope, L.R. Frank, C. Greenwalt, H.L.C. Meuzelaar and J.H. Futrell, An investigation of the pyrolysis of a composite Green River oil shale by TGA-MS and fast-scanning Py-MS, in *Proc. 28th Annual ASMS Conf. on Mass Spectrometry and Allied Topics*, New York, 1980 pp. 458-459.
- 198 H. Solli, S.R. Larter and A.G. Douglas, The analysis of kerogens by pyrolysis-gas chromatography-mass spectrometry using selective ion detection. 2. Use of alkylbenzenes for geochemical correlations studies, in A.G. Douglas and J.R. Maxwell (Eds.) *Adv. in Organic Geochemistry*, 1979, Pergamon Press, Oxford, 1980, pp. 591-597.
- 199 H. Solli, S.R. Larter and A.G. Douglas, The analysis of kerogens by pyrolysis-gas chromatography-mass spectrometry using selective ion monitoring 2. Alkyl-naphthalenes, *J. Anal. Appl. Pyrol.*, 1 (1980) 231-241.
- 200 S.R. Larter, H. Solli and A.G. Douglas, Analysis of kerogens by pyrolysis-gas chromatography-mass spectrometry using selective ion detection. *J. Chromatog.* 167 (1978) 421-431.
- 201 D. van de Meent, S.C. Brown, R.P. Philp and B.R.T. Simoneit, Pyrolysis-high resolution gas chromatography and pyrolysis gas chromatography-mass spectrometry of kerogens and kerogen precursors. *Geochim. Cosmochim. Acta*, 44 (1980) 999-1013.
- 202 W.E. Robinson, Kerogen of Green River formation in organic geochemistry - Methods and results. in G. Eglinton and M.T.J. Murphey (Eds.), *Organic Geochemistry*, Springer Verlag, Berlin, 1969, pp. 619-637.
- 203 P.H. van der Meide, P. Westbroek, E.W. de Jong, J.W. de Leeuw and H.L.C. Meuzelaar, Characterization of macromolecules from fossil shells by immunology and Curie-point pyrolysis mass spectrometry, in M. Omori and N. Watabe, (Eds.) *The Mechanisms of Biomineralization in Animals and Plants*, (Proc. 3rd Int. Symp. on the Mechanisms of Biomineralization in the Invertebrates and Plants, Kashikojima, Japan, 1977), Tokai Univ. Press, Tokyo, 1980, pp. 251-256.

- 204 H.L.C. Meuzelaar and S.M. Huff, Characterization of leukemic and normal white blood cells by Curie-point pyrolysis-mass spectrometry. *J. Anal. Appl. Pyrol.*, 3 (1981) 111-129.
- 205 J. Haverkamp, W. Windig, D. Valerio and P.G. Kistemaker, Advances in pyrolysis mass spectrometry, in *Proc. 28th Annual ASMS Conf. on Mass Spectrometry and Allied Topics*, New York, USA, 1980, pp. 49-50.
- 206 S.R. Larter, A geochemical study of kerogen and related materials, Thesis, University of Newcastle upon Tyne, UK, 1978.
- 207 B.R. Thomas, Modern and fossil plant resins, in J.B. Harborne (Ed.) *Phytochemical Phylogeny*, 1970, Acad. Press, London, pp. 59-79.
- 208 G.O. Poinar and J. Haverkamp, Use of pyrolysis mass spectrometry in the identification of amber samples, *Gems and Gemology*, submitted for publication.
- 209 F.J.E.M. Küppers, Pyrolyse van cannabidiol, Ph.D. Thesis, University of Utrecht, The Netherlands (1973).

SUBJECT INDEX

A

Acetic acid, 19
 Acetylcholine, 10
 Acrolein, 35
 Adenosine phosphate, C.3,C.4,C.5,C.6
 Adrenocorticotrophic hormone (ACTH),
 B.1,B.2,B.3
 Adrenocorticotropin, 22
 Agarose, A.6
 Air particulates, 77
 - non-linear map, 92
 Albumin, 3,12,32,34,35,41
 Alginic acid, A.9
 Alkenes, 27,40,94,95
 Alkaptonuria, 84
 Alkylpyrroles, 87
 Amber, F.27
 Amino acids, 10,15
 - aliphatic, 21
 - aromatic, 21
 - sulphur-containing, 21
 Amino sugars, 17
 Ammonia, 13
 Ampicillin, G.7
 Amylose, 12, A.2
 Analogue ion detection, 45,46
 Ancillary analytical methods, 13,42
 Anhydrosugars, 17,A.5,A.6
 Antibiotics, 7, 24
 Antigens (bacterial), 85
 Arabinan (from apple juice), A.11
Arenicola marina, 86
 Aromatic components, 87,89
Arthrobacter, 78
 Automation, 6,7
 Azo compounds, 31

B

Bacillus, 78
 - *subtilis*, 86,A.19,A.19a,A.22,A.25,A.25a
 Background (instrument), 8,31,47,48
 Bacteria
 - classification and identification, 77
 - colonies, 29,31
 - strains, 7,10,11
 Base phosphate condensates, 19
 Batch coating of sample wires, 32
 Benzene, 27,93,95

Benzofurans, 96
 Benzoic acids (substituted), 6
 Beverages, 77
 Bile, 83
 Bilirubin, G.10
 Bimolecular reactions, 10
 Biochemical fractions, 77
 Biogeochemical applications of Py-MS,
 92,105,F.1-F.29
 Biological applications of Py-MS, 77,
 86,87,88
 Bituminous coal, 12,F.17-F.21
 Body fluid, 49,77,83
 Bovine milk (homogenized), 12
 Bovine serum albumin, 12,51
 Brain tissue, 10
 Burlap, E.3

C

Cannabidiol, G.8,G.8a
 Capsular polysaccharide, 85
 - *Neisseria meningitides*, A.14,A.15,
 A.20,A.20a,A.23
 - *Haemophilus influenzae*, A.24
 Carbohydrate-protein mixtures, 35,36
 Carbohydrates, 35,36,71,110,A.1-A.27
 - anhydrohexose, A.6
 - deoxyhexose, A.10
 - hexosamine, A.12
 - hexose, A.1-A.6,A.22,A.26,A.27
 - hexuronic acid, A.8,A.9,A.16-A.19a
 - keto-deoxyoctonate (KDO), A.20,
 A.20a,A.21
 - ketose, A.7
 - muramic acid, A.25,A.25a
 - N-acetyl-hexosamine, A.13-A.20a,
 A.25-A.27
 - N-acetylneuraminic acid, A.23,A.27
 - pentose, A.11,A.24
 Carbon disulphide, 29
 Carbowax 20M, H.4
 Carrageenan, A.5
 Catalysts, 15
 Catalytic reactions, 31
 Cataractous eye-lens tissue, 84
 Cattle food, 90
 Cells, 9,29
 Cell identification, 5,84
 Cell wall composition, 86

- Cellulose, 12,15,16,17,18,93,94, A.1, A.1a
 Ceruloplasmin, B.13
 Channel electron multiplier arrays, 6
 Char, 22,37,41,49,96
 Characteristicity, 59,60
 Chemical ionisation mass spectrometry, 4,7,14,24,41,42,43
 Chemical interpretation, 11,68
 Chi-squared coefficients, 62
 - algorithm, 63
 Chitin, 17,18,86,A.13,A.13a
 Chitosan, A.12,A.12a
 Cholesterol, 49,D.9
 Choline, 10,25,26,71, D12, D12a
 Chondroitin sulphate, A.17-A.18a
 Chromic acid, 31
 Clinical detection and diagnosis, 85
 Coal, 5,27,29,49,70,95,96
 - bituminous, 12,96
 - boghead, F.22,F.23
 - brown, 93,94
 - conversion behavior, 27
 - high volatile bituminous, F.17-F.20
 - medium volatile bituminous, F.21
 - subbituminous, 12,93
 Coating techniques, 29-33
 Coatings, 77
 Coffee rust, 86,87
 Collagen, 68,B.12
 Collisional induced dissociation, 11, 14,19
 Computer-assisted chemical interpretation, 68
 Computer-assisted quantitative analysis, 70
 Computerised data processing, 7,46,55
 Computerised mass analysis, 43,46
 Condensation, 24,37,39,44,52
 Connective tissue, 4
 Contaminants (detection of), 86
 Contamination of ion-source, 37,39,40
 Coorongite, F.8
 Cork, E.12
 Cotton, E.1
 Cresol, 21,35
 Curie-point pyrolysis mass spectrometry,
 - automated, 44
 - diagram, 39
 - technique, 29
 Cyanocobalamin (vitamin B12), G.9
 Cysteine, 21,69
 Cytochrome C, B.9
- D
- DNA, 4,8,14,19,20,21,C.2
 Data analysis procedures, 55-76
 DEAE-dextran, 10,70,72,H.12
 Decarboxylation, 16
 Degradation reactions, 16,34,35
 Dehydrated nucleosides, 19
 Dehydration, 16
 Dehydrogenated pyrolysis products, 47
 Dendrograms, 65
 Deoxysugars, 17,A.10,A.21
 Deoxyribonuclease I, B.6
 Deoxyribonucleic acid (DNA), 4,8,14,19
 20,21,C.2
 Deoxyribose, 19,20
 Depolymerisation, 15,24
 Dibenzyl, 7,10
 Diethylaminoethyl(DEAE)-dextran, 10,70
 72, H.12
 Difference spectrum, 68
 Diffusion limited pumping, 43
 Digitonin, G.3
 Digitoxin, G.1
 Digoxin, G.2
 Dihydroxybenzene, 93,95
 Diketopiperazine, 10
 Dimethoxyphenyl, 25
 Dimethylaminoethanol, 25,26
 Dimethylvinylamine, 26, D12, D12a
 Dimethylvinylammoniumchloride, 26
 Dinucleotide, 8,20
 Dipalmitoyl, D.12,D.12a
 Dipeptides, 23,24
 Direct probe pyrolysis mass spectrometry, 3,4,7,19,23,24,25,41
 Discriminant analysis, 55,75
 Diseases (plant), 86
 Distance
 - Euclidean, 63
 - city block, 62,63
 Douglas fir, 12,52,53,E.11
 Dowex, H.9-H.11
 Drugs, 11,77,111,G.1-G.9
 Duchenne muscular dystrophy (DMD), 55, 69,71
- E
- Eddy currents, 33
 Electron energies, 41,52
 Electron impact ionisation, 3,4,13,19,
 20,24
 Electro-optical ion detectors, 6,14
 Electrophoretic bands, 24
Endogonaceae, 86
 Equilibrium temperature, 33,34,35,36
 Ergosterol, D.11
Escherichia coli, 78
 Estuarine sediment, 12
 Ethylcellulose, H.13
 Etioporphyrin, G.11
 Euclidean distance algorithm, 63
 Expansion chamber, 7,37,38,40,43,44,52
 Extraterrestrial life, 3,4,77

F

Factor analysis, 10,55,69,71,72
 Fatty acid, 24,D.2-D.5
 - salts, 6
 Feature plots, 60
 - scatter, 61
 Ferromagnetic cylinders, 7,31,36,37,39
 Ferromagnetic filament, 6,7,29,36,39
 Fibres, 77
 Fibroblasts, 84
 Fibroin, E.4
 Field desorption, 8
 - mass spectrometry, 19
 Field ionisation mass spectrometry, 3,
 7,17,19,41,42,43
 Filament cleaning, 35
 Filament pyrolysis mass spectrometry,
 3,6,7,10,23,25,31
 Fingerprinting, 3,9,42,47,49,55,77,
 80,85
 Flax, E.2
 Foods, 77
 Forensic science, 77
 Fourier transform ion cyclotron
 resonance mass spectrometry, 43
 Frog embryo cell clones, 84
 Fucoïdan, A.10
 Fulvic acid, 87,88,F.5
 Fungal phospholipids, 25,26
 Fungi, 86
 Furan, 16,89
 Fusinite, F.24

G

Galacto-gluco-glucurono-araban, 48
 Ganglioside, A.27
 Geochemical applications of Py-MS, 7
 Geopolymers, 5,11,27,42,77,100,110,
 116.F.9-F.29
 Gilsonite, F.13
 Glass reaction tubes, 31,38
 Glucan, 16
 Glucose utilisation, 78,79
 Glycoconjugates, 110,A.25-A.27,B.13
 Glycogen, 7,15,16,17,31,34,35,41,50,
 51,A.4
 - muscle, 69
 Glycoproteins, 24,35,B.13
 Glycosphingolipid, A.26,A.27
 Gold-coated expansion chamber, 7
 Guaiacyl, 25,92

H

Hair (camel), E.6
 Heavy metal, 89
 Hemicellulose, 93,94
Hemileia vastatrix spores, 86,87

Hemoglobin, B.8
 Herring DNA, 21
 Hexose polymers, 17,75,A.1-A.4
 Hexosyl moieties, 19
 Hexuronic acids, 17, A.8,A.9,A.16-
 A.19a
 High frequency coil, 6
 High resolution mass spectrometer, 8,
 13,14,17,19,42,43
 High resolution magnetic sector
 instrument, 14
 High speed ion counting, 7
 Homogeneity, 12
 Homogentisic acid, 84
 Humic acid, 27,87,88,F.6,F.7
 Humic materials, 7,11,27,77,110,116,
 F.1-F.7
 Hyaluronic acid, A.16
 Hydrocarbons, 36,42,94,96,E.7,F.13,
 H.1-H.3
 Hydrogen, 31
 Hydrogen sulphide, 13,21,35,40
 Hydroxymethylfurfural, 17
 Hydroxymethylglutaric acid, 84
 Hydroxyproline, 21,69
 Hydroxystyrene, 35

I

Indanes, 96
 Indenes, 96
 Indoles, 21,22,35,89
 Induction coil, 33
 Induction heating, 6
 Inorganic salts, 10
 Insulin, B.4,B.4a
 Intracellular electrolytes, 5
 Inulin, A.7
 Ion counting, 7,44,45,46
 Ion detection, 45
 Ion exchange resins, 12,H.9-H.11
 Ion molecule complexes, 5,6
 Ion transmission efficiency, 52
 Ionisation
 - CI, 41,42
 - FI, 41,42
 - Low voltage EI, 41,42
 Iron wires, 29
 Isomeric structures, 14
 Isoprene, 24,E.7,H.8

K

Kanamycin sulphate, G.5
 Keratin, 12,B.11,E.5,E.6
 Kerogens, 27,40,96,98
 Ketodeoxyoctonate (KDO), A.21
Klebsiella, 78,82
 - non-linear map, 82,83

L

Laser microprobe mass analyser (LAMMA), 5,6
 Laser pyrolysis mass spectrometry, 3, 5,6,19,21,23
 - CO₂ laser, 5
 - ruby laser, 5
 Lecithin, 25, D.12,D.12a
 Leukemic cells, 4,84
 Levoglucosan, 17
 Levoglucosenone, 17,19
 Library spectra, 49
 Lignite, F.16
 Lignins, 10,13,25,87,89,90,91,93,96, 97,98,112,E.9,E.10
 - Björkmann, 26,E.9
 - Brauns, E.10
 - grass, 26,93
 - straw, 26,E.9,E.10
 Linear programmed thermal degradation mass spectrometry (LPTDMS), 4
 Linoleic acid, D.2
 Linolenic acid methylester, D.3,D.4
 Lipids, 10,13,24,26,44,105,110,115, D.1-D.12a
 Lipopolysaccharide, 85
 Liquid nitrogen-cooled screen, 43,44,47
Listeria, 60,78
 Lugworm, 86
 Lysozyme, B.7

M

Magnetic sector instruments, 42,43,54
 - slow scanning, 5
 - high-resolution, 14
 Mammalian cells, 84
 Mass analysis, 42
 Matrices (re-ordered), 65
 Matrix effect, 29
 Medical applications of Py-MS, 7,77-85
 Memory effects, 41
 Metabolites, 31,105
 Methanol, 19,29,105
 Methanethiol, 21
 Methionine, 21,22,69,80
 Methoxyphenols, 87
 Methoxyphenyl, 25
 Methylchloride, 10,25,26
 Methylindole, 21,35
 Methylpyrrole, 21
 Microbiology, 3
 - clinical, 77
 Microorganisms, 3,4,29,77
 Micropipette, 31
 Milk homogenate, 12
 Milk powder (instant), 13
 Model compounds, 7
 Modular instrument design, 40

Multicellular organisms, 86
 Multicomponent mixtures, 14,38
 Muscle glycogen, 69
 Muscle tissue, 7,55,68,84
Mycobacterium, 14,49,78,80
 - *bovis*, 80
 - *bovis-BCG*, 80
 - *fortuitum*, 81
 - *gastri*, 82
 - *kansasii*, 81,82
 - *terrae*, 81
 - *tuberculosis*, 80
 - *xenopi*, 81
 - non-linear map, 81
 Myoglobin, 69,B.10

N

N-acetyl aminosugars, 17,73,75,80,86, 90,107,A.13-A.20a,A.25-A.27
 N-acetylglucosamine, 17
 N-acetylhexosaminyl polymers, 17,A.13-A.20,A.25,A.25a
 N-acetylneuraminic acid (sialic acid), 85,A.23, A27
 N-acetylneuraminic acid polymers (sialopolymers), 18,A.23
 NADH, C.9
 NADPH, C.8
 Naphthalenes, 27,93,95
 National Bureau of Standards, 11,13
 Natural rubber, 15,24,25,29
 Nearest neighbor tables, 65
Neisseria meningitidis, 85,A.14,A.15, A.20,A.20a,A.23
Neisseria gonorrhoea, 78,79
 - non-linear map, 78,80
 Nicotinamide adenine dinucleotide (NADH), C.9
 Nicotinamide adenine dinucleotide phosphate (NADPH),C.8
 Nigeran, A.3
 Nitric oxide, 89
 Nitriles, 21
 Nitro compounds, 31
 Nitrogen (liquid), 29,43,47
 Non-hexosyl polysaccharides, 17,A.11, A.21,A.23, A.24
 Non-linear maps, 65,67
 Normalisation, 56
 - iterative, 58
 Nucleic acids, 4,5,19,21,110,115,C.1, C.2
 Nucleosides, 19
 Nucleotides, 20,110,115,C.3-C.9

0

Octadecadiynoic acid, D.5
 Oligopeptides, 22,24,35,36,B.1-B.3

Oligosaccharides, 35,36,A.26,A.27
 Orchard leaves, 12
 Oven pyrolysis, 3,7
 - Curie-point, 10,36
 Oyster tissue, 12

P

P-Lipotropin, 22
 Palaeotaxonomy, 98,100
 Pastes, 31
 Peat, 92
 - bog, F.14
 - sphagnum, 93, F.15
 Penicillin, 84,116,G.6,G.7
 Pentoses, 17,75,A.11,A.24
 Pepsin, 3
 Peptides, 110,B.1-B.3
 Peptidoglycan, A.25,A.25a
 Pesticide residues, 89
 Phenol, 21,22,27,35,91,93,95,96
 Phenyl, 25
 Phenylacetoneitrile, 21
 Phenylalanine, 21,22,80
 Phenylbutanoic acid, 7,10
 Phosphatidylcholine, 25
 Phospholipids, 10,25,26,71, D12, D12a
 Photodiode array, 6
 Photographic plates, 6,8,13,43
 Photolysis, 5,6
 Pigment dyes, 6,7
 Pine needles, 12
 Plant development, 87
 Plastics, 77,110,H.1-H.8
 Polar compounds, 42
 Poliomyelitis virus vaccine, 10,70,72
 Pollen, 100,E.13
 Pollutants (organic), 91
 Polybutadiene, H.8
 Polybutene, H.2
 Polycaprolactam (Nylon 6), H.5
 Polydimethylsilicone (OV-1), H.7
 Polyethylene, H.1
 Polyethyleneglycol (Carbowax 20M), H.4
 Poly(ethyleneterephthalate), 4
 Polygalacturonic acid, 29,31,A.8
 Polyisoprene, 15,24,25,E.7,H.8
 Polyphosphates, 19
 Polysaccharides, 10,15,16,47,88,A.1-A.25a
 - non-linear map, 85
 Polystyrene, 15,16,48,H.3
 Polyterpene, 24,E.7
 Polytetrafluoroethylene, 15
 Polyvinylchloride, H.6
 Porphyrins, 68
 Pre-processing (data), 56
 Pressure/time profiles, 37,40
 Principal component analysis, 55,75
 Process monitoring, 9

Proline, 68,80
 Propylamine, 14
 Prosthetic implant devices, 4
 Proteins, 10,21,24,35,36,41,47,69,71,73,75,85,105,112,113,B.4-B.13,E.4-E.6
Proteus, 78
Pseudomonas, 78
 Pulse counting, 45
 Pyran-type fragments, 16
 Pyrrole, 21,27,68,89
 Pyrrolidine, 21
 Pyrogram variability, 51
 Pyroprobe, 7
 Pyrolysate transfer, 37,38,51
 Pyrolysis FD-MS, 8
 Pyrolysis gas chromatography (Py-GC), 3,35
 Pyrolysis GC/MS, 11,14,26,83
 Pyrolysis high resolution MS, 11
 Pyrolysis mechanisms, 7,11,13,22
 - in biomaterials, 15
 Pyrolysis pathways, 10
 Pyrolysis reactor, 7

Q

Quadrupoles, 7,42,43
 - computerised systems, 46
 Quality control, 9,85
 Quantitative applications, 10,70,71
 Quartz, 31
 Quasi-molecular ions, 5,41

R

Rabbit liver, A.4
 Rank (coals), 27
 RNA, 19, 20,C.1
 Recombination reactions, 10,37
 Redwood residues, 93,94
 Reference spectra, 10
 Re-ordered matrices, 65,67
 Reproducibility between instruments, 10
 Reproducibility in Curie-point pyrolysis mass spectrometry, 35,51
 - inter-laboratory, 11,49,52,54
 - long-term, 3,5,35,41,49,50,51,52
 - qualitative, 47
 - quantitative, 49
 Resins, 110,H.10,H.11
 Resinite, F.27
 Retroaldolisation, 16
 Ribonuclease, B.5
 Ribonucleic acid (RNA), 19,20, C.1
 Ribose, 19,20
 Rice flour, 12
 Ring fragments, 19
 River clay, F.2
 River sediment, 12,F.3

Rotation

- factor, 73
 - graphical, 73
 - Varimax, 73
 - vector, 70
- Rubber (natural), 12,15,24,25,29,E.7
Rust spores, 86
Rusting pyrolysis wires, 29

S

- Saline, 29
Salts, 15
Sample
- blow-off, 31
 - preparation, 29,50,51,105
 - size (minimum), 48,51
 - transfer conditions, 11,50,51
- Scaling, 56
- feature, 58
 - pattern, 56
- Scission, 15
Screening, 9
Secondary reactions, 7,10,19,25,36,41
Sediments, 12,77,86
Serum, 83
Shale (oil), 29,93,96,98
- Green River, 97,F.11
 - ion profiles, 40
 - Messel, 97,F.12
- Signal averaging, 7,14,45,46
Signal recording, 45
Signal-to-background ratio, 48
Silk, E.4
Similarity coefficients, 62
Simultaneous ion detection, 6,43
Skin effect, 33
Sludge, 29,31,77,89,90
Slurries, 31
Sodium lauryl sulphate, D.1
Soil (granite brown), F.1
Soil fertility, 87
Soil fertilizer, 90
Soil polymers, 27
Soil polysaccharide, 88,89,F.4
Soils (whole), 7,29,88
Solvents, 29,51,53
Space probes, 3
Spectrum presentation format, 111
Spinal fluid, 83
Spinach, 12
Sphagnum, 92,93
Sphagnum moss, E.16
Spores, 100
Sporinite, F.25
Standard reference materials, 11,13
- NBS, 12
- Staphylococcus*, 78,82
Stationary phases (GC), 12, H.7

Statistical analysis

- multivariate, 46,55,62
 - univariate, 60
- Stigmasterol, D.10
Streptococcus, 78
Streptomycin sulphate, G.4
Structural investigation, 9
Styrene, 15,21,35,H.3
Subbituminous coals, 12,93-95
Subtraction techniques, 68
Sulphur, 40,89,90,93,95,97,112
Sulphur dioxide, 40
Synovial fluid, 83
Synthetic polymers, 3,5,12,42,77,110,
H.1-H.13
Syringyl, 25,92,E.9,E.10

T

- Tandem mass spectrometer, 11,14,25
Tannin, E.8
Technical polymers, 11,H.1-H.13
Teichoic acid, 86,A.22
Teichuronic acid, 86,A.19,A.19a
Temperature rise times, 5,34,35
Temperature/time profiles for wires,
34,35
Terpenes, 24,E.7
Tetrafluoroethylene, 15
Tetrahexosylceramide, A.26
Thermal degradation, 24
Thermolability of carbohydrates, 35
Thymidine phosphate, C.7
Time-of-flight mass spectrometry, 5,6,
42,43
Time-resolved pyrolysis mass spectrom-
etry, 14,40,41,46
Tissues, 29,49,71,77,84,86
Toilet paper, 89
Toluene, 21,35
Tomato leaves, 12
Torbanite, F.9,F.10
Total heating time, 34,35,51
Tricaprylin, D.6
Trilaurin, D.7
Trimethylamine, 14,25,26, D12, D12a
Trimethylammonium, 10
Tripalmitin, D.8
Trisialosyl-tetraglycosylceramide,
A.27
Tryptophan, 21,22,69,80,B.1,B.2,B.4-
B.7
Tuna, Albacore, 12
Tyrosine, 21,22,B.4,E.4

U

- Ultrasonic suspension, 29
Unicellular organisms, 86

Urban particulate, 12,52,54
Urine, 29,83,84,116
- freeze-dried, 12
- scatter plot, 84

V

Vaccines, 77,85
Vidicon, 6
Vinyl dimethylamine, 25,26, D12a
Virus, 72,85,87
Vitamins, 110,G.9
Vitrinite, F.26

W

Water, 29,77,90,91
Wheat flour, 12,E.15
Wood
- Douglas fir, 53,E.11
- fossil, F.28
- fossil conifer, F.29
- petrified, 96
- powder (soft), 12
- silicified, 96
Wool (sheep), E.5

Y

Yeast (brewer's), 12,73,86,E.14

This Page Intentionally Left Blank